

1.1.



## D3.1 THE CONCEPT, PLANNING AND OPERATIONAL PROCEDURES OF FERA-WOC

SECURITY: PUBLIC



Lead beneficiary: CARERI

Contractual Due Date: 31/12/2022

Actual Submission Date: 02/02/2023

<b>Grant Agreement number:</b>	875154
<b>Project acronym:</b>	GREAT
<b>Project title:</b>	GREENER AIR TRAFFIC OPERATIONS
<b>Funding scheme:</b>	RIA/ H2020
<b>Start date of the project:</b>	January 1st, 2020
<b>Duration:</b>	42 months
<b>Project coordinator (organisation):</b>	Michael Finke (DLR)
<b>E-mail:</b>	Michael.Finke@dlr.de
<b>Project website address:</b>	<a href="http://www.project-great.eu">www.project-great.eu</a>



This project has received funding from the European Union's Horizon 2020 research and innovation programme under grant agreement No 875154 Great.

## Table of Contents

1. Introduction.....	1
1.1. Purpose of the Report.....	1
1.2. Scope .....	2
1.3. Intended Readership .....	2
1.4. Structure of the Document .....	2
2. Concept Definition of Heterogeneous En Route Airspace Management (HERAM) in China .....	4
2.1. Baseline Situation of En route Airspace in China.....	4
2.1.1. Overview .....	4
2.1.2. Static Airspace Structure .....	5
2.1.2.1 Waypoints and Air Routes Segments.....	5
2.1.2.2 Air Routes .....	6
2.1.2.3 Control Areas and Control Sectors .....	9
2.1.2.4 FIRs and Special Airspaces .....	10
2.1.3. Airspace Operational Situation Analysis .....	11
2.1.3.1 Regional Busy Waypoints.....	11
2.1.3.2 Busy Entry/Exit Points.....	13
2.1.3.3 Regional Busy Air Route Segments and Route Operation Efficiency.....	14
2.1.3.3.1 Traffic Flow .....	14
2.1.3.3.2 Horizontal Flight Efficiency .....	15
2.1.3.3.3 Vertical Flight Efficiency .....	16
2.1.3.4 Temporary Air Routes .....	17
2.1.3.5 Busy Area Control Sectors and Approach Control Sectors ...	20
2.1.4. Flight Rules.....	22
2.1.4.1 Rules for the Use of Temporary Routes .....	22
2.1.4.1.1 Concept of temporary routes .....	22
2.1.4.1.2 Current situation of temporary routes.....	22
2.1.4.2 Rules for the Use of International Routes.....	23



- 2.1.5. Comparison of Airspace Situation Between China, USA and Europe ..... 24
  - 2.1.5.1 Baseline Operational Situation of En-Route Airspace in Europe and USA ..... 24
    - 2.1.5.1.1 USA—Rapid routes network planning and construction based on parallel routes..... 24
    - 2.1.5.1.2 Europe-Coordination and autonomous operation planning of fragmented airspace ..... 25
  - 2.1.5.2 Comparison of Airspace Planning Concepts Between China, USA and Europe ..... 28
- 2.2. Fundamentals and Requirements for HERAM Transition ..... 29
  - 2.2.1. HERAM Transition Motivated by Greener Air Traffic Management Concept ..... 29
  - 2.2.2. Requirements for HERAM Transition ..... 30
- 2.3. En route airspace resource availability analysis ..... 32
  - 2.3.1. Meta-data of National-wide En-route Airspace Sectors ..... 32
  - 2.3.2. Resource Availability Measurement ..... 33
    - 2.3.2.1 Definition ..... 33
    - 2.3.2.2 Methodology ..... 34
    - 2.3.2.3 FSRA Modelling ..... 37
    - 2.3.2.4 Computational Procedures ..... 38
  - 2.3.3. Result Analysis ..... 41
- 2.4. Method for Boundaries Identification of Flexible En Route Airspace (FERA) ..... 43
- 2.5. FERA-WOC Concept..... 46
  - 2.5.1. General Concept ..... 46
  - 2.5.2. Specific Improvements ..... 47
  - 2.5.3. Challenges ..... 48
  - 2.5.4. Relation to ICAO and SESAR Concepts and Trends ..... 49
- 3. Complexity studies of Flexible En Route Airspace (FERA) Operation ..... 50
  - 3.1. Air Traffic Complexity Modeling and Uncertainty Analysis ..... 50
    - 3.1.1. Historical flight ADS-B data and national airspace sector data .... 50
    - 3.1.2. Complexity indicator system ..... 50

- 3.1.2.1 Complexity indicator system ..... 50
- 3.1.2.2 Statistical methods for complexity indicators..... 55
  - 3.1.2.2.1 FLIGHT TRAJECTORY RESAMPLING..... 55
  - 3.1.2.2.2 trajectory clustering method..... 58
- 3.1.2.3 Statistical results of complexity indicators ..... 60
- 3.1.3. Uncertainty Analysis of Complexity Indicators..... 66
- 3.2. Complexity-based Sector Capacity Estimation for Dynamic FERA management..... 75
  - 3.2.1. Fast-time simulation ..... 75
    - 3.2.1.1 Baseline model validation ..... 76
    - 3.2.1.2 Scenarios ..... 79
    - 3.2.1.3 Simulation and Outputs..... 81
  - 3.2.2. Complexity-based workload estimation using based on XGBoost. 84
    - 3.2.2.1 Introduction of XGBoost ..... 84
    - 3.2.2.2 Controller workload prediction based on XGBoost ..... 86
    - 3.2.2.3 Performance Analysis..... 86
    - 3.2.2.4 The relationship between uncertainty and importance of complexity indicators ..... 92
- 4. FERA-WoC Planning and dynamic sector operation..... 94
  - 4.1. Collaborative Entry and Exit points planning for sectors in FERA-WoC.. 94
    - 4.1.1. Overview ..... 94
    - 4.1.2. Problem description ..... 94
    - 4.1.3. Sector boundary point planning model based on great circle ..... 95
      - 4.1.3.1 Assumptions ..... 95
      - 4.1.3.2 Data processing ..... 96
      - 4.1.3.3 Great circle paths generation ..... 97
      - 4.1.3.4 Collaborative planning of multi-sector entry and exit points ..... 100
  - 4.2. Optimal reconfiguration of FERA sectors adapting to time-varying demand ..... 112
    - 4.2.1. Dynamic configuration model of FERA sectors..... 112
    - 4.2.2. Dynamic partitioning algorithm of FERA sectors ..... 115

- 4.2.3. Sector boundary optimization algorithm..... 117
- 4.2.4. Case Analysis ..... 120
  - 4.2.4.1 Description of the Lanzhou en-route airspace scenarios and related parameters setting..... 120
  - 4.2.4.2 Accuracy validation of XGBoost-based workload estimation model ..... 121
  - 4.2.4.3 Discussion of Results ..... 123
- 4.3. Operation procedures for FERA management..... 129
  - 4.3.1. The operation mode of FERA-WoC..... 129
  - 4.3.2. The workflow of dynamic airspace management ..... 131
    - 4.3.2.1 Strategic dynamic airspace management..... 131
      - 4.3.2.1.1 Development of policies and regulations by agencies 132
      - 4.3.2.1.2 Collection and validation of airspace requirement.... 133
      - 4.3.2.1.3 Coordination and conciliation of airspace requirements ..... 133
      - 4.3.2.1.4 Design and validation of airspace structures ..... 134
      - 4.3.2.1.5 Publication and implementation of airspace structure 136
    - 4.3.2.2 Pre-tactical airspace management ..... 136
    - 4.3.2.3 Tactical real-time operations..... 138
  - 4.3.3. Emerging Situation ..... 138
    - 4.3.3.1 Communication failure ..... 138
      - 4.3.3.1.1 Aircraft on-board communication equipment can receive normally but transmission failure ..... 139
      - 4.3.3.1.2 The aircraft's on-board communication reception and transmission are both faulty ..... 139
    - 4.3.3.2 Loss of Cabin Pressurisation..... 140
    - 4.3.3.3 engine failure..... 141
    - 4.3.3.4 Spatial disorientation ..... 141
    - 4.3.3.5 radio compass failure ..... 141

- 5. References ..... 143
- Annex 1: Abbreviation..... 145
- Annex 2: Resource Availability of En-route Sectors in China ..... 147



Annex 3: The uncertainty of complexity indicators in representative sectors in China..... 192

PROPRIETARY RIGHTS STATEMENT

This document contains information, which is proprietary to the GreAT consortium. Neither this document nor the information contained herein shall be used, duplicated or communicated by any means to any third party, in whole or in parts, except with the priori written consent of the GreAT consortium. This restriction legend shall not be altered of obliterated on or from this document.

*DISCLAIMER*

*The information, documentation and figures in this document are written by the GreAT consortium under EC grant agreement no. 875154 and do not necessarily reflect the views of the European Commission. The European Commission is not liable for any use that may be made of the information contained herein.*

## 2. INTRODUCTION

In the existing airspace administrative system in China, due to the existence of restricted and prohibited airspace, especially within heavy traffic regions, aircraft are only permitted to fly along fixed air routes with very limited robustness and flexibility, resulting in more flight time, fuel consumption and emissions. In order to adapt to the increasing traffic demand and support the Greener Trajectory-Based Operation (G-TBO), in Performance improvement area 3, namely Optimal Capacity and Flexible Flight of ASBU, Free-route Operations (FRTO) is identified as a thread that describes the capability evolution by introducing flexible and free routing, which may reduce potential congestion on trunk routes and busy intersections, resulting in reduced flight distance and fuel burn. Free Route Airspace is one of the significant features in SESAR ATM master plan, overcoming the aviation sector's efficiency, capacity and environmental problems by helping in the reduction of fuel consumption and emissions, while improving flight efficiency.

In order to explore the feasibility of new operational concepts in China, with a prior knowledge of China's airspace features in the western region (i.e., medium density of air traffic, more available airspace, accommodate long haul flights to EU, Asian and partial US), the concepts of FRA, FUA (Flexible use of Airspace), and FCA (Flight Centric ATC) will be taken into account to develop a new concept of Heterogeneous En Route Airspace Management (HERAM) by identifying a refined boundary to distinguish between structured (eastern region) and flexible (western region) en route airspace system based on the en route airspace resource availability analysis. Further, reconfiguration principles and technologies of Flexible En Route Airspace in the West of China (FERA-WoC) will be explored by investigating the operational characteristics of FRA when specifically applied in China, supported by the European Consortium in the project. This is done in terms of complexity, uncertainty and capacity, in order to achieve seamless and flexible en route airspace in China, which is adapted to user-preferred and green 4-D trajectory operation.

### 2.1. PURPOSE OF THE REPORT

Following the proposed Greener Air Traffic Concept in WP2.1, this final document of WP3.1 analyzes the characteristics of en route airspace system and available space-time resources in China. The boundary division methods of structural (eastern region) and flexible (western region) en route networks are studied. The concept of Heterogeneous En Route Airspace Management (HERAM) is developed, and the elemental characteristics of flexible en route airspace is explored, such as complexity, uncertainty and traffic capacity. The reconfiguration principles, methods and operation procedures of the Western Flexible En Route Airspace (FERA-

WoC: Flexible En Route Airspace in the West of China) is established to identify, research and verify the general scientific problems and key technologies of the FERA-WoC operation, which provides a theoretical basis for promoting the refined reformation of China's airspace system.

## 2.2. SCOPE

This report studies the technologies and methods for Flexible En Route Airspace in the west of China (FERA-WoC) in MWP3, Greener Long-Haul operation. The concept of Heterogeneous En Route Airspace Management (HERAM) is developed by identifying a refined boundary to divide the China's en route network into "flexible" and "structured" 3-D regions. Boundary division, complexity analysis and robust, self-adaptive reconfiguration algorithm is studied to derive solutions to the general scientific problems and required technologies of the FERA-WoC operation in China's heterogeneous en route network, which would give preliminary information to WP3.2 and WP3.3 to understand the profile of flexible en route airspace.

## 2.3. INTENDED READERSHIP

This section describes the intended audience for this report. In general, readers of this report can be:

- 1) Readers internal to the project, using this report as input for their own activities or connections between work packages;
- 2) Readers from the GreAT Advisory board, to provide input and to follow the developments from a stakeholder point of view.
- 3) Readers from air navigation service providers or other stakeholders not involved in the project but would be effected by its improvements (especially military side in China).
- 4) Standardization bodies and regulating authorities / organizations, such as ICAO, EASA, EUROCONTROL or CAAC.

All other interested members of aviation community.

## 2.4. STRUCTURE OF THE DOCUMENT

This report contains the following sections:



**Chapter 1 Introduction** – describes the purpose and scope of the report, the intended audience and the report structure.

**Chapter 2. CONCEPT DEFINITION OF HETEROGENEOUS EN ROUTE AIRSPACE MANAGEMENT (HERAM) IN CHINA** – outlines the current en-route airspace information and practices in China, and illustrates the essential elements or assumptions that are needed to construct the HERAM framework. The parameterization of en route airspace structure in China and the modelling of en-route airspace resource availability are illustrated in detail. The distribution of the availability in different air traffic control regions of China are analyzed. Based on this, boundary identification of FERA-WoC is illustrated based on sector clustering according to resource availability. FERA-WoC concept, which is one of the cornerstones of achieving green long-haul flight between city pairs of China and Europe, is proposed including general definition, specific improvements, challenges and relations to ICAO and SESAR concepts and trends.

**Chapter 3. COMPLEXITY STUDIES OF FLEXIBLE EN ROUTE AIRSPACE (FERA) OPERATION** – 12 complexity indices are proposed in terms of airspace availability, traffic distribution and trajectory interactions at both microscopic and macroscopic view. Aiming at supporting strategic and pre-tactical DAC, low, medium and high level of uncertainty of complexity indicators are categorized by empirically analyzing the variations in 76 sectors. The sector ZLLL04 is taken as an example and the baseline simulation model using AirTOP is validated with the help of air traffic controllers from Northwest ATMB. Three different sector scenarios (i.e., low, moderate and high flexibility) with 1,200-hour random flight plans are designed to generate the operation data for XGBoost-based modeling of the relationship between complexity and simulated workload. Additional discussions are made on uncertainty and prediction accuracy.

**Chapter 4. FERA-WOC PLANNING AND DYNAMIC SECTOR OPERATION**– develops optimal entry and exit points planning model in multi-sector scenario that supports “direct route” flight based on the concept of FERA-WoC. The FERA sectors dynamic configuration model is established, and the Binary Space Partition (BSP) algorithm and the A\*-based sector boundary tuning algorithm is designed for sectors configuration. The Lanzhou en-route airspace is taken as an example for sectors dynamic configuration experiment to verify the feasibility and effectiveness of the proposed method. In addition, the operational procedures of dynamic airspace management and emerging air traffic control is preliminarily proposed.

**ANNEX 1 ABBREVIATION.**

**ANNEX 2 RESOURCE AVAILABILITY OF EN-ROUTE SECTORS IN CHINA.**

**ANNEX 3 THE UNCERTAINTY OF COMPLEXITY INDICATORS IN DIFFERENT SECTORS IN CHINA.**

# 3. CONCEPT DEFINITION OF HETEROGENEOUS EN ROUTE AIRSPACE MANAGEMENT (HERAM) IN CHINA

## 3.1. BASELINE SITUATION OF EN ROUTE AIRSPACE IN CHINA<sup>a</sup>

### 3.1.1. OVERVIEW

By the end of 2019, in China, there are 992 air routes, with a total distance of 234,509 kilometers calculated by non-repeated distance, a net increase of 9,275 kilometers over the previous year. The density of air route per unit airspace is about 0.023 kilometers/square kilometers and the density of airspace traffic is about 0.56 sorties/square kilometers. In total, 47 entry/exit points have been set up, accomplishing the organic connection with the international air route network of neighboring countries and remote countries and regions. At present, 4237 airports, 16,996 city pairs, and 11,345 flight air lines have been announced. The average non-linear coefficient of city-pair flight air lines is about 1.14<sup>[1]</sup>.

There are 11 FIRs in China with a total area of 10.81 million square kilometers. By the end of 2019, China has set up 15 high-altitude control areas, 28 medium/low-altitude control areas, 44 approach control areas and 2 terminal control area; in total, 402 control sectors are set, a net increase of 24 control sectors over the previous year, including 256 area control sectors and 146 approach (terminal) control sectors in maximum configuration; in total, 1 prohibited airspace, 66 danger airspaces, 201 restricted airspaces and 1 air defense identification zone are set.

By the end of 2019, the towers have offered services to 10,766 million flights for takeoffs and landings (excluding flight school training), an increase of 7.60% year-on-year; the ATC industry serviced a total of 42,181 million flights throughout the year, an increase of 6.6% year-on-year. 45 airports with the air traffic control system and control services serviced approximately 8,127 million take-offs and landings, accounting for 75.49% of the total number of airports, a year-on-year increase of 2.57%.

In 2018, 5,624 million flights have been accomplished, surpassing 1/3 of the USA (16,122, 500 flights) and 1/2 of Europe (11,022,800 flights), a year-on-year

increase of 5.65% which is 2.78 times that of USA (2.03%) and 1.49 times that of Europe (3.80%).

### 3.1.2. STATIC AIRSPACE STRUCTURE

#### 3.1.2.1 WAYPOINTS AND AIR ROUTES SEGMENTS

By the end of 2019, there were 1,829 waypoints in China in total, a net increase of 232 waypoints over the previous year, including 409 navigation station waypoints, 425 P code waypoints, 995 five-character waypoints. Among them, there are 527 waypoints where more than 3 air routes (including 3 air routes) interact, accounting for 28.81% of the total number of waypoints (See Figure 2.1). In 2019, there were 3,021 air routes segments in China, 330 more than the previous year. Figure 2.2 shows the changes in the number of various waypoints in the past five years.

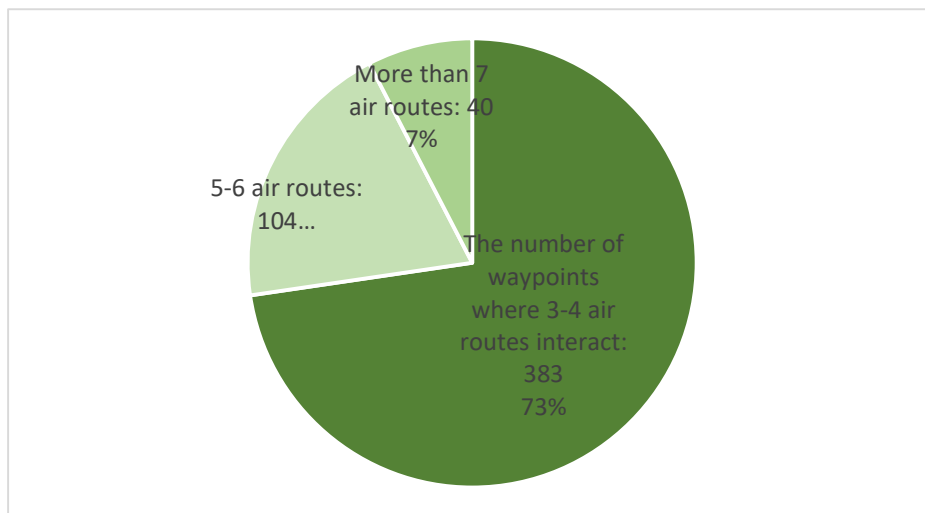
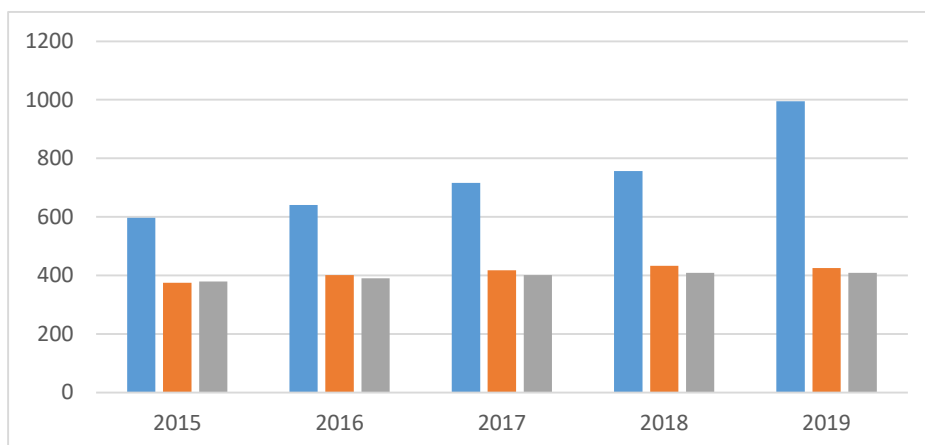


Figure 2.1 Interacts of air routes



	2015	2016	2017	2018	2019
P code waypoints	597	641	716	756	995
Five-character waypoints	375	401	417	433	425
NDB and VOR/DME	379	390	401	408	409
In total	1351	1432	1534	1597	1829

Figure 2.2 Changes of various waypoints (2015-2019)

Figure 2.3 shows the basic situation of existing waypoints and air routes segments in FIRs in China. Among them, the number of basic airspace elements in Shanghai, Kunming and Guangzhou FIR ranks top three.

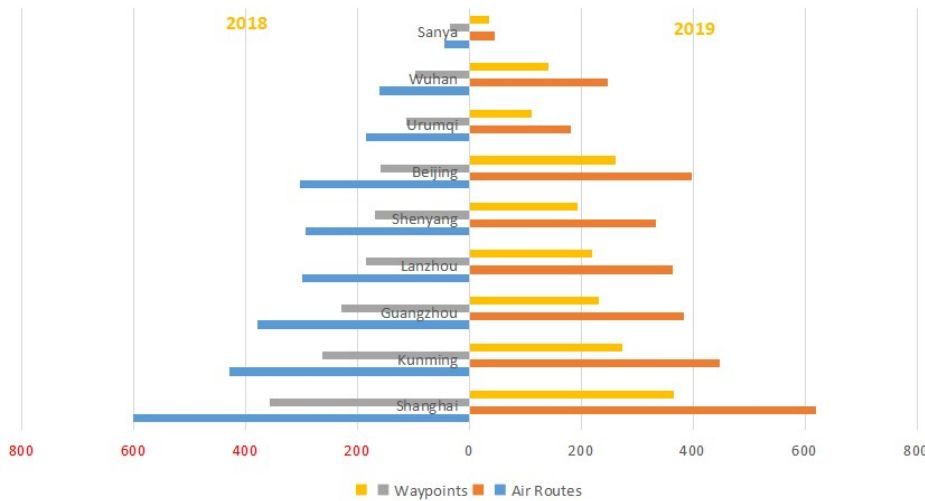


Figure 2.3 Comparison of the basic airspace elements in FIRs (2018-2019)

### 3.1.2.2 AIR ROUTES

By the end of 2019, in China, there are 992 air routes, with a total distance of 234,509 kilometers calculated by non-repeated distance. Among them, there are 743 fixed air routes, with a total distance of 183,966 kilometers, accounting for 78.45% of the total mileage of air routes; and 249 temporary air routes with a total distance of 50,543 kilometers (including 154 X air routes (only for Chinese airlines) with a total distance of 34,676 kilometers and V air routes (open for foreign airlines) with a total distance of 15,867 kilometers), accounting for 21.55%. Among the fixed air routes, there are 7,362 conventional air routes with a total distance of 134,907 kilometers (including 34 unconventional air routes with a total distance of 38,327 kilometers and 328 conventional air routes with a total distance of 96,580 kilometers); 8,365 arrival/departure air routes, with a total distance of 38,984 kilometers; and 916 regional navigation air routes, with a total distance of 10,075 kilometers (see Figure 2.4). In total, there are 471 international air routes, with a total distance of 134,923 kilometers; and 521 domestic air routes, with a total distance of 99,586 kilometers.

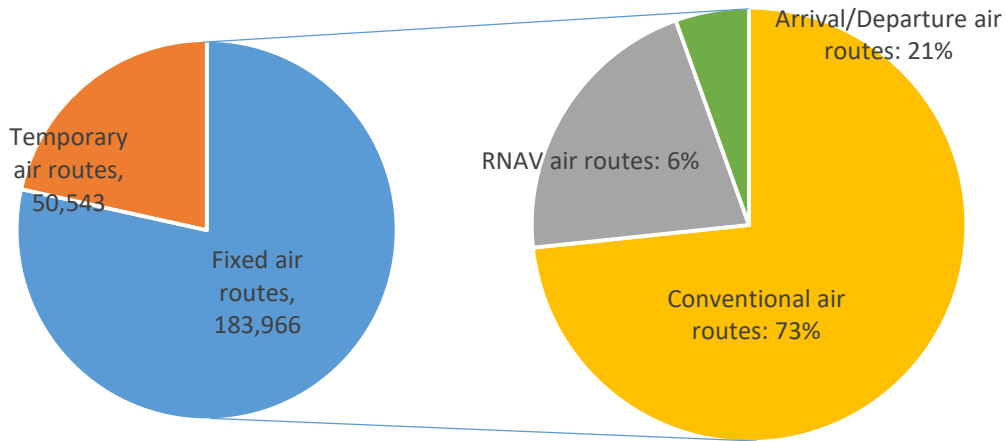


Figure 2.4 Composition of air route

Compared with 2018, the total mileage of air routes in 2019 increased by approximately 9,275 kilometers, a year-on-year increase of 4.12% (Figure 2.5). Among them, a net increase of 34 fixed air routes, totaling 4,193 kilometers; a net increase of 35 temporary routes, totaling 5082 kilometers. According to the statistics of opening to the outside world, compared with last year, there were a net increase of 73 international air routes, totaling 17,853 kilometers; a net reduction of 4 domestic air routes, totaling 8,578 kilometers.



Figure 2.5 Change of air route mileage (2010-2019)

In general, the total mileage of air routes has increased relatively slow, with an average annual growth rate of about 4.02% in the past ten years (Figure 2.5). Under the current airspace management system, the civil aviation management system is in line with the national social and economic development strategy, focusing on deepening the adjustment of the systematic structural layout, steadily promoting the continuous growth of available airspace, and promoting the efficient, intensive and safe allocation and use of airspace resources. A series of phased results were achieved: Firstly, five major corridors, including Beijing-Kunming and

Guangzhou-Lanzhou, were successively completed and put into use, and the layout of the trunk line network entered a virtuous circle. Secondly, the opening of air routes has been continuously pushing forward. In 2019, the mileage of international air routes reached 134,923 kilometers, and the average annual growth rate in the past five years was 7.36%, which was much higher than the average annual growth rate of domestic air routes of 0.21% (Figures 2.6). Thirdly, the airspace resources around the airport have increased significantly, with an average annual growth rate of 8.27% in the past five years, which is the fastest growth rate of various air routes. Fourthly, the mileage of temporary routes maintained a relatively rapid growth rate, with an average annual growth rate of 7.20% in five years, which was significantly higher than the average annual growth rate of 3.23% for fixed route routes, and its proportion in the total mileage of air routes also maintained a steady increase year by year. (Figure 2.7).

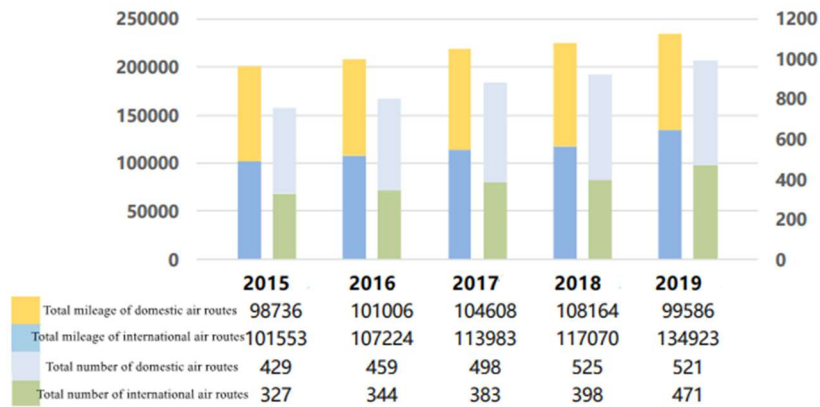


Figure 2.6 Change of international/domestic air route mileage/number (2015-2019)

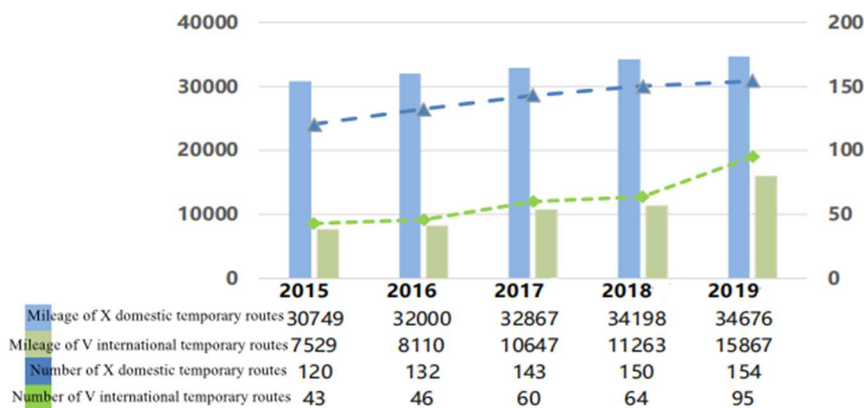


Figure 2.7 Change trend of temporary route mileage/number (2015-2019)

### 3.1.2.3 CONTROL AREAS AND CONTROL SECTORS

In total, there are 15 high-altitude (above 6000m) ACCs, 28 medium/low-altitude ACCs, 42 approach control areas and 2 terminal control areas, and their specific distribution is shown in Figure 2.8.

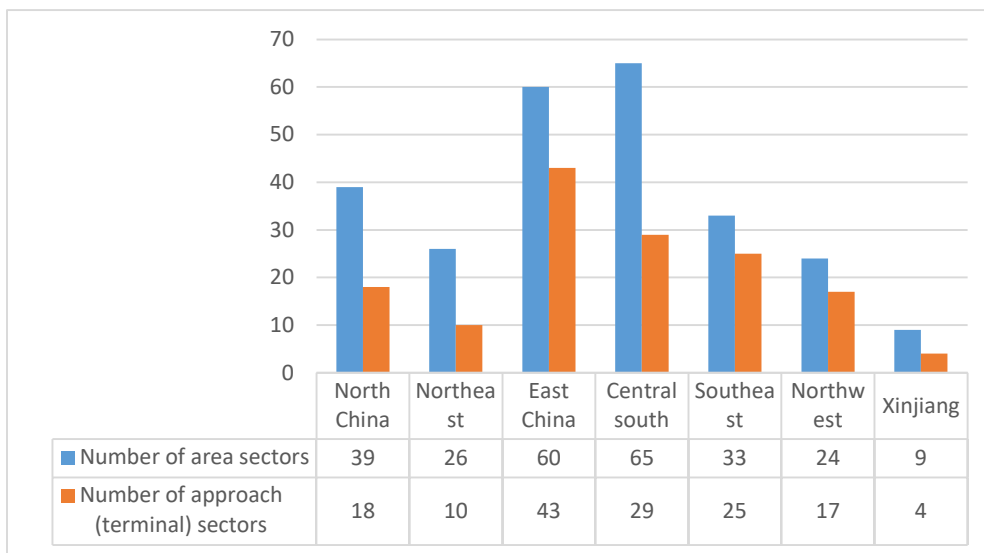
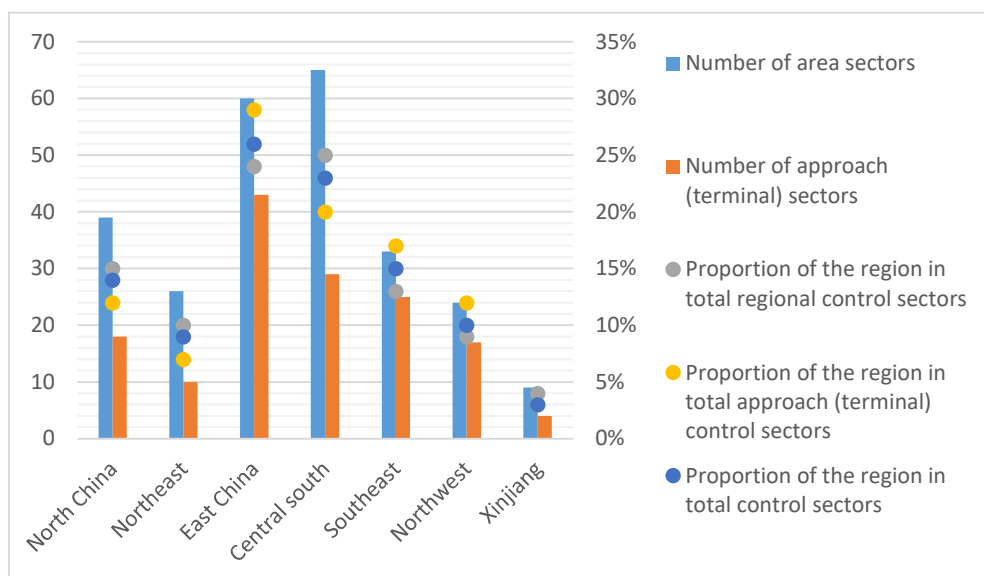


Figure 2.8 Area and approach (terminal) control sectors distribution in each region

In 2019, 402 control sectors are set in total, including 256 area control sectors and 146 approach (terminal) control sectors. 385 control sectors are actually used nationwide, including 243 area control sectors and 142 approach (terminal) control sectors.



	North China	Northeast	East China	Central south	Southeast	Northwest	Xinjiang
Number of area sectors	39	26	60	65	33	24	9
Number of approach (terminal) sectors	18	10	43	29	25	17	4
Proportion of the region in total regional control sectors	15%	10%	24%	25%	13%	9%	4%
Proportion of the region in total approach (terminal) control sectors	12%	7%	29%	20%	17%	12%	3%
Proportion of the region in total control sectors	14%	9%	26%	23%	15%	10%	3%

Figure 2.9 Geographical distribution of the number of control sectors

Among the seven regions, the total number of control sectors in East China, Central South and Southwest China ranks the top three, with 103, 94 and 58 sectors respectively, each accounting for 26%, 23% and 15% of the total number of control sectors in China (see Figure 2.9).

### 3.1.2.4 FIRS AND SPECIAL AIRSPACES

At present, China has 11 FIRs, namely Beijing, Shanghai, Shenyang, Guangzhou, Wuhan, Lanzhou, Urumqi, Kunming, Sanya, Taipei and Hong Kong. The nine mainland FIRs have a total area of 10.26 million square kilometers, the details are as shown in Figure 2.10.

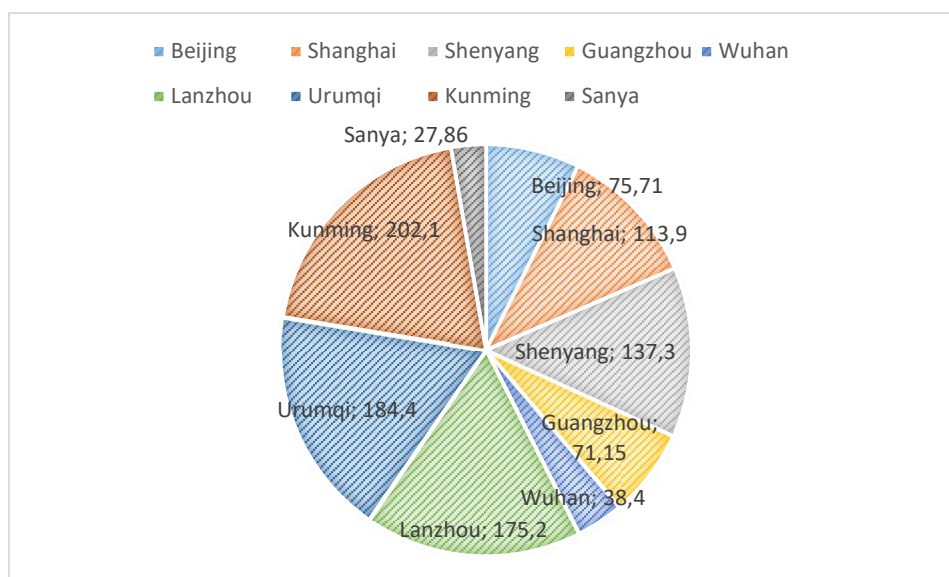


Figure 2.10 Each FIR (10,000 square kilometers) and its proportion

At present, 269 various types of special airspaces have been set, including 1 prohibited airspace, 66 danger airspaces, 201 restricted airspaces, and 1 air defense identification zone. See Figure 2.11 and Figure 2.12 for details of the number and distribution proportion of special airspaces in each FIR.



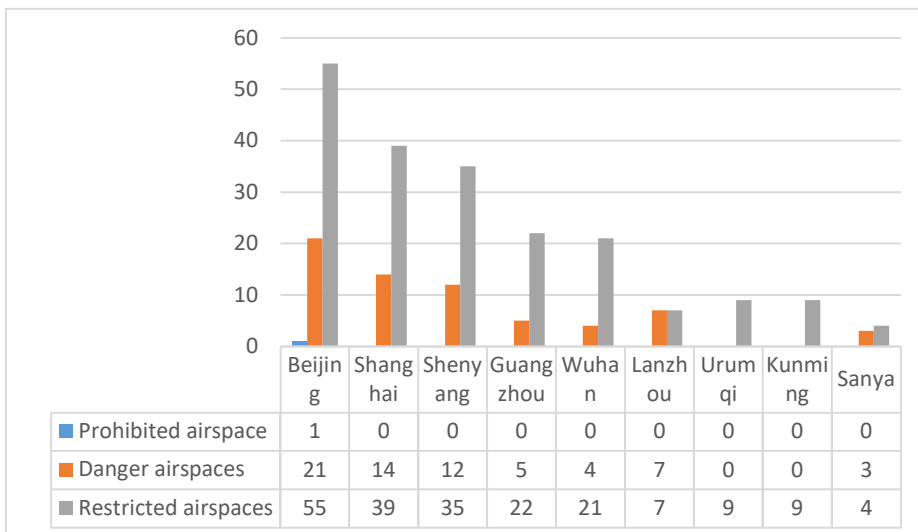


Figure 2.11 Number of special airspace in each FIR

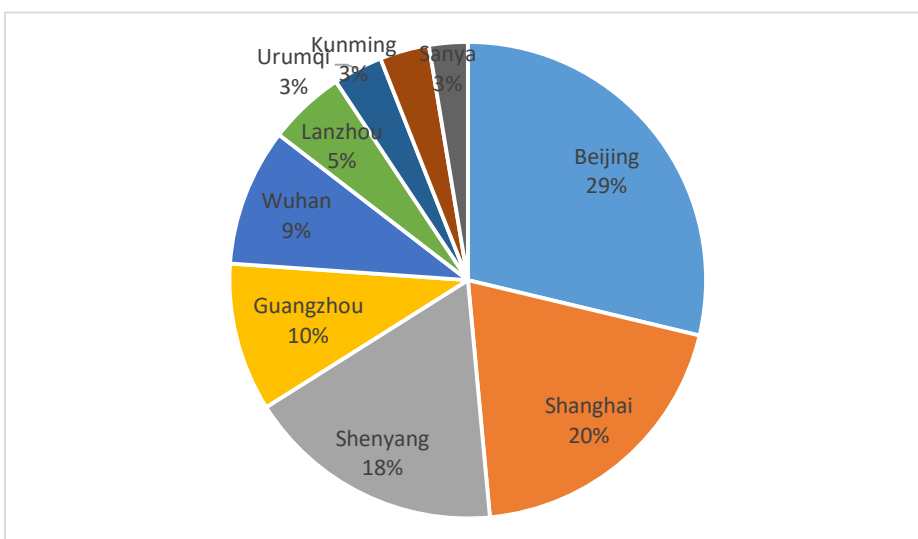


Figure 2.12 Proportional distribution of special airspace number

### 3.1.3. AIRSPACE OPERATIONAL SITUATION ANALYSIS

#### 3.1.3.1 REGIONAL BUSY WAYPOINTS

According to the top 20 regional waypoints regarding daily average flow in 2019. HFE (Hefei VOR), LKO (Longkou VOR), PAVTU, TOL (Tonglu VOR) and OBLIK rank the top 5, with average daily flow of more than 1000 flights. They are also converged intersection nodes of multiple air routes. The flight flow of the above waypoints is large and the airspace structure is relatively complex, therefore the structure of relevant air routes can be appropriately optimized so as to release the operation load at the bottleneck (Figure 2.13).

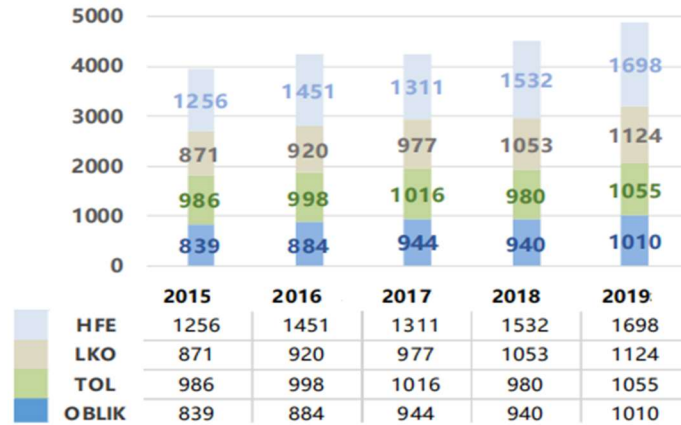


Figure 2.13 Comparison of some busy waypoints in recent five years

The five air route points with the highest increasing rate in daily average flow are DST, HFE (Hefei VOR), MADUK, ESDOS and TOL, with year-on-year increases of 14.04%, 10.84%, 10.33%, 7.88% and 7.65% respectively. On the whole, the flow of the primary busy waypoints in China still maintains the trend of rapid growth (Figure 2.14). Among them:

—TOL (Tonglu VOR) is converged intersection node of 6 air routes including A470, A599, H24, W508, etc. 949 flight routes are passing this point. Due to the rapid increase of flights to and from the southwest and central regions, as well as Nanjing and Hangzhou airports, traffic flow at this point has increased significantly.

—DST (Dongshan VOR) is located in Wenzhou, with a complex airspace structure. It is converged intersection node of 8 air routes including B221, H22, R596, and W117. 900 flight routes are passing this point. The reasons for increase in traffic flow mainly come from two aspects. One is seasonal changes in flight volume, the other is large increase in flights from the Northeast to East China and further as well as Midwest and Zhejiang to Taipei.

—HFE (Hefei VOR) and MADUK are both converged intersection nodes of R343 trunk route and other routes, with as many as 1,715 and 1,542 flight routes respectively. The apparent increase in these two points are mainly due to the increase in flights between East China and Northwest and further as well as the rapid increase in small and medium-sized airports in Jiangsu.

—ESDOS is located at converged intersection nodes of A461 and W118 in Wuhan. Especially after the Daxing Airport airspace plan is launched, this point has become a converging intersection node for two traffic flows in Beijing to enter Central South. In addition, the traffic flow in Beijing-Guangzhou continues to increase, so the traffic volume has increased steadily.

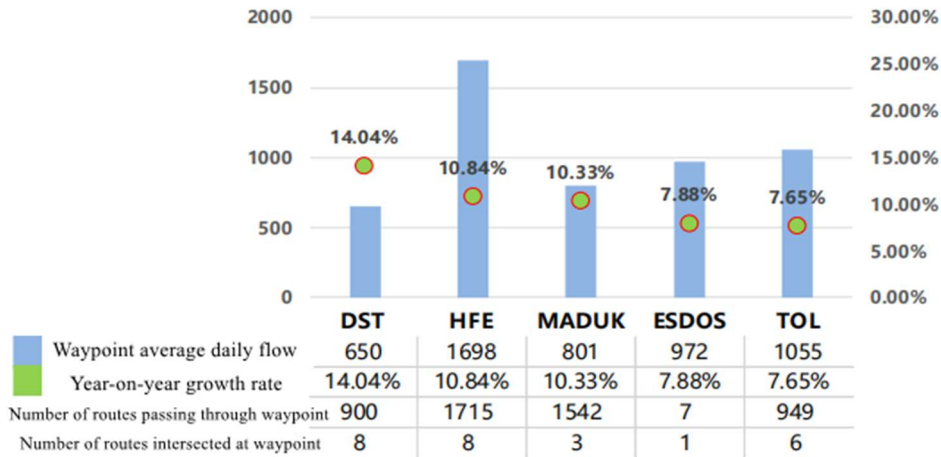


Figure 2.14 Related airspace indicators of top 5 waypoints of average daily traffic increase

It can be seen from the analysis that busy waypoints are concentrated on trunk routes such as A461, A470, A599, B221, R343, and the increase in waypoint traffic has the obvious property of transmitting, which means that the operating pressure of the trunk road network is increasing and the airspace structure needs to be further optimized and different operation modes should be adopted to realize capacity expansion and efficiency enhancement.

### 3.1.3.2 BUSY ENTRY/EXIT POINTS

In 2019, there were 1,468,110 inbound and outbound flights in China in total, a year-on-year decrease of 12.74%. Figure 2.15 shows the flow comparison of the top-20 busiest entry/exit points regarding flight flow in the recent three years. It can be seen from the figure that in the past three years, the flow at TAMOT (Hong Kong), SARIN (China-Kazakhstan) and ARGUK (China-Russia) has been increasing year by year; on the contrary, BUNTA (China-Vietnam), DOTMI (Hong Kong), OLDID (Taipei), INTIK (China-Mongolia), and SULEM (Taipei) have shown a downward trend. Some entry/exit points, such as SIKOU (Hong Kong), SAGAG (China-Laos), KAMUD (China-Kyrgyzstan), and MORIT (China-Mongolia) have basically maintained a flat trend in the past three years, with a relatively stable growth rate.

Rank	Entry/exit points	2017	2018	2019
1	AGAVO	108848	166504	129762
2	LINSO	89591	84677	85493
3	SIKOU	76826	78727	80079
4	BUNTA	64725	52246	52246
5	POLHO	52411	104187	51150
6	BEKOL	47441	47064	49702
7	SAGAG	46236	43308	43900
8	SULEM	50088	36490	43130
9	ASSAD	54329	52738	43028
10	NIXAL	38039	76397	36373
11	INTIK	26621	45273	29695
12	MAGOG	25995	27419	27718
13	SARIN	23636	23527	27070
14	SIERA	27615	26274	25647
15	DOTMI	25973	23373	23826
16	TAMOT	32148	22677	22757
17	MORIT	19896	17077	20601
18	OLDID	15545	20965	17722
19	ARGUK	7789	7780	9140
20	KAMUD	11055	10331	8563

Figure 2.15 Comparison of top 20 entry/exit points flight flows over the past three years (2019)

### 3.1.3.3 REGIONAL BUSY AIR ROUTE SEGMENTS AND ROUTE OPERATION EFFICIENCY

#### 3.1.3.3.1 TRAFFIC FLOW

In 2019, the top-20 regional air route segments regarding average daily flow mainly concentrates on traditional trunk air routes such as A461, A470, A593 and R343, and the average daily number of flights is 770. Among them, B208-NIXAL-FYG, B215-VYK-APOGO and A470-TOL-CJ (Qijianqiao) segments have the most prominent increases in traffic flow, increasing by 117.63%, 30.88% and 12.47% respectively.

It can be seen from Figure 2.16 that the congestion of A461 on Beijing-Guangzhou air route is the most prominent, followed by A593 and A470.

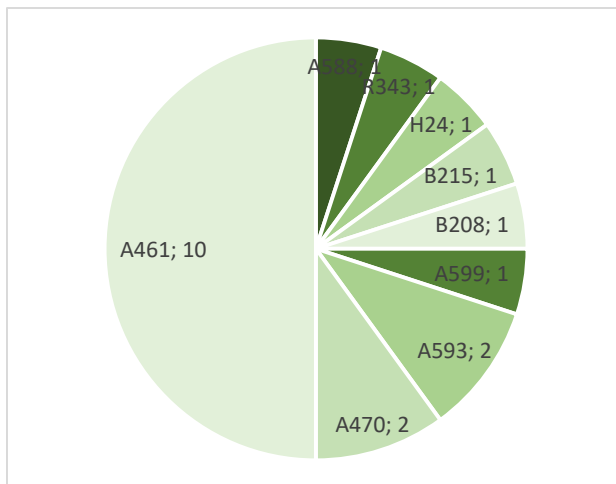


Figure 2.16 Distribution of top-20 segments of average daily flow in different routes

The section from WXI (Weixian VOR) to PAVYU in central and southern China accounts for 60% of the total length of air route A461, and keeps a large flow state (16 flights/kilometers) throughout the year. From the perspective of the airspace structure, the air route segment is vertical and horizontal, covering a wide range, connecting W4, B208, B213, A581, R343, H24 and many other main east-west routes, with converged intersection nodes of more than 3 air routes (average daily flow exceeds 700 flights), WXI, ZHO, HOK, LKO, DAPRO, LIG, which have become one of the most complex trunk air route segments in the current airspace structure.

### 3.1.3.3.2 HORIZONTAL FLIGHT EFFICIENCY

In China, horizontal flight efficiency (also named as non-linear coefficient) is defined as the ratio of FPL route distance to the great circle distance. In 2019, the average non-linear coefficient of city-pair flight air lines is about 1.14, which means that the average actual flight distance of each flight is about 14% more than the optimal route.

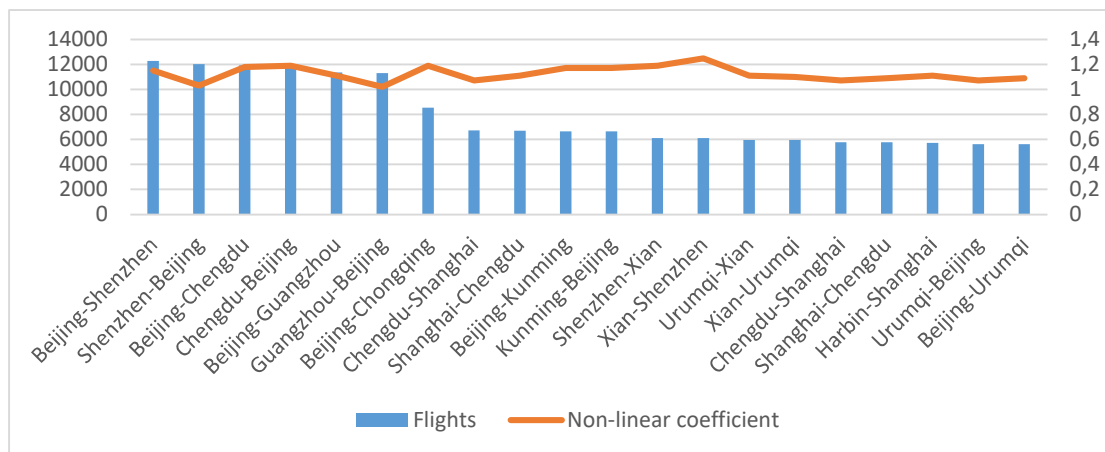


Figure 2.17 Non-linear coefficients of some busy city pairs

Figure 2.17 selects top 20 cities with flight distance greater than 1500 kilometers and the busiest flight routes (in descending order of busyness). The average non-linear coefficient is 1.12, which is slightly better than the national average of 1.14. Among them, the non-linear coefficient of air lines from Guangzhou to Beijing is the lowest at about 1.02; the non-linear coefficient from Xi'an to Shenzhen is the highest, at about 1.25.

### 3.1.3.3.3 VERTICAL FLIGHT EFFICIENCY

Calculated on the peak traffic day (August 3, 2019), A461 route carries the largest traffic at 6,900, 7,500, and 8400 meters, accounting for 9.02%, 10.36% and 9.98% of the total available altitudes respectively (See Figure 2.18).

Figure 2.19 shows controlled flight hours in different flight levels in Europe. It can be seen that prevailing air traffic flow is distributed at FL340 to FL390. Figure 2.20 shows the traffic flow at different flight levels of busy air routes in China. Most of the flights are allocated below 9800m. The vertical flight efficiency of Europe is higher than that of China.

高度层	A461-LKO-HOK	A461-OBLIK-ZHO	A461-ZHO-IDULA	A461-LUMKO-LKO	A461-P385-WXI	A461-PAVTU-LUMKO	A461-LIG-PAVTU	A461-ESDOS-OBLIK	A461-HOK-ESDOS	A461-IDULA-P385
S1550	81	0	0	7	0	4	12	0	0	0
S1490	0	0	0	0	0	0	0	0	0	0
S1430	0	0	0	0	0	0	0	0	0	0
S1370	0	0	0	0	0	1	0	0	0	0
S1310	0	0	0	0	0	0	0	0	0	0
S1250	18	2	3	10	1	2	0	2	3	1
S1220	16	0	4	31	29	26	28	0	3	4
S1190	31	1	3	35	1	10	1	0	11	0
S1160	26	1	5	51	42	41	45	1	15	5
S1130	54	74	70	53	73	19	10	57	51	42
S1100	22	3	7	50	40	44	51	0	2	2
S1070	72	23	10	2	23	35	59	0	5	5
S1040	11	3	8	2	2	1	1	0	4	5
S1010	67	4	75	13	17	24	0	3	10	2
S0980	88	93	97	87	95	48	31	77	72	68
S0950	59	2	8	113	76	93	100	3	16	6
S0920	159	130	136	127	115	62	21	117	110	60
S0890	168	3	121	6	43	147	3	0	10	7
S0840	231	46	21	89	182	132	192	6	26	27
S0810	137	101	119	119	118	30	31	90	72	73
S0780	161	15	135	99	53	56	54	8	46	1
S0750	156	79	86	92	119	24	28	2	71	29
S0720	67	17	9	76	64	7	3	0	65	11
S0690	167	5	67	100	122	109	15	3	57	46
S0660	128	101	101	151	88	50	43	91	80	26
S0630	38	34	8	104	54	16	11	22	20	16
S0600	23	16	7	48	28	1	4	3	10	8

Figure 2.18 Flow on A461 at different flight levels on peak day (August 3)

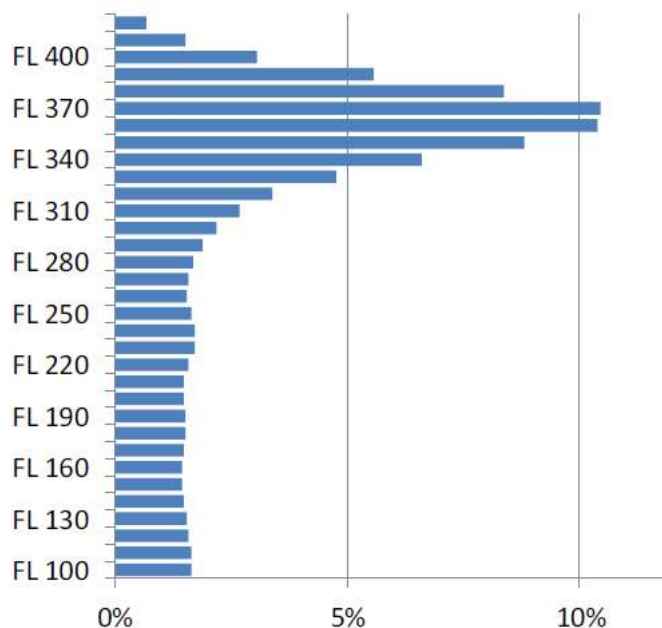


Figure 2.19 Controlled flight hours by FL in Europe (2018)

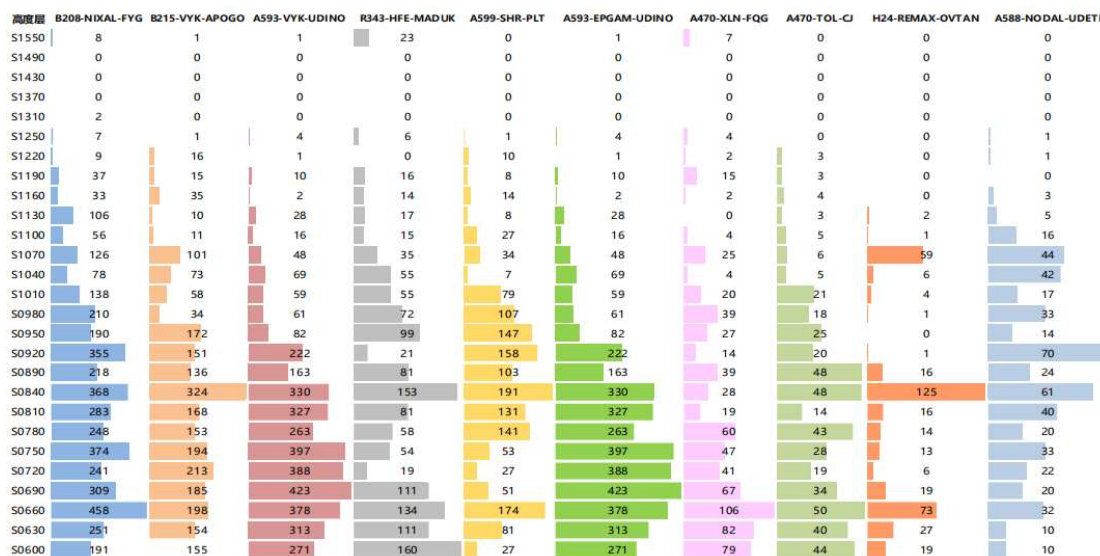


Figure 2.20 Flow on busy routes at different flight levels on peak day (August 3)

### 3.1.3.4 TEMPORARY AIR ROUTES

The use of temporary routes in 2019 is roughly the same as in 2018. There are 54 temporary routes actually used (Figure 2.21). Some temporary routes (such as X136, X64, V12, V78, etc.) have large daily average traffic flow and long service time. In the whole year, a total of 373,000 flights used temporary routes, shortened the flight distance of 15.7 million kilometers, saved 84,800 tons of fuel consumption, and reduced carbon dioxide emissions by 267,000 tons, a year-on-year decrease of 4.36%, 0.25%, 0.24%, and 0.37% respectively.

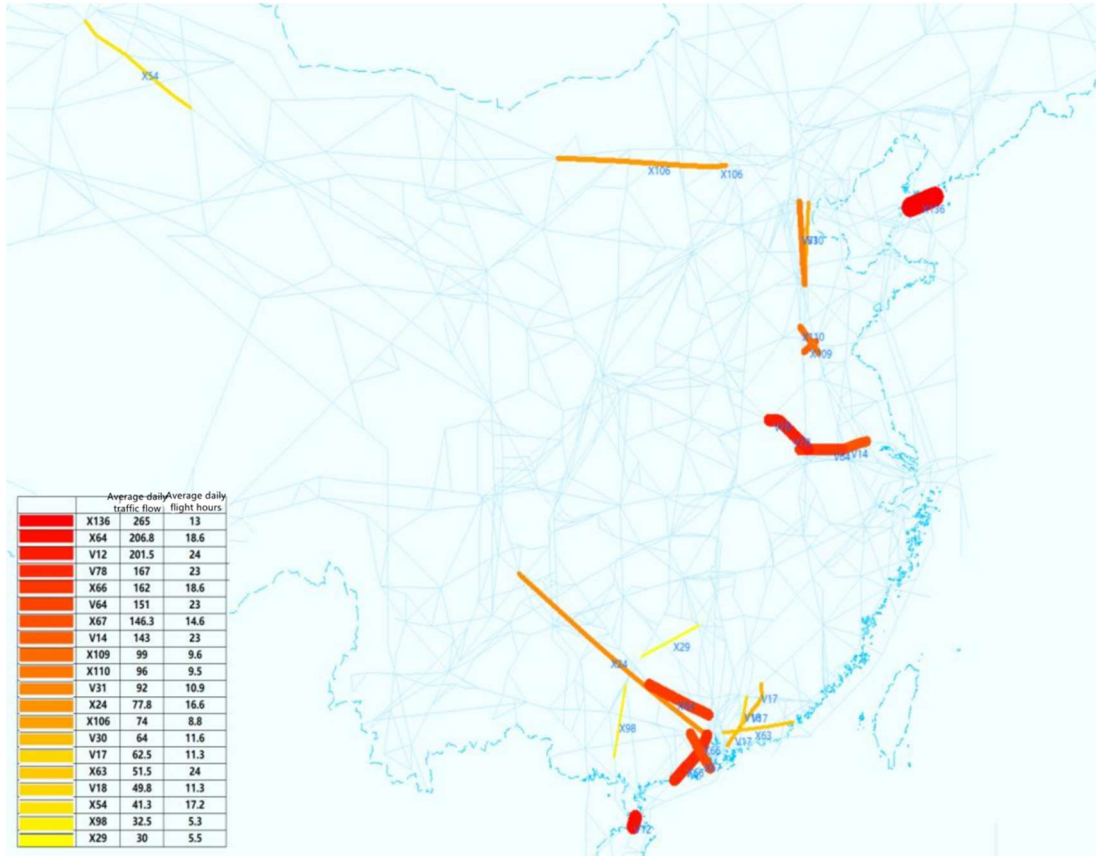


Figure 2.21 Top-20 temporary routes of daily average traffic flow

As shown in Figure 2.22, in the past five years, although the use of temporary routes in 2016 has shown a downward trend year-on-year, it has improved since 2017 and maintained a relatively stable momentum from 2018 to 2019. On the whole, the enthusiasm for the use of shared airspace between the military and civilians has gradually increased, the use of temporary air routes to save flight distance has steadily increased, the efficiency of regional temporary air routes has been significantly improved.

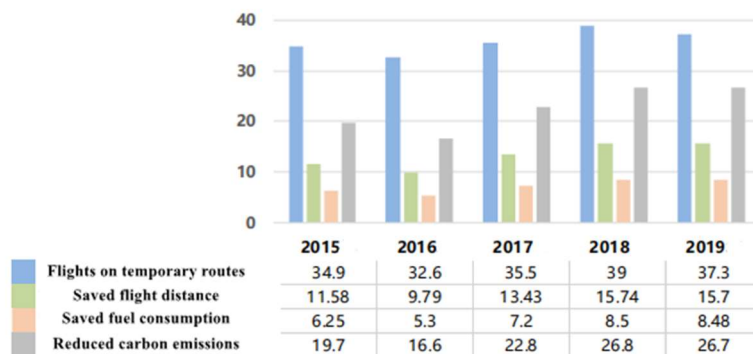


Figure 2.22 Change trend of relevant indicators of temporary routes (2015-2019)

In 2019, the top-20 temporary air routes regarding daily average flow are mainly distributed in North China, Central South China and East China, which are also the



regions with the most active flight activities. On the whole, the average daily flow of the above temporary air routes reaches 111 flights, and the average daily use time is about 14.97 hours, with the year-on-year decrease of 15.2% and 3.84% respectively (see Figure 2.23).

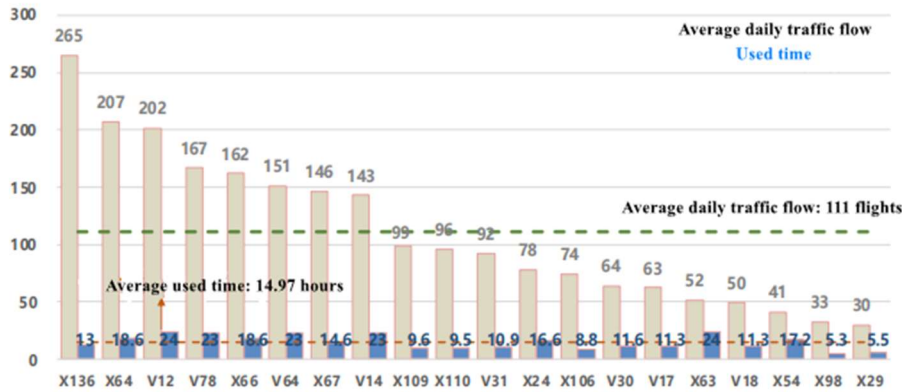


Figure 2.23 Average daily traffic flow and average daily service hours of top-20 temporary routes in 2019

Figure 2.23 listed the average daily flow and average daily use hours of the top 20 temporary air routes respectively. Some temporary air routes in busy regions, such as X136, X64 and V12, have an average daily flight quantity of more than 200 flights, which has become a useful supplement to the fixed air route network in this region and played an important role in improving the regional airspace operation environment. For temporary routes that are open for a long time (the average daily opening time is more than 20 hours), such as V14, V64, V78, X63, the use should be further strengthened, and the mechanism of "normal default open use" should be continuously improved. Taking the Central and South China region as an example, according to statistics, 9 temporary routes (V101, V103, V106, V107, V108, V109, V66, X171, X172) were newly added in 2019. The total number of flights using temporary routes throughout the central and southern regions reached 106,700 flights, reducing the flight mileage of 4.51 million kilometers, effectively promoting energy conservation and emission reduction, improving regional operation efficiency, and playing a positive role in improving the airspace operation environment.

However, there are still some problems in the use of temporary air routes across the country. Firstly, inter-regional temporary routes involve a number of military and civil aviation units, which not only require a large amount of coordination work, but also require each section of temporary routes in different regions to be open before they can be used. This leads to limited use of some temporary routes and the reduction should be effective. Secondly, although the "normalized opening" mechanism has been established, there are still problems such as insufficient available time and less available height. The potential of the airspace needs to be further tapped and released.

### 3.1.3.5 BUSY AREA CONTROL SECTORS AND APPROACH CONTROL SECTORS

In 2019, 90% of the top-20 sectors regarding average daily flow concentrate in Central South and East China. Compared with 2018, about 94% of them show the trend of positive growth. Figure 2.24 compares average daily traffic with peak hourly traffic. Among them, Chengdu 08 (+26.51%), Hefei 01 (+11.59%) and Hefei 04 (+11.22%) sectors have a large increase in flow and Chengdu 23 (-12.04%) have a large decrease in flow.

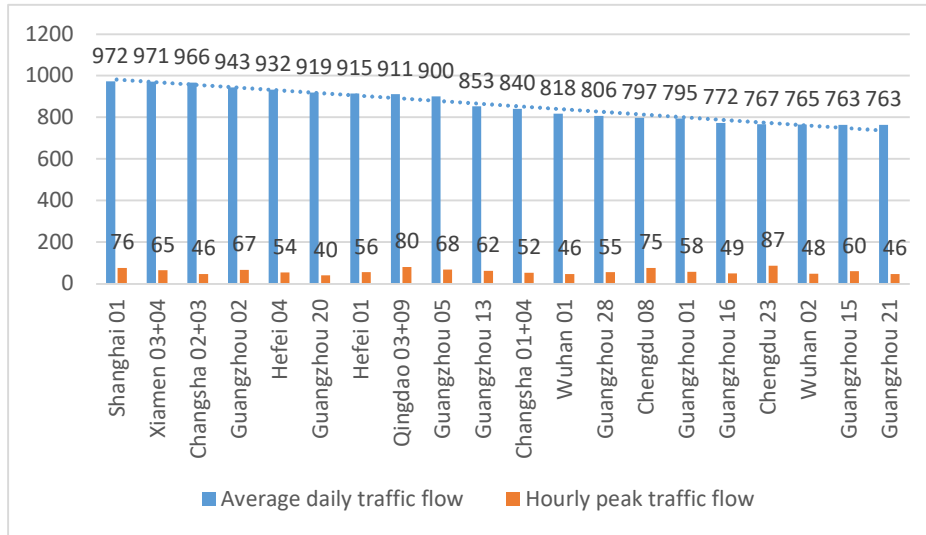


Figure 2.24 Top-20 sectors of area average daily flow

Among the top-20 sectors, 19 sectors have completed capacity assessments. About 36.8% sectors have peak hour traffic exceeding the capacity baseline, with an average overcapacity ratio of -1.95%. Figure 2.25 shows the five sectors with the largest excess capacity ratio, including the air routes network density and main intersections within the sector, and examines the airspace structure and operational characteristics of each sector from more perspectives. For example, Hefei 01 has a very dense internal air routes (density of air routes network is about 0.08). As mentioned above, HFE not only bears the main traffic flow from East China to North China, but also a conflict-prone area where multiple air routes converge (There are as many as 11 intersections in the sector), due to year-round high-level operation and continuous increase in traffic flow, the sector is obviously over-capacity. The road network density of Xiamen 03+04 is about 0.02, and there are 7 intersections inside. It is mainly responsible for the take-off and landing of Xiamen, Fuzhou, Wuyishan and Quanzhou airports and the control of flights in other areas. In addition, the continuous increase of flights in various places has exceeded. The capacity is relatively large.

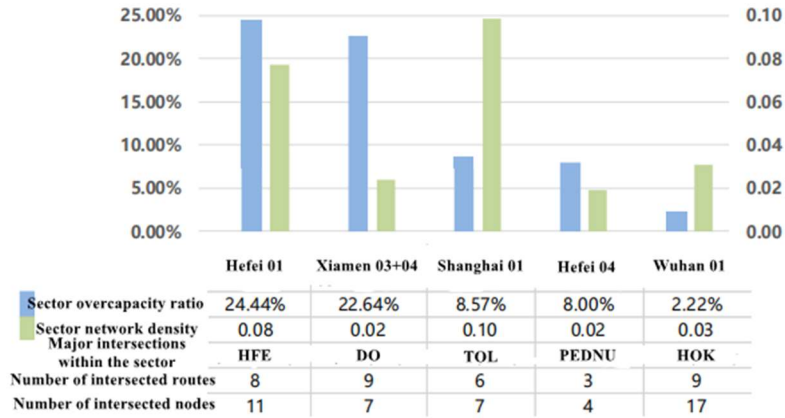


Figure 2.25 Top-5 overcapacity ratio sectors

Figure 2.26 lists the average flight time, maximum instantaneous flights, and number of route intersections for some busy air routes sectors on the peak traffic day (August 3, 2019). Through analysis of relevant indicators, it can be seen that Guangzhou 05 and 15 sectors have a large number of intersections, a higher maximum instantaneous flights, a relatively short average flight time, a complex airspace structure, high instantaneous control pressure, and difficulty in deployment. And adjusted number of intersections in Chengdu 08 is relatively small, the maximum instantaneous flights are low, the average flight time is relatively long, and the overall airspace operation environment and control difficulty have been improved.

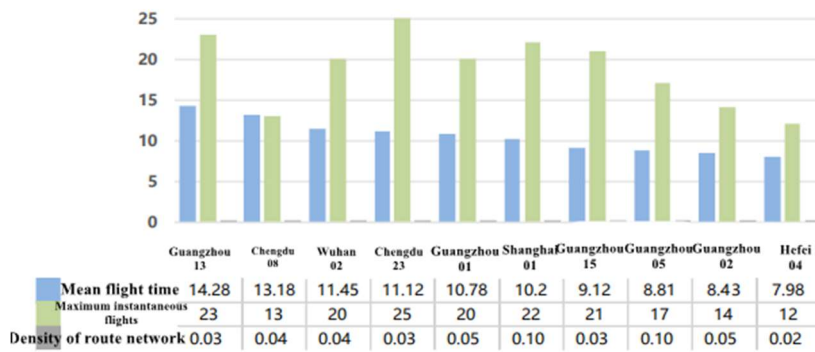


Figure 2.26 Airspace related indicators of some busy sectors on traffic peak day (August 3)

Based on the current airspace operational situation, there are still some sectors in various regions operating under high load. Combining actual situations, we can further optimize the airspace structure, scientifically adjust the number and use of sectors, and strive to increase deployment space, reduce control difficulty, and make the workload among the sectors is more balanced, achieving the best match between capacity, traffic and personnel, and comprehensively improving the quality of sector airspace operation.

### 3.1.4. FLIGHT RULES

#### 3.1.4.1 RULES FOR THE USE OF TEMPORARY ROUTES

##### 3.1.4.1.1 CONCEPT OF TEMPORARY ROUTES

Temporary routes are segments with designated code and determined direction that are authorized by relevant state departments to fulfil flight needs. They are managed by the Air Force, and instructed by civil aviation. Temporary routes are divided into temporary international routes and temporary domestic routes. Temporary international routes can be publicly announced for foreign and domestic airlines to choose from. Temporary domestic routes can only be used by domestic airlines. The main difference between temporary routes and fixed routes is that temporary routes are air routes with restrictions. Most countries in the world have similar routes, such as point-to-point direct flights with the consent of the controller, seasonal routes that can be used during a certain period of the year, and weekend routes that are open on weekends. Temporary routes in Europe are called Conditional Routes. Their use and management methods are relatively mature, and they have become a successful example of the flexible use of airspace. Due to the particularity of temporary routes, the diversity of limiting factors and uncertainty, the use of temporary routes must comply with the principle of declaration before use. When airlines (or flight crews) wish to use temporary routes, they must apply to the civil aviation administration. After the application is coordinated by the civil aviation ATC department and the air force ATC department, and clear approval is obtained, the temporary flight route can be entered <sup>[2]</sup>.

##### 3.1.4.1.2 CURRENT SITUATION OF TEMPORARY ROUTES

Currently, there are 117 temporary routes announced nationwide, with a total distance of more than 34,000 kilometers, accounting for nearly 20% of the total distance of air routes. The basic model of current airspace management system is under the leadership of the National Air Traffic Management Committee, the Air Force organizes and implements national flight control, and military and civil aviation provide air traffic control services in accordance with their respective responsibilities. In other words, whether and when temporary air routes can be opened to civil aviation are determined by the Air Force ATC department. The civil aviation ATC department is responsible for temporarily assigning and directing civil aircraft overflights during the air route opening period.

Administrative Measures for the Use of Temporary Routes promulgated by the Air Traffic Management Commission in 2008 set clear requirements on the application methods, application channels, and notification of approval information for temporary routes. When the military aviation has flight activities, the temporary

route can be used only after the approval of the relevant flight control department. Under normal circumstances, the air traffic control units of the Air Force will formulate flexible airspace use plans based on the next day's combat readiness training plan and issue temporary route use permits. The civil aviation control department will direct flights to use temporary routes based on the information issued by the Air Force. However, in actual operations, there are problems such as insufficient airspace release, unsmooth information release channels, and inconsistent implementation standards and operating methods of various control departments. The use of temporary routes will not be announced in NOTAM, and it is almost impossible for airlines to obtain temporary route use permits during the flight planning stage. Only a few flights are permitted in the air or are directed by controllers to use temporary routes <sup>[3]</sup>.

### 3.1.4.2 RULES FOR THE USE OF INTERNATIONAL ROUTES

Allocation and Use of International Air Rights Resources to classify the allocation and management of international Air rights resources, gradually breaking the rule of "one long-distance international route, one carrier", and establishing the principles and quantitative index system for the allocation of navigation rights resources, and strictly manage the use of navigation rights. According to the Measures, international routes are divided into first-category international routes and second-category international routes. The first-category of international routes refer to routes from China to foreign countries with open air rights or open air routes under agreements with countries with partial open air rights. The second-category international routes refer to the international routes in the market with restricted air rights other than the first- category international routes, which are divided into the second- category long-range international routes and the second-category non-long-range international routes. Second-category international routes from domestic destinations in China to destinations in the Americas, Europe (excluding Russia), Oceania, and Africa are second-category long-range international routes, and the others are second-category non-long-range international routes <sup>[4]</sup>.

The measures adopt categories for different types of routes. First- category international routes do not limit the number of designated carriers, route schedules, operational frequency and capacity arrangements. Second-category long-distance international routes gradually introduces competition. For the second-category long-range international routes operated by existing airlines, if they meet the new carrier access standards stipulated in the Measures, a new carrier can be added, thereby gradually breaking the rule of "one long-distance international route, one carrier" and encourage airlines to participate in international competition.

The Measures also set requirements for new carriers on second-category long-range passenger international routes, clearly complying with the air rights regulations and there are two or more airline companies competing for the same

air rights (including applications by airline companies to increase the number of flights). In accordance with the principles of international air rights resource allocation and the contents of declarations by air transport companies, comprehensive evaluations were made on the basis of consumer interest indicators, hub development indicators, resource utilization efficiency indicators and enterprise operational quality, and the scoring standards and calculation methods for these indicators were clarified. At the same time, there is no restriction on the number of carriers for second-category long-range international routes and non-long-range international routes subject to air rights arrangements.

The Measures require that airlines must operate strictly in accordance with the approved routes, schedules, models, and execution dates, and cannot change or cancel without authorization. Air transport companies with operating permits for international routes should make full use of the air rights they have, otherwise the Civil Aviation Administration will cancel them according to law, or take back the air rights that are not fully used and re-allocate them. CAAC will establish and improve the flight operation monitoring system and information analysis and notification system of international routes, and conduct supervision and inspection to strictly manage the use of air rights<sup>[5]</sup>.

### 3.1.5. COMPARISON OF AIRSPACE SITUATION BETWEEN CHINA, USA AND EUROPE

#### 3.1.5.1 BASELINE OPERATIONAL SITUATION OF EN-ROUTE AIRSPACE IN EUROPE AND USA

##### 3.1.5.1.1 USA—RAPID ROUTES NETWORK PLANNING AND CONSTRUCTION BASED ON PARALLEL ROUTES

The USA aviation industry is highly developed, with sufficient airspace resources available for civil aviation and fewer restrictions on use. The United States National Airspace System (NAS) is divided into 21 en-route control centers (ARTCC) to provide control services, forming 11 metropolitan areas in the overall airspace operation, and radiating air routes from the metropolitan area as the center, forming "spokes" type air routes structure<sup>[6]</sup>.

In order to better meet the needs of rapid operation of large-volume traffic flows, the USA is vigorously promoting the planning and construction of high-altitude routes network, which mainly include "sky corridors" and "tube network."

#### (1) Sky corridor

At present, the Sky corridor is a set of parallel J type high-altitude routes guided by the VOR navigation station. Its route design and operational rules are similar to those of traditional routes. Its structure is a nearly parallel long tube, which only

accepts the function of self-separation (automatically maintain interval). When the aircraft enters, the four-dimensional trajectory program is used to avoid flight conflicts, so the "sky corridor" can ensure that the aircraft in the structure is separated from other traffic flows in the program. Sky corridor is implemented along the best path and height, and can move dynamically in order to avoid bad weather or take advantage of favorable wind, so it is also called Flow Corridor. Currently, the sky corridors that the United States has built mainly include the East-West Corridor and the Northeast Corridor. The East-West Corridor has been fully implemented, and the Northeast Corridor is still being implemented gradually.

#### (2) Tube network

At present, the USA Tube Network structure is a high-altitude grouped parallel Q-type routes (RNAV2 route). Its purpose is to directly connect major USA airports through planning and grouping parallel routes to ensure the operation of flights in densely trafficked areas. More efficient and smoother. In general, the route numbers of the tube network in the USA are used separately according to parity, with odd numbers for north-south directions and even numbers for east-west directions. There is the distribution of existing formations of parallel Q routes in the United States. For example, the parallel route groups Q1, Q3, Q5 and Q7, Q9, and Q11 are the north-south routes running through the western USA, and Q140 and Q812 are the east-west routes running through the northern USA.

Sky corridor and tube network are effective improvements to the North American airway network, which is conducive to maximizing the advantages of the road network structure, achieving expansion and high-speed and smooth traffic flow; while constructing the backbone airway network, it cooperates with the sector Re-optimization can further improve the overall operating efficiency of the airspace.

### 3.1.5.1.2 EUROPE-COORDINATION AND AUTONOMOUS OPERATION PLANNING OF FRAGMENTED AIRSPACE

Due to the large number of EU member states, there are many busy hub airports in its airspace, the distance between airports is relatively short, and the operation is relatively independent, which makes the structure of European airspace very different from that of the USA. In order to further coordinate and efficiently use the fragmented airspace between different countries, Europe has mainly adopted and developed Functional Airspace Blocks (FABS), Flexible Use of Airspace (FUA) and Free Route Airspace (FRA) and other airspace planning and implementation methods.

#### (1) FABS

FABS are airspace blocks established from the perspective of operational requirements. The purpose is to

- provide the best air navigation services and related functions, regardless of how national borders are established.
- provide integrated air traffic services by strengthening cooperation between air navigation service providers or, where appropriate, from a performance-driven perspective.

So far, the EU has formulated 9 FAB initiatives, including Nordic FAB (NEFAB), Denmark-Sweden FAB, Baltic FAB, European Center FAB (FABEC), Central Europe FAB (FABCE), Danube FAB, Blue Mediterranean, United Kingdom-Ireland FAB, and Southwest FAB (See Figure 2.27).

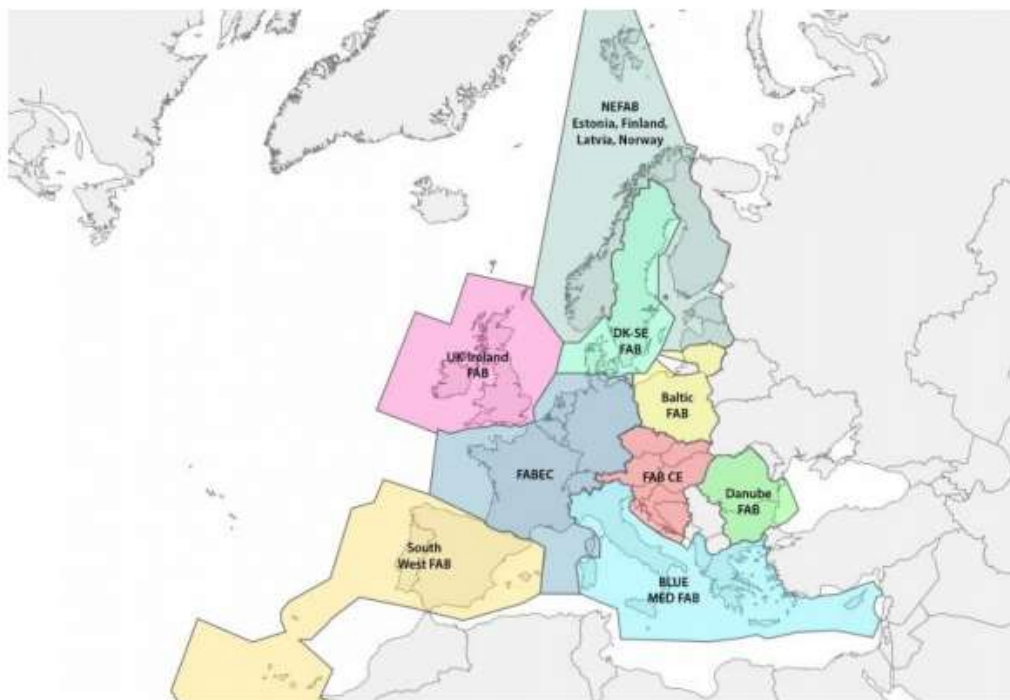


Figure 2.27 European Functional Airspace Block (FAB) distribution

## (2) FUA

European FUA is mainly based on the overall management of the three-level airspace management (ASM) mechanism (including three levels: strategy, pre-tactics and tactics), through scientific planning and flexible allocation of airspace resources (including temporary segregated areas), focusing on design three types of conditional routes (CDRs) are used to effectively integrate fragmented airspace and fully tap its potential to better meet the needs of different users at different times. By actively releasing and dynamically deploying corresponding airspace resources, the overall airspace utilization efficiency is improved<sup>[7]</sup>.

## (3) FRA

Free route airspace is another airspace planning concept that Europe has vigorously promoted and implemented in recent years. By the end of 2018, 54 area control



centers across Europe have implemented FRA in whole or in part, and about 50% of them have implemented 24-hour operation (See Figure 2.28).

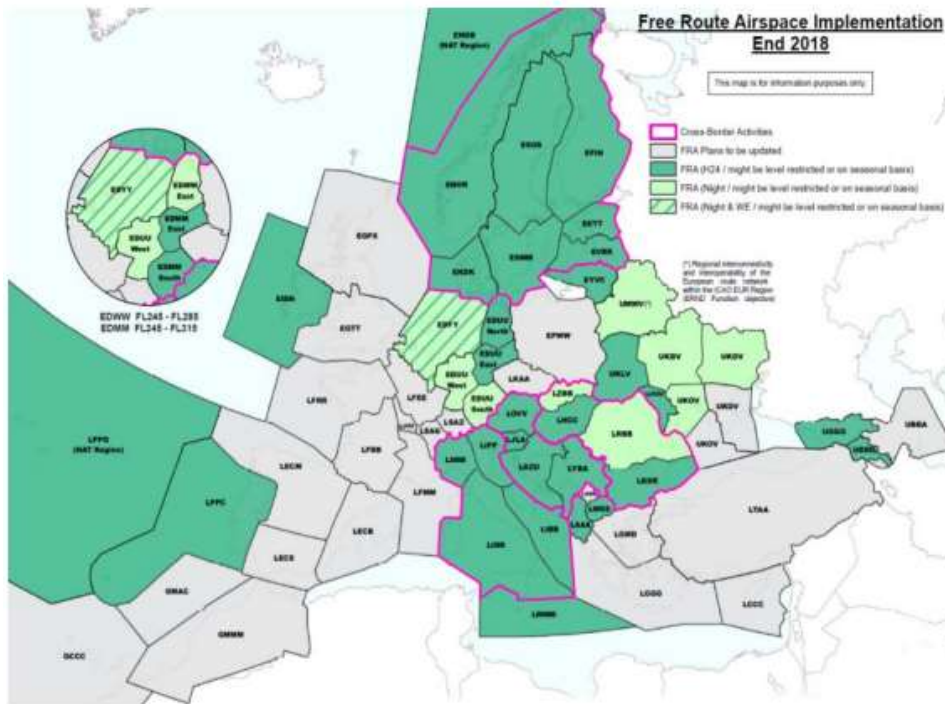


Figure 2.28 Implementation of European FRA at the end of 2018

European flights reached a record low in terms of en-route flight extension at the end of 2017. Route extension - the difference between the flight flown and the corresponding portion of the great circle distance - reached an average of 3.17% in 2012. In 2017, this fell to 2.77%, very close to the Europe-wide performance target of 2.6% by 2019, thanks in part to initiatives like free route airspace. FRA is a key landmark in achieving free routing across European airspace on the road to SESAR's business trajectories and 4D profiles. It will make possible to meet the demands of future airspace users over the next 50 years, including civil and military Unmanned Aircraft Systems (UAS), hypersonic transport, and spaceplane operations to sub-orbit, wireless network balloons and airships.

Free Route Airspace (FRA) is a specified volume of airspace where users may freely plan a route between a defined entry and exit point. Subject to airspace availability, routing is possible via intermediate waypoints, without reference to the ATS route network. Inside this airspace, flights remain subject to air traffic control. FRA is a way of overcoming the aviation sector's efficiency, capacity and environmental problems by helping in the reduction of fuel consumption and emissions, while improving flight efficiency. At the same time, it paves the way for further enhanced airspace design and ATM operational concepts [8].

### 3.1.5.2 COMPARISON OF AIRSPACE PLANNING CONCEPTS BETWEEN CHINA, USA AND EUROPE

From the perspective of air traffic service providers, both China and the USA are single air traffic service providers (ANSP), while European air traffic services are mainly provided by various countries (the number of European ANSPs in 2018 was 39). Therefore, in 2018, the number of area/en-route control areas between China and the USA is almost the same, 28 and 25 respectively.

In the air traffic service airspace of the USA and Europe, civil aviation has fewer restrictions on airspace planning and design and organization and implementation of air flight. The overall air route structure is reasonable, rich in layers, and dense. Aviation users can choose routes flexibly according to their needs. In comparison, the available airspace resources of China's civil aviation are not sufficient, and the route density of air routes is much lower than that of Europe and the USA. City pairs can often only fly on a fixed route, with fewer alternative routes, and the degree of flexible use of airspace is not high.

Combining the current status, problems and actual development of domestic airspace operations, the Air Traffic Management Bureau of the Civil Aviation Administration summarized and put forward the key themes of the current airspace planning, which is expanding increments and revitalizing the stock, connecting and opening up the broken sections in the entire road network and the bottleneck section to achieve the ideal effect of adding a section, connecting one section, equalizing the flow, and revitalizing the whole. The main concept of airspace planning currently adopted is to build a nationwide unidirectional circulation channel in the air. The construction method is mainly to reorganize the relatively idle route network of existing routes on both sides of the main route to form a route that is dual to the original route, realize the unidirectional operation of air traffic flow, and improve the overall operation of the road network Efficiency, while achieving flow balance configuration.

Since 2012, the civil aviation management system has actively implemented the concept of one-way circulation channel airspace planning and construction. By the end of 2019, Beijing-Kunming, Guang-Lan, Shanghai-Lan, Shanghai-Ha, China, South Korea, and Beijing-Guangzhou (Northern section) have been completed. The construction of 5 major corridors, including Chengdu-Lhasa, Lanzhou-Urumqi one-way parallel double-track, optimizes the operation pattern of China route network to a certain extent, makes the traffic flow more balanced, and reduces the relative flight risk.

## 3.2. FUNDAMENTALS AND REQUIREMENTS FOR HERAM TRANSITION

This section describes the motivation of HERAM based on the current situation in China and the Greener Air Traffic Management Concept proposed in MWP2. In addition, some requirements for HERAM transition are illustrated, which lead to the following steps of airspace resource availability analysis, FERA-WoC boundary identification and studied in other MWPs.

### 3.2.1. HERAM TRANSITION MOTIVATED BY GREENER AIR TRAFFIC MANAGEMENT CONCEPT

Concept elements of Greener Air Traffic Management have been identified in D2.1. Greener En-route operations concept elements mentioned there include free route during cruise flight, standardized cross border ATM, in-flight wind-optimal trajectory planning, free vertical movement and free cruise speed. Obviously, flexibility and efficiency of airspace resource utilization is the key in enabling free choice of preferred flight trajectory to achieve such green en-route operation. It is essential to develop a new operational framework of en-route airspace in China to support the greener long-haul flight.

As illustrated in baseline situation of airspace in China, there are two main features in en-route operation that give us motivation and enlightenment of deriving HERAM framework.

- (1) **Restricted use of airspace outside the air route.** Due to the national airspace management regulation, aircraft's movement in the en-route sector is generally limited only along air route with a predefined width (e.g. 20km) depending on specific situation in China. Rerouting outside the air route is allowed in some emergency situation (e.g. thunderstorm) when authorized by the military. Temporary Route (TS) is the main means of civil-military coordination on use of airspace. In recent years, the initiative to share airspace use has been gradually raised. The utilization of TS increased year by year. However, the availability is not transparent to airlines by NOTAM due to high uncertainty of military activities. For the cross-region TS, the coordination becomes more complicated. For airlines, the predictability of the availability of certain routes is very important for fuel-efficient path planning, especially for long haul flights. Such en route airspace operation of low freedom shall be significantly improved to support greener en-route operations concept.
- (2) **Significant differences of airspace situation between east and west part of China.** Based on analysis of baseline situation of en-route airspace, the busiest route points, route segments and sectors are all located in east and south of China. As for the prohibited/restricted/danger areas, almost half of

them are in Beijing, Shanghai and Guangzhou FIR, while 11.5% of them are in the northwest, i.e., Lanzhou and Urumqi FIR. Intuitively, airspace in the west possess more potential to implement free route and flexible use of airspace, which will be quantitatively measured in Section 2.3. The difference in en-route airspace situation provide illumination for proposing a feasible conceptual framework to enhance the flexibility of en-route operation in China.

### 3.2.2. REQUIREMENTS FOR HERAM TRANSITION

According to the elements of greener en-route operations concept, as well as the baseline situation of en-route airspace in China, we propose a new airspace management concept named Heterogeneous En Route Airspace Management (HERAM). HERAM is a novel conceptual framework that defines a refined boundary to distinguish between structured (the nominal eastern region) and flexible (the nominal western region) en route airspace system without changing the existing air route structure. In the west, the Flexible En Route Airspace (FERA) will be developed to provide semi-free routing options with adaptive Flexible Use of Airspace (FUA) mechanism. The general concept of FERA will be elaborated in Section 2.4. Everything remains unchanged in the east part.

In order to transit into HERAM, some fundamentals and requirements shall be guaranteed, which will be addressed in MWP3 and MWP5, including:

- (1) **Large-scale airspace with higher resource availability.** To ensure the continuity of operation and management, and to maximally improve the flexibility of trajectory planning, larger-scale airspace comprised of connected sectors with higher resource availability are needed to construct FERA. That means, the FERA-WoC is an integral continuum spatially in west of China, which will be identified in WP3.1.
- (2) **Re-configuration of FERA sectors.** Splitting airspace into small sectors has been an effective way to reduce ATC workload that could further increase the airspace capacity. However, trajectory-based operation in FERA apparently has new features which require re-configuration of existing sectors. Firstly, new modules for increasing airspace flexibility like conditional routes, entry and exit points or free movement zones will be introduced in FERA as supplements to the ATS routes, which requires a thorough update of current sector boundaries to adapt to new elements. Besides, adhering to the Controlled Time of Arrival (CTA) in conflict resolution based on air-ground negotiation would be a new challenge to air traffic controllers. Trajectory flexibility and robustness shall be taken into consideration in FERA sector design. Furthermore, new elements and tasks may bring additional operational complexity to controllers' mental workload, and requires new complexity metrics in sector design. Overall, reconfiguration of sectors is a crucial step towards FERA implementation, which will be addressed in WP3.1.

- (3) **A refined FUA mechanism between military and civil coordination.** In current national airspace management regulation, the foundation of enhancing the flight flexibility is to establish a refined coordination mechanism between civil and military to improve the utilization of airspace resource. That means the advanced FUA with Chinese characteristics are required for the implementation of FERA-WoC, e.g. CDR-I, RCA, etc.
- (4) **Ground-based DSS for trajectory negotiation.** As mentioned above, adhering to the Controlled Time of Arrival (CTA) in conflict resolution based on air-ground negotiation at tactical level would be a new task to the controllers, which demands high mental workload within limited time interval. To achieve the TBO in FERA with green targets, Decision Support System (DSS) for ATC is required to make maximum use of the FERA, which will be studied in WP3.2 and WP3.3.
- (5) **Advanced Avionics equipment.** Aircraft are airborne nodes of next generation of ATM system. Advanced Flight Management System, CNS equipment, and Human-Machine Interface will provide more choice of routes and more freedom during flight through air-ground cooperation. The greener operation in FERA will certainly benefit from upgrading avionics.

### 3.3. EN ROUTE AIRSPACE RESOURCE AVAILABILITY ANALYSIS

#### 3.3.1. META-DATA OF NATIONAL-WIDE EN-ROUTE AIRSPACE SECTORS

We collected basic structural information of airspace above 6000m in China, including 223 en route control sectors, 881 air routes and 268 PRDs (Prohibited, Restricted and Dangerous Areas) . Meta-data has been extracted and stored in a Geodatabase for further use.

For each sector, it consists of sector boundary point, sector boundary segment, sector entry/exit point, altitude range, interactions between boundary segments and air routes and interactions between sector boundary and PRDs.

Table 2.1 Meta-data of the en-route sector

Metadata	Attribute
<b>Sector boundary point</b>	the coordinate of latitude and longitude that make up the boundary of a sector
<b>Sector entry/exit point</b>	the coordinate of latitude and longitude that an en route pass through a sector
<b>Sector Altitude</b>	Altitude range of a sector, including minimum altitude(m) and maximum altitude(m).
<b>PRDs boundary point</b>	the coordinate of latitude and longitude that make up the boundary of PRDs
<b>PRDs Altitude</b>	Altitude range of PRDs, including minimum altitude(m) and maximum altitude(m).
<b>Air route point</b>	Basic component of an air route; navigation point or report point.
<b>Air route segment</b>	The connecting lines of air route points; some air route segments can make up an integrated air route.
<b>Interactions</b>	Interactions between air routes and sector boundary segment; interactions between PRDs and sector boundary segment.

With the data above, the overall en route sector and PRDs above 6000m in 2D view is shown in Figure 2.29. We randomly select an example sector as show in Figure 2.30 in both 2D and 3D view. The projection of PRDs onto horizontal plane

is irregular polygon. Relative position relations between air routes, PRDs and sector boundaries are quite complicated. Detouring around the restricted area is a common way in air route design. The availability of sector resource will be measured based on the airspace data in section 2.3.2.



Figure 2.29 En-route Sectors and PRDs in China

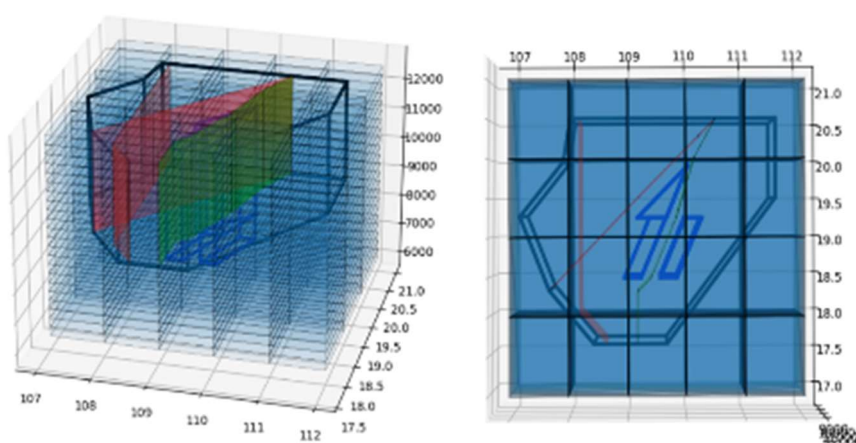


Figure 2.30 Example sector in 2D and 3D view

### 3.3.2. RESOURCE AVAILABILITY MEASUREMENT

#### 3.3.2.1 DEFINITION

##### 1) Resource Availability

Resource Availability (RA) at sector level refers to the volume of airspace resource available for civil flights operation in a sector. To explore the flexibility potential of en route airspace, RA at sector level can be simply derived through the Total Sector Volume (TSV) and PRDs Volume. However, RA defined by such static volume relations can hardly present the constraints imposed on air traffic flow operation by PRDs.

## 2) Flow-based Sector Resource Availability (FSRA)

A Flow-based Sector Resource Availability (FSRA) is defined as a ratio of structural sector capacity (network capacity) in the presence of active PRDs to the ideal structural sector capacity, for a certain traffic flow pattern. Here, structural capacity of a sector is determined by the maximum throughput at the bottleneck. Figure 2.31 shows the sector structure with flow patterns. From the figure we can see that the green solid lines represent the traffic flow and the direction is from left to right. So the blue dashed line on the left represents the s(source) and the right one represents the t(sink). Take the direction of the traffic flow as reference, the left side edges, except for the source s and sink t, is defined as top T (top); the right side of the traffic flow, except for source s and sink t, is defined as bottom B (bottom). P1, P2 and P3 represent the PRDs in the sector. The red dashed lines represent the shortest distance from the T/B to the PRDs, as well as shortest distance between polygonal PRDs.

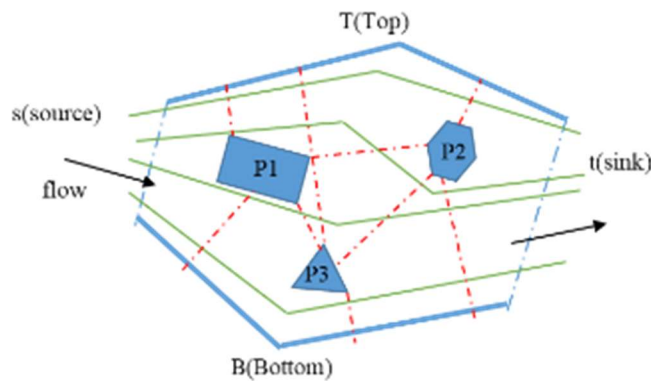


Figure 2.31 Sector structure with flow patterns.

### 3.3.2.2 METHODOLOGY

#### 1) The maximum flow minimum cut theorem

In any network  $G$ , the maximum flow from the source to the sink is equal to the capacity of the Minimum Cut (MC) separating the source and the sink<sup>[9]</sup>. This theorem is the maximum flow minimum cut theorem. The sector is abstracted into network according to certain rules, and the maximum flow of the network can be obtained by the above theorem. The structure of the network changes with the different placements of the source and the sink node, and the bottleneck capacity is obtained.

A discrete network is a directed graph  $G=(N,A)$ , where  $N$  is the set of nodes and  $A$  is the set of (directed) arcs connecting certain pairs of nodes. Each arc  $e$  has a capacity,  $c(e)$ . Two nodes,  $s$  and  $t$  in  $N$ , are designated as the source and sink, respectively. All other nodes of  $N$  are internal nodes. A flow in  $G$  is an assignment of a flow value,  $f(e) \leq c(e)$ , to each arc  $e$  in  $A$ , so that the total flow into each



internal node is equal to the total flow out of it. The value of the flow is the total flow out of  $s$ . By flow conservation, this is also the total flow into  $t$ .

The maxflow problem is to find a flow with maximum value. A cut in  $G$  is a partition of the nodes into two sets  $S$  and  $T$ , such that  $s$  is in  $S$ , and  $t$  is in  $T$ . An arc  $e$  is said to cross the cut if one of its endpoints is in  $S$ , and the other is in  $T$ . The capacity of a cut is the sum of the capacities of the arcs that cross it. No flow in  $G$  can possibly have a larger value than the capacity of any cut. A mincut is a cut of minimum capacity, and therefore its capacity is an upper bound on the value of any flow. It is also said that the capacity of a mincut equals the value of a maxflow<sup>[10]</sup>.

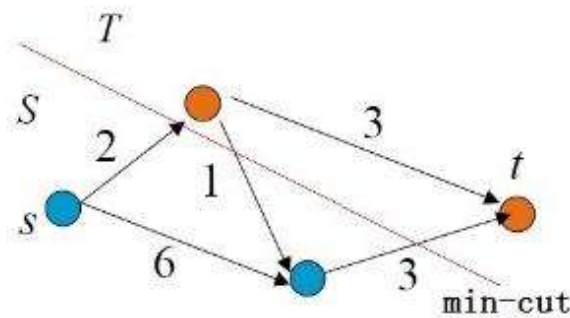


Figure 2.32 Min-cut in discrete network

The notions pertinent to discrete network flows can be extended naturally to flows in 2D domains<sup>[11]</sup>. Instead of a discrete network, a continuous domain, such as a simple polygon  $P$ , is considered (Figure 2.33). Two boundary edges,  $s$  and  $t$ , of the polygon are designated as the source and the sink. A flow  $f$  in  $P$  is a vector field. The constraints  $P_1 \dots P_K$  are pairwise-disjoint simple hazard polygons that lie fully inside  $P$ ; the flow is not allowed to pass through any of the constraints, i.e., for any point  $x$  within a constraint,  $f(x) = 0$ .

The  $s$ - $t$  cut of polygon  $P$  divides the polygon  $P$  into two parts  $S$  and  $R$ ,  $P = S \cup R$ ,  $S \cap R = \emptyset$ , and  $s \in S$ ,  $t \in R$ . The polygon is set as follows: according to the direction in which the flow flows through the polygon, the left side of the flow, except for the source  $s$  and sink  $t$ , is set as the top  $T$  (top), and the right side of the flow, except for the source  $s$  and sink  $t$ , is set as the bottom  $B$  (bottom)<sup>[12]</sup>.

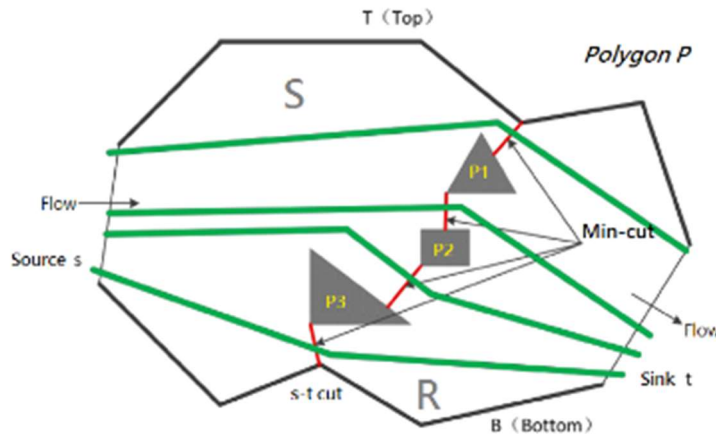


Figure 2.33 Min-cut in continuous domain

The maxflow problem is to find an  $s$ - $t$  flow of maximum value. A cut in  $P$  is a partitioning of the polygon into two parts so that  $s$  is in one of the parts, and  $t$  is in the other. The capacity of a cut is the length of the boundary between the parts from the top  $T$  to the bottom  $B$ , where only the part of the boundary that is interior to  $P$  (and not on the boundary of  $P$  or within a constraint) is included in the length. We use the term “mincut” to refer to the path(s) within  $P$  that comprise the boundary of the cut (shown as the red paths in Figure 4.5), as well as to refer to the capacity (length) of the mincut<sup>[13]</sup>.

Therefore, the maximum flow minimum cut problem is transformed into a problem of searching for the shortest path from the top  $T$  to the bottom  $B$ . In this research, we are concerned with computing a mincut in polygonal domains, which represents the maximum theoretical throughput of an airspace with respect to a given set of PRDs constraints.

## 2) The shortest path problem: Dijkstra algorithm

Dijkstra algorithm is a representative shortest path algorithm, which is used to calculate the shortest path from one node to other nodes<sup>[14]</sup>. It uses the idea of breadth-first search, extending from the starting point to the end. It is essentially a greedy algorithm.

Let  $G=(V,A,W)$  be a weighted directed graph, and divide the vertex set  $V$  in the graph into two groups. One group is the set of vertices whose shortest path has been found (denoted by  $S$ ). At the beginning, there is only one source point in  $S$  at the beginning. After each shortest path is obtained, the vertex will be added to the set  $S$  until all vertices are added to  $S$ , and the algorithm will end. The other group is the set of the remaining vertices (denoted by  $U$ ) that have not determined the shortest path. The vertices in  $U$  is added to  $S$  in turn in order of the increment of the shortest path length. During the process of joining, the length of shortest path from the source point  $v$  to each vertex in  $S$  is not greater than that from the source point  $v$  to any vertex in  $U$ . In addition, each vertex corresponds to a distance. The

distance of the vertices in  $S$  is the shortest path length from  $v$  to the vertex. The distance of the vertices in  $U$  is the current shortest path length from  $v$  to this vertex, only including the vertex in  $S$  as the middle vertex.

The algorithm steps are as follows (see Figure 2.34).

- ① At the beginning,  $S$  only contains the source point, that is,  $s = \{v\}$ , and  $dis^{(0)}(v) = 0$ .  $U$  includes other vertices except  $v$ , that is,  $U = \{\text{other vertices}\}$ . If  $v$  has edges with the vertex  $u$  in  $U$ ,  $\langle u, v \rangle$  normally has weight; if  $u$  is not the adjacent point of  $v$ , the weight of  $\langle u, v \rangle$  is  $\infty$ , that is  $w(u, v) = \infty$ .
- ② Select a vertex  $k$  from  $U$  with the smallest distance between it and  $v$ , and add  $k$  to  $S$  (the selected distance is the shortest path length from  $v$  to  $k$ ).
- ③ Taking  $k$  as the new intermediate point, the distance of each vertex in  $U$  is modified. If the distance from the source point  $v$  to the vertex  $u$  (passing through the vertex  $k$ ) is shorter than the original distance (not passing through the vertex  $k$ ), the distance value of vertex  $u$  is modified, and the modified distance value is the distance of vertex  $k$  plus the weight on the edge  $\langle k, u \rangle$ , that is,  $dis^{(n+1)}(u) = \min\{dis^{(n)}(k), dis(v, k) + w(k, u)\}$ .
- ④ Repeat step ② and ③ until all vertices are included in  $S$ .

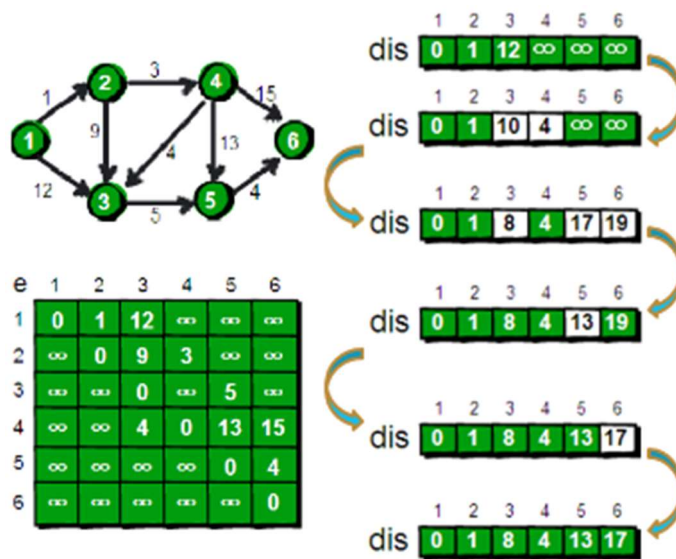


Figure 2.34 Dijkstra algorithm schematic diagram

### 3.3.2.3 FSRA MODELLING

#### 1) Assumptions

- (1) Consider a region of airspace specified by a constant flight level and a two-dimensional (2D) polygonal domain  $P$ .
- (2) One portion of the airspace boundary serves as the source while another portion serves as the sink. Restrict all flights to enter at the source and exit the airspace

at the sink. Do not allow flow to originate or to terminate within the airspace (i.e., no aircraft exit or enter the flight level within the interior of P).

(3) Assume that aircraft can come arbitrarily close to constrained area as long as they do not enter it.

**2) Mathematical representation by graph theory**

The polygon sector and PRDs are modelled as an undirected weighted graph, where the vertices present the top and bottom edges of polygon sector, as well as PRDs, the edge of the network shows the connectivity between vertices, the weight of the edge is given by the shortest physical distance between any two connected vertices<sup>[15]</sup>.

The top and bottom edges of polygon sector is determined by the traffic pattern, which shows the source and sink edges.

For a given traffic pattern, the structural capacity is measured by MC from top vertex to the bottom one in the graph, i.e., the distance of the shortest path between the top and bottom vertex.

For a given sector and flow pattern, the MC with and without PRDs are denoted as  $\gamma^*$  and  $\gamma$ , respectively. Then,  $FSRA = \gamma^*/\gamma$ .

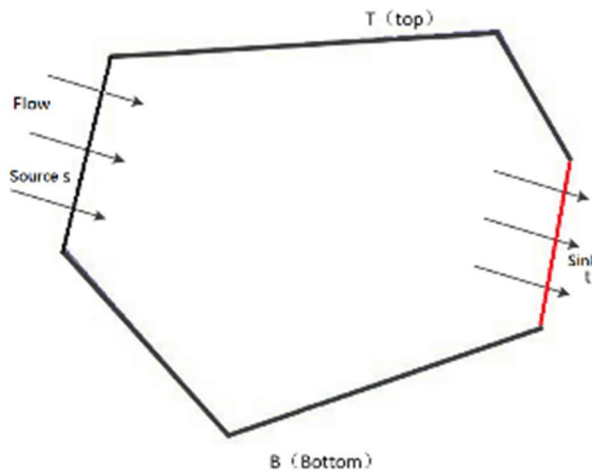


Figure 2.35 Min-cut in area without PRDs

**3.3.2.4 COMPUTATIONAL PROCEDURES**

- 1) Identifying the source and sink edges of a polygon according to the traffic flow pattern of the sector.
- 2) Marking the PRDs of a sector as the most approximate polygons of different shapes in the graph.
- 3) Finding out the corresponding top and bottom edge of a traffic flow pattern in a polygon sector at FL  $h$ .

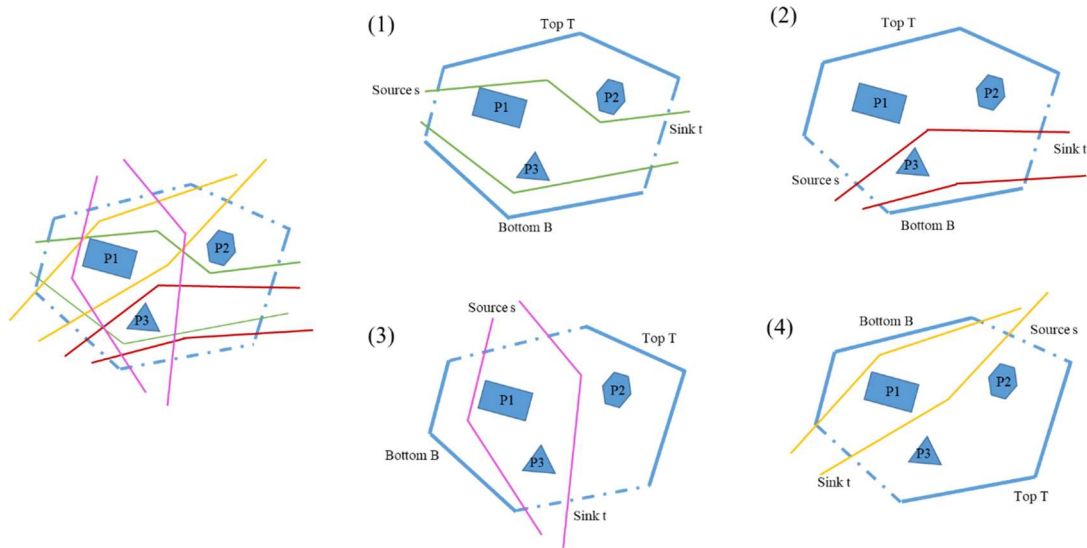


Figure 2.36 Top edge and bottom edge of different traffic flow patterns

4) Generating the resource network graph by analyzing the connectivity relationship between vertices, i.e., top edge, bottom edge and PRDs. Let the set of top edge, bottom edge and PRDs be  $\Omega = \{e_f^{Top}, P1, P2, \dots, Pm, e_f^{Bottom}\}$ . The shortest distance between vertices in  $\Omega$  is calculated as the weight of edges in the resource graph and denoted as  $d^{(0)}(e_f^{Top}, Pm)$ .

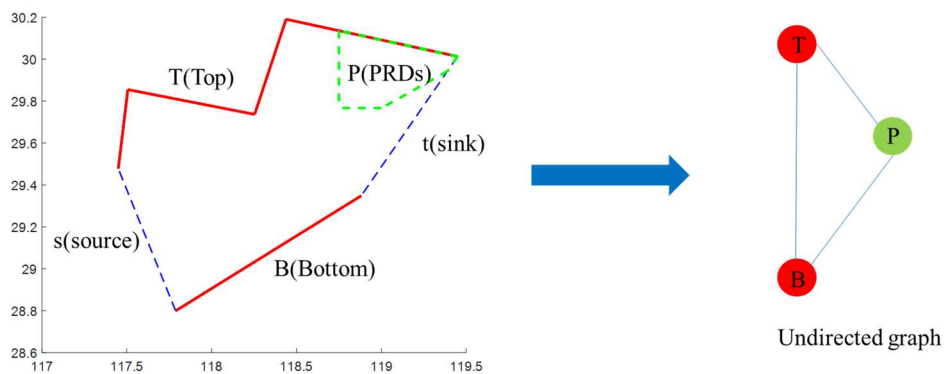


Figure 2.37 Resource network structure schematic diagram

5) Establishing the initial distance matrix

$$D = \begin{pmatrix} 0 & d^{(0)}(e_f^{Top}, P_1) & d^{(0)}(e_f^{Top}, P_2) \dots & d^{(0)}(e_f^{Top}, P_m) & d^{(0)}(e_f^{Top}, e_f^{Bottom}) \\ \vdots & 0 & d^{(0)}(P_1, P_2) \dots & d^{(0)}(P_1, P_m) & d^{(0)}(P_1, e_f^{Bottom}) \\ \vdots & \vdots & 0 & \ddots & \vdots \\ \vdots & \vdots & \vdots & d^{(0)}(P_{m-1}, P_m) & d^{(0)}(P_{m-1}, e_f^{Bottom}) \\ \vdots & \vdots & \vdots & \ddots & d^{(0)}(P_m, e_f^{Bottom}) \\ 0 & \dots & \dots & 0 & \dots & 0 \end{pmatrix}$$

6) Dijkstra algorithm is used to search the shortest path from the top edge to the bottom edge in the presence of the PRDs. Since the flow flows from the source edge to the sink edge, the capacity limitation of the source edge and the sink edge should also be considered. The length of the shortest path is the minimum of the shortest path from the top edge to the bottom edge, the length of the source and sink edge, that is,  $d^* = \min\{d^{(m)}(e_f^{Top}, e_f^{Bottom}), len(e_f^{Source}), len(e_f^{Sink})\}$ . The length of the path is denoted as  $\gamma_{i,h}^*$ .

7) The shortest path between the top edge and the bottom edge without PRDs is found, that is,  $d = \min\{len(e_f^{Source}), len(e_f^{Sink})\}$ . The length of the path is denoted as  $\gamma_{i,h}$ .

8) The FSRA corresponding to the traffic flow pattern and FL  $h$  is  $\eta_{i,h} = \frac{\gamma_{i,h}^*}{\gamma_{i,h}}$ .

9) The FSRA of all traffic flows at FL  $h$  is obtained as follows:  $\eta = \frac{\sum_{i=1}^N \eta_{i,h}}{N}$ , where  $N$  is the number of flow patterns at FL  $h$  in the sector.

The schematic diagram of FSRA is shown in Figure 2.39.

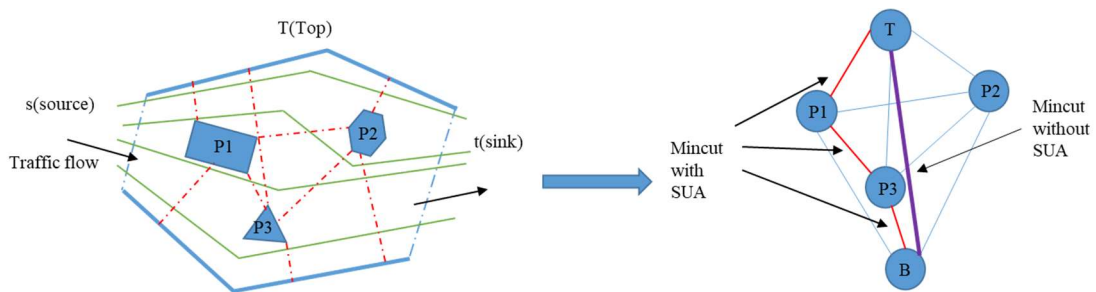


Figure 2.39 FSRA schematic diagram

### 3.3.3. RESULT ANALYSIS

Figure 2.40 shows the Resource Availability Map (RAM) of en route airspace in China based on FSRA measurement. From the figure, we can see that the FSRA in western China is higher than that in eastern China, which is consistent with the actual situation and common sense. Figure 2.41 shows the cumulative probability distribution of FSRA in China. It can be seen from the figure that only less than 50% of the sectors have FSRA values larger than 0.8, 80% of which is higher 0.9.

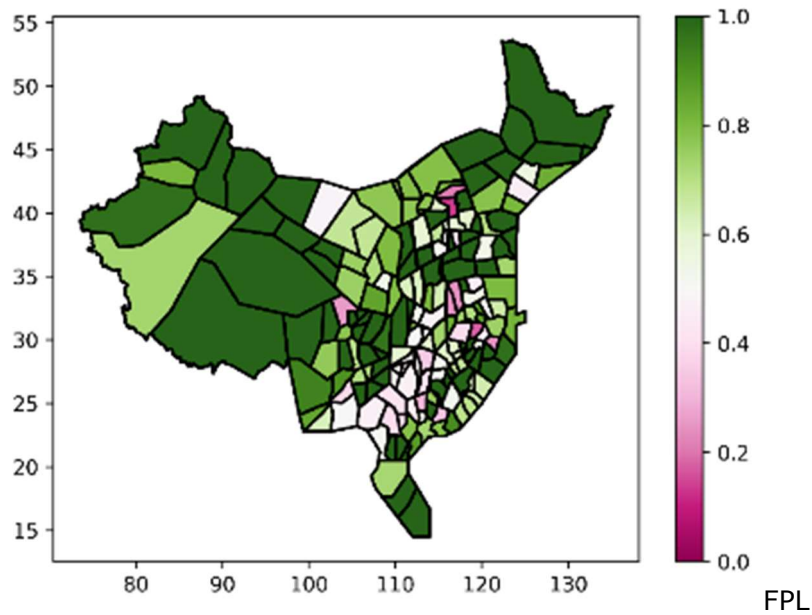


Figure 2.40 Resource Availability Map (RAM) of en route airspace in China

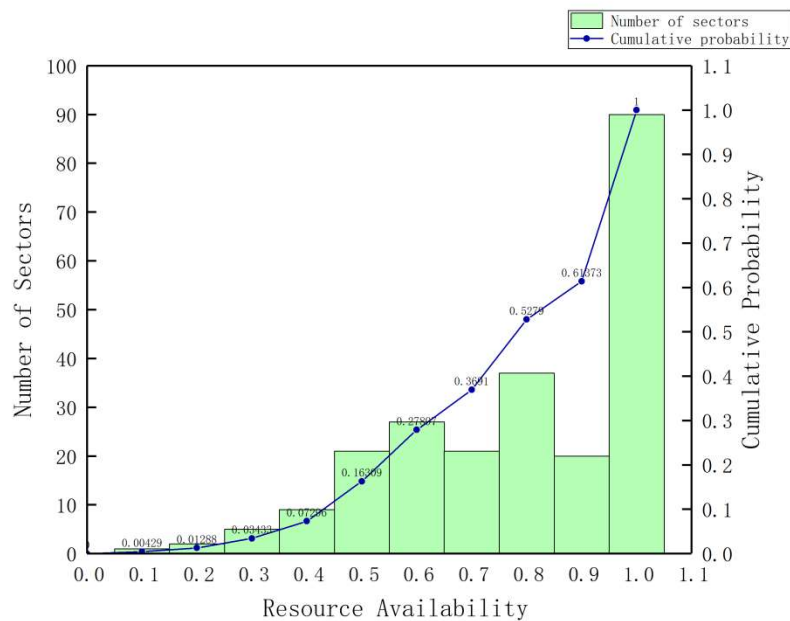


Figure 2.41 Cumulative probability distribution of FSRA in China

Figure 2.42 shows the distribution of FSRA in China's FIRs (except for Hongkong and Taipei). It can be seen that the median value of FSRA in Kunming and Shenyang FIR are 1, and that in Urumqi FIR is close to 1, which indicate the potential of implementing FERA. The top 3 constrained areas are Guangzhou, Wuhan and Shanghai FIRs. Besides, the box-plot of Beijing, Guangzhou, Wuhan and Shanghai FIRs have a longer box, which shows that the FSRA value distribution in the above regions is relatively scattered, while the constraints imposed by PRDs in Sanya, Lanzhou, Urumqi, and Shenyang are more even across sectors.

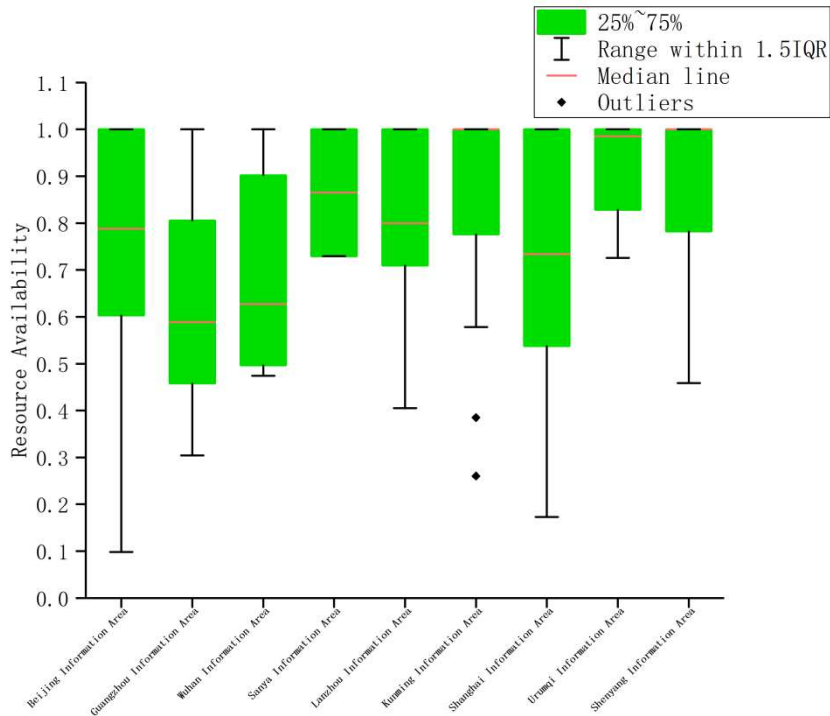


Figure 2.42 Distribution of FSRA in some FIRs

Figure 2.43 shows the distribution of FSRA in China's Control Areas. It can be seen that the median value of FSRA in Lanzhou, Harbin, Dalian, Taiyuan, Chengdu, Lhasa, and Jinan are 1, and that in the control areas of Urumqi and Guiyang are close to 1. Beijing, Sanya, Shanghai, Hefei, Kunming, Shenyang, Xi'an, Zhengzhou, Qingdao, and Hohhot have the FSRA values between 0.7 and 0.9. Besides, the FSRA values in Beijing, Shanghai, Lanzhou, Nanchang, Hefei, Guangzhou, Kunming, Wuhan, Shenyang and Qingdao control areas are relatively scattered, while the distribution of FSRA Urumqi, Nanning, Harbin, Lhasa, Guilin, Jinan, Guiyang and Changsha is more concentrated. Some outliers are observed in Chengdu, Xi'an and Hohhot, indicating that the spatial flexibility of sectors in these control areas vary greatly.



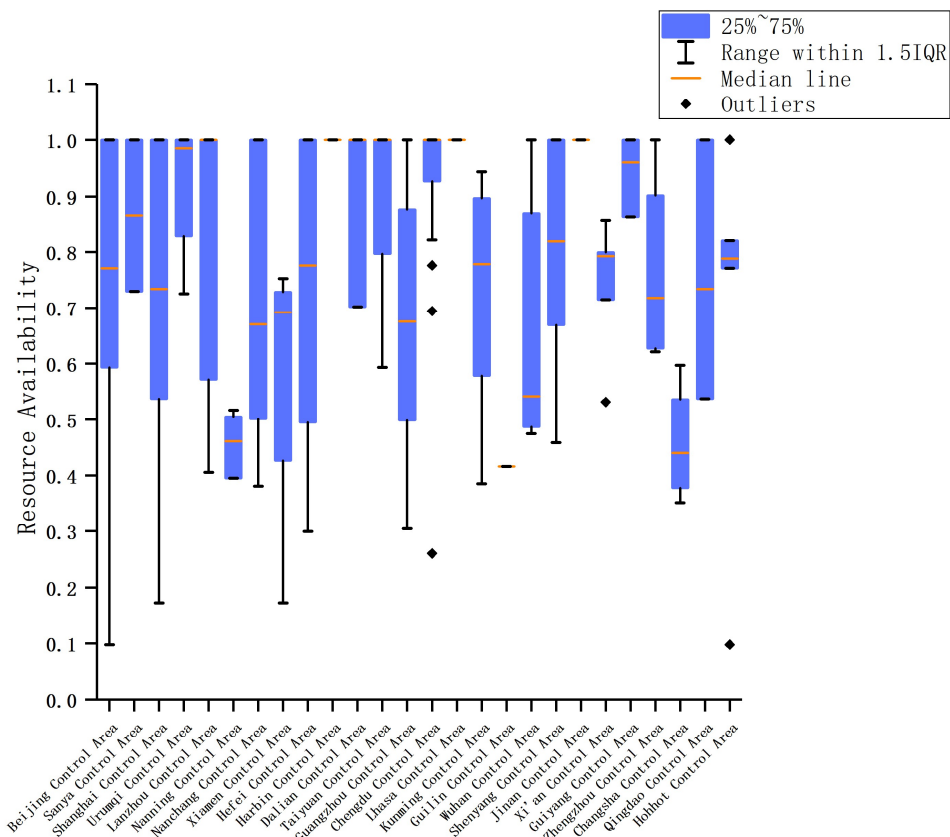
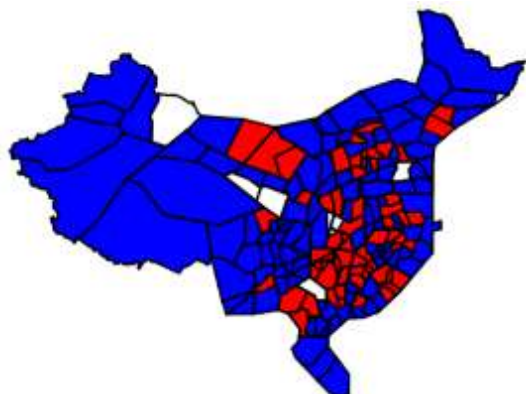


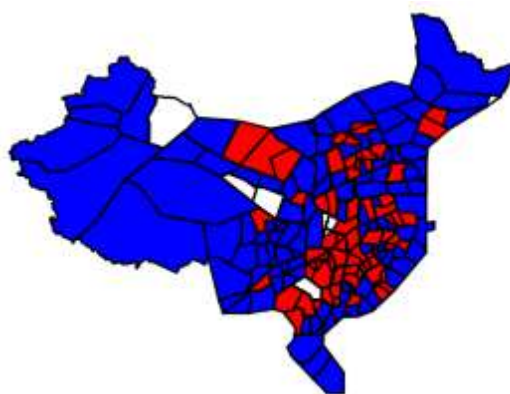
Figure 2.43 Distribution of FSRA in China's control areas

### 3.4. METHOD FOR BOUNDARIES IDENTIFICATION OF FLEXIBLE EN ROUTE AIRSPACE (FERA)

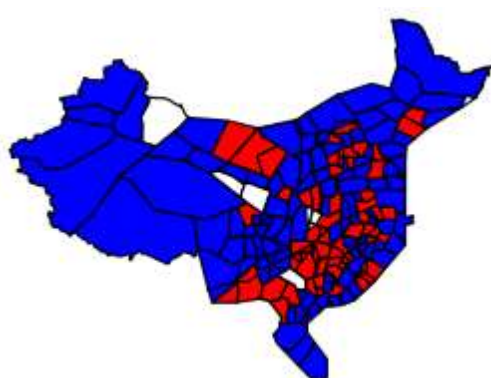
Based on the FSRA analysis in section 2.3.3, we look at the resource availability of different flight level range to derive the vertical and horizontal boundary of the FERA-WoC simultaneously. For each vertical range (600m), all en route sectors are categorized into two parts based on K-means clustering algorithm: lower (in red) and higher (in blue) FSRA, as shown in Figure 2.44.



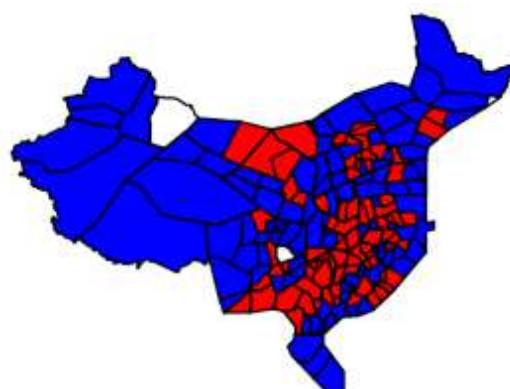
(a) 6000-6600m



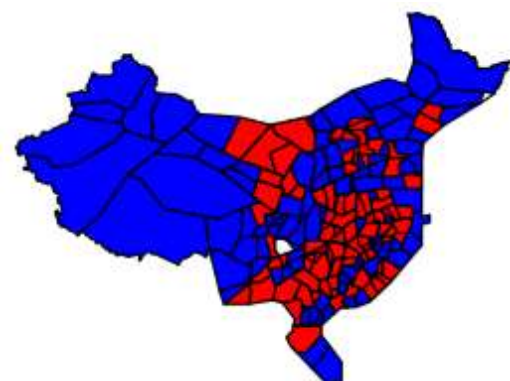
(b) 6600-7200m



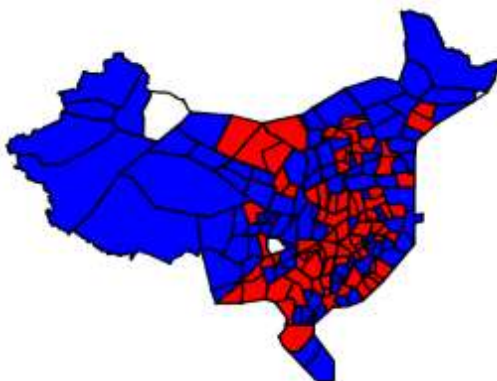
(c) 7200-7800m



(d) 7800-8400m



(e) 8400-8900m



(f) 8900-9500m

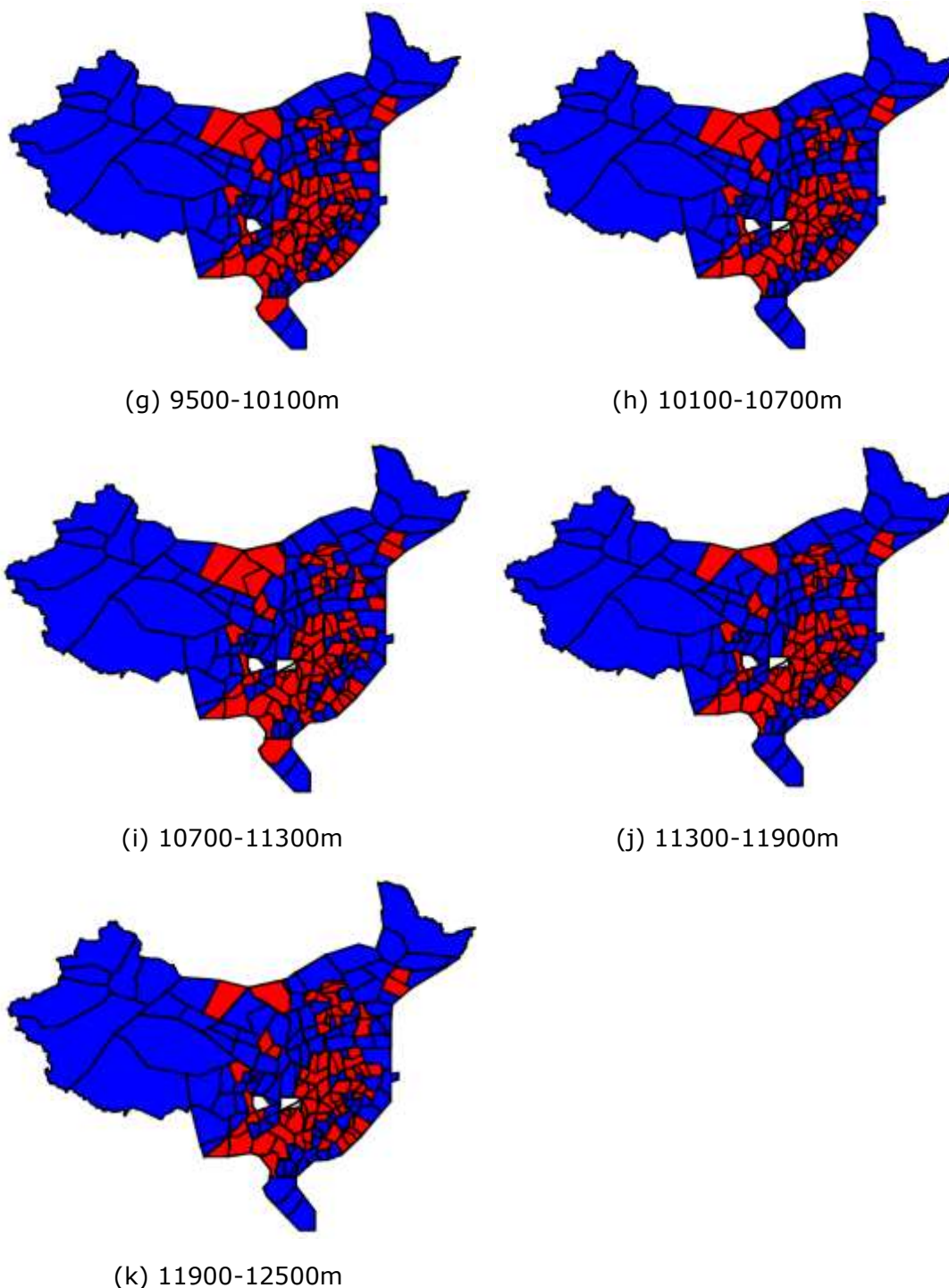


Figure 2.44 Clustering results of FSRA for different flight level ranges

The purpose of boundary identification is to divide China’s en route network into “Flexible” and “Structured” regions, and then to support trajectory-based greener air traffic operation in “Flexible” airspaces. It can be seen from Figure 2.45 that the FSRA in western China is relatively high, and almost all sectors with low FSRA are located in eastern China. **Finally, the vertical boundary above (including) 8900m is identified by considering the consistency of horizontal**

**boundaries in different vertical range, see Figure 2.44. The horizontal boundary FERA-WoC based on FSRA is shown in Figure 2.45.**

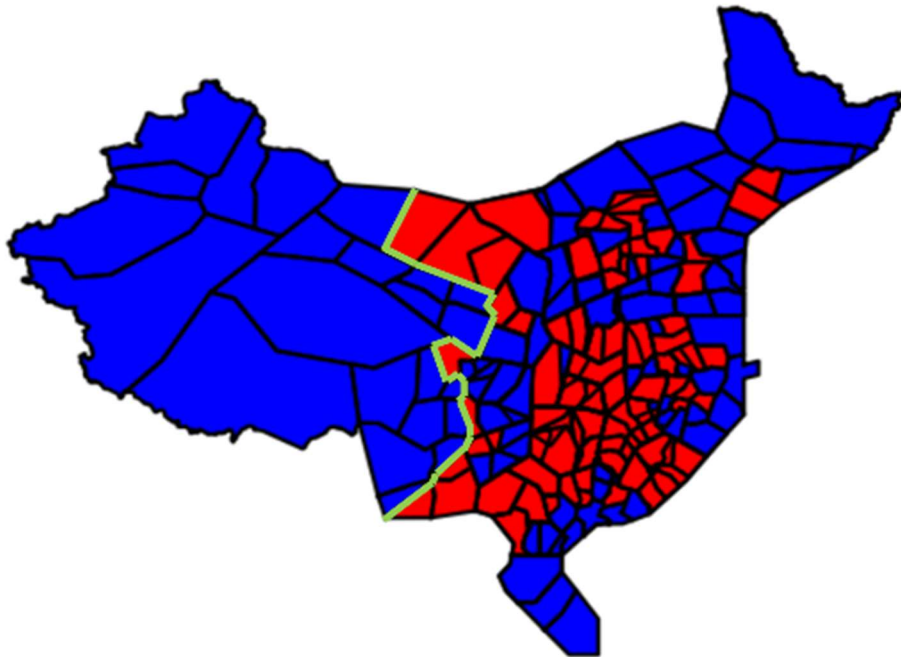


Figure 2.45 The horizontal boundary of FERA-WoC.

## 3.5. FERA-WOC CONCEPT

FERA-WoC is the core of the HERAM, since the operation in the rest part of China divided by the boundary is assumed to be unchanged. This section only gives a brief introduction to the concept of FERA-WoC by outlining its features to understand the structural improvements. Further studies of airspace complexity and sector dynamic configuration in WP3.1 will follow this concept.

### 3.5.1. GENERAL CONCEPT

By taking aforementioned HERAM transition requirements, Flexible En Route Airspace in West of China (FERA-WoC) concept is proposed as a form of modularized en route airspace comprised of on-demand elements for improving spatial freedom, which is capable of supporting semi-free route operation in west China underpinned by refined Flexible Use of Airspace (FUA) mechanisms with Chinese characteristics.

The FERA can retain or adjust the original ATS route, and configure sector entry and exit points, intermediate waypoints, conditional routes, and free maneuvering

zones based on the availability of airspace resources and FUA rules. It should be made clear that, to improve the trajectory selection flexibility (such as adapting to high-altitude wind changes) of 4D-capable aircraft, the sector entry and exit points could be the published significant points, as well as arbitrary coordinates defined by latitude and longitude. Noted that the intermediate waypoints can only be defined by navigational aids.

Airspace Users may freely plan a route between a pair of entry/exit point and intermediate waypoints subject to published route availability (national or international route category) without reference to the ATS route network. Tactical rerouting guided by air traffic controller via intermediate waypoints or inside FMZ is feasible. Inside this airspace, flights remain subject to air traffic controllers. The conceptual structure of FERA sector is shown in Figure 2.46.

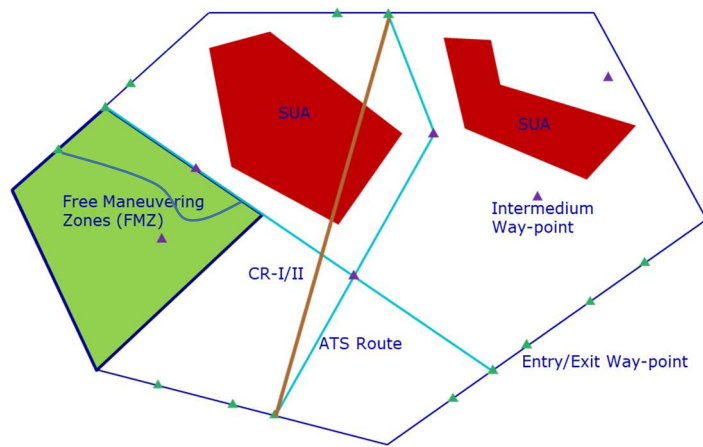


Figure 2.46 The modularized structure of FERA sector

### 3.5.2. SPECIFIC IMPROVEMENTS

Compared with traditional structured en route operations, FERA-WoC expands the spatial dimensions of operations by tapping available airspace resources and establishing a FUA mechanism, providing friendly airspace environmental support for flexible trajectory selection and green air traffic operations. Specific improvements include:

(1) **Diversified combination of modularized airspace elements to improve en route operation flexibility.** FERA-WOC carries out the design by integrally considering the ideal economic trajectory including prevalent high-altitude wind, the boundary of east and west en route airspace, the special used airspace and nav aids, etc. In view of the inadequate ground-based nav aids in western China and the complicated military flight activities, a variety of on-demand combinations of sector entry and exit points, intermediate points, conditional routes, and free maneuvering zones are used to supplement ATS routes expanding the feasible en route operation space to a certain extent, to improve the flexibility and efficiency.

(2) **A localized and enriched civil-military coordination of FUA in west of China.** FERA-WOC is based on a more dynamic and refined FUA mechanism. Considering the current overall principles of military and civil flight operations in China, as well as the restrictions in the western airspace, ways such as CAT I and CAT II Conditional Routes (CR), and Reduced Coordinated Airspace (RCA) are may adopted to supplement the existing FUA mechanism with temporary routes as the main means.

(3) **Support aircraft with different onboard capabilities.** In view of the practical problems of insufficient ground-based nav aids in western China and uneven capabilities of aircraft onboard equipment, considering we are now in the transition period from traditional operation to trajectory-based operation, the designed FERA-WOC sector entry and exit points include significant points and arbitrary coordinates. Aircraft that do not have 4D capabilities can choose to take significant points as the entry and exit points or simply fly along the ATS route; aircraft with advanced 4D capabilities can fly between any feasible entry and exit points of FERA-WOC.

### 3.5.3. CHALLENGES

The realization of the FERA-WOC goal requires a more flexible airspace use mechanism as a guarantee on the one hand, and focus on the uncertainty of the traffic structure caused by the expansion of spatial dimensions and its impact on the ATC workload on the other hand. The above-mentioned concerns are also the main challenges faced by the operation of FERA-WOC.

(1) **The uncertain effect of the proposed FUA mechanism.** Establishing a military-civilian coordination mechanism and improving the ability of flexible allocation of airspace resources are the main approaches to build FERA-WOC. The FERA-WOC concept clarifies the key elements to improve the utilization of airspace resources, such as increasing sector entry and exit points, conditional routes, free maneuvering areas, etc., but may be restrained by frequent military activities in local airspace that leads to the difficulty in airspace coordination. These obstacles that could jeopardize the full application of the mechanism will in turn affect the flexibility of trajectory selection in the overall western airspace, which is one of the main challenges facing the implementation of FERA-WOC.

(2) **Highly dynamic traffic situation.** FERA-WOC is an adaptive combination of multiple types of airspace elements. The air traffic flow pattern has changed from a highly regular structure to a dynamic and random decentralized type. The complexity of air traffic situation awareness would increase, which in turn affects the workload of controllers and flight safety. How to accurately predict the operational capacity of the FERA-WOC sector is the basic work for carrying out Demand and Capacity Balancing (DCB) and trajectory planning, and it is also another key challenge facing the implementation of FERA-WOC.

### 3.5.4. RELATION TO ICAO AND SESAR CONCEPTS AND TRENDS

ICAO ASBU Performance Improvement Area 3: Optimum capacity and flexible flights, states that introduction of free routing in defined airspace, where the flight plan is not defined as segments of a published route network or track system to facilitate, adherence to the user-preferred profile. Free Route Airspace (FRA) is a key element of future ATM architecture in Europe. FERA-WOC is a flexible (not fully free) airspace model with localized characteristics based on the actual problems of China's en-route airspace and future development needs.

Compared with FRA, their similarities are:

(1) The goals are both to improve the utilization of airspace resources and support more flexible 4D trajectory operations.

(2) Aircraft can dynamically plan flight trajectories in the internal airspace between available entry and exit points.

(3) Compatible with ATS routes and support aircraft operations that do not have 4D capabilities.

(4) A complete mechanism of FUA is needed.

(5) Flights must follow the controller's instructions.

(6) The issue of sector dynamic capacity and planning needs to be carefully reconsidered.

Considering the uniqueness of China's airspace management system, the differences are:

(1) FRA adopts a mature FUA framework. Considering the characteristics of military activities in western China, FERA-WOC is a flexible transformation of traditional structural airspace under the flexible use of limited airspace. Therefore, according to the differences in the availability of airspace resources in each sector, we shall configure one or more elements (e.g., entry and exit points, conditional routes, and free maneuvering zones) as supplements to the ATS route, and design a corresponding FUA mechanism.

(2) FRA sector entry and exit points are generally significant points, and in special circumstances, it allows significant points to deviate from sector boundaries. For the FERA-WOC, sector entry and exit points can be significant points, or any coordinates determined by the latitude and longitude. On the one hand, it is used to deal with the shortcomings of the lack of ground-based nav aids in the west; on the other hand, it can also increase entry and exit points to make up for the insufficient flexibility in actual operations caused by airspace restrictions.

## 4. COMPLEXITY STUDIES OF FLEXIBLE EN ROUTE AIRSPACE (FERA) OPERATION

### 4.1. AIR TRAFFIC COMPLEXITY MODELING AND UNCERTAINTY ANALYSIS

This section illustrates a complexity indicator system (CIS) constructed based on the operational characteristics of aircraft in the flexible en route airspace sectors as exemplified in Chapter 2. Based on historical ADS-B data of flights within national sectors, the complexity indicators are measured and self-compared in the same time slice of different days. By integrating the uncertainties of the complexity indicators for all sectors, we classify the uncertainty into the low, medium and high levels as the basis of sector capacity estimation and dynamic sector configuration in FERA-WoC for strategic and pre-tactical phase.

#### 4.1.1. HISTORICAL FLIGHT ADS-B DATA AND NATIONAL AIRSPACE SECTOR DATA

Nationwide historical flight ADS-B data from November 1st to 7th, 2019 was collected. The data mainly includes flight number, aircraft type, record time, latitude and longitude coordinates, altitude, airspeed, vertical speed, angle, departure airport, arrival airport and other information.

National airspace sector data is also collected, including basic information of 232 element control sectors. The airspace sector data consists of the upper and lower bound of the flight level and the latitude and longitude of the boundary points of each control sector.

#### 4.1.2. COMPLEXITY INDICATOR SYSTEM

##### 4.1.2.1 COMPLEXITY INDICATOR SYSTEM

###### 1) Number of Main Flows (MF)

Based on the aircraft trajectory information in sector  $sec$  of time slice  $t_k$ , the traffic flows  $TF_{sec,t_k}^i$  in sector  $sec$  of time slice  $t_k$  are identified using the flight trajectory clustering method, thus the traffic volume  $FV_{sec,t_k}^i$  of each traffic flow  $TF_{sec,t_k}^i$  in



time slice  $t_k$  is counted. The traffic flow whose traffic volume exceeds 25% of the total volume in the time period is defined as the main flow<sup>[16]</sup>, and the number of main flows in sector  $sec$  of time slice  $t_k$  is  $MF_{sec,t_k}$ .

## 2) Traffic Flow Distribution (FD)

The standard deviation of the distribution of traffic volume over the traffic flows describes the level of unevenness in the distribution of flight flows in sector  $sec$  of time slice  $t_k$ , denoted as  $FD_{sec,t_k}$ . The higher the value of the indicator is, the more unevenly the traffic is distributed over the traffic flows:

$$FD_{sec,t_k} = \sqrt{\frac{\sum_{i=1}^{Fnum_{sec,t_k}} (FV_{sec,t_k}^i - \overline{FV}_{sec,t_k})^2}{Fnum_{sec,t_k}}} \quad (3.1)$$

where  $\overline{FV}_{sec,t_k}$  is the average value of traffic flows in sector  $sec$  of time slice  $t_k$ ,

and  $Fnum_{sec,t_k}$  is the number of traffic flows in sector  $sec$  of time slice  $t_k$ .

## 3) Number of Trajectory Intersection (TI)

It mainly refers to the number of track intersections formed by the intersection of aircraft trajectories<sup>[17]</sup> operating in sector  $sec$  of time slice  $t_k$  in spatial position, denoted as  $RI_{sec,t_k}$ .

## 4) Conflict Intensity (CI)

In the airspace sector, the value of conflict intensity between aircraft pairs increases as the spatial distance between aircraft pairs decreases. The minimum spatial distance between aircraft  $AC_{sec,t_k}^k$  and aircraft  $AC_{sec,t_k}^i$  operating in sector  $sec$  of time slice  $t_k$  is  $Dmin_{sec,t_k}^{i,k}$ . The intensity of the conflict between aircraft pairs

$AC_{sec,t_k}^k$ ,  $AC_{sec,t_k}^i$  is defined in terms of a power function:

$$CI_{sec,t_k}^{i,k} = (Dmin_{sec,t_k}^{i,k} + a)^n \quad (3.2)$$

where  $n$  is the power exponent and  $a$  is a correction factor to correct for excessive conflict intensity values when the distance  $Dmin_{sec,t_k}^{i,k}$  value is extremely small.

The average value of conflict intensity between all aircraft pairs is calculated to obtain the conflict intensity in sector  $sec$  of time slice  $t_k$ :

$$CI_{sec,t_k} = \sum_{i=1}^{num_{sec,t_k}} \sum_{k=1}^{num_{sec,t_k}} CI_{sec,t_k}^{i,k} \quad (3.3)$$

where  $num_{sec,t_k}$  is the number of aircraft in sector  $sec$  of time slice  $t_k$ .

### 5) Airspace Uses (AU)

Airspace uses is defined as the utilization rate of sector area, i.e., the used area and unused area within the sector. The sector area utilization rate is related to the number of airways in the sector, and has a positive and negative influence on the operational complexity. On the one hand, sector area utilization rate and complexity of the sector increase as the number of airways in the sector increases. On the other hand, flexibility of aircraft operation increases as the available sector area get larger, which is positively significant for alleviating the difficulty of conflict deployment<sup>[18]</sup>.

The number of airways within the sector  $sec$  of time slice  $t_k$ , is  $m$ , the length of the  $j$ <sup>th</sup> airway in sector  $sec$  of time slice  $t_k$  is  $a_{sec,t_k}^j$ , and the width is  $b_{sec,t_k}^j$

(according to the Chinese civil aviation air traffic management rules, the width of the flight path is 10 km on both sides of the centerline, which shall not be less than 8 km in any case). In sector  $sec$  of time slice  $t_k$ , the area of restricted airspace is

$S_{sec,t_k}^{prds}$ , then the airway area is:

$$RS_{sec,t_k} = \sum_{j=1}^m a_{sec,t_k}^j \times b_{sec,t_k}^j \quad (3.4)$$

Airspace uses of sector in sector  $sec$  of time slice  $t_k$  is defined as followed:

$$rsu_{sec,t_k} = \frac{RS_{sec,t_k}}{S_{sec} - S_{sec,t_k}^{prds}} \quad (3.5)$$

### 6) Altitude Variation (AV)

Variation level of aircraft altitude distribution is expressed as the standard deviation of the flight altitude set  $H_{sec,t_k}$  of all aircrafts operating in sector  $sec$  of time slice

$t_k$ , and the flight altitude of aircraft  $AC_{sec,t_k}^i$  is  $h_{sec,t_k}^i \in H_{sec,t_k}$ . Then the altitude variation is:

$$AV_{sec,t_k} = \sqrt{\frac{\sum_{i=1}^{num_{sec,t_k}} (h_{sec,t_k}^i - \bar{h}_{sec,t_k})^2}{num_{sec,t_k}}} \quad (3.6)$$

where  $\bar{h}_{sec,t_k}$  is the average of the flight altitude of all aircrafts.

### 7) Speed Variation (SV)

Variation level of aircraft speed is expressed as the standard deviation of the set  $S_{sec,t_k}$  of the speeds of all aircrafts operating in sector  $sec$  of time slice  $t_k$ , and the flight speed of aircraft  $AC_{sec,t_k}^i$  is noted as  $s_{sec,t_k}^i \in S_{sec,t_k}$ . Then the speed variation is:

$$SV_{sec,t_k} = \sqrt{\frac{\sum_{i=1}^{num_{sec,t_k}} (s_{sec,t_k}^i - \bar{s}_{sec,t_k})^2}{num_{sec,t_k}}} \quad (3.7)$$

where  $\bar{s}_{sec,t_k}$  is the average speed of all aircrafts.

### 8) Occupancy (per ATCO position) (OC)

Occupancy refers to the number of aircrafts at a given time instant in sector  $sec$  of time slice  $t_k$ :

$$OC_{sec,t_k} = \frac{num_{sec,t_k}}{T_{t_k}} \quad (3.8)$$

where  $T_{t_k}$  is the duration of the time slice  $t_k$ .

### 9) Traffic Entry (per ATCO position) (TE)

Traffic Entry indicates the number of aircrafts entering sector  $sec$  in time slice  $t_k$  [19]:

$$TE_{sec,t_k} = \sum_{ACTE_{sec,t_k}^i \in ACTE_{sec,t_k}} ACTE_{sec,t_k}^i \quad (3.9)$$

where  $TE_{sec,t_k}^i \in TE_{sec,t_k}$ ,  $TE_{sec,t_k}$  denotes the set of aircrafts entering sector  $sec$  in time slice  $t_k$ .

### 10) Total flight time of the aircraft under ATCO responsibility in the given timeframe (FT)

$ACFT_{sec,t_k}^i$  denotes the controlled flight time of aircraft  $AC_{sec,t_k}^i$ , then in sector  $sec$  of time slice  $t_k$ , the controlled flight time  $ACFT_{sec,t_k}$  for all flights is denoted as:

$$ACFT_{sec,t_k} = \sum_{i=1}^{num_{sec,t_k}} ACFT_{sec,t_k}^i \quad (3.10)$$

### 11) Number of control transfers (CT)

The number of control transfers indicates the number of aircraft in sector  $sec$  for which controllers make control transfers with the adjacent sectors during time slice  $t_k$  [20]:

$$CT_{sec,t_k} = \sum_{ACTE_{sec,t_k}^i \in ACTE_{sec,t_k}} ACTE_{sec,t_k}^i + \sum_{ACTL_{sec,t_k}^i \in ACTL_{sec,t_k}} ACTL_{sec,t_k}^i \quad (3.11)$$

where  $ACTE_{sec,t_k}^i \in ACTE_{sec,t_k}$ ,  $ACTE_{sec,t_k}$  denotes the set of aircraft entering sector  $sec$  in time slice  $t_k$ .  $ACTL_{sec,t_k}^i \in ACTL_{sec,t_k}$ ,  $ACTL_{sec,t_k}$  denotes the set of aircraft leaving sector  $sec$  in time slice  $t_k$ .

### 12) Flow-based Sector Resource Availability (FSRA)

FSRA is the ratio of the sector capacity under a certain traffic flow organization when there is a restricted area within the airspace sector to the sector capacity when there is no restricted area, and this ratio can reflect the level of the sector resource availability. The detailed modelling was stated in progress report of MS6, here we only provide a short description.

In sector  $sec$ , the inflowing sector boundary of the traffic flow  $TF_{sec}^i$  is  $s_{sec}^i$  and the outflowing sector boundary is  $t_{sec}^i$ . The direction of the flow through the polygonal sector, the left side of the traffic flow, except for  $s_{sec}^i$  and  $t_{sec}^i$ , the remaining edges form the top edge  $L_i^T$ ; the right side of the flow, except for  $s_{sec}^i$  and  $t_{sec}^i$ , the remaining edges form the bottom edge  $L_i^B$ .  $P_{sec}^j$  denotes the restricted area within the polygon, i.e., the area through which the traffic flow cannot pass. The shortest distance from the top edge  $L_i^T$  to the bottom edge  $L_i^B$  is the minimum cut, and the maximum flow through the polygon sector is equal to the minimum cut capacity. The minimum cut under the action of the traffic flow  $TF_{sec}^i$  and the presence of the restricted area is  $MC_i^{SA}$ ; the minimum cut of the traffic flow  $TF_{sec}^i$  and without the presence of special airspace is  $MC_i^{NS}$ , and the sector resource availability corresponding to the traffic flow  $TF_{sec}^i$  is:

$$FSRA_i = \frac{MC_i^{SA}}{MC_i^{NS}} \quad (3.12)$$

The weight of traffic flow  $TF_{sec}^i$  is:

$$\omega_i = \frac{FV_i}{\sum_{i=1}^n FV_i} \quad (3.13)$$

The flow-based sector resource availability is:

$$FSRA = \sum_{i=1}^n \omega_i \times FSRA_i \quad (3.14)$$

## 4.1.2.2 STATISTICAL METHODS FOR COMPLEXITY INDICATORS

### 4.1.2.2.1 FLIGHT TRAJECTORY RESAMPLING

Flight trajectory data of aircraft is generally collected by radar, ADS-B surveillance equipment, etc., and consists of a set of discrete points with the same time interval.

Each trajectory data not only contains time  $t$  and space  $(x, y, z)$  information, but

also sometimes includes flight characteristics information such as heading and ground speed, which is a typical high-dimensional data. The number of aircraft flying in the flexible airspace is large, and the scale of the generated flight trajectory data is huge, which has a certain impact on the processing speed and calculation accuracy of the flight trajectory. In addition, because the change of flight state of aircraft in the flight process is smooth transition, there are few emergency maneuvers, and the surveillance equipment takes a fixed time interval in the data acquisition process, which will definitely lead to a large amount of redundancy in the generated flight trajectory data. Especially the aircraft in the straight-line flight process, its heading, ground speed and other flight characteristics are basically fixed. Therefore, before the clustering analysis of flight trajectories, each trajectory should be resampled to reduce the scale of data while maintaining its main flight characteristics, so as to facilitate subsequent processing.

Resampling technique can effectively reduce the data size while preserving the data features, and is one of the core techniques in massive data processing<sup>[21]</sup>. In this section, we adopt the uniform parameterization method to realize the resampling of flight trajectory data. Let a flight trajectory consist of  $n$  trajectory points  $(p_1, p_2, \dots, p_n)$ , where each trajectory point is a four-dimensional vector

$p_i = (t_i, x_i, y_i, z_i), i = 1, 2, \dots, n$  . The cumulative chord length in Eq. (3.15), or the cumulative time in Eq. (3.16), is chosen as a parameter to parameterize the whole trajectory to the interval  $[0, 1]$ .

$$\left. \begin{aligned} u_1 &= 0 \\ u_i &= u_{i-1} + \frac{\sqrt{(x_i - x_{i-1})^2 + (y_i - y_{i-1})^2 + (z_i - z_{i-1})^2}}{\sum_{j=2}^n \sqrt{(x_j - x_{j-1})^2 + (y_j - y_{j-1})^2 + (z_j - z_{j-1})^2}} \end{aligned} \right\} \quad (3.15)$$

$$\left. \begin{aligned} u_1 &= 0, \\ u_i &= u_{i-1} + \frac{|t_i - t_{i-1}|}{\sum_{j=2}^n |t_j - t_{j-1}|} \end{aligned} \right\} \quad (3.16)$$

where  $u_i$  is the value of the parameter corresponding to the trajectory point  $p_i$ ,  $u_1 = 0, u_n = 1$ ;  $(x_i, y_i, z_i)$  is the 3D coordinate represented by  $p_i$  and  $t_i$  is the recording moment of  $p_i$ .

After parameterization, keep the first and last trajectory points unchanged, and calculate the trajectory points corresponding to the parameter nodes as resampling points according to the sampling points (or sampling rate).

For example, the number of sampling points is  $m$ . In addition to keeping the first and last trajectory points, it is sufficient to calculate the trajectory point  $q_k$  corresponding to the parameter node  $\frac{k-1}{m-1} (k = 2, 3, \dots, m-1)$ , then the flight trajectory

after resampling can be expressed as  $(q_1, q_2, \dots, q_m)$ , and  $q_1 = p_1, q_m = p_n$ . Figure 3.1 shows a two-dimensional schematic of the resampling process.

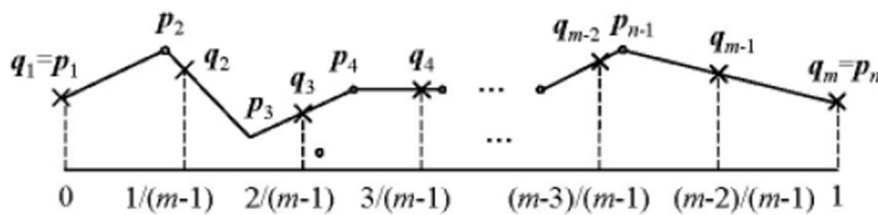


Figure 3.1 Flight trajectory resampling process

In the Figure 3.1: "o" indicates the initial trajectory point; "x" indicates the resampling point. It should be noted that the method may generate new points in the resampling process, and the flight characteristics of the initial trajectory can be better maintained by using linear interpolation. The three-dimensional sampling process is similar.

The resampling results are shown in Figure 3.2. In Figure 3.2: Blue dots indicate the initial flight trajectory points; red dots indicate the resampling points. The number of sampling points is 50. Similarly, the resampling calculation can also be performed with the accumulation time as the parameter.

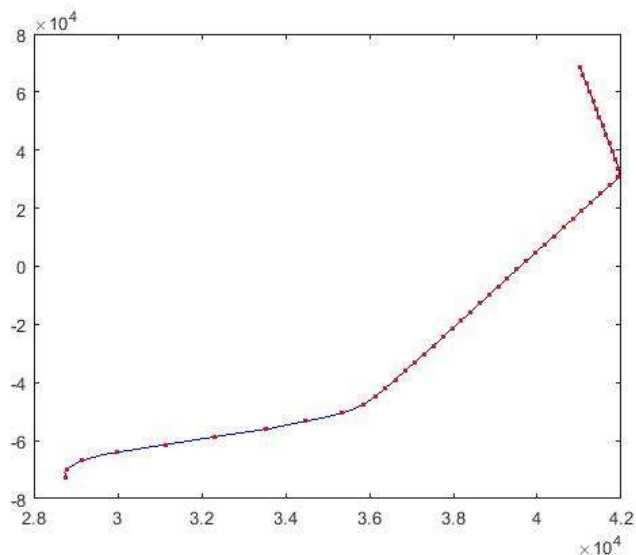


Figure 3.2 Cumulative chord length resampling results (50 sampling points)

In the resampling process, the number of the sampling points or the sampling rate can be controlled according to the change of the flight state of the trajectory. In addition to the resampling result with 50 sampling points shown in Figure 3.2, the resampling results with 30 and 100 sampling points are shown in Figure 3.3 and Figure 3.4.

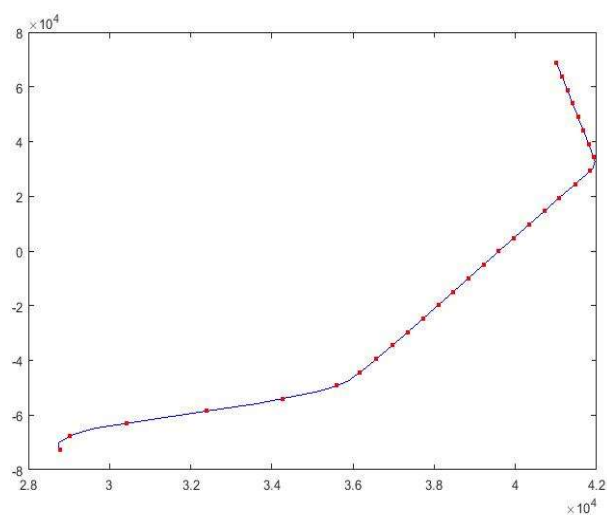


Figure 3.3 Cumulative chord length resampling results (30 sampling points)

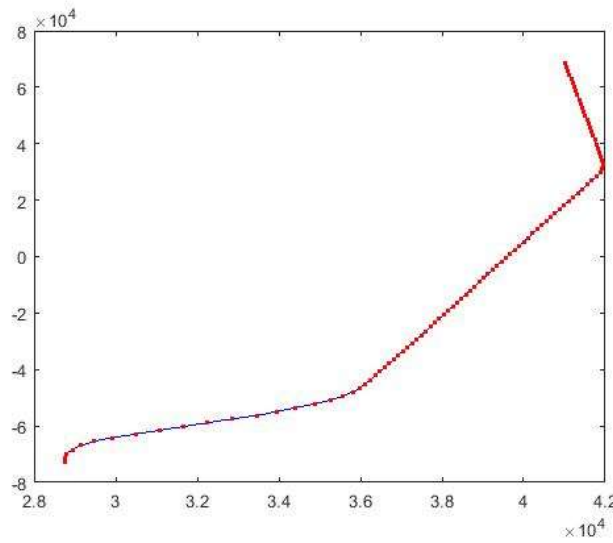


Figure 3.4 Cumulative chord length resampling results (100 sampling points)

#### 4.1.2.2.2 TRAJECTORY CLUSTERING METHOD

In this section, the aircraft flight trajectories are clustered using K means after resampling<sup>[22]</sup>, and  $\Omega$  is noted as the set of  $L$  trajectory sequences,  $\Omega = \{X_1, X_2, \dots, X_L\}$ , where each element is the trajectory sequence after the resampling process. The Euclidean distance is chosen as the similarity measure between data samples, and the steps of the track clustering algorithm are as follows:

- Step1 :Initialize the clustering centers. First, one trajectory is randomly selected from all trajectories as the center of the first category:  $C_1 \leftarrow X_1$ . Then another one trajectory  $X_2$  is selected from the remaining  $L-1$  trajectories as the center of the second category  $C_2$ , while a threshold  $\rho$  is set so that  $d(C_2, C_1) \geq \rho$ .
- Step2 :The Euclidean distance from the initial cluster center is calculated for each trajectory in all the trajectory datasets and the cluster to which it belongs is determined. Each trajectory in the trajectory dataset is assigned to the corresponding cluster with the closest distance to the cluster center.

$$d(X_1, C_1) = \min\{D_{X_1, C_1}, D_{C_1, X_1}\} \quad (3.17)$$

$$class(X_1) = \arg(\min(d(X_1, C_i))), i = 1, 2, \dots, K \quad (3.18)$$

- Step3 :Adjusting the clustering center. The number of trajectories



corresponding to each cluster,  $n_1, n_2, \dots, n_k$ , is obtained from the previous step. For each cluster of trajectories, a new representative is found that minimizes the spatially similar distance to all trajectories within that cluster, and that representative is the new cluster center.

$$C_i \leftarrow \arg \min_{l=1, \dots, n_i} \sum_{k=1}^{n_i} d(X_{l,i}, X_{k,i}) \quad (3.19)$$

where  $X_{l,i}$  is the  $l$ th sample belonging to class  $i$ .

- Steps 2 and 3 are repeated until the central trajectory of the cluster no longer changes. At this point the center is the central trajectory, and as it belongs to the same cluster, the trajectories in each cluster can be considered to belong to the same type of trajectory pattern. The flow chart for the above steps is shown in Figure 3.5.

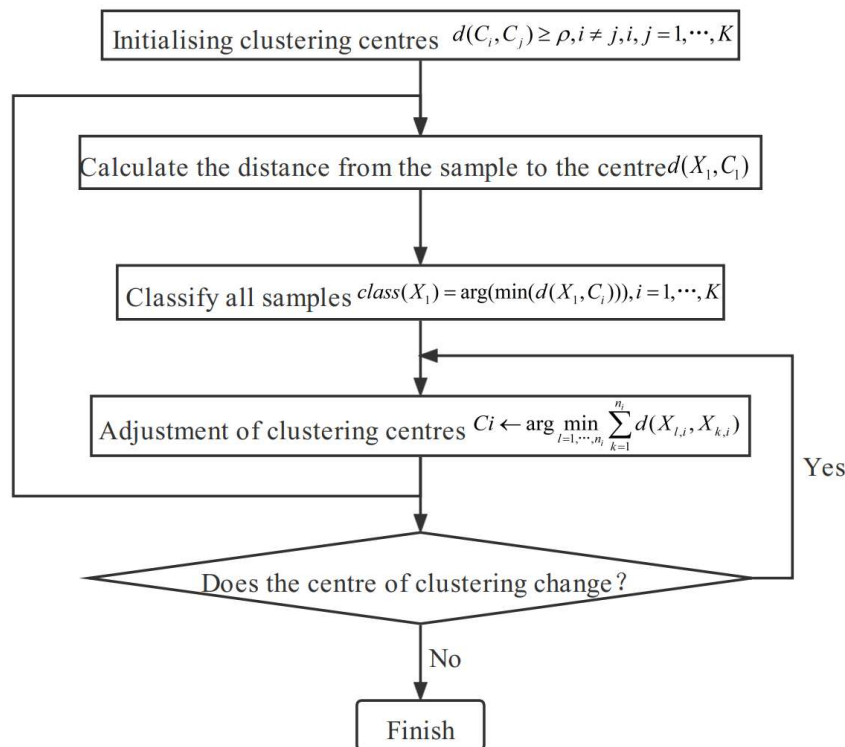


Figure 3.5 The flow chart of trajectory clustering

Elbow method is used to determine the optimal K value of the K-means algorithm in the process of trajectory clustering. The sum of squared errors under different number of clusters is calculated to form a descending curve, and the K value located at the elbow of the curve is selected as the optimal K value of the algorithm. Figure 3.6 shows the trajectory clustering results of sector ZUUUAR11 from 16:00-17:00 on November 1, 2019, and the K value of K-means algorithm is taken as 4.

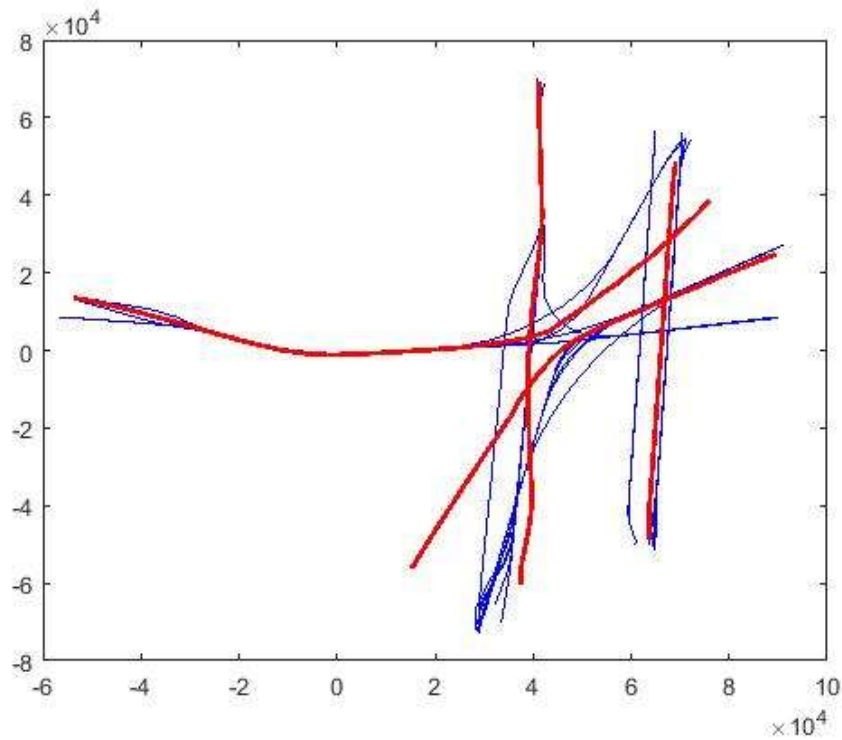


Figure 3.6 Sector ZUUAR11 trajectory clustering results

#### 4.1.2.3 STATISTICAL RESULTS OF COMPLEXITY INDICATORS

Using November 1, 2019 to November 7, 2019 as the statistical period, nationwide aircraft flight ADS-B data and 76 airspace sector base data were used to count the daily complexity indicator values of different airspace sectors nationwide at the time granularity of 1 hour and 15 minutes. Since the number of aircraft per unit time slice is small under the time granularity of 15 minutes, the statistical results of the number of main flows, traffic flow distribution, number of trajectory intersection, and conflict intensity indicators are less useful for the complexity indicator uncertainty analysis, the above four indicators are not counted for the time granularity of 15 minutes. Since the value of the traffic flow-based sector resource availability indicator is fixed for each sector, the indicator can be considered with low-level uncertainty, so the statistical results of this indicator are not shown in the subsequent charts. The number of sampling points for the resampling process of flight trajectory clustering is 50.

For the 25 Upper Control Areas in the country, 3 representative sectors with high, medium and low traffic volume are selected for each Upper Control Area. Therefore, the complexity indicators of 75 sectors are calculated for uncertainty analysis. Taking the sector ZUUAR11 as an example, Figure 3.7 – Figure 3.17 shows the results of the sector ZUUAR11 for each of the 11 airspace sector complexity metrics other than the flow-based sector resource availability indicator, at a time granularity of 1 hour. The complete results of all sectors are shown in the Appendix.

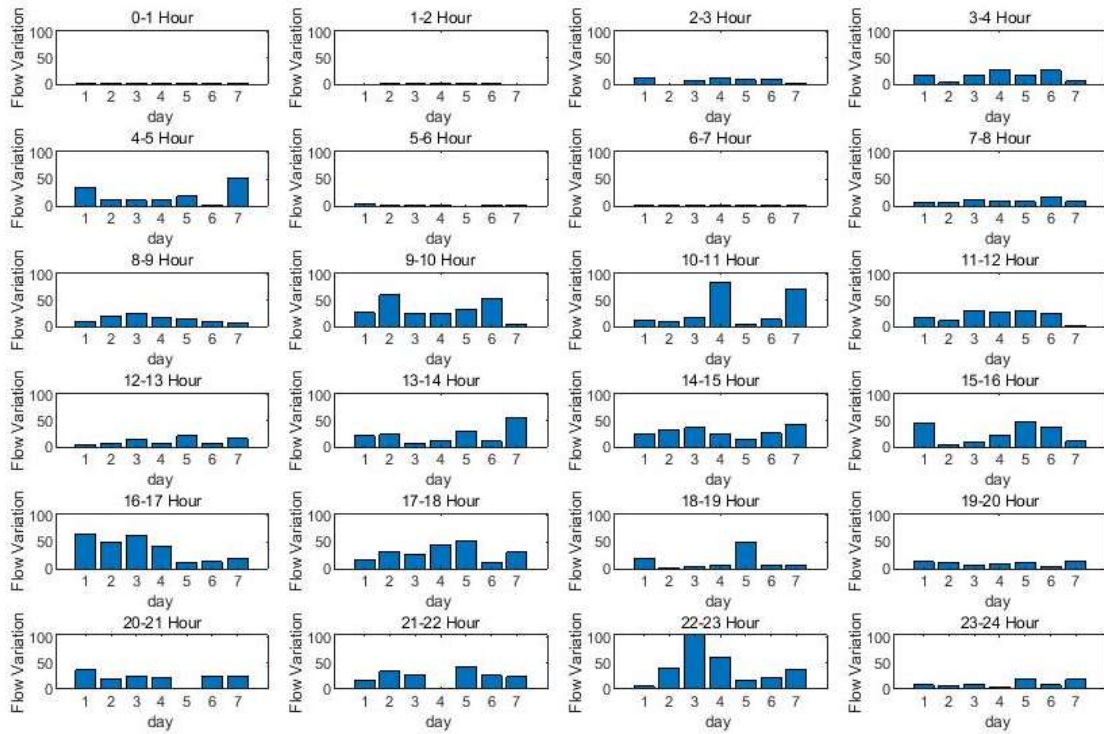


Figure 3.7 Number of main flows in sector ZUUUAR11 (1 hour)

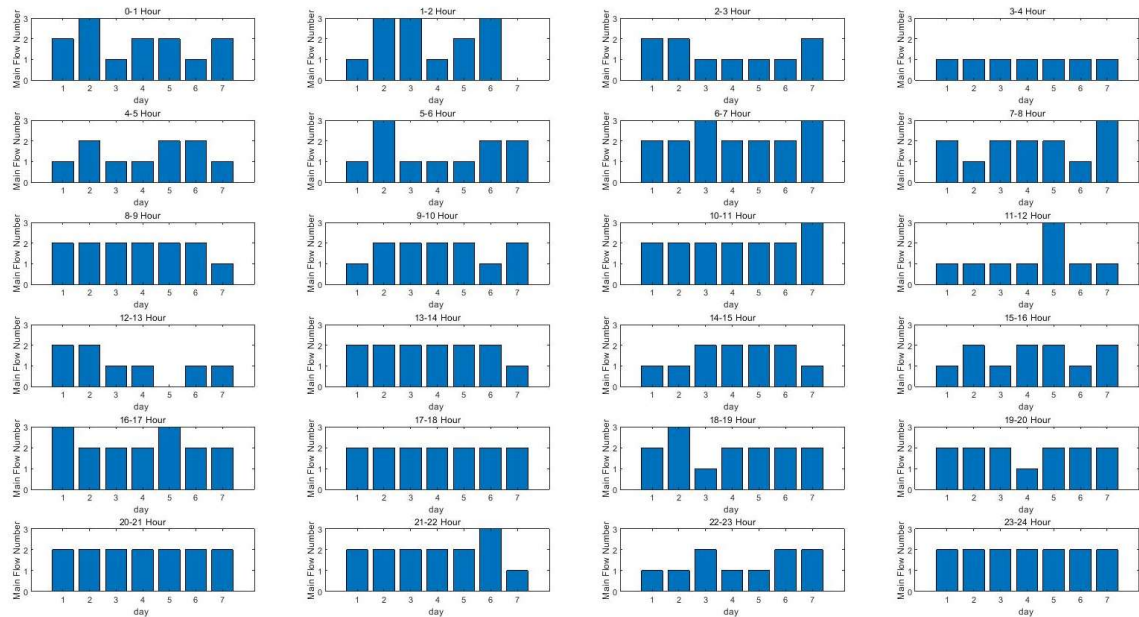


Figure 3.8 Traffic flow distribution in sector ZUUUAR11 (1 hour)

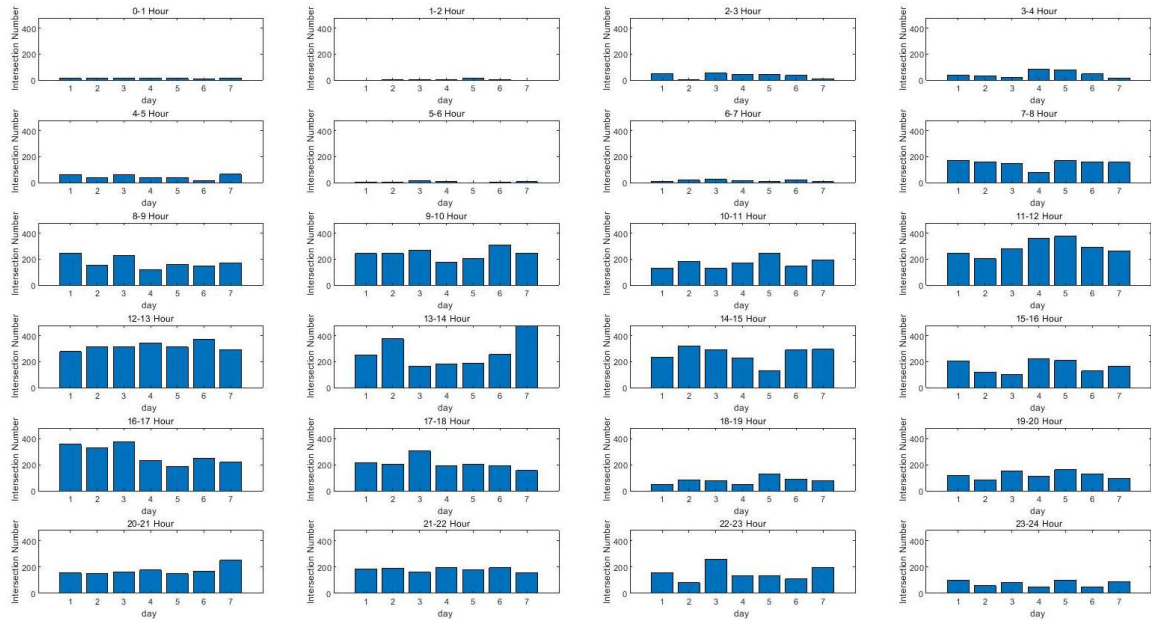


Figure 3.9 Number of trajectory intersection in sector ZUUAR11 (1 hour)

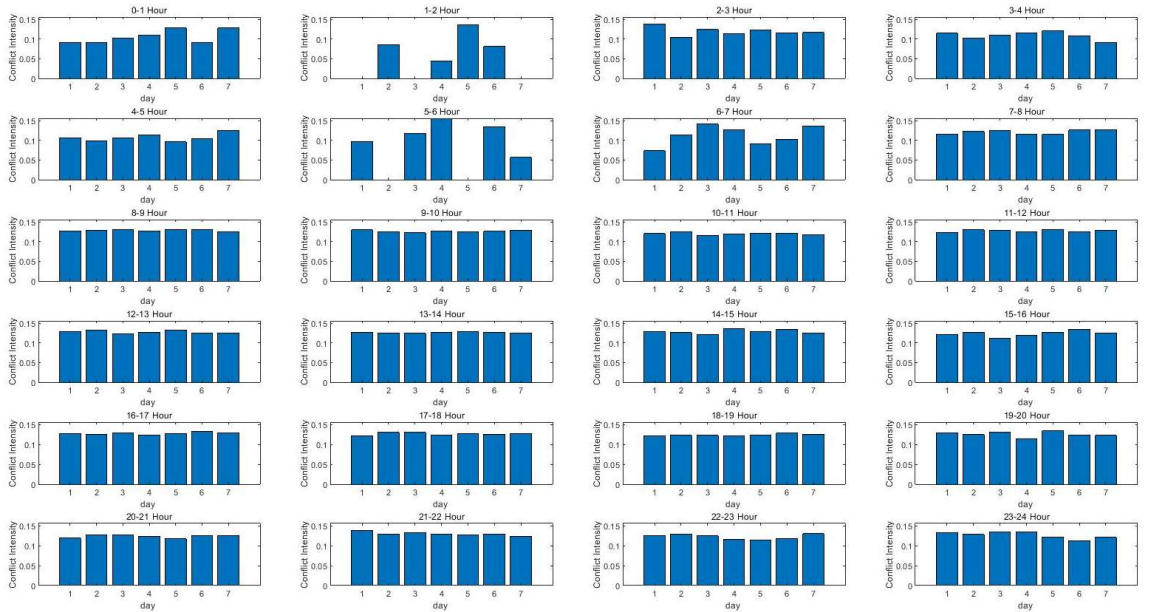


Figure 3.10 Conflict intensity in sector ZUUAR11 (1 hour)

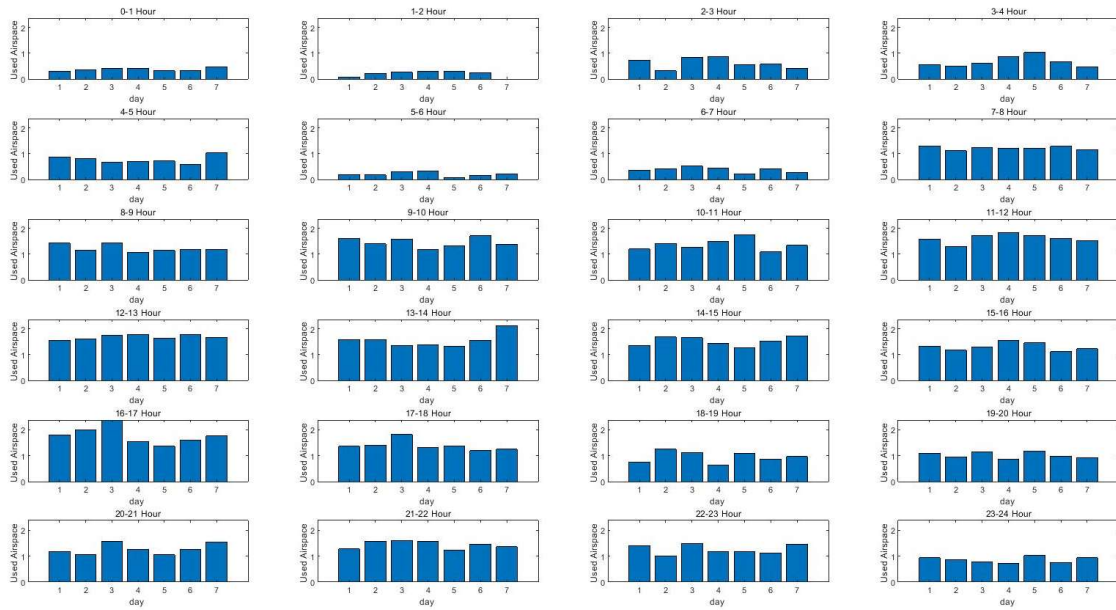


Figure 3.11 Airspace uses in sector ZUUUAR11 (1 hour)

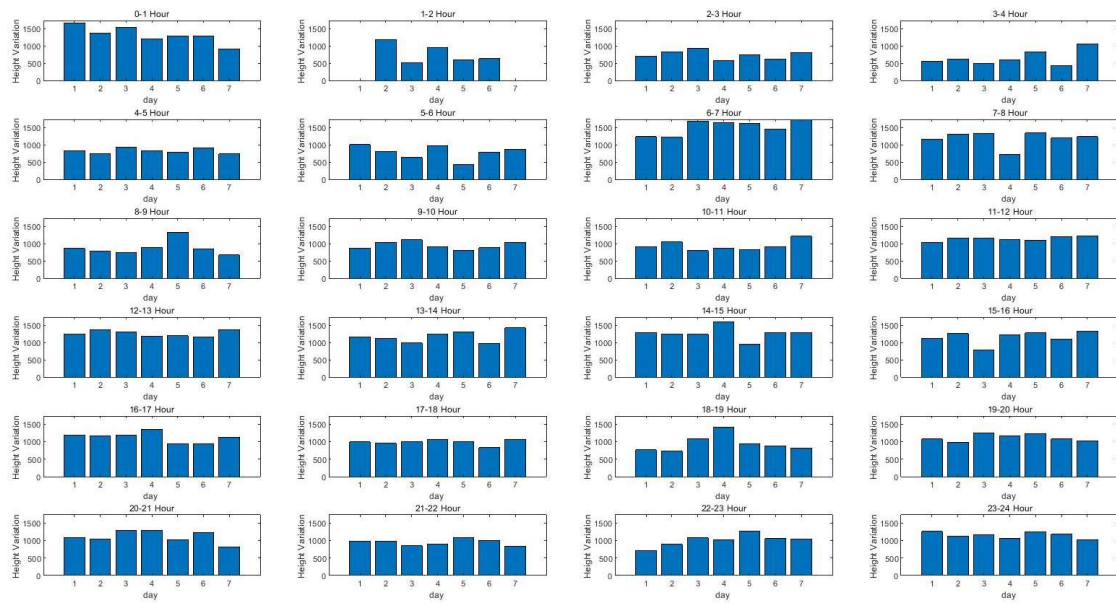


Figure 3.12 Altitude variation in sector ZUUUAR11 (1 hour)

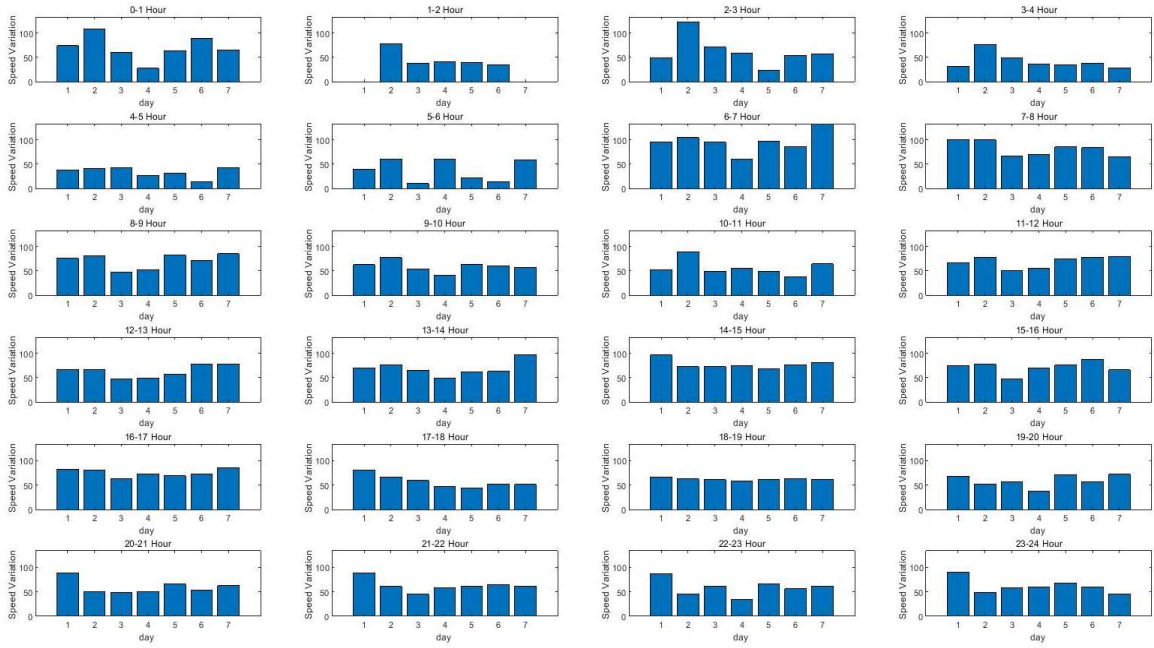


Figure 3.13 Speed variation in sector ZUUUAR11 (1 hour)

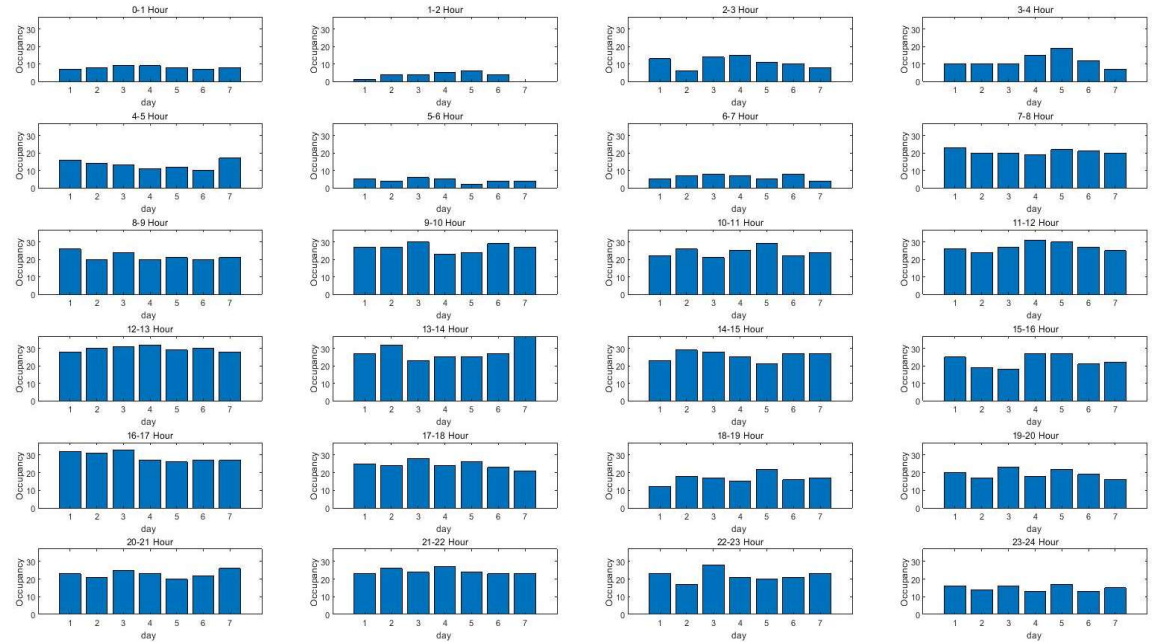


Figure 3.14 Occupancy in sector ZUUUAR11 (1 hour)

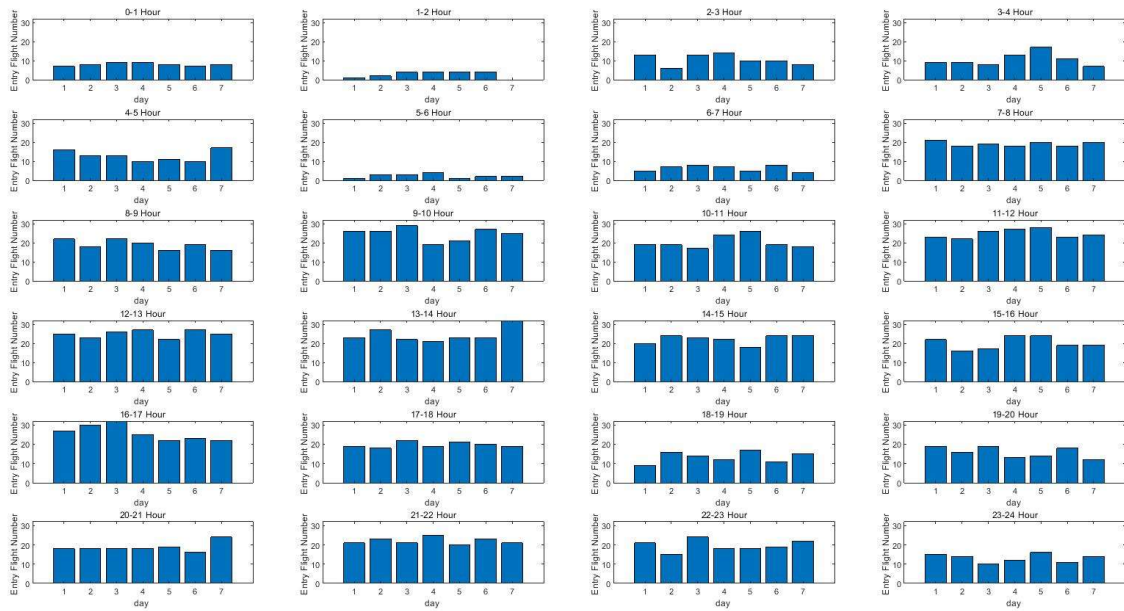


Figure 3.15 Traffic entry in sector ZUUUAR11 (1 hour)

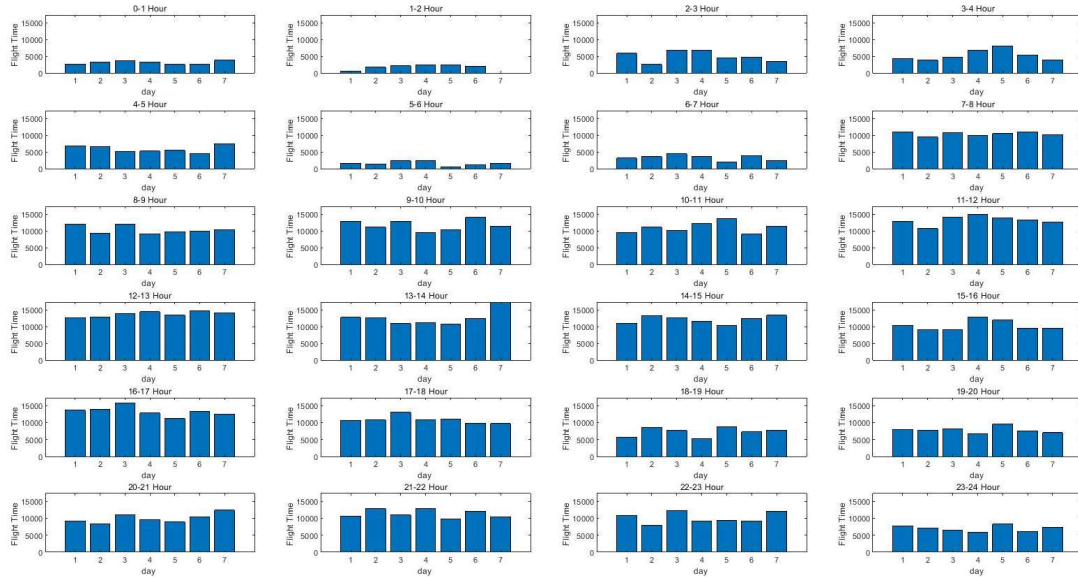


Figure 3.16 Total flight time of the aircraft in sector ZUUUAR11 (1 hour)

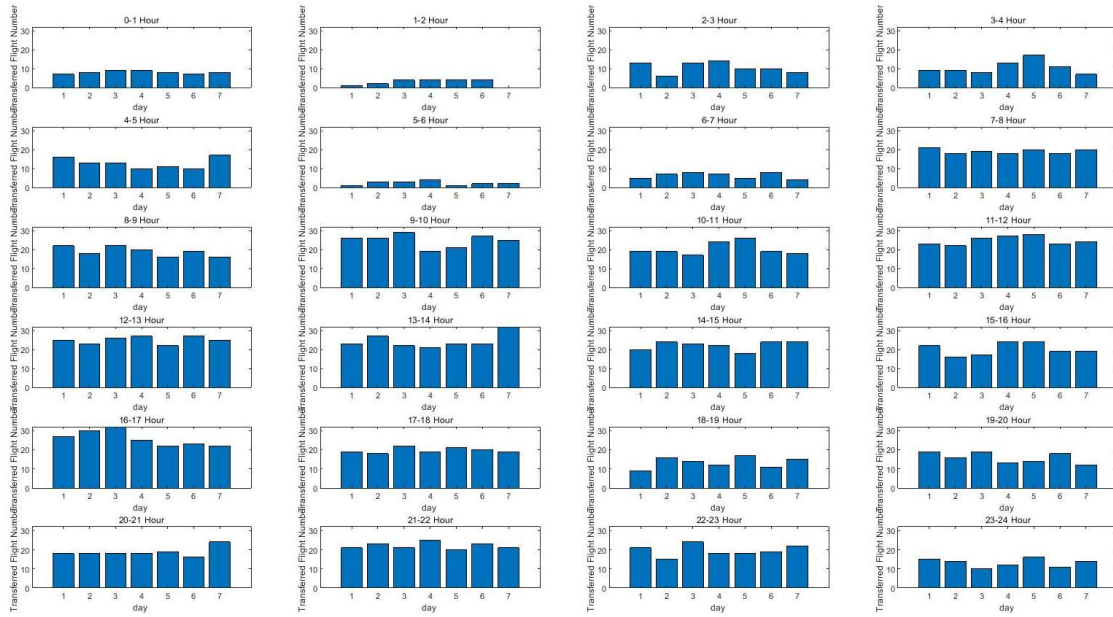


Figure 3.17 Number of control transfers in sector ZUUUAR11 (1 hour)

#### 4.1.3. UNCERTAINTY ANALYSIS OF COMPLEXITY INDICATORS

In order to analyze the uncertainty of the airspace complexity indicators mentioned above, the values of complexity indicators of the sector in different time slices of the statistical period are calculated according to the basic data of the airspace sector and the historical ADS-B data of flights in the sector.

The value of the statistical sector complexity indicator  $k$  in the time slice  $i$  of the statistical period  $j$  is  $x_{i,j}^k$ . To eliminate the influence of the dimension on the uncertainty of the complexity indicator, the values of indicators is normalized, so that the numerical range of different complexity indicators is within the interval  $[0,1]$ , while remaining the same distribution as the original data:

$$\bar{x}_{i,j}^k = \frac{x_{i,j}^k - x_{\min}^k}{x_{\max}^k - x_{\min}^k} \tag{3.20}$$

where  $x_{\max}^k$  is the maximum value of the indicator  $k$ , and  $x_{\min}^k$  is the minimum value of the indicator  $k$ .

Based on the normalized value of airspace complexity indicators, the standard deviation of the distribution is used to measure the variation of the indicator in each time slice during the statistical period:



$$\sigma_i^k = \sqrt{\frac{\sum_{j=1}^m (\bar{x}_{i,j}^k - \bar{x}_{i,avg}^k)^2}{m}} \quad (3.21)$$

where  $\bar{x}_{i,avg}^k$  is the average value of indicator  $k$  in the time slice  $i$ .

The average value of the standard deviation  $\sigma_i^k$  of each complexity indicator  $k$  over all time slices is calculated to measure the uncertainty of the indicator  $k$ :

$$\bar{\sigma}^k = \frac{1}{n} \sum_{i=1}^n \sigma_i^k \quad (3.22)$$

According to the statistical results of the airspace complexity indicators, the uncertainty of the corresponding complexity indicator is calculated as the basis for the uncertainty analysis of the complexity indicator. For the 25 Upper Control Areas of China, 3 sectors of each Upper Control Area are selected with high, medium and low traffic volume respectively. Therefore, a total of 76 sectors are selected for the uncertainty analysis of airspace complexity indicators. Figure 3.18 and Figure 3.19 present the uncertainty of the complexity index of the ZGGGAR12 sector in the eastern airspace with time granularity of 1 hour and 15 minutes respectively. Figure 3.20 and Figure 3.21 present the uncertainty of the complexity index of the ZUUUAR11 sector located in the western airspace with time granularity of 1 hour and 15 minutes respectively. The detailed statistical results of other sectors are listed in the appendix.

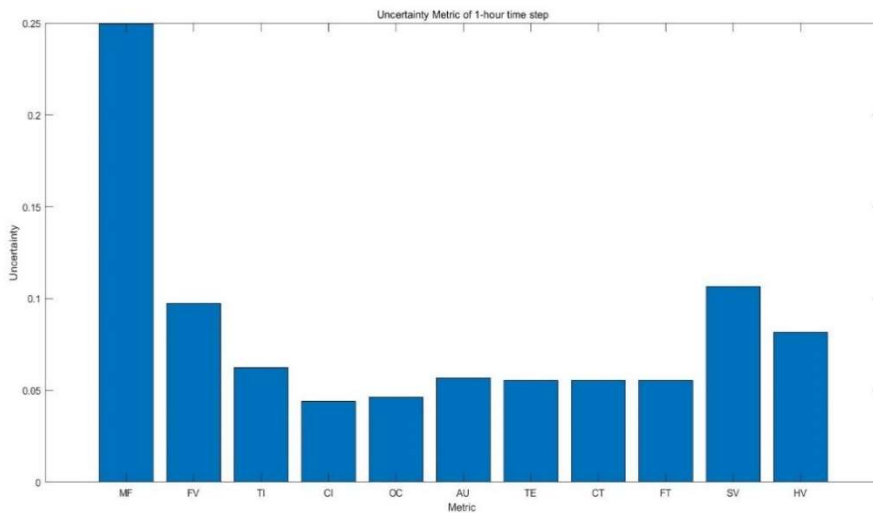


Figure 3.18 Uncertainty of the complexity index of ZGGGAR12 (1 hour)

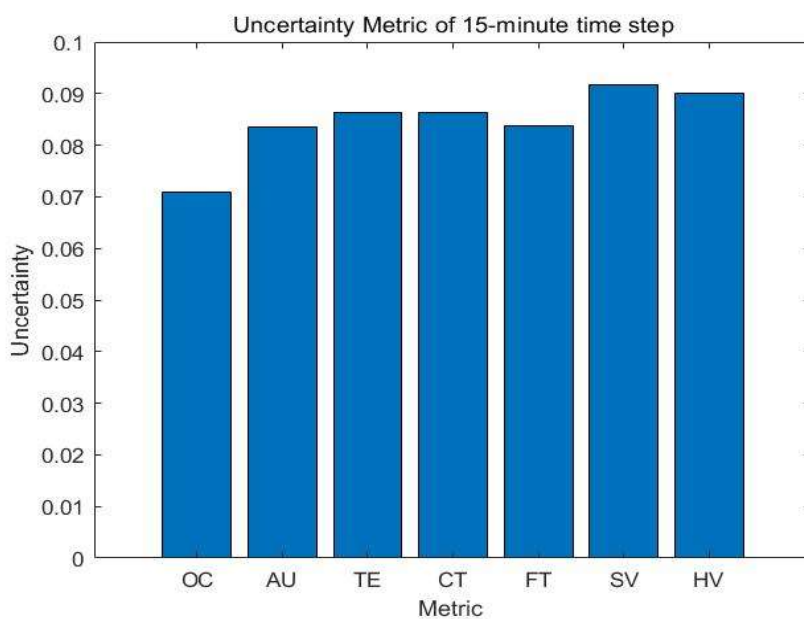


Figure 3.19 Uncertainty of the complexity index of ZGGGAR12 (15 minute)

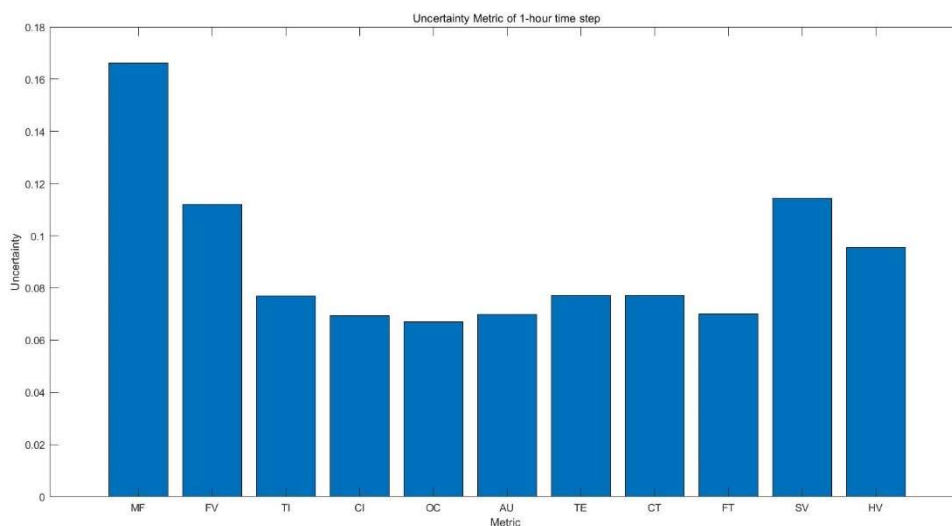


Figure 3.20 Uncertainty of the complexity index of ZUUUAR11 (1 hour)

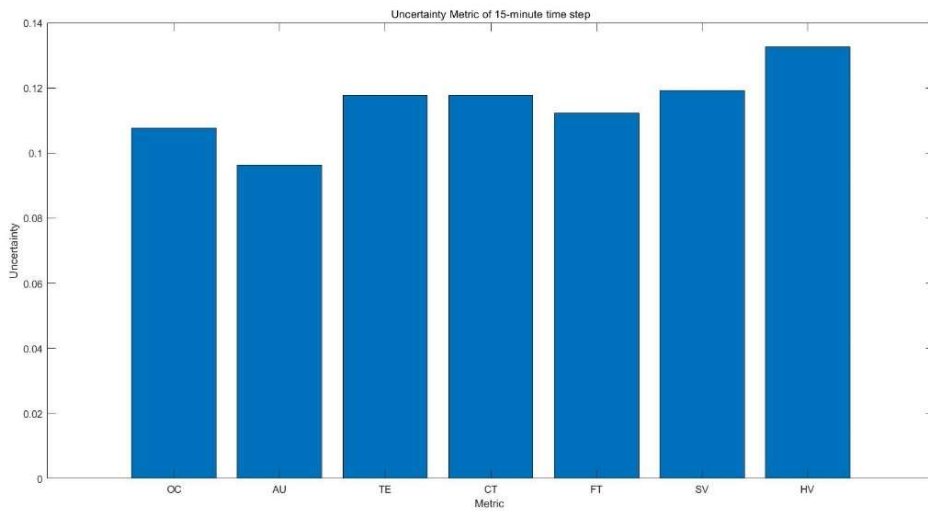


Figure 3.21 Uncertainty of the complexity index of ZUUUAR11 (15 minute)  
 The results of the uncertainty (1 hour) for each complexity indicator of the 76 sectors are compared and analyzed, as shown in Figure 3.22 - Figure 3.32.

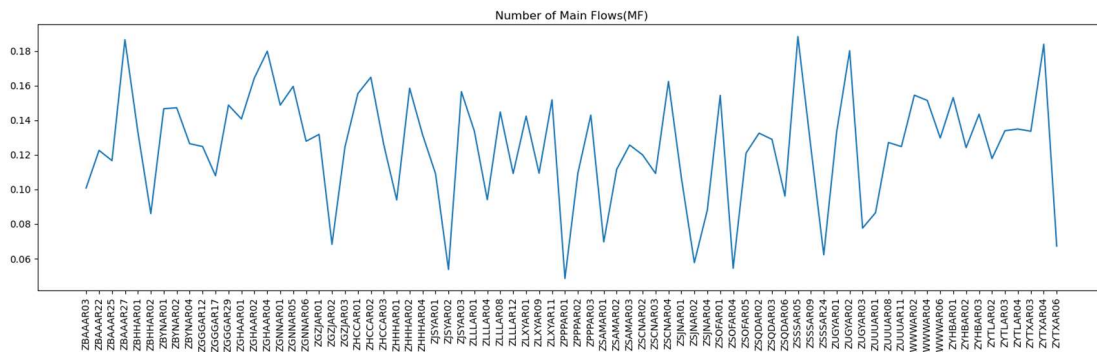


Figure 3.22 Uncertainty of the number of main flows of the 76 sectors

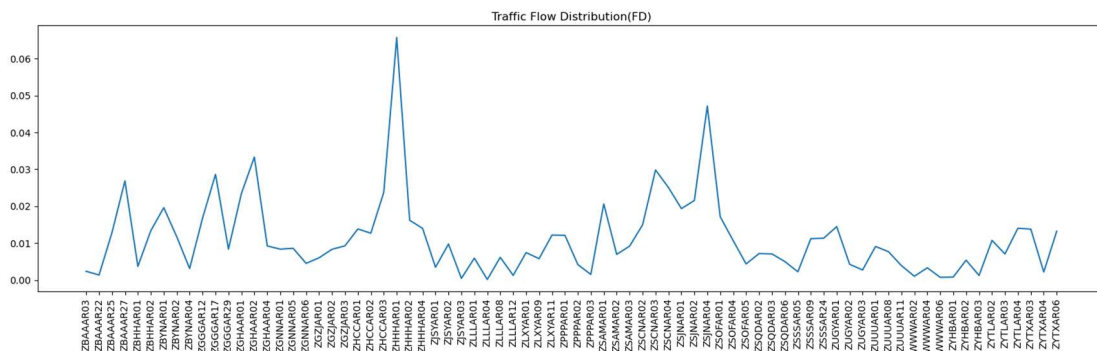


Figure 3.23 Uncertainty of the traffic flow distribution of the 76 sectors

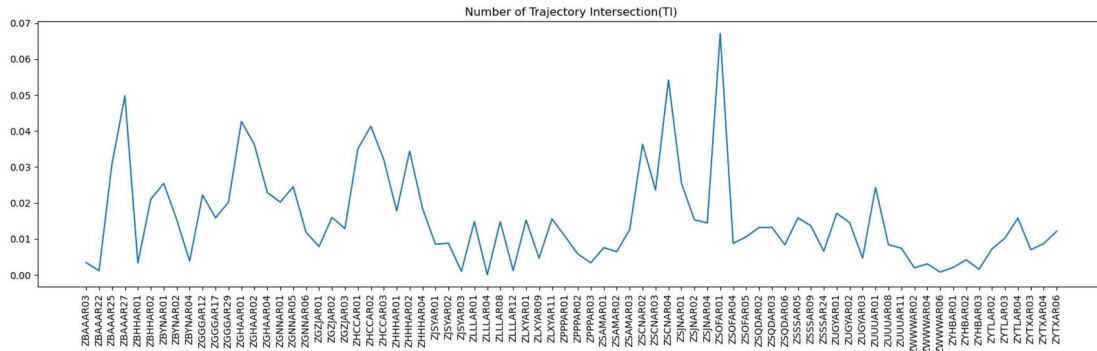


Figure 3.24 Uncertainty of the number of trajectory intersection of the 76 sectors

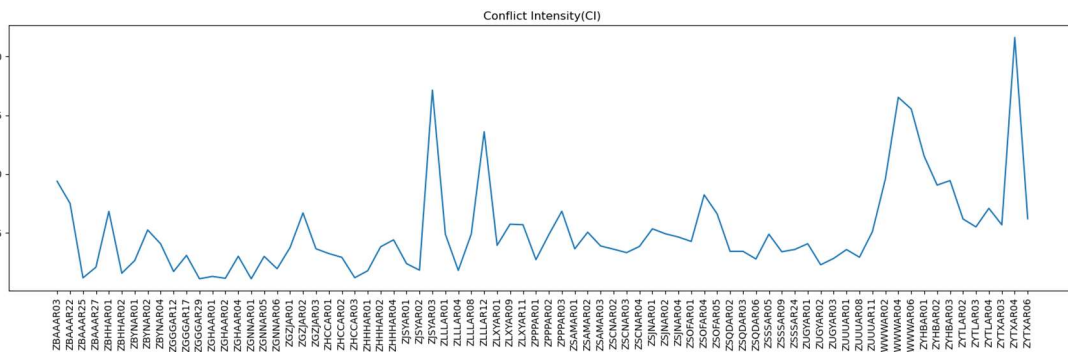


Figure 3.25 Uncertainty of the conflict intensity of the 76 sectors

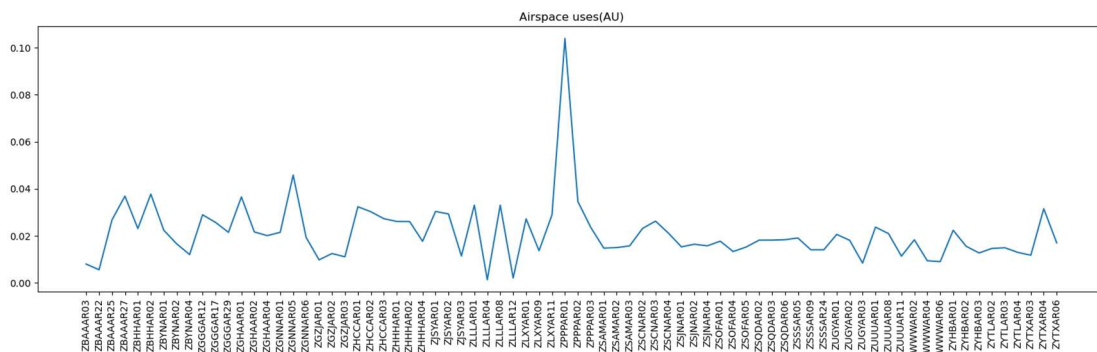


Figure 3.26 Uncertainty of the airspace uses of the 76 sectors

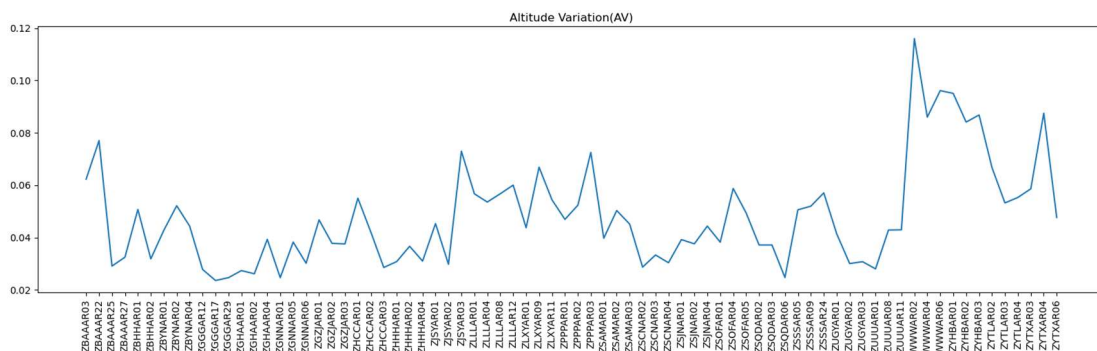


Figure 3.27 Uncertainty of the altitude variation of the 76 sectors

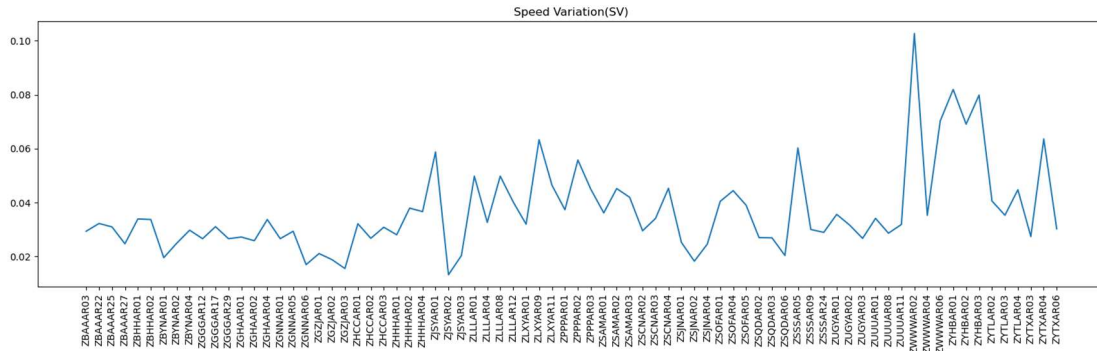


Figure 3.28 Uncertainty of the speed variation of the 76 sectors

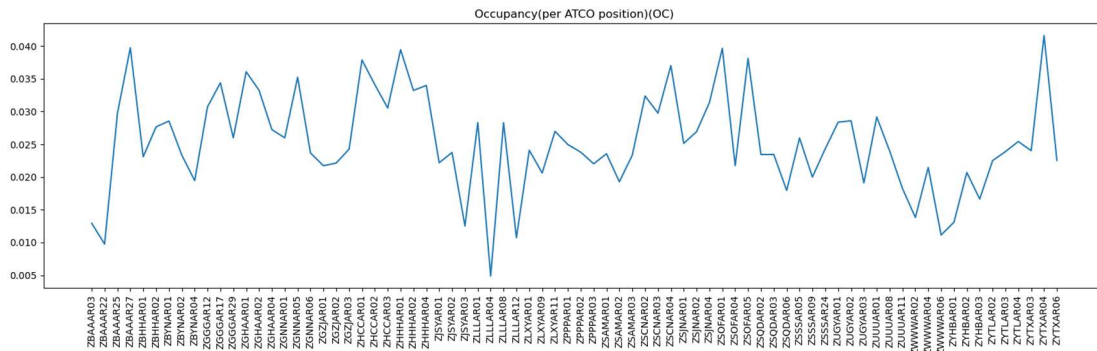


Figure 3.29 Uncertainty of the occupancy of the 76 sectors

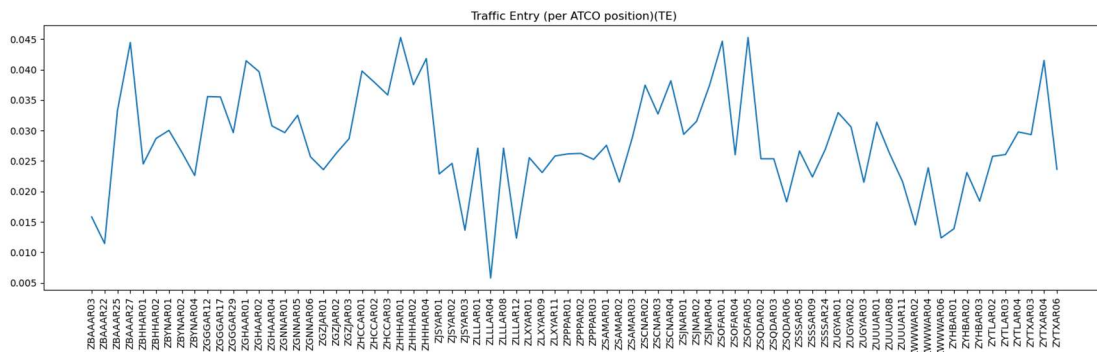


Figure 3.30 Uncertainty of the traffic entry of the 76 sectors

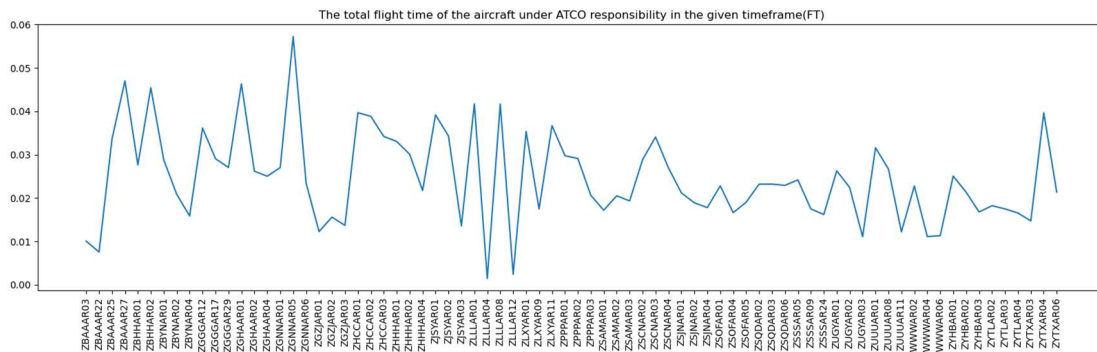


Figure 3.31 Uncertainty of the total flight time of the 76 sectors

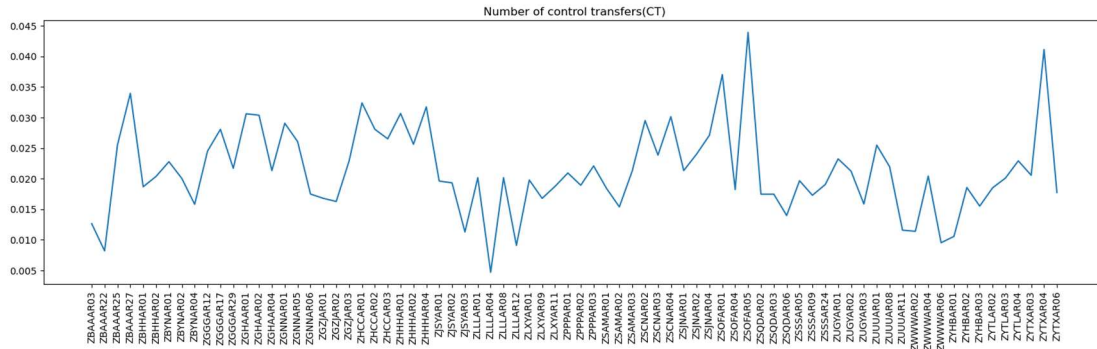


Figure 3.32 Uncertainty of the number of control transfers of the 76 sectors

The average value and the standard deviation of each complexity indicator uncertainty of 76 sectors is calculated, and the results are shown in the Table 3.1.

Table 3.1 Average value and standard deviation of complexity indicator uncertainty of 76 sectors

Indicators	Average	Standard Deviation
Number of Main Flows, MF	0.12498	0.03256
Traffic Flow Distribution, FD	0.01138	0.01070
Number of Trajectory Intersection, TI	0.01574	0.01317
Airspace uses, AU	0.02105	0.01288
Number of control transfers, CT	0.02133	0.00716
The total flight time of the aircraft under ATCO responsibility in the given timeframe, FT	0.02466	0.01063
Occupancy (per ATCO position), OC	0.02532	0.00755
Traffic Entry (per ATCO position), TE	0.02805	0.00840
Speed Variation, SV	0.03660	0.01606
Altitude Variation, AV	0.04796	0.01921
Conflict Intensity, CI	0.05122	0.03879

Based on the calculation results of complexity indicator uncertainty of different sectors, K-Means clustering algorithm is used to cluster the complexity indicators above, where the feature of the clustering sample is the complexity indicator uncertainty of different sectors. The cluster label of each complexity indicator is shown in the Table 3.2, and the centers of the clusters are shown in the Figure 3.33.

Table 3.2 Cluster label of each complexity indicator

Cluster 1	Number of Main Flows, MF
Cluster 2	Conflict Intensity, CI Altitude Variation, AV Speed Variation, SV
Cluster 3	Traffic Entry (per ATCO position), TE Occupancy (per ATCO position), OC Traffic Flow Distribution, FD Number of Trajectory Intersection, TI Airspace uses, AU Number of control transfers, CT

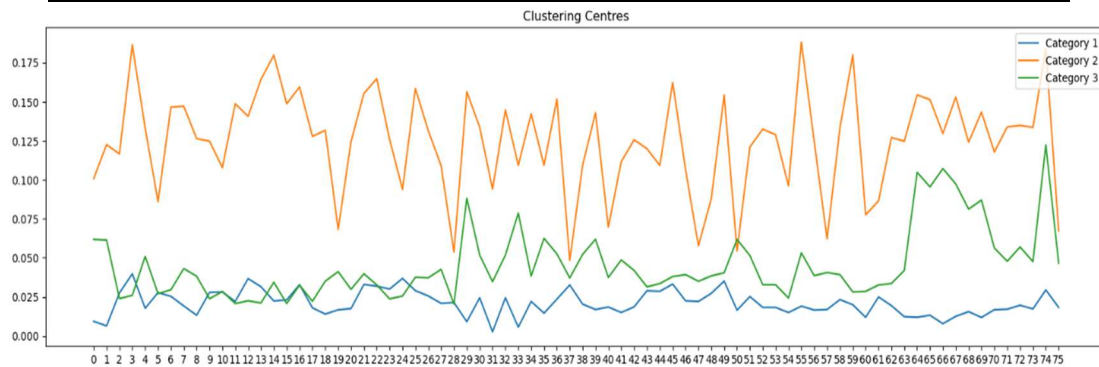


Figure 3.33 Centers of the cluster

Based on the K-Means clustering results and Table 3.2, the main traffic flow quantity (MF) can be classified as the high-level uncertainty indicator. The Conflict Intensity (CI), Altitude Variation (AV), and Speed Variation (SV) can be classified as the medium-level uncertainty indicators. Traffic Entry (TE), Occupancy (OC), Traffic Flow Distribution (FD), Number of Trajectory Intersection (TI), Airspace uses (AU), Number of control transfers (CT) are classified as low-level uncertainty indicators. Since the value of the Flow-based Sector Resource Availability is fixed for each sector, this complexity indicator can also be considered as low-level uncertainty. The uncertainty classification of the complexity indicators is shown in the Table 3.3.

Table 3.3 Uncertainty classification of the complexity indicators

High uncertainty indicator	Number of Main Flows, MF
Medium uncertainty indicator	Conflict Intensity, CI Altitude Variation, AV

	Speed Variation, SV
Low uncertainty indicator	Traffic Entry (per ATCO position), TE Occupancy (per ATCO position), OC Traffic Flow Distribution, FD Number of Trajectory Intersection, TI Airspace uses, AU Number of control transfers, CT Flow-based Sector Resource Availability



## 4.2. COMPLEXITY-BASED SECTOR CAPACITY ESTIMATION FOR DYNAMIC FERA MANAGEMENT

This section describes a complexity-based sector capacity estimation model using pioneering ML technologies. A fast-time simulation using AirTop supported by ATCOs from NorthWest ATMB helping the validation of the baseline model is setup to generate simulated operation data for learning. The generated workload prediction model underpins the dynamic sector configuration in next study.

### 4.2.1. FAST-TIME SIMULATION

In order to measure the capacity of flexible en route airspace sector, ZLLAR04 sector in the western sector is selected as the research object. The sector is located in Lanzhou region, with large sector area and higher sector resource availability, which has the potential to implement the flexible routing. The flight level of ZLLAR04 is ranged from 8900m to 12500m. The 3D boundary is inside the FERA-WoC defined in MS6. The horizontal structure is shown in Figure 3.34.



Figure 3.34 The structure of ZLLAR04 sector

**4.2.1.1 BASELINE MODEL VALIDATION**

In this project, the method of modeling research and evaluation based on computer simulation platform is selected, because the software modeling method can fully consider the complexity of airspace itself, and can quantitatively analyze some factors of the model, which has a high degree of simulation effect on the overall operation process of the evaluation object. Therefore, this project is based on the AirTOP modeling and simulation platform for research.

Because AirTOP simulation software mainly adopts event-based load generation method to calculate controller load. By counting the number of events in the simulation process and accumulating the time spent by the controller to process the corresponding events, the cumulative working time of the controller per unit time is obtained. Then divide the accumulated working hours of the controller by the unit time to obtain the controller workload.

Before the simulation, the baseline model must be verified first<sup>[23]</sup>. The project designs the operation scenario based on the historical typical day, and then randomly generates an array of flight plans according to the actual airspace static structure of ZLLAR04 sector, control operation rules, controller workload, aircraft quality and other parameters. The baseline model is verified and corrected by comparing the controller workload, and the parameters that are more consistent with the actual situation are determined. After several debugging, the main control events and their parameters can be obtained, as shown in Table 3.4. At the same time, the change between the controller experience scoring workload and the controller workload obtained by AirTOP simulation is shown in Figure 3.35. It can be seen that with the continuous adjustment of parameters, the workload of the above two gradually becomes consistent, indicating that the model parameters are gradually reasonable. During the AirTOP simulation of the flight plan, the aircraft operation situation is shown in Figure 3.35.

Table 3.4 Main control events and their parameters

Event	Total event time	Monitor	Air/Ground Communication	Height statement	Conflict detection	Conflict Resolution	Coordination
Sector Entry	0:00:15	0:00:05	0:00:08				0:00:02
Sector Exit	0:00:08		0:00:08				
Level Change	0:00:08			0:00:08			
Conflict Detection - crossing	0:00:20				0:00:20		

both cruising							
Conflict Detection - crossing both in vertical	0:00:30				0:00:30		
Conflict Detection - crossing one in vertical	0:00:25				0:00:25		
Conflict Detection - opposite both cruising	0:00:20				0:00:20		
Conflict Detection - opposite both in vertical	0:00:30				0:00:30		
Conflict Detection - opposite one in vertical	0:00:25				0:00:25		
Conflict Detection - same track both cruising	0:00:10				0:00:10		
Conflict Detection - same track both in vertical	0:00:20				0:00:20		
Conflict Detection - same track one in vertical	0:00:15				0:00:15		
Conflict Resolution -	0:01:00					0:01:00	

crossing both cruising							
Conflict Resolution - crossing both in vertical	0:01:00					0:01:00	
Conflict Resolution - crossing one in vertical	0:01:00					0:01:00	
Conflict Resolution - opposite both cruising	0:01:00					0:01:00	
Conflict Resolution - opposite both in vertical	0:01:00					0:01:00	
Conflict Resolution - opposite one in vertical	0:01:00					0:01:00	
Conflict Resolution - same track both cruising	0:01:00					0:01:00	
Conflict Resolution - same track both in vertical	0:01:00					0:01:00	
Conflict Resolution - same track one in vertical	0:01:00					0:01:00	

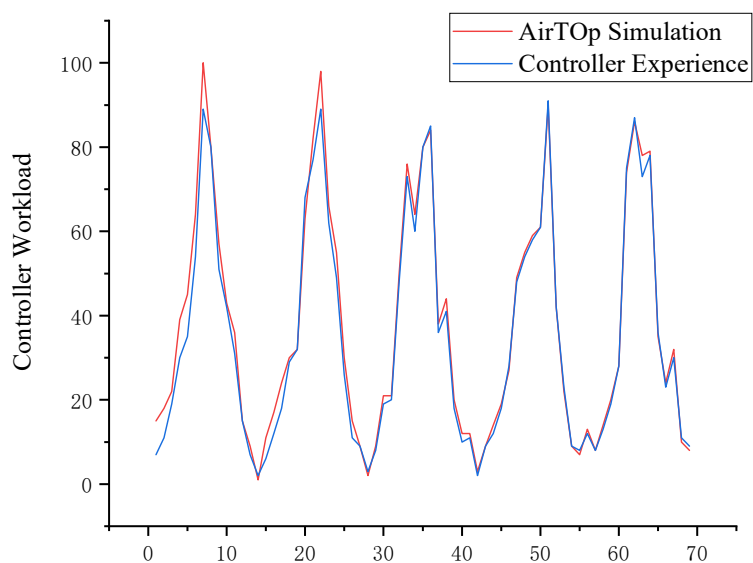


Figure 3.34 AirTOP simulation controller workload and controller experience scoring workload change trend chart

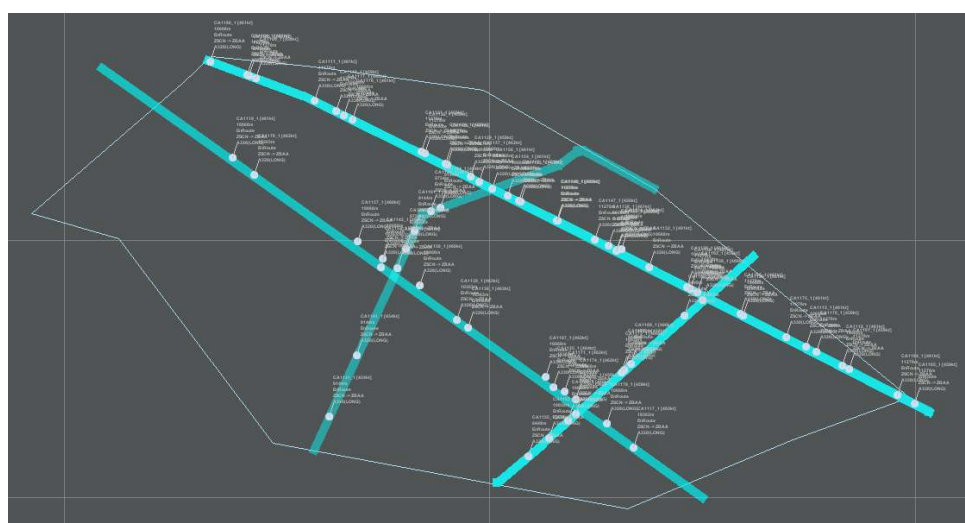


Figure 3.35 Flight operation simulation based on AirTOP

#### 4.2.1.2 SCENARIOS

##### 1) Sector configuration

In order to investigate the impact of route flexibility on operation performance, for comparison, the original route structure and sector boundary points are now retained as a structural sector (Case 1). Then, according to the optimal cluster number and upper limit of sector boundary points, we re-clustered the points less

than the optimal cluster number (Case 2). The optimal cluster (Case 3) characterizing the balanced flexibility of airspace sector is directly adopted from Chapter 2. Therefore, Case 1 represents a purely structural airspace sector with a **flexibility of none** (Figure 3.35); Case 2 represents an airspace sector with **moderate flexibility** (Figure 3.36); Case 3 represents the route airspace sector with **Optimal flexibility** (Figure 3.37).

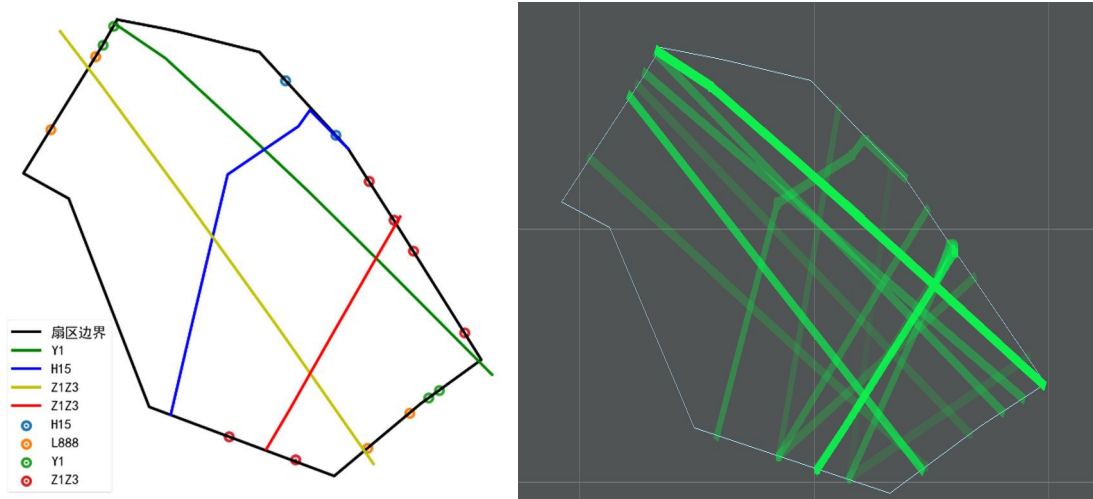


Figure 3.36 The layout of ZLLL04 with moderate flexibility

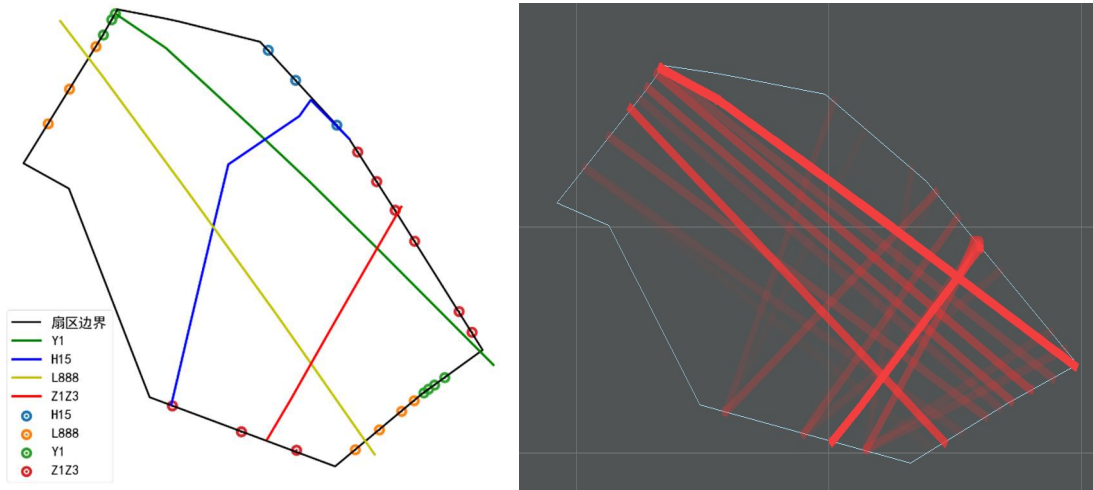


Figure 3.37 The layout of ZLLL04 with optimal flexibility

## 2) Traffic condition

In order to perform a Monte Carlo simulation, the random flight plans shall be prepared. The historical data is analysis to obtain the specific traffic conditions of the sector, so as to make the flight plan more reasonable and realistic. Specific steps are as follows:

(1) Based on the ADS-B data, the actual trajectory data of the aircraft passing through the sector can be obtained. The aircraft types, cruising level, ground speed, route in used is then analyzed.

(2) Then, a simulated flight planning is generated. Since the interval time between flights entering the sector cannot be negative, it is a distribution of non-negative random variables. The most commonly used distribution is Poisson distribution, as shown in formula (3.23):

$$P(N(t) = n) = \frac{(\lambda t)^n e^{-\lambda t}}{n!} \quad (3.23)$$

where  $t$  is the total time span of a flight plan,  $P(N(t) = n)$  is the probability of  $n$  flights in a single flight plan, and  $\lambda$  is the mean value of the Poisson distribution, that is, the mean value of the traffic flow within the time span of a random flight plan.

The number of flights for each flight planning generally obeys the Poisson distribution with parameter  $\lambda$ . The total duration of a single flight planning is 2 hours. The number of flights that fly into the sector every 15 minutes is shown in Figure 3.38. A total of 200 flight plans are generated.

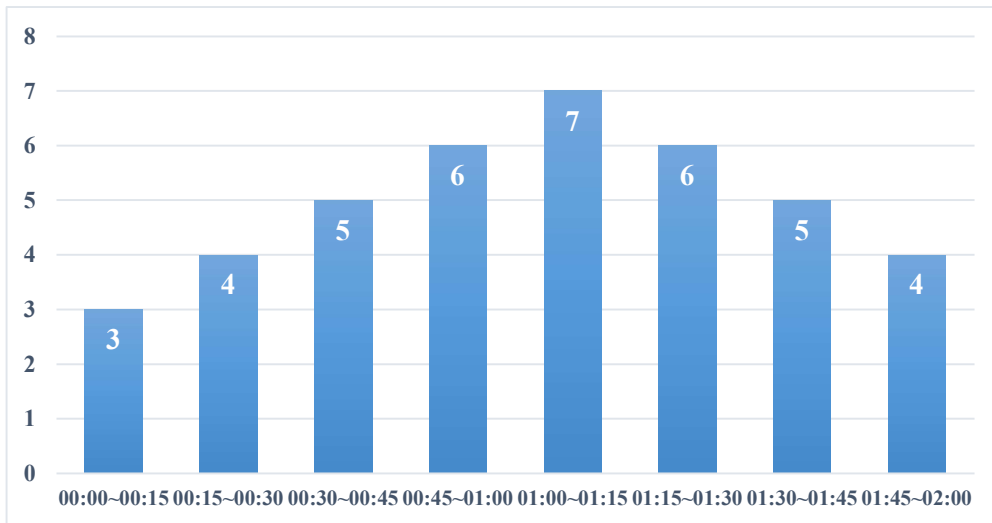


Figure 3.38 Time series pattern of simulated traffic flow

(3) The prepared 200 flight plans are used for all 3 cases for comparative studies. For Case 2 and Case 3, each route is randomly assigned with its corresponding flexible route.

#### 4.2.1.3 SIMULATION AND OUTPUTS

##### 1) Monte Carlo simulation

Monte Carlo simulation has been rapidly popularized in recent 10 years. Monte Carlo method, also known as statistical simulation method and random sampling

technology, is a numerical calculation method based on "random number" and probability statistics theory. The Monte Carlo method is used to randomly generate the flight sequence and then form a large number of flight plans that can be imported by the computer simulation model. By analyzing the simulation results, the situation of aircraft entering and exiting the sector within a certain period of time can be obtained, and the workload of controllers can be calculated.

**2) Simulation based on AirTOP**

Based on the Monte Carlo simulation application theory, an AirTOP simulation model is built to simulate the actual operation of ZLLAR04 sector. For the above three cases, 200 flight planning for each case are imported into the validated AirTop simulation model. The above complexity indicators are quantified by analyzing the simulation data, and the workload of controllers can be obtained accordingly. The AirTOP simulation modeling process is shown in Figure 3.39.

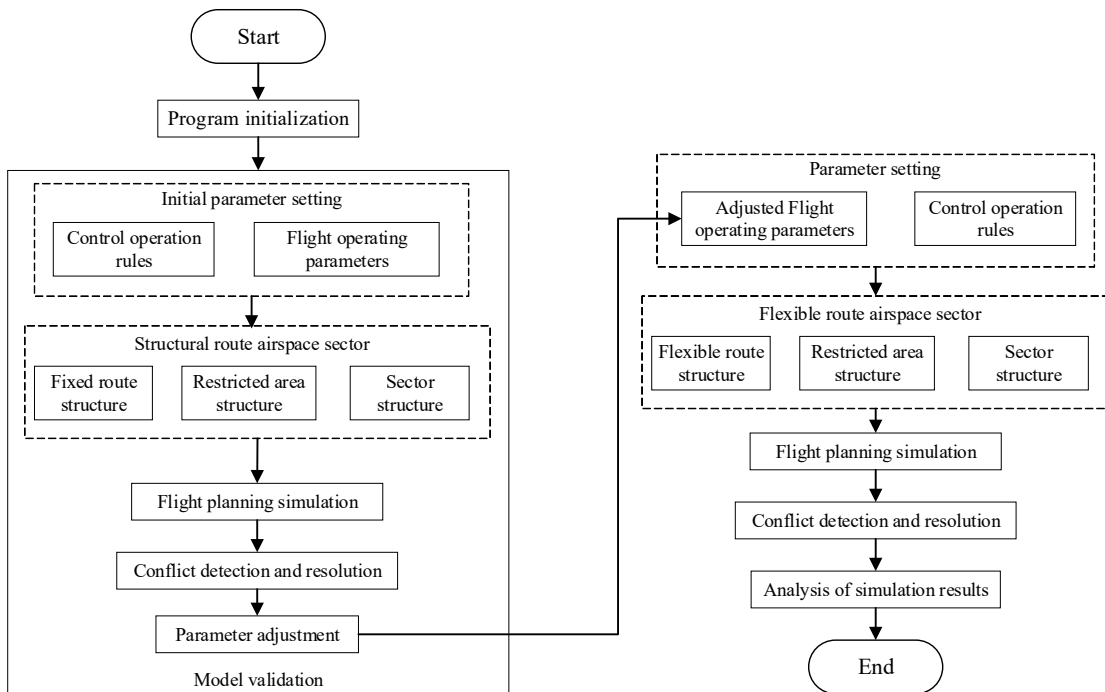


Figure 3.39 Flow chart of AirTOP simulation modeling

In AirTOP, the controller workload is mainly calculated from the following aspects:

- a. General workload, including aircraft entering and exiting sectors, aircraft passing through waypoints, aircraft altitude changes, issuing instructions according to air traffic control rules or waypoint rules, etc.;
- b. Conflict detection and resolution workload, including actual conflict detection, potential conflict detection, conflict resolution, etc.;
- c. Approach sequencing workload, including instructions to change route, instructions to change altitude, speed and heading, etc.;



d. Traffic flow management workload, including speed monitoring under time constraints, speed change instructions under time constraints, etc.

The simulation interface based on AirTOP simulation is shown in Figure 3.40.

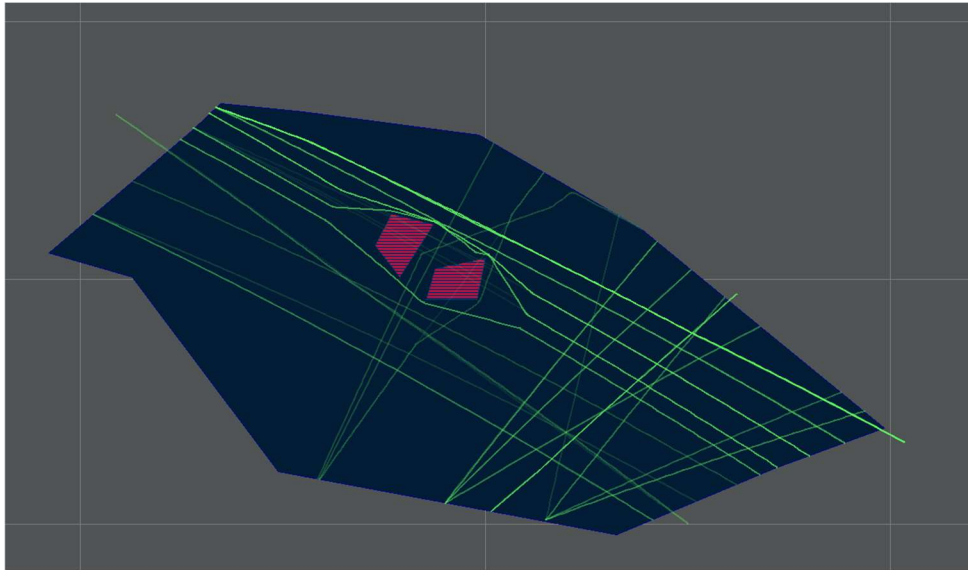


Figure 3.40 Interface of AirTOP simulation

### 3) Analysis of simulation results

According to the AirTOP simulation, the controller workload of each case is shown in Figure 3.41. It can be seen that with the continuous increase of flexibility, the average controller workload is gradually decreasing. The controller workload distribution in the structural airspace sector is relatively scattered and has great volatility. With the increasing flexibility of the en-route airspace sector, the controller workload is gradually stable and the fluctuation becomes smaller.

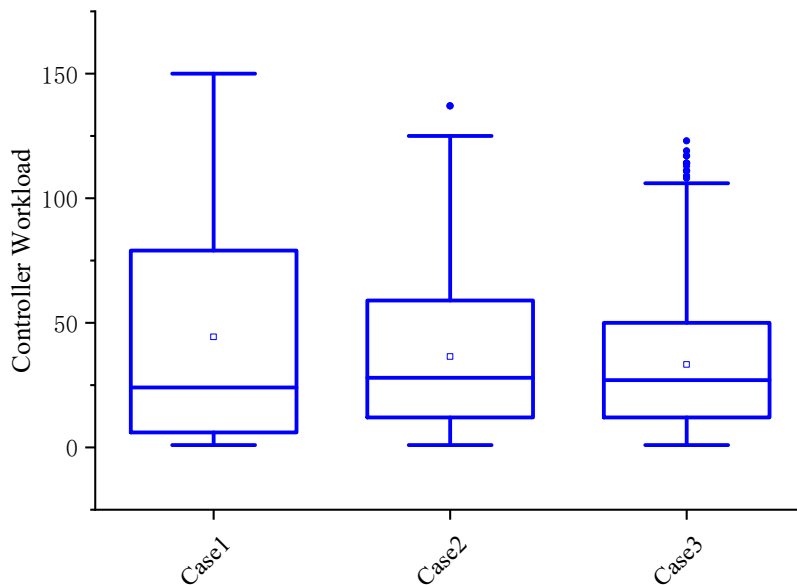


Figure 3.41 Comparison of control workload in different cases

## 4.2.2. COMPLEXITY-BASED WORKLOAD ESTIMATION USING BASED ON XGBOOST

### 4.2.2.1 INTRODUCTION OF XGBOOST

The XGBoost algorithm is an ensemble learning algorithm improved on the basis of the Gradient Boosting Decision Tree (GBDT) [24]. Its core idea is to integrate the weak classifier into a strong classifier, that is, the residual of the previous weak learner training is fitted by introducing a new weak learner. After the training, the prediction score corresponding to each sample will be generated. The final sample prediction value can be obtained by summing the prediction scores generated by all weak learners. The structure of XGBoost is shown in Figure 3.42.

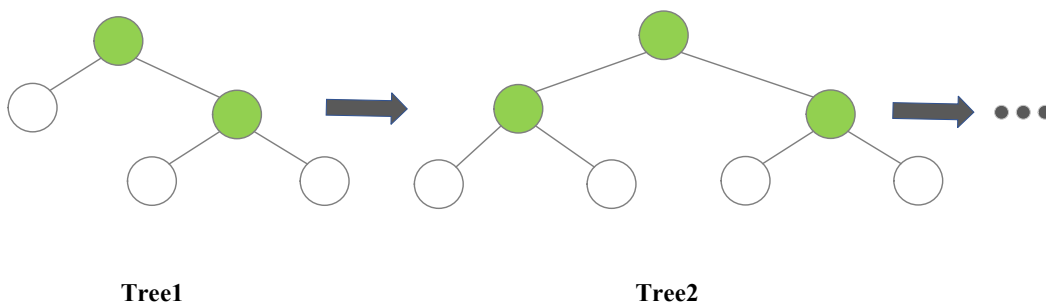


Figure 3.42 Structural diagram of XGBoost

For each case of route airspace sector, it is assumed that it has  $n$  sets of data, and each group of data has  $m$  characteristics, which is represented by  $M = \{(x_i, y_i)\} (x_i \in R^m, y_i \in R, i = 1, 2, \dots, n)$ . XGBoost uses CART regression tree model as weak learner. For the prediction of the group  $i$ , the prediction function is:

$$\hat{y}_i^{(t)} = \sum_{j=1}^t w_{ij} \quad (3.24)$$

In Equation (3.24):  $\hat{y}_i^{(t)}$  represents the predicted value of group  $i$ ;  $t$  represents the iteration times of the decision tree;  $w_{ij}$  represents the score of the leaf nodes in each decision tree;  $i, j$  represents the data sequence number and the decision tree sequence number.

During the training of the model, the objective function is defined as:

$$Obj^{(t)} = \sum_{i=1}^n l(y_i, \hat{y}_i^{(t)}) + \sum_{j=1}^t \Omega(f_j) \quad (3.25)$$

In Equation (3.25):  $\sum_{i=1}^n l(y_i, \hat{y}_i^{(t)})$  represents the loss function, usually the mean

square error function, which is used to determine the difference between the predicted value and the real value, and then measure the accuracy of the model;

$\sum_{j=1}^t \Omega(f_j)$  represents the complexity function, that is, the sum of the complexity of  $t$

trees, which is used to control the complexity of the model and reduce the risk of over fitting.

For the Taylor second-order expansion of the loss function in the Equation (3.25), the objective function can be approximately obtained:

$$Obj^{(t)} = \sum_{i=1}^n \left[ l(y_i, \hat{y}_i^{(t-1)}) + g_i f_i(x_i) + \frac{1}{2} h_i f_i^2(x_i) \right] + \sum_{j=1}^t \Omega(f_j) \quad (3.26)$$

In Equation (3.26):  $\hat{y}_i^{(t-1)}$  represents the sum of the scores of the sample  $i$  in the

previous  $t-1$  trees, which is a certain value;  $f_i(x_i)$  represents the score of the

sample  $i$  in the tree  $t$ ;  $g_i$  and  $h_i$  represent the first-order and second-order derivation of the loss function for this model respectively<sup>[25]</sup>.

In the XGBoost algorithm, the complexity of a single decision tree can be calculated by Equation (3.27):

$$\Omega(f_j) = \gamma T + \frac{1}{2} \lambda \sum_k w_k^2 \quad (3.27)$$

In Equation (3.27):  $T$  and  $\gamma$  represent the number of leaf nodes and their

penalty terms respectively;  $w_k$  represents the score of the node  $k$ ;  $\lambda$  represents

L2 regular penalty term.

Based on Equation (3,27), the complexity function composed of  $t$  trees can be obtained:

$$\sum_{j=1}^t \Omega(f_j) = \Omega(f_j) + const = \gamma T + \frac{1}{2} \lambda \sum_k w_k^2 + const \quad (3.28)$$

In Equation (3.28):  $const$  is a constant representing the sum of the complexity of the previous  $t-1$  trees.

Since the constant will not affect in the process of optimizing the function, the objective function can be simplified as follows after  $t$  iterations:

$$Obj^{(t)} = \sum_{i=1}^n \left[ g_i f_i(x_i) + \frac{1}{2} h_i f_i^2(x_i) \right] + \gamma T + \frac{1}{2} \lambda \sum_k^T w_k^2 \quad (3.29)$$

#### 4.2.2.2 CONTROLLER WORKLOAD PREDICTION BASED ON XGBOOST

The flow chart of controller workload prediction based on XGBoost is shown in Figure 3.43.

- a. According to the AirTOP output data corresponding to each case, each index in the flexible route airspace complexity index system is quantified and standardized;
- b. Divide the sample into training sample and test sample;
- c. Input the training sample into the XGBoost model and adjust the parameters to meet the accuracy requirements;
- d. Import the test sample into the model whose parameters have been adjusted, and finally get the prediction result.

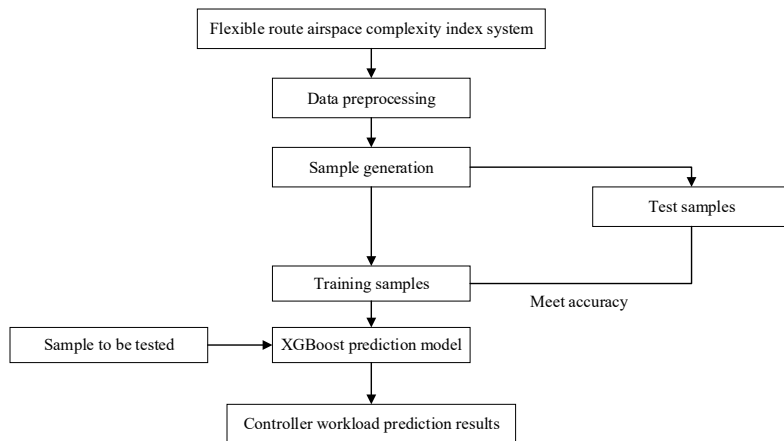


Figure 3.43 Flow chart of controller workload prediction based on XGBoost

#### 4.2.2.3 PERFORMANCE ANALYSIS

##### 1) Prediction results of each case

According to the AirTOP output data corresponding to each case, the data is divided respectively, and 90% of them are selected as the training set and 10% as the test set.

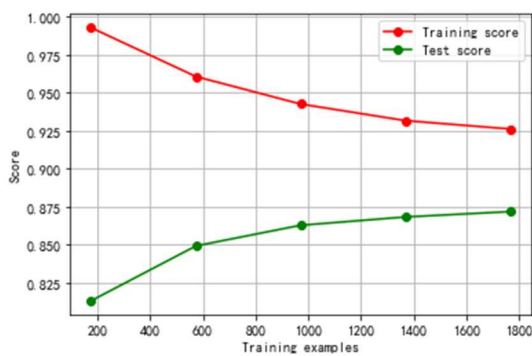
The prediction performance of the model mainly depends on two factors: the quality of the data itself and the adjustment of the model parameters<sup>[26]</sup>. In order to further improve the prediction effect of the model, it is necessary to adjust the parameters of the controller workload prediction model based on XGBoost. Among them,  $n\_estimators$  is the number of weak estimators in the ensemble algorithm. The larger the parameter value, the stronger learning ability of the model, but the

easier the model is to overfit. The *min\_chil\_weight* parameter controls the minimum sample size required on the leaves, and its adjustment is more effective for data with larger sample sizes. The *max\_depth* controls the maximum depth of the tree in the model. The larger the parameter value, the more complex the model is, and the model is prone to overfitting. The *Subsample* controls the proportion of randomly sampled data for training, and the *learning\_rate* parameter controls the iteration rate, both of which prevent the model from overfitting. The *reg\_lambda* and *reg\_alpha* are the L1 and L2 regularization terms of the weight respectively. *Gamma* controls the minimum loss function drop value required for node splitting. They can reduce the complexity of the model and speed up the algorithm convergence.

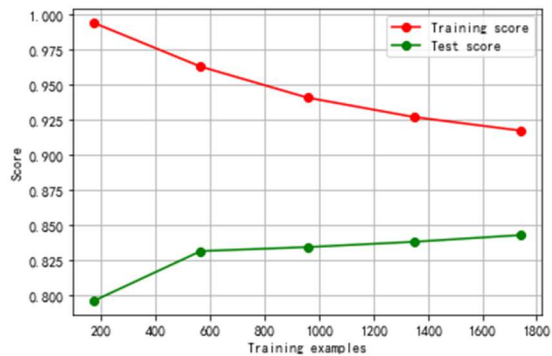
The key parameters of the XGBoost algorithm are adjusted using grid search, and the cross-validation results are used as the criterion for parameter selection. Finally, after several rounds of testing and parameter adjustment, the optimal values of some key parameters are shown in Table 3.5. Meanwhile, the learning curve of each case is shown in Figure 3.44.

Table 3.5 The optimal value of the key parameters of each case model

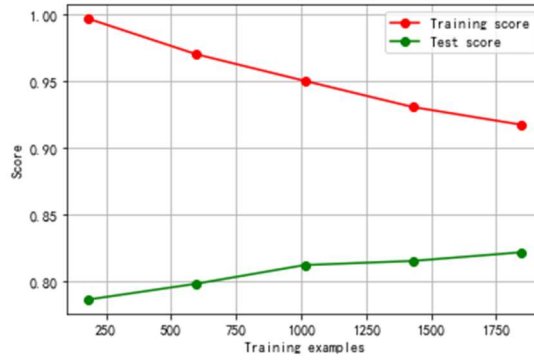
	<i>n_estimators</i>	<i>max_depth</i>	<i>Subsample</i>	<i>learning_rate</i>	<i>Gamma</i>
Case1	80	4	1	0.06	0.4
Case2	100	4	1	0.07	0.4
Case3	120	4	1	0.1	0.4



(a) Case1



(b) Case2



(c) Case3

Figure 3.44 Learning curve of each case

After the model parameters are determined, the XGBoost prediction model is trained with the training set, and then the test set is imported into the trained model to obtain the predicted value of the controller workload in the test set. In order to quantitatively analyze and compare the prediction results of the models, the complex correlation coefficient  $R^2$ , Root Mean Square Error (RMSE) and Mean Absolute Error (MAE) were used as indicators to evaluate the performance of the model. The calculation formula is as follows:

$$R^2 = 1 - \frac{\sum_{i=1}^n (x_i - x_p)^2}{\sum_{i=1}^n (x_i - x'_0)^2} \tag{3.30}$$

$$RMSE = \sqrt{\frac{1}{n} \sum_{i=1}^n (x_i - x_p)^2} \tag{3.31}$$

$$MAE = \frac{1}{n} \sum_{i=1}^n |x_i - x_p| \tag{3.32}$$

In Equation (3.30)-(3.32),  $x$  is the value of the variable (this study refers to controller workload),  $x_i (i=1,2,\dots,n)$  is the actual value of controller workload;  $x'_0$  is the average value of  $x_i$ ;  $x_p$  is the predicted value of  $x_i$ ;  $n$  is the number of samples in the test set.

Finally, the evaluation results of prediction error of each case are obtained, as shown in Table 3.6.

Table 3.6 Performance of workload prediction model based on XGBoost

	Case1	Case2	Case3
RMSE	3.96	4.25	4.08
MAE	2.84	3.73	3.65

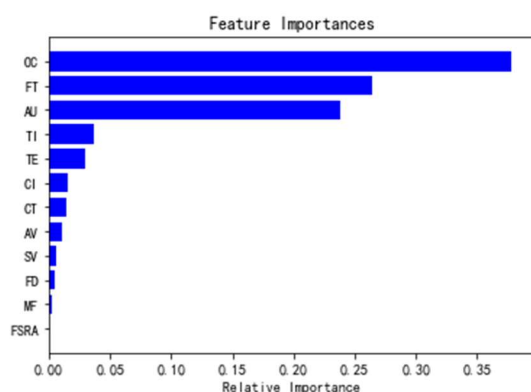
$R^2$                       0.89                      0.83                      0.84

It can be seen from Table 3.6 that all the three cases get higher  $R^2$  values and smaller error values, which proves that the model controller has good performance in controller workload prediction. The prediction accuracy of the model within the range of  $\pm 2$ ,  $\pm 4$ ,  $\pm 6$ ,  $\pm 8$  and  $\pm 10$  between the prediction results and the actual controller workload is shown in Table 3.7. In terms of controller workload prediction, the model accuracy for the three cases are around 90% within  $\pm 8$  error. Compared with case 1, the accuracy of case 2 and 3 is slightly lower due to higher freedom of air traffic flow leading to more complex and less predictable impact of traffic patterns on workload.

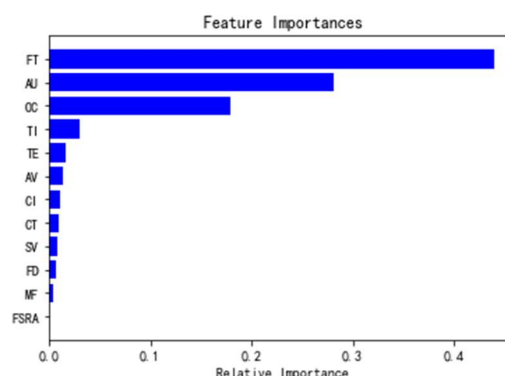
Table 3.7 Prediction accuracy of workload

	$\pm 2\%$	$\pm 4\%$	$\pm 6\%$	$\pm 8\%$	$\pm 10\%$
Case1	36.273%	59.546%	82.312%	93.445%	96.234%
Case2	32.997%	56.823%	79.624%	89.452%	93.221%
Case3	33.367%	55.762%	77.416%	92.983%	95.664%

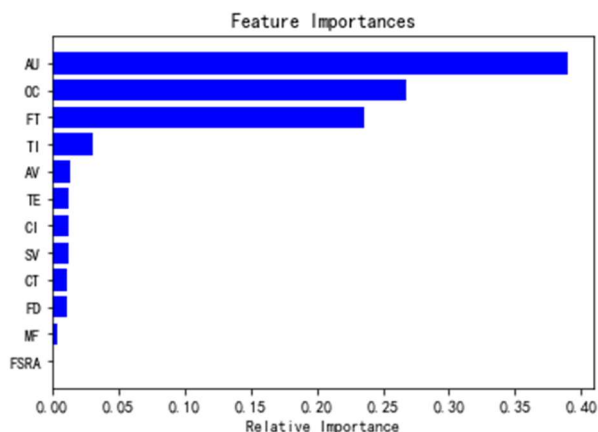
According to XGBoost, the importance ranking of each indicator can be obtained to explore the impact of the air traffic complexity on controller workload prediction. Figure 3.45 shows the importance ranking of the complexity indicators of each case based on XGBoost. It can be seen that for all cases, the top three important indicators are FT, AU and OC. As the flexibility of the airspace sector increases in terms of more flight routes, the importance level of AU is gradually improved.



(a) Case1



(b) Case2



(c) Case3

Figure 3.45 The importance ranking of the complexity indicators of each case based on XGBoost

**(2) Prediction results of all cases**

With the improvement of flexibility in route airspace sector, the number of flexible routes in the sector also increases. Therefore, we developed route length (RL) index as a new complexity indicator with low uncertainty, which measures the sum of the length of fixed route and flexible route in the sector. Then we merged the data of three cases to train a more comprehensive workload prediction model based on XGBoost incorporating the flexibility of airspace sector. The specific training and testing process is consistent with the previous one. The optimal hyper-parameter values are shown in Table 3.8, and the learning curve is shown in Figure 3.46. The training performance of the comprehensive prediction model, as shown in Table 3.9 gets better compared with the numbers of case 2 and 3 in Table 3.6.

Table 3.8 The optimal value of the key hyper-parameters

	<i>n_estimators</i>	<i>max_depth</i>	<i>Subsample</i>	<i>learning_rate</i>	<i>Gamma</i>
Optimum value	100	5	1	0.07	0.4

Table 3.9 Training performance the comprehensive prediction model based on XGBoost

Performance parameters	result
RMSE	4.17
MAE	3.32
R <sup>2</sup>	0.87

The model prediction accuracy in the range of  $\pm 2$ ,  $\pm 4$ ,  $\pm 6$ ,  $\pm 8$  and  $\pm 10$  respectively is shown in Table 3.10. It can be seen that within the error range of  $\pm 8$ , the prediction accuracy of the model reach at 93.65%, indicating that with the increase of sample data and the introduction of the index of RL, the prediction performance of the model has been further improved.



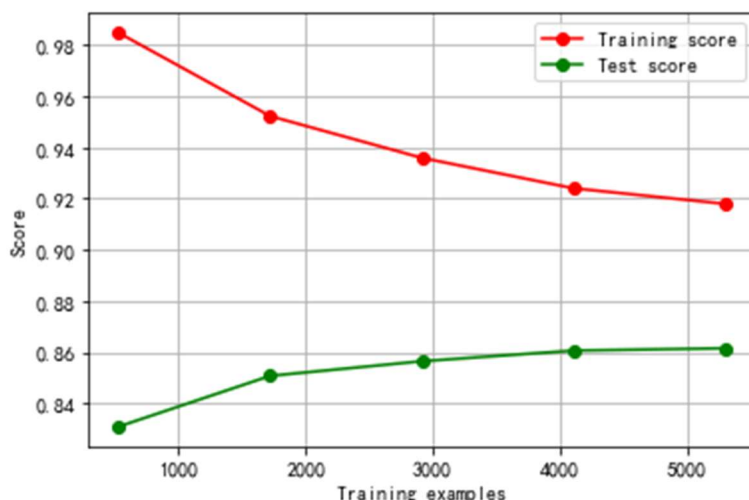


Figure 3.46 learning curve

Table 3.10 Prediction accuracy of controller workload

	±2%	±4%	±6%	±8%	±10%
Accuracy	42.724%	59.336%	80.963%	93.648%	96.815%

The importance ranking of the complexity index of controller workload prediction model based on XGBoost is shown in Figure 3.47. It can be seen from the figure that AU, OC ,FT and TI rank the top four, and the index of RL ranks fifth. Therefore, under the premise of considering the flexibility of the route airspace sector, RL is a relatively key indicator. And it is positively correlated with the controller workload.

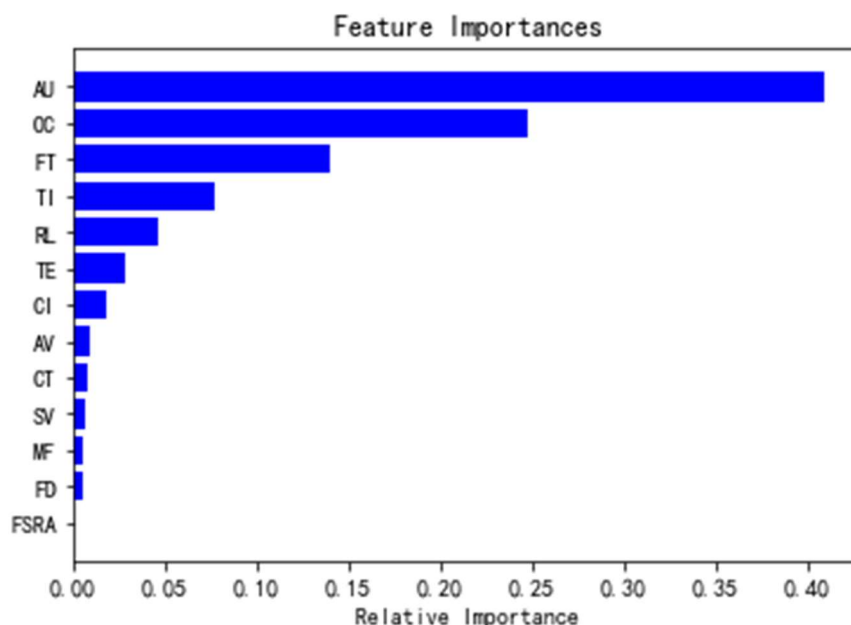


Figure 3.47 The importance ranking of the complexity indicators

#### 4.2.2.4 THE RELATIONSHIP BETWEEN UNCERTAINTY AND IMPORTANCE OF COMPLEXITY INDICATORS

Based on the complexity index uncertainty classification table given in Section 3.13 and the complexity index importance ranking given in Figure 3.47, the relationship matrix between the importance and uncertainty is presented in Table 3.11.

Table 3.11 Characteristics of complexity indicators

Influence \ Uncertainty	Low influence	Medium influence	High influence
High uncertainty	MF	CI	-
Medium uncertainty	SV	AV,TE	-
Low uncertainty	FD,FSRA	CT,RL	TI,AU,OC,FT

It can be seen from the above table that there is great uncertainty in some complexity indicators. At strategic stage, it would be more robust to select the complexity indicators with lower uncertainty to predict the controller workload thus dynamically optimizing the sector configuration. In order to investigate the prediction performance of the model trained without the high uncertainty indicators, we set two new cases : a low uncertainty indicators (Case4) including FD, FSRA, CT, RL, TI, AU, OC and FT, and a Low and medium uncertainty indicators (Case5) including FD, FSRA, CT, RL, TI, AU, OC, FT, SV, AV and TE. The performance of case 4 and 5 is compared with that of the comprehensive model, as shown in Table 3.12 and 3.13.

Table 3.12 Prediction error for each case

	Comprehensive prediction	Case4	Case5
RMSE	4.17	5.34	4.86
MAE	3.32	4.26	3.97
R <sup>2</sup>	0.87	0.85	0.85

It can be seen from the above evaluation results that reducing the dimension of complexity features imposed negative impact on the accuracy of the controller workload prediction. High uncertainty indicators (i.e., MF and CI) representing the air traffic characteristics at macroscopic and microscopic level respective are significant for workload prediction. However, the accuracy of the lighted model with less uncertain factors is still acceptably.

In next study, the models with different complexity indicators will be used to dynamically manage the sector configuration in FERA-WoC according to different time span based on quantified uncertainty level.

Table 3.13 Comparison of prediction accuracy

	±2%	±4%	±6%	±8%	±10%



Comprehensive prediction	42.724%	59.336%	80.963%	93.648%	96.815%
Case4	36.952%	52.419%	78.494%	87.248%	92.921%
Case5	39.368%	56.297%	79.861%	90.735%	93.164%

## 5. FERA-WOC PLANNING AND DYNAMIC SECTOR OPERATION

### 5.1. COLLABORATIVE ENTRY AND EXIT POINTS PLANNING FOR SECTORS IN FERA-WOC

#### 5.1.1. OVERVIEW

The FERA-WoC concept supporting HERAM is given in the progress report WP3.1-MS6. Such airspaces can retain or adjust the original ATS routes, configure sector entry and exit points, intermediate waypoints, conditional routes, and free maneuvering zones. It should be noted that, in order to improve the flexibility of 4D aircraft's trajectory selection (such as adapting to changes in wind direction at high altitudes) and make up for the lack of ground-based navigation facilities in the western region, the entry and exit points of the sector can be announced as important points, or can be defined arbitrarily latitude and longitude coordinates. Intermediate waypoints can only be defined by nav aids.

Under this concept, flexibly setting and assigning sector entry and exit points is one of the important ways to improve the freedom of FERA sector operation. In this section, a sector boundary point planning model based on great circle and boundary point constraints is proposed. The model integrates two factors, the horizontal efficiency of the trajectory and the degree of clustering distortion. The goal is to minimize the total distance of the horizontal trajectory considering the constraints of the boundary points, explore a flexible route airspace sector boundary point layout that is moderate in number and responds to demand, provide a "sample" sector for the subsequent development of flexible route airspace complexity and capacity prediction as well as a framework for the next stage to carry out research on sector dynamic configuration.

#### 5.1.2. PROBLEM DESCRIPTION

The main goal of flexible route airspace sector boundary point planning is to support airspace users' preferred trajectory on demand, and dynamically respond to users' different requirements for flight distance, flight time, and fuel consumption. For en-route flight, the level flight distance is the most important variable affecting fuel consumption and emissions under the condition of constant available altitude. Therefore, based on the concept of green long-haul route operation in D2.1 and progress report WP3.1-MS6, this chapter takes the Western Flexible Route Airspace (FERA-WoC) as the research object, extracts the city (airport) pair information of

all flights in the airspace, identifies and clusters intersections of trajectories and sector boundaries based on the great circle trajectories in FERA-WoC, finds a balance between the number of clusters and the flight distance so as to realize the coordinated configuration of multi-sector entry and exit points in FERA-WoC. Aiming at this problem, this chapter takes the flight distance of the planned flight as the objective function, comprehensively considers the degree of clustering distortion in the solution process, and proposes a flexible route airspace sector entry and exit point configuration model. To simplify the calculation, this chapter treats the aircraft as a mass point, treats the airspace as Euclidean space, and converts the latitude and longitude of the Earth's surface to Cartesian coordinates.

### 5.1.3. SECTOR BOUNDARY POINT PLANNING MODEL BASED ON GREAT CIRCLE

#### 5.1.3.1 ASSUMPTIONS

In order to simplify the model, according to the actual airspace conditions, the following assumptions are made:

- (1) The initial in-point and target out-point of the flight in FERA-WoC are known. Considering that the connection points between the flexible route airspace and the eastern airspace and the western low-altitude airspace (such as approach airspace) remain unchanged, neither the initial entry point nor the target exit point participate in clustering and optimization;
- (2) The influence of uncertain weather such as high-altitude wind on the optimal horizontal trajectory is not considered. In fact, we have also carried out planning considering the horizontal trajectory of the wind and the entry and exit points of the sector. However, due to the vast area of the west, the wind direction of each sector is quite different, and the current data cannot support the analysis of prevailing winds. Sector entry and exit point planning based on trajectory, provides a more flexible and robust airspace structure for the 4D trajectory planning in WP3.
- (3) This chapter retains the original fixed ATS routes, and adds new boundary points to the original sector boundaries to support the differential operation of airspace users equipped with different airborne equipment capabilities;
- (4) This chapter plans out that "direct flight paths" between sector boundary points may pass through restricted areas. In view of this situation, you can negotiate with the military to open conditional routes for high-traffic routes, and delete or set detour points in the sector to avoid routes that are used infrequently. This content will be discussed in the third stage and is beyond the scope of this chapter

### 5.1.3.2 DATA PROCESSING

The following data are required to carry out flexible route airspace sector boundary point planning:

(1) Basic airspace data, including flexible route airspace, east-west boundary, sector boundary, waypoint and border point information, especially location point name and coordinates. Location point data were obtained from the National Aeronautical Information Publication (NAIP).

(2) Flight plan data, including flight plan, pilot plan report and trajectory data. Through the matching of three types of data, determine the city-to-flight plan information flying through FERA-WoC, and extract the initial entry point and target exit point of the flight in FERA-WoC. It is worth noting that since there may be alternative routes between airports, the great circle planning of the corresponding flight within FERA-WoC also takes into account the different entry and exit points available for the flight.

We selected 1251 flights in a week in November 2019 in FERA-WoC, involving 21 sectors in the western flexible route airspace, see Figure 4.1, with a total of 42 edges, including 1 airspace boundary and 41 sector boundaries. Table 4.1 shows the planned flight waypoints of some flights in the western airspace. Among them, ZGGG-EHAM passing through the flexible route airspace has two optional flight routes, and the city pairs that only take off or land in the flexible route airspace include ZLXN-ZHHH, etc. , the city pairs that take off and land in the flexible en route airspace are ZUUU-ZLXY, etc.

Table 4.1 Example route waypoints

Departure airport	Destination airport	Planned waypoint
ZGGG	EHAM	PASLU P265 WLY FJC JTG CDX P247 P142 P143 OMBON ELPAN BESMI XIXAN SUNUV BUKPU ANDIM LELUX LAXEV P434 NOGEX P407 OMGUP IGDON TODOD NIXUK IBANO BIKNO IPMUN KEXAB FKG VARMU UGPEL IKARA OMKEN P221 SALMO PIBIG TCH SARIN
ZGGG	EHAM	PASLU P265 WLY FJC JTG CDX P247 P142 P143 OMBON ELPAN BESMI XIXAN SUNUV MUDAP JTA AKMAT P92 YBL P435 GOBIN MORIT
ZLXN	ZHHH	P15 DNC XIXAN IRSUM JIG VISIN SADB U HO P396 P404 P397 UGSUT P17 P62 KIKIV ML P403 REVKU ONIXO
ZUUU	ZLXY	NOBIK AGULU IGNOL NSH

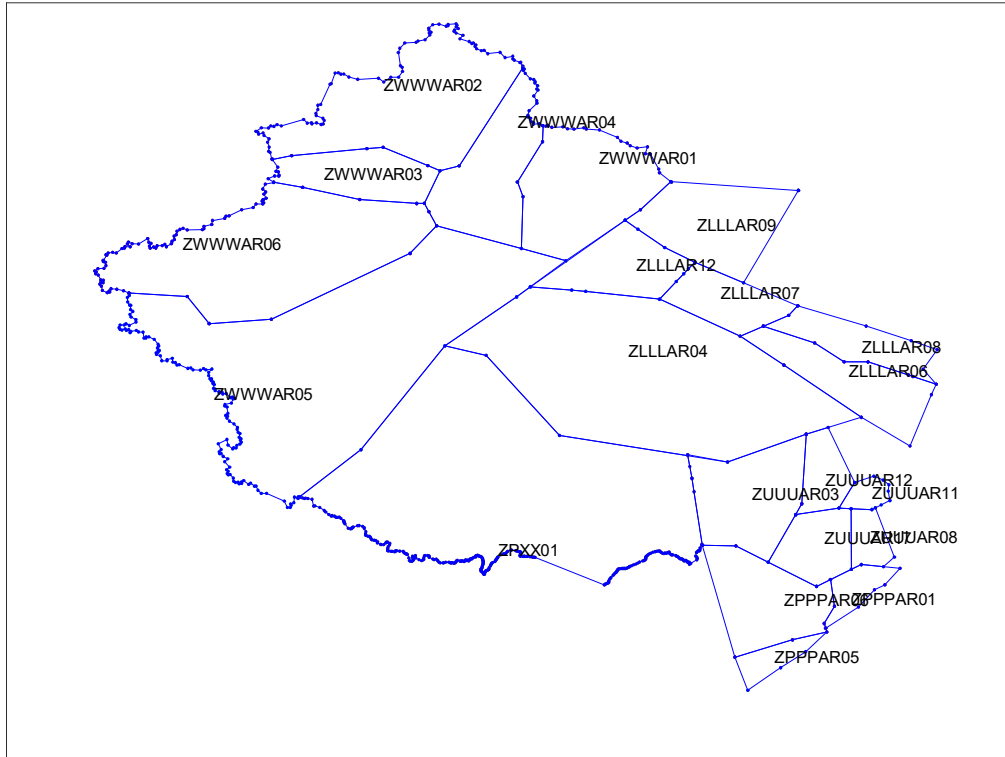


Figure 4.1 Boundaries and sectors of FERA-WoC

### 5.1.3.3 GREAT CIRCLE PATHS GENERATION

Based on the above data, filter out the flight plan information in FERA-WoC, ① determine which city pairs or airport pairs of flights pass through FERA-WoC, denoted as  $F_j (j=1,2,\dots,J)$ ; ② flight plan information under the current route structure; ③ Location information of the entry and exit points of flights in the FERA-WoC are denoted as  $I_j (j=1,2,\dots,J)$  and  $O_j (j=1,2,\dots,J)$  respectively.

If the sum of the entry and exit points is known, the angle between the flight segment and the center of the earth can be known by using the great circle flight principle as follows (4.1):

$$\cos \theta = \sin \lambda_\alpha \sin \lambda_\beta + \cos \lambda_\alpha \cos \lambda_\beta \cos (\varphi_\beta - \varphi_\alpha) \tag{4.1}$$

From the included angle of the flight segment at the center of the earth, the spherical distance of the flight segment can be calculated as follows (4.2):

$$D = R \cdot \arccos \theta \tag{4.2}$$

Among them,  $R$  is the radius of the earth, which is 6,371,000 meters.

According to the distance formula, the great circle and the distance between any two entry and exit points can be calculated. Next, according to the sector horizontal boundary, all sector edges in FERA-WoC are numbered, as shown in Figure 4.2, the boundary information is stored in the set. The FERA-WoC boundary (ie, the east-west boundary and the national border) is numbered as 1 and does not participate in clustering.

According to the great circle function and sector edge information, the intersection of the great circle between the entry and exit points of FERA-WoC and the boundary of each sector can be obtained, see Figure 4.3, that is, the sector boundary point, and the position information of the boundary point is stored in the set. The number of intersection points of each sector boundary is shown in Table 4.2.

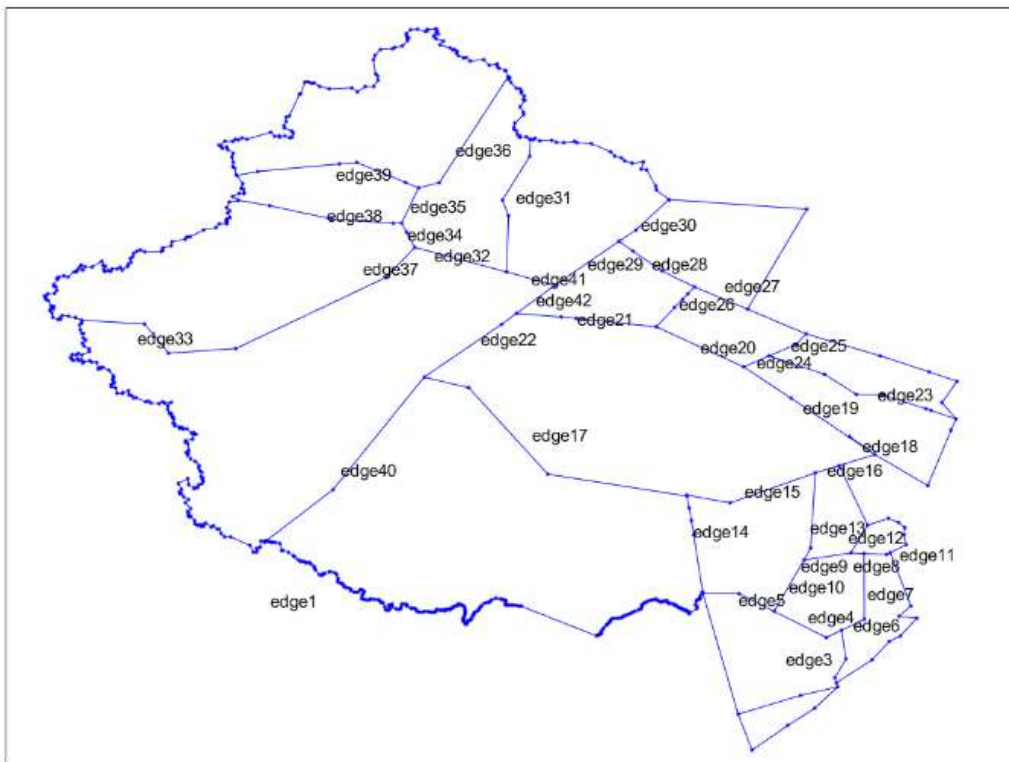


Figure 4.2 Sector boundary numbers in the FERA-WoC



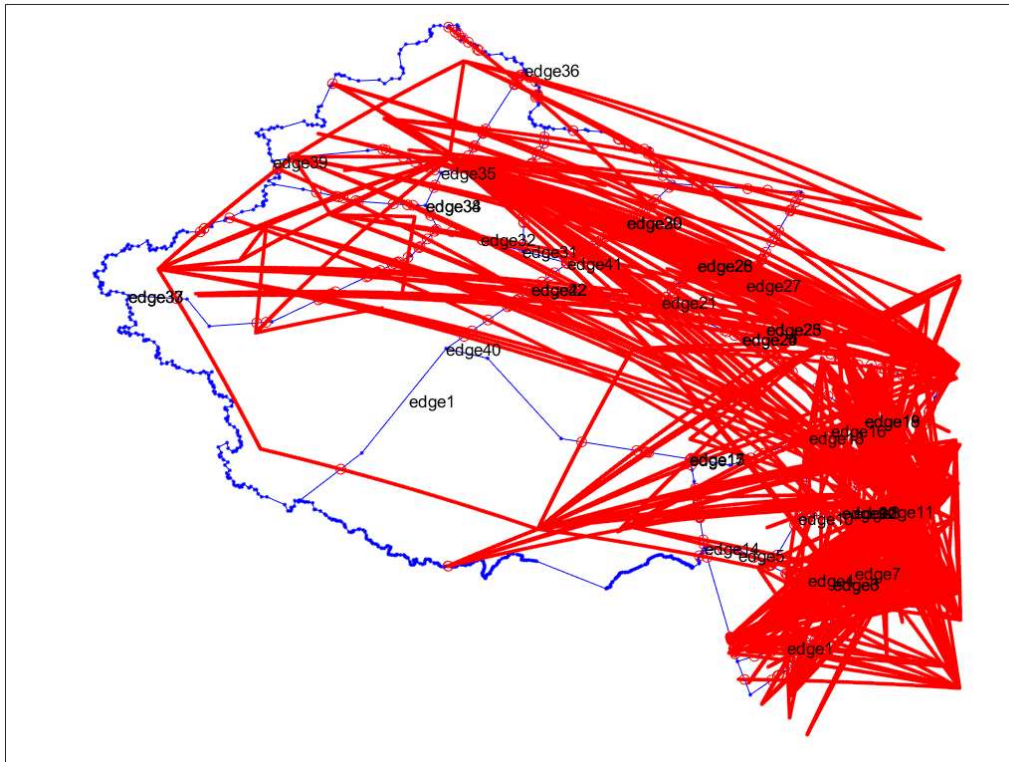


Figure 4.3 The intersections of the planned great circle paths and the sector boundaries

Table 4.2 Number of intersections of planned paths with sector boundaries

Edge number	2	3	4	5	6	7	8	9	10	11	12	13	14	15
Number of intersections	36	112	109	8	27	122	7	22	15	48	45	81	36	64
Edge number	16	17	18	19	20	21	22	23	24	25	26	27	28	29
Number of intersections	18	12	42	71	23	48	31	120	15	37	44	8	33	103
Edge number	30	31	32	33	34	35	36	37	38	39	40	41	42	
Number of intersections	137	252	12	44	6	8	227	44	19	40	2	2	11	

### 5.1.3.4 COLLABORATIVE PLANNING OF MULTI-SECTOR ENTRY AND EXIT POINTS

#### 1) Decision variables

The number of intersections between the great circle and the sector boundary is large and most of the intersections are close in space. Considering the trade-off between flexibility, economy, and airspace situational complexity in trajectory-based operations, this section conducts a collaborative optimization of the number and layout of multi-sector boundary points within FERA-WoC. The number of boundary points on the corresponding edge is introduced as an integer decision variable.

#### 2) Objective function

To maintain a high level of efficiency after clustering the entry and exit points of the sector, the model optimization goal is to connect the sector boundary points after clustering optimization in turn to form the shortest total distance of the trajectory. Among them, the great circle is still used for horizontal path planning between adjacent boundary points.

#### 3) Algorithm flow

##### (1) Overall process

Based on the distribution of the intersection points between the great circle and the sector boundary, the spatial position clustering is performed according to the latitude and longitude data of each intersection point to form a reasonable number of sector boundary points; The initial great circle determines the sector boundary points that the flight passes through, that is, the new trajectory after sector boundary points are clustered. The optimized trajectory fully considers the short trajectory distance and the rationality of sector boundary point layout. The specific implementation steps are as follows<sup>[27]</sup>:

- According to the flight plan and pilot plan report, obtain the entry and exit points of each flight  $j$  in the FERA-WoC in the flight set  $F_j$ ;
- Plan the great circle of each flight between the entry and exit points;
- Find the intersection of each great circle and the sector boundary, and store it in the set;
- Using the nested clustering optimization algorithm to optimize the number and layout of sector boundary points;
- Determine the optimized horizontal flight trajectory and flight distance according to the corresponding relationship between the flight and the cluster center of the sector boundary intersection.

##### (2) Solution algorithm

In the above optimization process, the boundary points of the sector are firstly clustered, and then the total flight distance of the flight after clustering is

calculated, and the balance point between the number of clusters and the flight distance is obtained in the iterative solution. Aiming at the mutual coupling effect of sector boundary point layout, an algorithm framework with nested structure as the core is proposed, and a heuristic algorithm of nested clustering is designed. First, the K-Means clustering algorithm is embedded in the genetic algorithm to continuously generate the solution of the number of sector boundary points; then, the good global search ability of the genetic algorithm and the law of imitating natural selection to preserve the excellent individuals are used to control the iterative process; finally, Taking the reciprocal of the total great circle distance as the fitness value of the genetic algorithm, and considering the pros and cons of the solution based on this, the synchronous optimization of the number of boundary points on all boundaries of the sector is realized.

#### ① K-Means clustering algorithm

In this section, the K-means algorithm is used to cluster the entry and exit points of the sector. The core is to use the intersection of the initial great circle and the sector boundary as the sample, and the Euclidean distance as the similarity measure between the data samples, so as to cluster all the samples into K clusters, so that the similarity of the samples within the cluster is the highest, and the similarity of the samples between the clusters is the lowest, and the center point of each cluster is obtained as the candidate entry and exit points<sup>[28]</sup>.

The basis of the K-means algorithm is to determine the K value. This section adopts the elbow method to determine the optimal K value to ensure the effectiveness of the clustering. The core of the elbow method is to calculate the sum of squares SSE (The Sum of Squares due to Error) under different numbers of clusters. There are three sums of squares, namely: the sum of squares of total errors, SSE, and the sum of squares of errors between clusters SSB. The elbow method used in this chapter stipulates that the number of clusters corresponding to the ratio of SSB to SSE of 90% is the optimal K value, and the squared error SSE represents the clustering error of the sample, indicating the quality of the clustering effect. SSE is the sum of SSB and SSW. As the number of clusters K increases, the sample division will become more and more refined, the degree of aggregation of each cluster will gradually increase, SSW will gradually decrease, and the ratio of SSB to SSE will gradually increase. When K is less than the real number of clusters, since the increase of K will greatly increase the degree of aggregation of each cluster, the decline of SSW will be large, and the ratio of SSB to SSE will also increase greatly; when K reaches the real clustering, the value of K is increased, the return on the degree of aggregation obtained by increasing the value of K will quickly become smaller, so the decline of SSW will decrease sharply, and it will become flat as the value of K continues to increase. Therefore, the relationship between the ratio of SSB to SSE and the K value is like an elbow, and the K value corresponding to the elbow is the most obvious turning point, that is, the number

of clusters with the largest aggregation degree return. The SSE calculation formula is as followed (4.3) :

$$SSE = \sum_{i=1}^N |x_i - \bar{x}|^2 \quad (4.3)$$

Among them,  $x_i$  is the sample point,  $\bar{x}$  is the center point of the entire data set.

The formula for calculating SSW is as follows (4.4):

$$SSW = \sum_{j=1}^k \sum_{x \in C_j} |x - \bar{x}_j|^2 \quad (4.4)$$

Among them,  $C_j$  represents the  $j$ th cluster;  $x$  is the sample point in  $C_j$ ;  $\bar{x}_j$  is the cluster center of  $C_j$ ;  $k$  is the number of clusters.

The formula for calculating the SSE between groups is as follows (4.5):

$$SSB = \sum_{j=1}^k |\bar{x}_j - \bar{x}|^2 n_j \quad (4.5)$$

Among them,  $n_j$  is the number of sample points of the  $j$ th cluster, and  $\bar{x}$  is the center point of the entire data set.

## ② Genetic algorithm

Genetic algorithm is a kind of heuristic algorithm, which can usually get the result approaching the optimal solution relatively quickly when solving complex problems. For the optimal planning of entry and exit points in flexible airspace, the algorithm implementation steps are as follows:

- *Chromosome coding.* The number of boundary points in each sector is taken as an individual, and a certain margin is added to the optimal K value determined by the elbow method and is set as the upper bound of the independent variable, which balances the solution efficiency and the result optimization degree to a certain extent.
- *Generate the initial population.* The population size is set to 200, and the number of initial sector boundary points is randomly generated according to the intersection of the great circle between all entry and exit points passing through the flexible route airspace and the sides of the sector.
- *Design a fitness function.* The original problem is a minimization problem, and the objective function is that the total distance of the trajectory formed by sequentially connecting the cluster-optimized sector boundary points along the great circle is the shortest. Therefore, the following

formula (4.6) is selected to represent the individual fitness evaluation function:

$$Fit = (f(N_i))^{-1} \tag{4.6}$$

Among them, *Fit* is the fitness function and  $f(N_i)$  is the objective function.

- *Genetic operators.* After the parent population is generated, the offspring population is obtained by mutation and crossover. The genetic algorithm control parameter settings are shown in Table 4.3.

Table 4.3 Nested clustering genetic algorithm parameter settings

parameter value	Value
Population size	200
Terminate Evolution Algebra	200
Crossover probability	0.8
Mutation probability	0.1
Variation mode	Random factor variation

- *Termination condition.* When the size of the evolutionary algebra in the genetic algorithm is equal to that of the termination evolutionary algebra, the iterative process is ended and the optimal layout of entry and exit points is obtained; otherwise, the genetic operation is continued.

### ③ Genetic Algorithm for Nested Clustering

In view of the complexity of this problem, it is difficult to solve it efficiently by using clustering and optimization methods alone. Therefore, combining the advantages of K-Means and genetic algorithm, an optimization algorithm for nested clustering is designed. First, calculate the optimal number of clusters according to the elbow method, and add a certain margin on this basis as the optimization space of each variable; then use the K-Means clustering algorithm to generate the initial number of clusters and layout. The result is fed back to the outer genetic algorithm. After calculating the total distance of the great circle, the genetic algorithm uses the result of the next generation of individuals as the input of the inner K-Means algorithm, and the objective function is the clustering of the inner layer. The algorithm and the outer layer of the genetic algorithm achieve the optimality in the continuous feedback. The specific steps of the algorithm are shown in Fig 4.4.

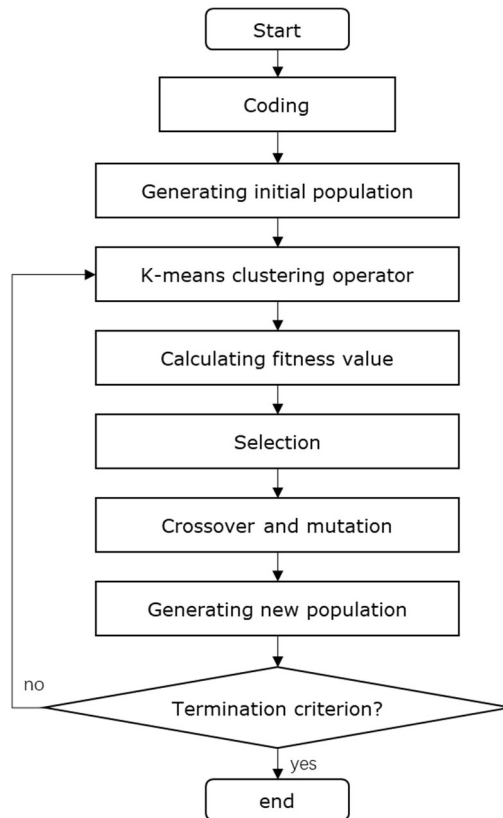
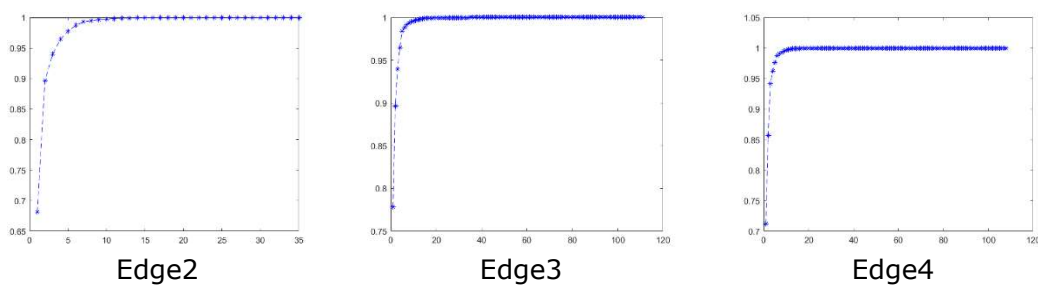
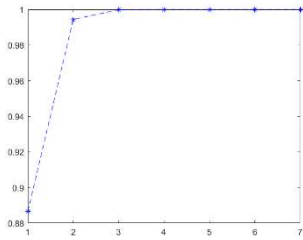


Figure 4.4 Flowchart of Nested Clustering Genetic Algorithm

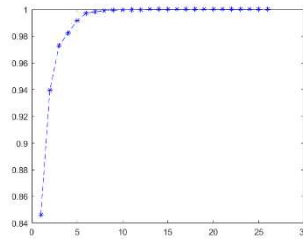
#### 4) Result analysis

First, based on the K-means algorithm, in order to obtain the optimal number of clusters for each edge, plot the relationship between the ratio of the sum of squared errors and the number of clusters, as shown in Figure 4.5. Specifically, taking edge 41 as an example, with the increase of the number of clusters K, the ratio of the sum of squares of the error shows an upward trend; when the value of K is 1~4, the ratio of the sum of squares of the error increases sharply; when the value of K exceeds 4, the squared error and SSE ratio are basically stable. To sum up, the optimal K value of edge 41 is determined to be 4 based on the elbow method. The optimal K values for all sector boundaries are shown in Table 4.4. In order to increase the search solution space, a certain margin is added on the basis of the optimal K value as the upper limit of the iteration of the independent variable. The upper limit of all sector boundary points is shown in Table 4.4.

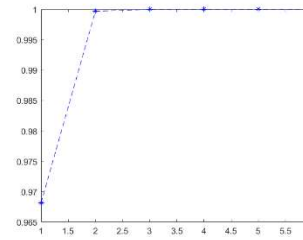




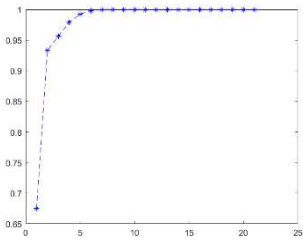
Edge5



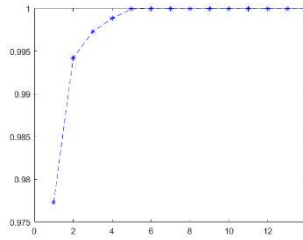
Edge6



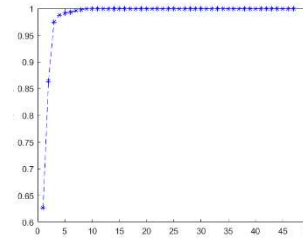
Edge8



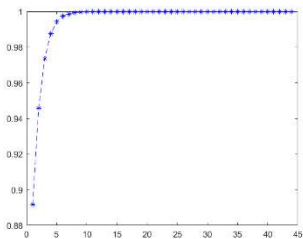
Edge9



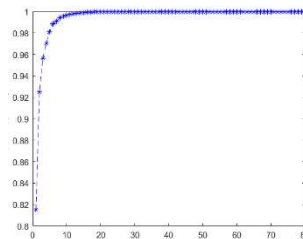
Edge 10



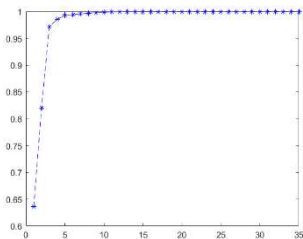
Edge 11



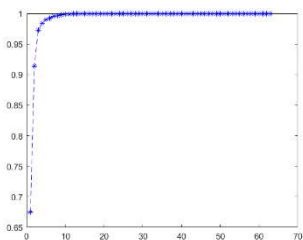
Edge 12



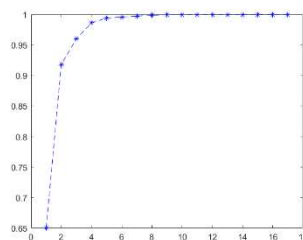
Edge 13



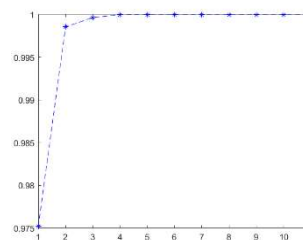
Edge 14



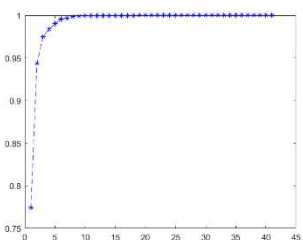
Edge 15



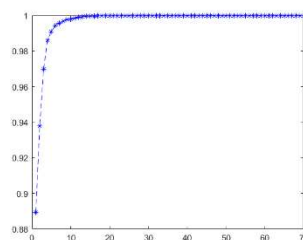
Edge 16



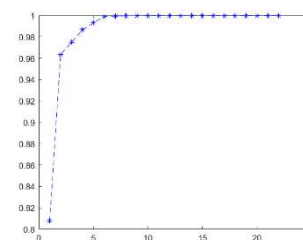
Edge 17



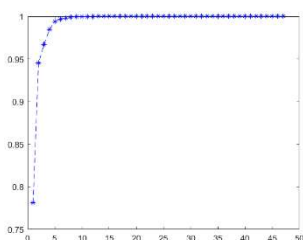
Edge 18



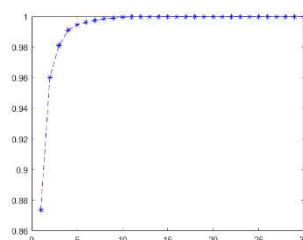
Edge 19



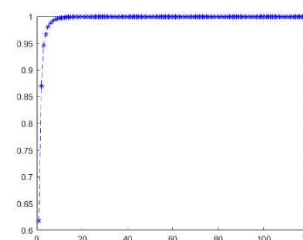
Edge 20



Edge 21



Edge 22



Edge 23

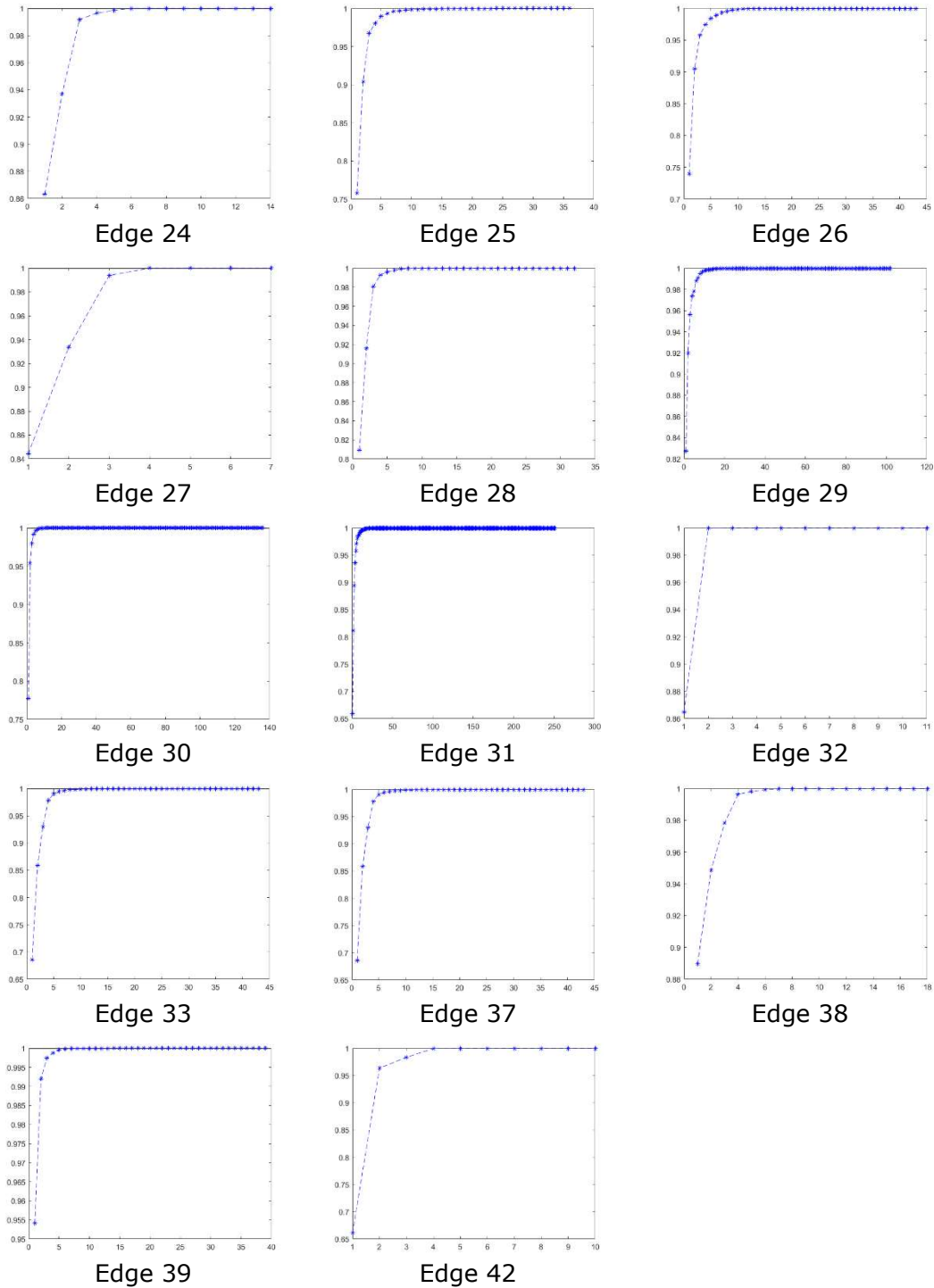


Figure 4.5 Relationship between the number of clusters of sector boundary points(x axis) and the ratio of SSE(y axis)

Table 4.4 Optimal number of clusters and the upper limit of the boundary points of each sector

Edge Number	2	3	4	5	6	7	8	9	10	11	12	13	14	15
-------------	---	---	---	---	---	---	---	---	----	----	----	----	----	----



Optimal number of clusters	6	8	7	3	5	28	2	5	4	6	6	8	5	6
Upper limit of cluster number	8	10	9	5	7	30	4	7	6	8	8	10	7	8
Edge Number	16	17	18	19	20	21	22	23	24	25	26	27	28	29
Optimal number of clusters	4	3	6	9	5	5	6	8	4	6	7	3	5	9
Upper limit of cluster number	6	5	8	11	7	7	8	10	6	8	9	5	7	11
Edge Number	30	31	32	33	34	35	36	37	38	39	40	41	42	
Optimal number of clusters	6	15	3	6	2	2	6	6	4	4	1	1	4	
Upper limit of cluster number	8	17	5	8	1	1	6	8	6	6	1	1	6	

The clustering upper limit is substituted into the genetic algorithm, and the model is solved based on the aforementioned nested clustering optimization algorithm. Experiments show that when the evolutionary generation of the population continues to increase, the individuals continue to approach the optimal direction. As shown in Figure 4.6, the total distance of the great circle based on boundary point constraints rapidly decreases to  $9.018257 \times 10^8$  meters within 15 generations stabilized after the 80th.

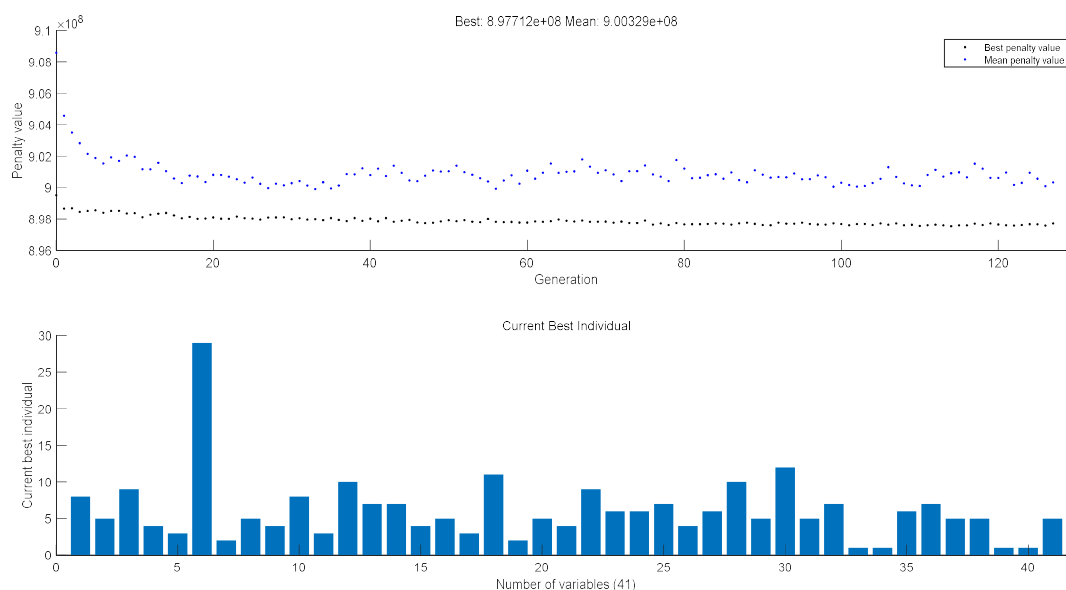


Figure 4.6 Iterative process of nested clustering genetic algorithm

The final results are shown in Table 4.5, the final objective function value is  $8.977427 \times 10^8$  meters. Figure 4.7 shows the airspace structure of flexible routes, including airspace information such as sector boundaries, sector entry and exit points, waypoints, and national border points.

Table 4.5 The number of sector boundary points after clustering optimization

Edge Number	2	3	4	5	6	7	8	9	10	11	12	13	14	15
Optimal number of points	8	5	9	4	3	29	2	5	4	8	3	10	7	7
Edge Number	16	17	18	19	20	21	22	23	24	25	26	27	28	29
Optimal number of points	4	5	3	11	2	5	4	9	6	6	7	4	6	10
Edge Number	30	31	32	33	34	35	36	37	38	39	40	41	42	
Optimal number of points	5	12	5	7	1	1	6	7	5	5	1	1	5	

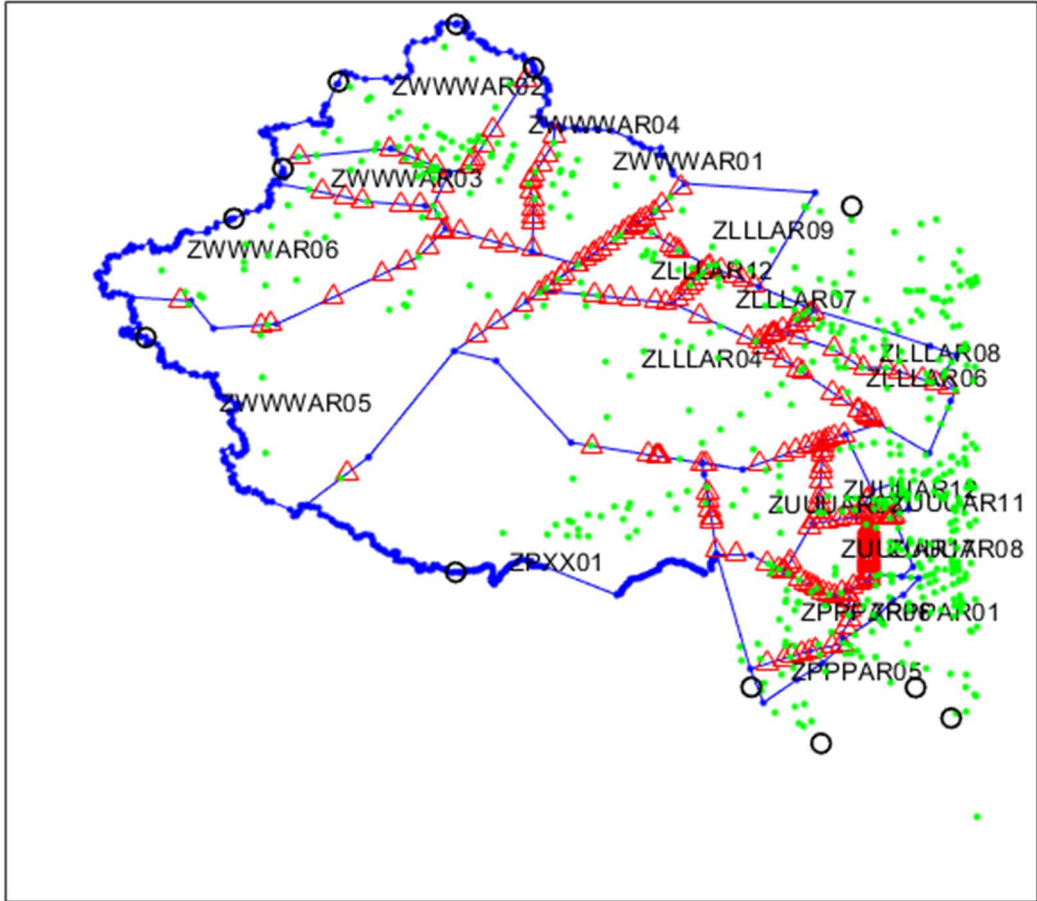


Figure 4.7 The new layout of route points in the FERA-WoC

The total length of the great circle (L1), the total length of the trajectory based on the sector boundary point planning (L2) and the total length of the trajectory based on the fixed routes currently in use (L3) were calculated respectively, as shown in Table 4.6. The influence of sector boundary point planning on horizontal trajectory efficiency is evaluated. Among them, after clustering the sector boundary points, the total flight distance of the flight was shortened by 6.10% compared with the fixed route airspace, and increased by 0.081615% compared with the ideal great circle.

Table 4.6 Horizontal trajectory efficiency in different types of airspace

Airspace type	Trajectory length ( $\times 10^8$ m)
Free airspace-Great circle (L1)	8.970106
Flexible route airspace- Trajectory based on planned sector points (L2)	8.977427
Structured airspace- trajectory along fixed routed (L3)	9.560033

Taking the planned route from Guangzhou Baiyun Airport to Amsterdam Schiphol Airport as an example. Figure 4.8 shows two optional routes in the current structured airspace, Figure 4.9 is the great circle between the entry and exit points in FERA-WoC, and the Figure 4.10 is The flight path after sector boundary point clustering. The length of the great circle with SARIN as the national boundary point is 3,030,943 meters, and the length of the trajectory in the full-structured airspace is 3,335,764 meters. The trajectory length after sector boundary point planning is 3,094,343 meters, which is 7.24% shorter than that in the full-structured airspace., with an increase of 2.10% over the length of the great circle.

To sum up, the collaborative optimization method for the layout of sector boundary points in the western flexible route airspace proposed in this section can effectively balance the number of boundary points and horizontal trajectory efficiency, and can provide a method for flexible route airspace and flight trajectory planning under the same sector configuration. The entry and exit points of the sectors generated in this section will also provide “sample” sectors for the subsequent modeling of complexity indicators, especially the complexity-based sector capacity (i.e., control workload) experiments.

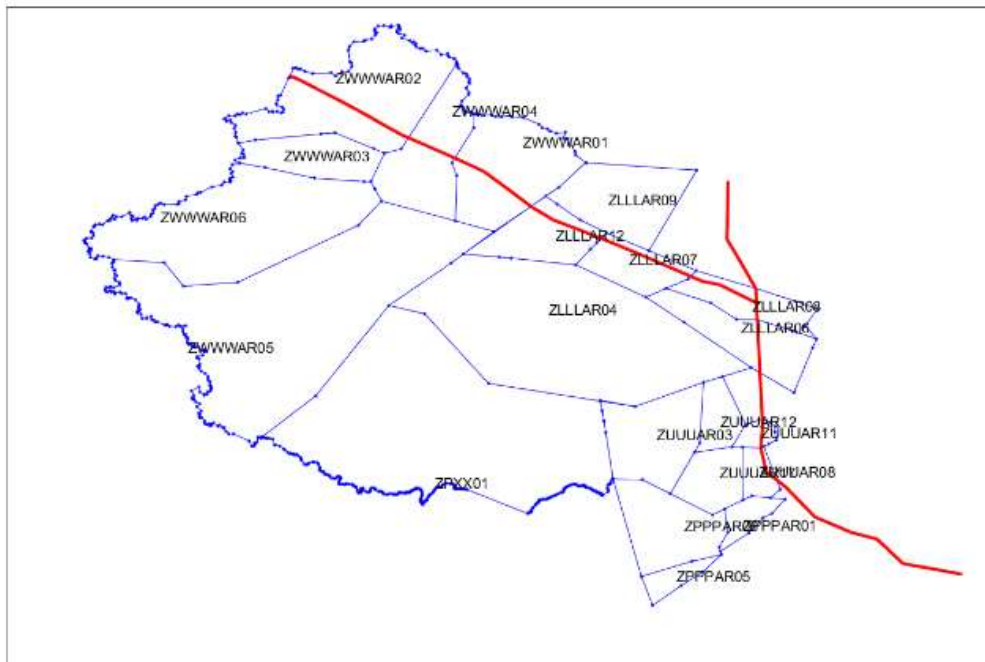


Figure 4.8 The flight path from Guangzhou to Amsterdam in structured airspace

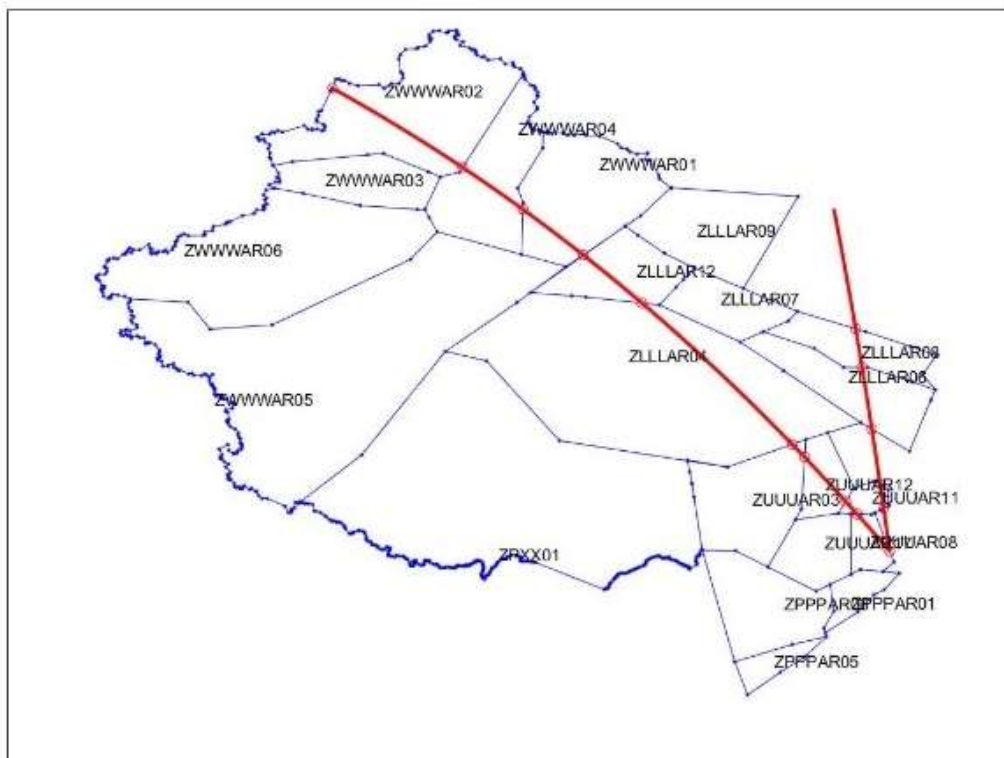


Figure 4.9 The great circle flight path from Guangzhou to Amsterdam

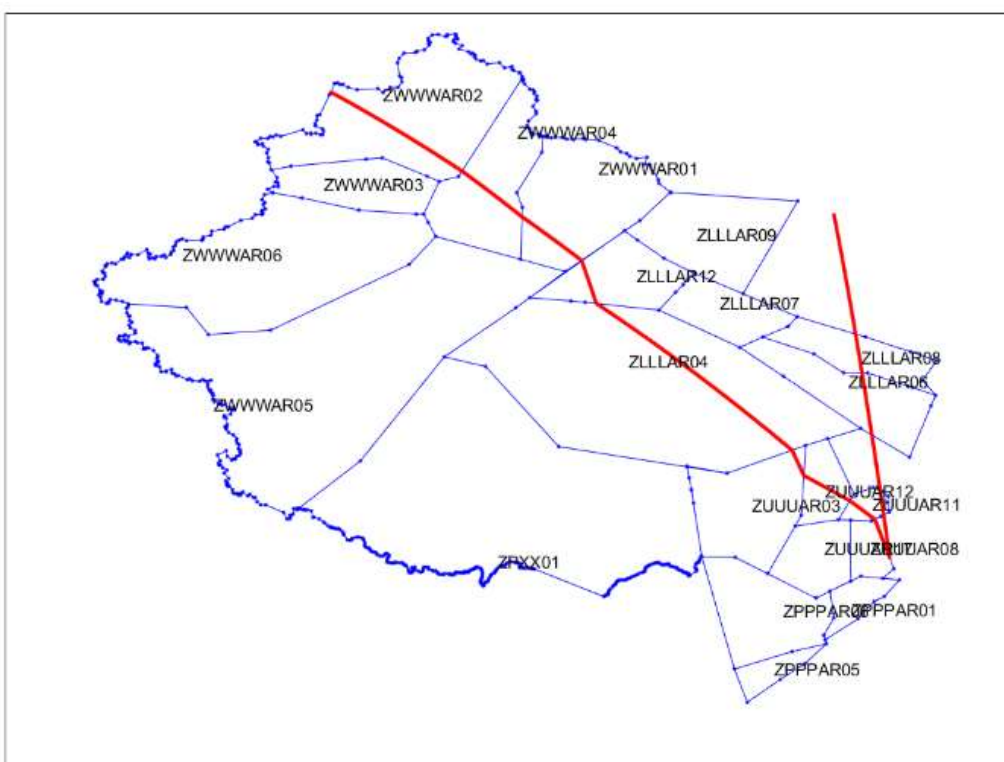


Figure 4.10 The flight path from Guangzhou to Amsterdam based on the constraints of planned sector boundary points

## 5.2. OPTIMAL RECONFIGURATION OF FERA SECTORS ADAPTING TO TIME-VARYING DEMAND

This section firstly establishes the FERA sectors dynamic configuration model, then uses the Binary Space Partition (BSP) algorithm and the A\*-based sector boundary tuning algorithm for sectors configuration, and finally takes Lanzhou en-route airspace as an example for sectors dynamic configuration experiment to verify the feasibility and effectiveness of the proposed method.

### 5.2.1. DYNAMIC CONFIGURATION MODEL OF FERA SECTORS

#### 1) Objective Function

The control workload of each sector in the airspace should be balanced as much as possible to ensure the maximum utilization of airspace resources. Therefore, the primary objective of dynamic configuration of FERA sectors is to balance the workload of each sector. For simplification, we assume that the subjective characteristics (e.g., acceptable workload threshold) of air traffic controllers are homogeneous. The objective function should be:

$$D = \min \sqrt{\frac{1}{M} \sum_{m=1}^M (W_m - \bar{W})^2} \quad (4.7)$$

where  $W_m$  is the ATC workload for the  $m$ th sector,  $\bar{W}$  is the average ATC workload of all sectors,  $M$  is the number of sectors,  $D$  is the degree of balance of workload.

In addition, it is necessary to try to ensure that the sector coordination load in the airspace is minimized, i.e., the number of aircraft crossing the sector boundaries is minimized at time  $T = [t_0, t_1]$ .

#### 2) Constraints

In the process of dynamic configuration of FERA sectors, the influence of the route structure, sector shape, and restricted area on the geometric boundary of the sector needs to be considered to ensure the flight safety of aircraft and reduce the difficulty of sector control.

In this paper, sector boundary optimization is required to satisfy the following constraints:

Convex constraint of the sector

Aircraft should avoid crossing the same sector two or more times during a flight. Convex constraints can ensure that aircraft do not repeatedly enter and exit the sector leading to increased sector coordination handover load. Concave boundaries are not unacceptable for all cases, as long as the sector boundary optimization does not cause traffic flow to enter the same sector twice or more.

Let the sequence of vertices of the sector be  $p_1, p_2, \dots, p_k, \dots, p_n$  counterclockwise ( $p_1 = p_n$ ) and the  $k$ th boundary be  $p_k p_{k+1}$ ;  $c_{hk}$  indicates whether route  $h$  intersects with the  $k$ th boundary,  $c_{hk} = 1$  indicates intersection, and  $c_{hk} = 0$  indicates disjunction or tangency. Defining  $C_h$  as the number of intersections of route  $h$  with the sector boundary, and  $C_h$  should be less than  $C_0$ , then:

$$C_h = \sum_{k=1}^{n-1} c_{hk}, C_h \leq C_0 \quad (4.8)$$

(b) Sector minimum flight time constraint

Flights in the sector receive the ATC services, including the transmission of control instructions and the monitoring of the proper execution of flight maneuvers. In addition, entering and exiting the sector involves the execution of handover tasks. If the flight time of aircraft in the sector is too short, it will inevitably lead to frequent control handover actions, which is not conducive to the establishment of situation awareness and maybe detrimental to flight safety. It is mathematically expressed as:

$$T_{flight \min} \geq 2t_{transfer} \quad (4.9)$$

where  $T_{flight \min}$  is the minimum value of the flight time of the aircraft in the sector and  $t_{transfer}$  is the time required for a single control transfer act to be executed.

(c) Safety distance constraint from the route intersection to the sector boundary

There are potential flight conflicts at the route intersection, which require a high concentration of ATCos for command. At the sector boundary, the aircraft handover work generates a large control handover load for ATC. Therefore, the proximity of the route intersection to the sector boundary is likely to lead to chaotic control behavior and increased workload. Define  $d_i$  as the shortest distance from the  $i$ th intersection to the sector boundaries,  $d_{\min}$  denotes the minimum value of the distance from the  $m$  intersections to the sector boundaries and should be larger than the specified value  $d_0$ . Then:

$$d_{\min} = \min\{d_1, d_2, \dots, d_i, \dots, d_m\}, d_{\min} > d_0 \quad (4.10)$$

(d) Crossing angle constraint between the route and the sector boundary

There is a left-right offset for aircraft flying along the route, and if the angle between the route and the sector boundary is too small, it will lead to an unclear distribution of control responsibilities at the sector boundary and higher possibility of aircraft flying out of the boundary. Let  $\theta_{ij}$  denote the angle of the  $i$ th flight segment when it crosses the  $j$ th sector boundary,  $\theta_0$  denote the minimum constraint value of the route crossing angle, the cross angle  $\theta$  between the flight path and the sector boundary needs to satisfy the following condition:

$$\theta = \begin{cases} \theta_{ij}, 0 \leq \theta_{ij} \leq \frac{\pi}{2} \\ \pi - \theta_{ij}, \frac{\pi}{2} < \theta_{ij} \leq \pi \end{cases}, \theta_0 \leq \theta \leq \frac{\pi}{2} \quad (4.11)$$

(e) Constraint on the location of sector boundary and restricted area

The location of the restricted area should be taken into account in dynamic configuration of sectors. The ideal result in placing the restricted area inside the sector and at a sufficient distance from the sector boundary. In this paper, it is specified that the sector boundary cannot cross the inside or edge of the restricted area.

Let the sequence of vertices of the restricted area be  $r_1, r_2, \dots, r_k, \dots, r_n$  counterclockwise ( $r_1 = r_n$ ) and the  $k$ th boundary be  $r_k r_{k+1}$ ;  $g_{bk}$  denotes whether the sector boundary  $b$  intersects with the  $k$ th boundary of the restricted area,  $g_{bk} = 1$  denotes intersecting or tangent, and  $g_{bk} = 0$  denotes not intersecting.

Define  $G_b$  as the number of intersection points between the sector boundary  $b$  and the boundaries of the restricted area, then:

$$G_b = \sum_{k=1}^{n-1} g_{bk} = 0 \quad (4.12)$$

(f) Sector horizontal and vertical scale constraint

The horizontal-to-vertical ratio is the ratio of the short side to the long side of the minimum external rectangle of the sector boundary, which reflects the similarity between the sector shape and the square, and the horizontal-to-vertical ratio constraint can avoid too short flight time and frequent control handover of the sector. Let  $\gamma$  be the ratio of the short side to the long side of the minimum external



rectangle of the sector, and  $\gamma_0$  be the minimum horizontal to vertical ratio of the sector, then:

$$\gamma \geq \gamma_0 \quad (4.13)$$

### 5.2.2. DYNAMIC PARTITIONING ALGORITHM OF FERA SECTORS

Binary Space Partition (BSP) is a heuristic space partitioning method, which is based on the idea that any plane can partition space into two half-spaces. In a two-dimensional plane, any line can partition that plane into two half-planes. For the airspace, the BSP algorithm will select different partition lines to gradually subdivide it into smaller subspaces.

In this paper, the specific steps for BSP to partition the airspace are as follows:

(a) Discrete the airspace boundaries

First, the shortest side of the target polygon is divided into 2~8 equal parts to obtain the shorter basic segments. Then, the length of each side of the polygon is the numerator and the length of the basic segment is the denominator, and the fractions are rounded down to get the number of segments corresponding to each side. Finally, each side is divided equally according to the corresponding number of segments, and the vertices of each segment are the discrete points of the boundaries of the null field.

(b) Obtain the set of partition lines

The discrete points located on different boundaries are combined in pairs to form the set of partition lines  $\{l_1, l_2, \dots, l_i, \dots\}$ .

(c) Select the partition line to divide the airspace

Select the partition line to divide the target space in turn, and judge whether the selected partition line satisfies each constraint of the sector boundary optimization. If meet, save this feasible partition line and subspaces; if not, delete it.

(d) Select the optimal partition line

Calculate the workload for the subspaces delineated by all feasible partition lines above, prioritizing the line whose subspaces load does not exceed the threshold, and selecting the line with the most balanced load. If there is more than one line with the most balanced load, the line with the most balanced subspace area is selected as the optimal one.

(e) Determine whether the number of subspaces is the same as before

After obtaining the optimal partition line and its delineated subspaces, determine whether the number of subspaces is the same as the original number of sectors. If

the number is insufficient, select the airspace with the largest load as the target airspace and repeat the above steps (a) to (d) to continue the division until the number of subspaces is the same as before.

The algorithm flowchart is shown in Figure 4.11.

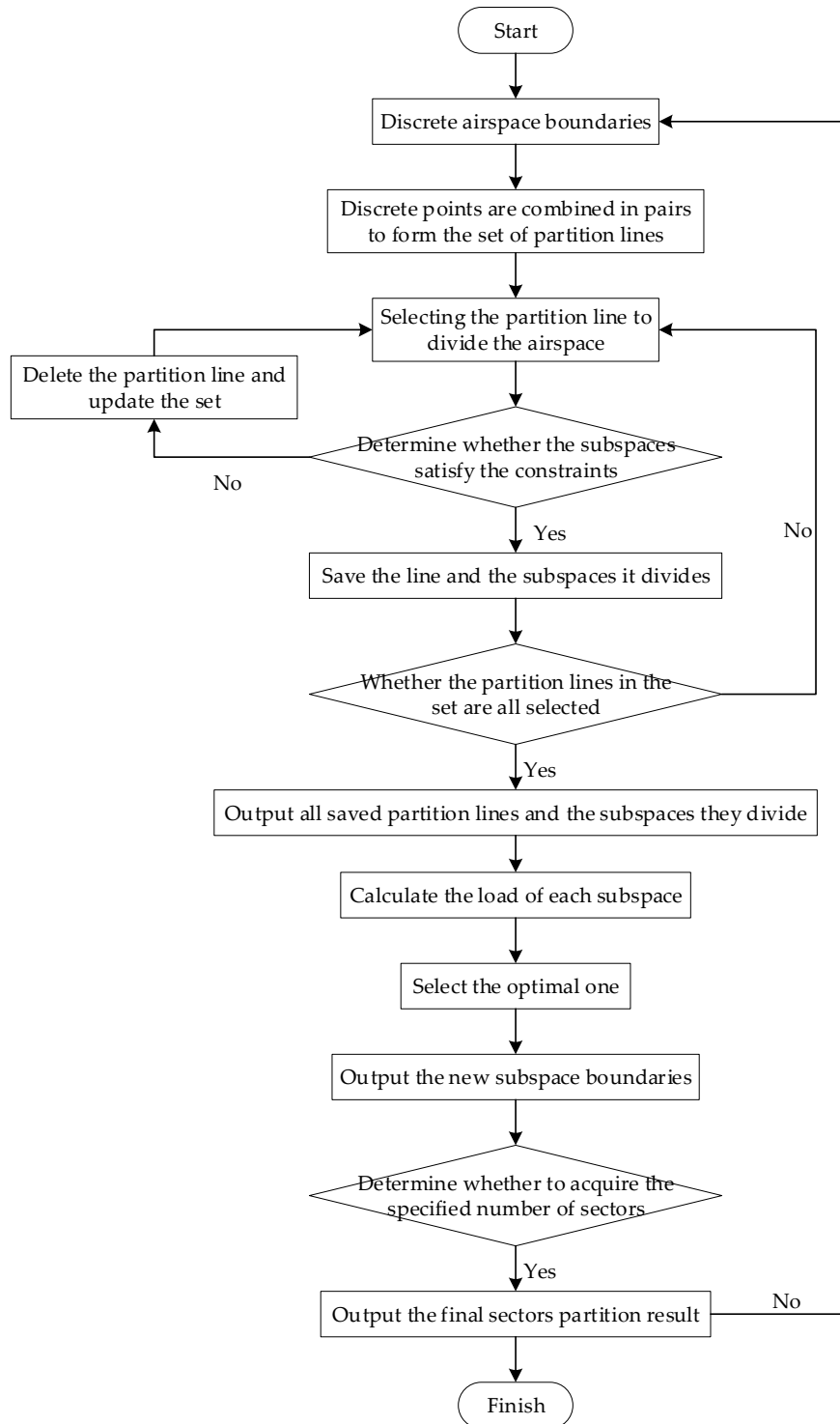


Figure 4.11 BSP algorithm flow chart.

### 5.2.3. SECTOR BOUNDARY OPTIMIZATION ALGORITHM

In order to facilitate control of aircraft operations, all the optimal partition lines obtained above will be tuned. The objectives of the optimization process are twofold:

- (a) Keeping the endpoint unchanged, the optimized line needs to connect as many waypoints as possible in the vicinity of the original partition line;
- (b) The optimized line is as similar as possible to the original partition line.

In this paper, we use the A\*-based heuristic algorithm, which employs a modified line segment Hausdorff distance (MLHD) to measure the similarity between line segments to calculate the valuation function to seek the optimal partition line setting scheme.

Chen et al. introduced a MLHD calculation method, which consists of three types of distances: angle distance, vertical and parallel distance, and compensation distance. In this paper, the three distances are calculated as follows:

- (a) Angle distance

As shown in Figure 4.12, let  $d_{\theta}(m_i, n_j)$  be the angle distance between the original line segment  $m_i$  and the new line segment  $n_j$ , then

$$d_{\theta}(m_i, n_j) = \min(l_{m_i}, l_{n_j}) \times \sin \theta_{(m_i, n_j)} \tag{4.14}$$

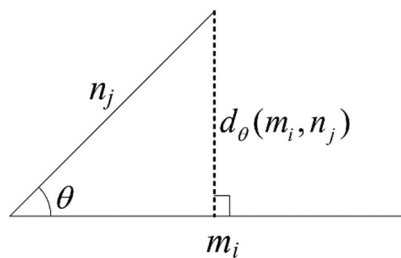


Figure 4.12 Angle distance illustration.

- (b) Vertical and parallel distance

Rotate the shorter of the original line segment  $m_i$  and the new line segment  $n_j$  around its midpoint until it is parallel to the other one. As in Figure 4.13, let  $d_{\perp}(m_i, n_j)$  be the vertical distance and  $d_{\square}(m_i, n_j)$  the parallel distance, then

$$d_{\perp}(m_i, n_j) = \begin{cases} l_{\perp}, l_{n_j} \geq l_{m_i} \\ \frac{l_{n_j}}{l_{m_i}} \times l_{\perp}, l_{n_j} < l_{m_i} \end{cases} \quad (4.15)$$

$$d_{\square}(m_i, n_j) = \min(l_{\square 1}, l_{\square 2}) \quad (4.16)$$

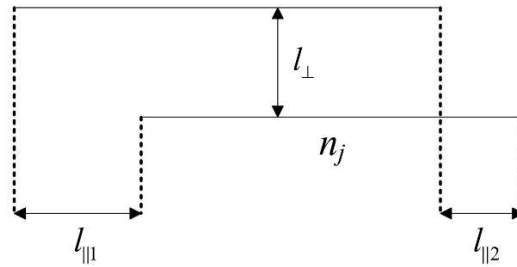


Figure 4.13 Vertical distance, parallel distance illustration.

(c) Compensation distance

Let  $d_S(m_i, n_j)$  be the compensating distance between the two line segments, then

$$d_S(m_i, n_j) = \begin{cases} l_{m_i} - l_{n_j}, l_{n_j} \leq l_{m_i} \\ 0, l_{n_j} > l_{m_i} \end{cases} \quad (4.17)$$

After calculating the above three distances, the MLHD of the original line segment  $m_i$  and the new line segment  $n_j$  is

$$d(m_i, n_j) = d_{\theta}(m_i, n_j) + d_{\perp}(m_i, n_j) + d_{\square}(m_i, n_j) + d_S(m_i, n_j) \quad (4.18)$$

For the optimization of the partition line, the two endpoints of the line can be considered as the starting point and the ending point. Referring to the A\* algorithm to find the connectable waypoints and known route entry/exit points, the steps are as follows:

(a) Filter connectable waypoints and known entry/exit points

Make two straight lines perpendicular to the partition line at the two endpoints, the waypoints and known entry/exit points within the range of the two straight lines are the connectable points.

(b) Make the projections of each point on the original partition line

Make the vertical line of the original partition line across the points, and the foot of each vertical is the projection.

(c) Number the points

The points are numbered (1,2,3, ...) according to the distance from each projection point to the starting point, from near to far. During the wayfinding process, only the points with larger numbers will be searched.

(d) Set the valuation function

Referring to the A\* algorithm, set the valuation function as:

$$f(x) = g(x) + h(x) - \omega \cdot N(x) \quad (4.19)$$

where  $f(x)$  is the valuation function of node  $x$ ,  $g(x)$  is the actual cost from the former node to the present node  $x$ , which in this paper is the MLHD of the former node and the present node  $x$  connected line segment and the segment projection on the original partition line;  $h(x)$  is the estimated cost of the best path from node  $x$  to the target node, which in this paper is the MLHD of the node  $x$  and the target node connected line segment and the segment projection on the original partition line;  $N(x)$  is the number of remaining connectable points after node  $x$ , and  $\omega$  is the weight value.

It is worth noting that since  $g(x)$ ,  $h(x)$ , and  $N(x)$  are of different magnitudes, they need to be subjected to Min-Max Normalization so that the values map between  $[0,1]$ . The conversion function is as follows:

$$\eta' = \frac{\eta - \min(\eta)}{\max(\eta) - \min(\eta)} \quad (4.20)$$

(e) Find the optimal partition line path

According to the above valuation function, find the node with the smallest valuation function value as the path node of the optimal partition line at each step until reaching the target endpoint.

(f) Verify the optimal partition line path

Verify that the path satisfies the constraints of the sector boundary optimization and that subspaces workload does not exceed the threshold. If not, find the optimal line path again by adjusting the weight values in the valuation function.

The algorithm flow is shown in Figure 4.14.

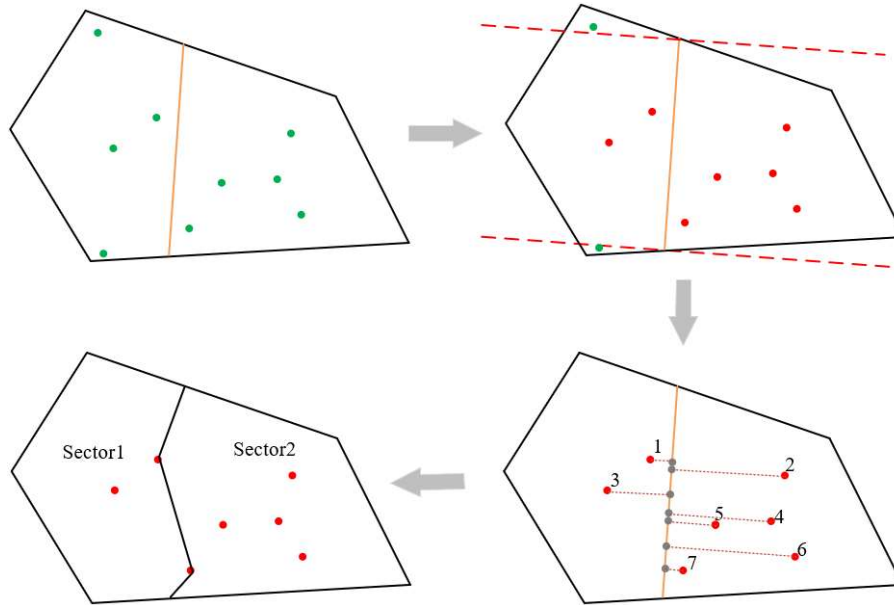


Figure 4.14 A\*-based heuristic algorithm process.

#### 5.2.4. CASE ANALYSIS

This section takes the Lanzhou en-route airspace in China as an example and implements the dynamic configuration of sectors.

##### 5.2.4.1 DESCRIPTION OF THE LANZHOU EN-ROUTE AIRSPACE SCENARIOS AND RELATED PARAMETERS SETTING

The sector data of Lanzhou en-route airspace is collected, mainly including the upper and lower bound of the flight level and the latitude and longitude of the boundary points of each control sector. We also collected the flight trajectory data of Lanzhou en-route airspace from 0:00 to 23:59 on 8 June 2019, which mainly included flight number, track point moment, latitude and longitude coordinates, altitude, angle, airspeed, etc. The location distribution of routes, restricted areas, trajectories, and sector boundaries are shown in Figure 4.15.

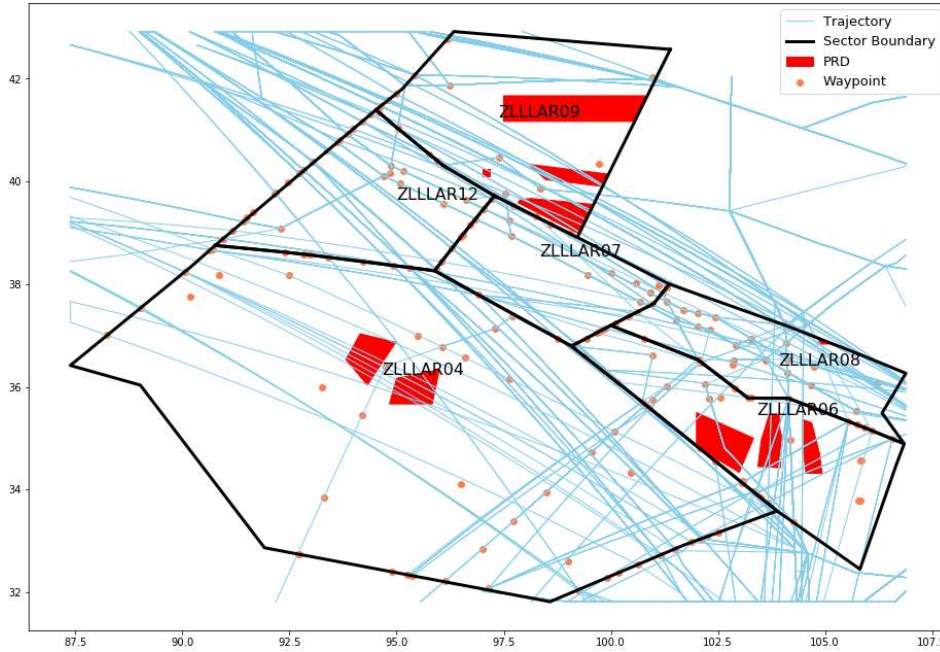


Figure 4.15 Lanzhou en-route airspace scenarios.

The experimental parameters are set as shown in Table 4.7:

Table 4.7 Experimental parameters setting.

Experimental Parameter Name	Value
Maximum number of intersections between the route and the sector boundaries $C_0$	2 pcs
Time required for the execution of a single control transfer $t_{transfer}$	5 min
The shortest distance between the route intersection and the sector boundary $d_0$	10,000 m
Minimum intersection angle between route and sector boundary $\theta_0$	$\frac{\pi}{6}$
Minimum Sector Horizontal-to-vertical Ratio $\gamma_0$	0.3

### 5.2.4.2 ACCURACY VALIDATION OF XGBOOST-BASED WORKLOAD ESTIMATION MODEL

The indicators with lower uncertainty and higher impact were selected to build the ATC workload estimation model: Conflict Intensity (CI), Altitude Variation (AV), Traffic Entry (per ATCO position) (TE), Number of control transfers (CT), Number

of Trajectory Intersection (TI), Airspace uses (AU), Occupancy (per ATCO position) (OC), and The total flight time of the aircraft under ATCO responsibility in the given timeframe (FT).

The data set is divided, and 90% of it is selected as the training set and 10% as the test set. In order to quantitatively analyze and compare the estimation results of the models, the complex correlation coefficient  $R^2$ , Root Mean Square Error (RMSE), and Mean Absolute Error (MAE) were used as indicators to evaluate the performance of the model. The calculation formula is as follows:

$$R^2 = 1 - \frac{\sum_{i=1}^n (x_i - x_p)^2}{\sum_{i=1}^n (x_i - x'_0)^2} \tag{4.21}$$

$$RMSE = \sqrt{\frac{1}{n} \sum_{i=1}^n (x_i - x_p)^2} \tag{4.22}$$

$$MAE = \frac{1}{n} \sum_{i=1}^n |x_i - x_p| \tag{4.23}$$

where  $x$  is the value of the variable (this study refers to ATC workload),  $x_i (i = 1, 2, \dots, n)$  is the actual value of controller workload;  $x'_0$  is the average value of  $x_i$ ;  $x_p$  is the predicted value of  $x_i$ ;  $n$  is the number of samples in the test set.

The evaluation results of estimation error are obtained, as shown in Table 4.8.

Table 4.8. Evaluation results of ATC workload estimation model based on XGBoost.

Evaluation Parameters	Evaluation Result
RMSE	11.16817
MAE	6.80012
$R^2$	0.89597

It can be seen from Table 4.8 that the  $R^2$  of the model is higher, while the MAE and RMSE are smaller, so it has a better effect on the estimation of ATC workload.

The model accuracy of the estimation results and the actual ATC workload error in the range of  $\pm 2$ ,  $\pm 4$ ,  $\pm 6$ ,  $\pm 8$ , and  $\pm 10$  is shown in Table 4.9. It can be seen that within the error range of  $\pm 8$ , the estimation accuracy of the model can reach 94.956%.



Table 4.9. Estimation accuracy of ATC workload.

Error	±2	±4	±6	±8	±10
Accuracy	43.635%	60.447	81.692%	94.956%	96.884%

### 5.2.4.3 DISCUSSION OF RESULTS

According to the ATC workload estimation model, Figure 4.16 shows the workload estimation results of each sector from 10:00 to 15:59 on 8 June 2019.

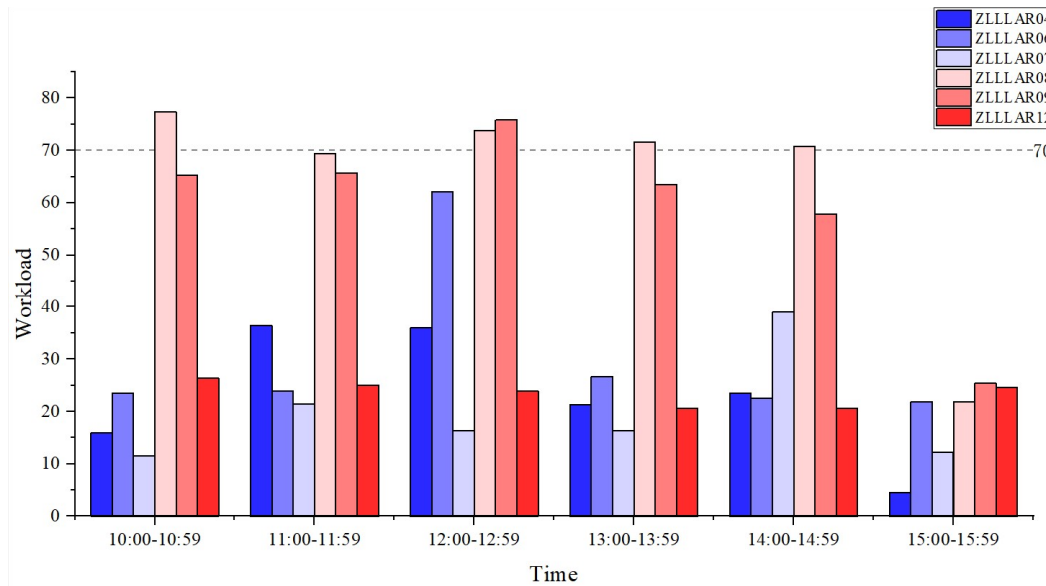


Figure 4.16 Lanzhou en-route airspace 8 June 2019 10:00–15:59 hourly workload forecast results for each sector.

Three time periods, 10:00–11:59, 12:00–13:59, and 14:00–15:59, are selected for the sector partitioning experiment. Setting the sector workload threshold to 70, then in the period 10:00–11:59, ZLLAR08 is overloaded; in the period 12:00–13:59, ZLLAR08 and ZLLAR09 are overloaded; in the period 14:00–15:59, ZLLAR08 is overloaded. The overloaded sectors are combined with their adjacent sectors as the target airspace, and the BSP algorithm is used to partition them in the first stage.

After obtaining the initial partition lines by the one-stage BSP algorithm, the sector boundaries can be further optimized by the A\*-based heuristic algorithm. Figure 4.20 shows the relationship between the number of points connected to all sector partition lines and the weight values for all three time periods. As shown in Figures 4.17-4.19, with the increase of the weight  $\omega$ , the more the number of points connected by the partition lines, the more the waypoints and known entry/exit points within the sector are used. In this way, it is more convenient for the ATC to control the aircraft operation and improve efficiency. The smaller the weight value  $\omega$ , the smaller the number of points connected to the partition line, and the smoother the sector boundaries.

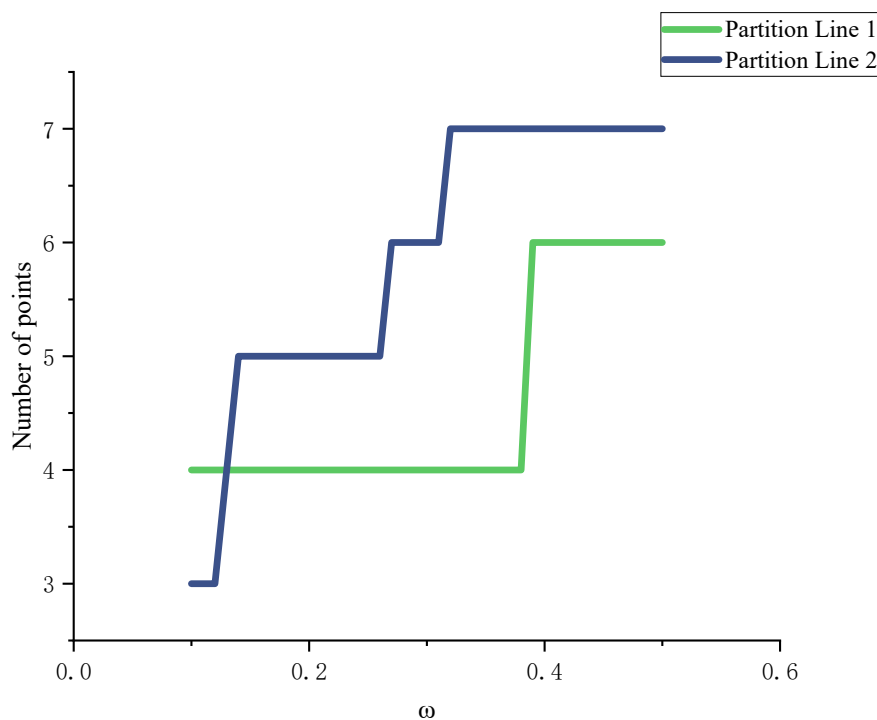


Figure 4.17 The relationship between the number of points connected by partition line 1-2 and  $\omega$

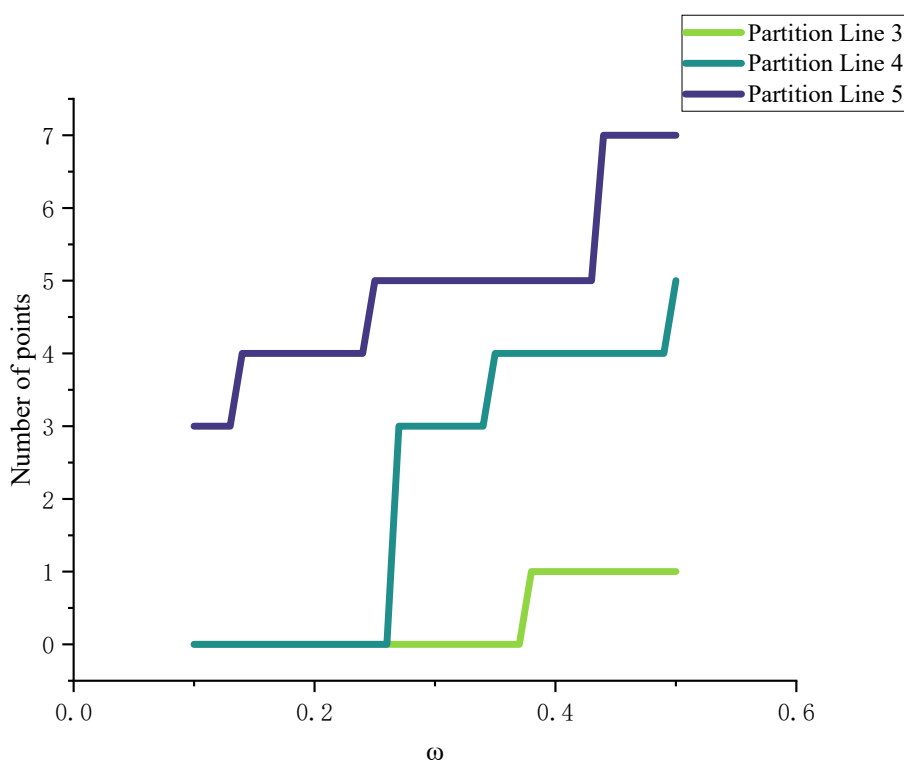


Figure 4.18 The relationship between the number of points connected by partition line 3-5 and  $\omega$

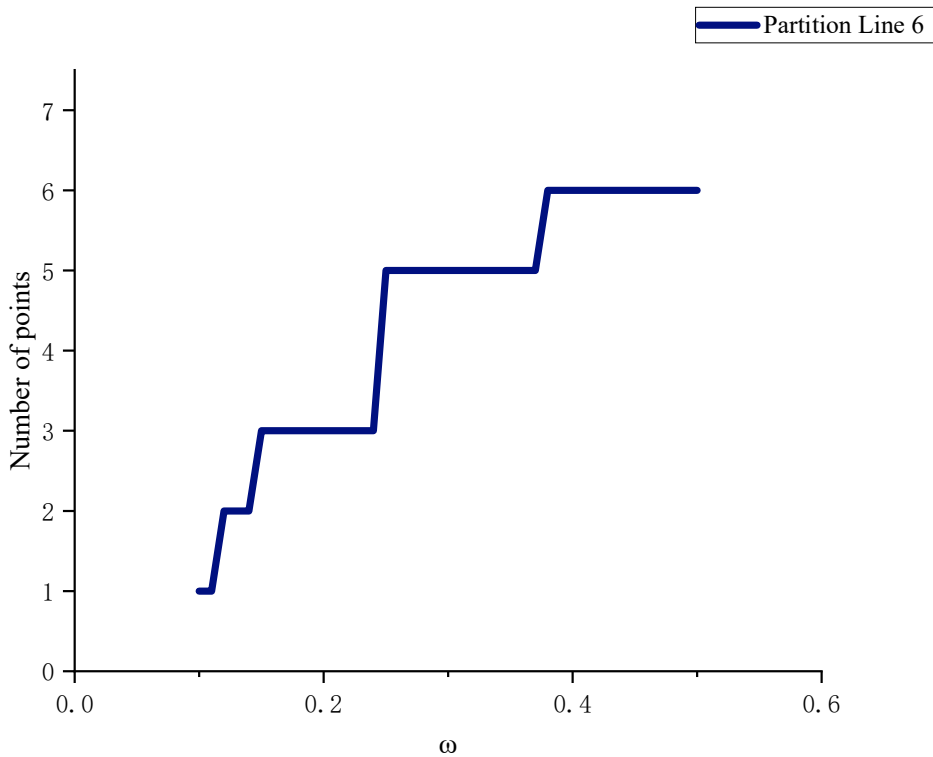


Figure 4.19 The relationship between the number of points connected by partition line 6 and  $\omega$

For the three time periods, we choose the weight value of 0.25 to optimize all the partition lines, taking into account the utilization rate of the points within the airspace as well as the smoothness of the sector boundaries. At the same time, it is still necessary to consider whether the optimized segmentation lines and new sectors satisfy the constraints of sector boundary optimization and the requirement that all workloads do not exceed the threshold. After experiments, at the weight value  $\omega$  of 0.25, the sector workloads delineated by the optimized partition lines 2 and 6 exceed the threshold, so the one-stage division results are maintained; the rest of the lines meet all requirements.

Figures 4.20(a)-4.22(a) show the sector structure after the first stage of partition for the three time periods. Figures 4.20(b)-4.22(b) show the sector boundary optimization results of the second stage. Tables 4.10-4.12 show the comparison of the workload of each sector before and after the division.

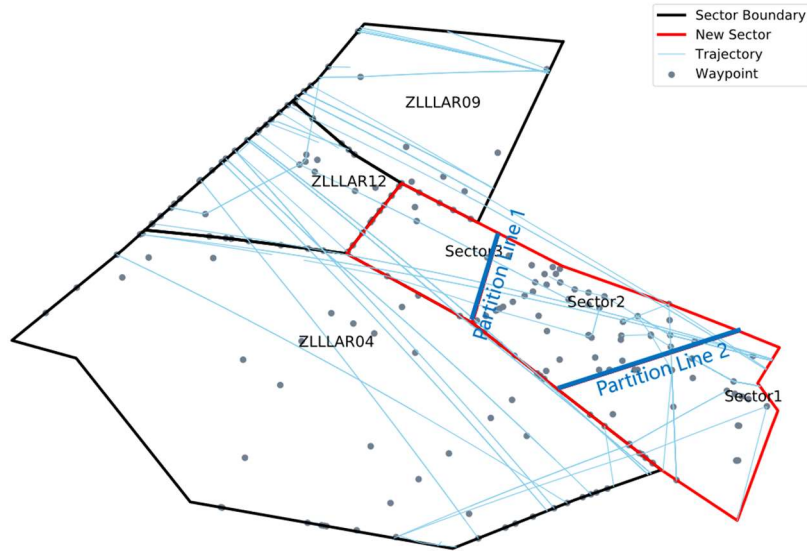


Figure 4.20(a) 10:00–11:59 After one-stage.

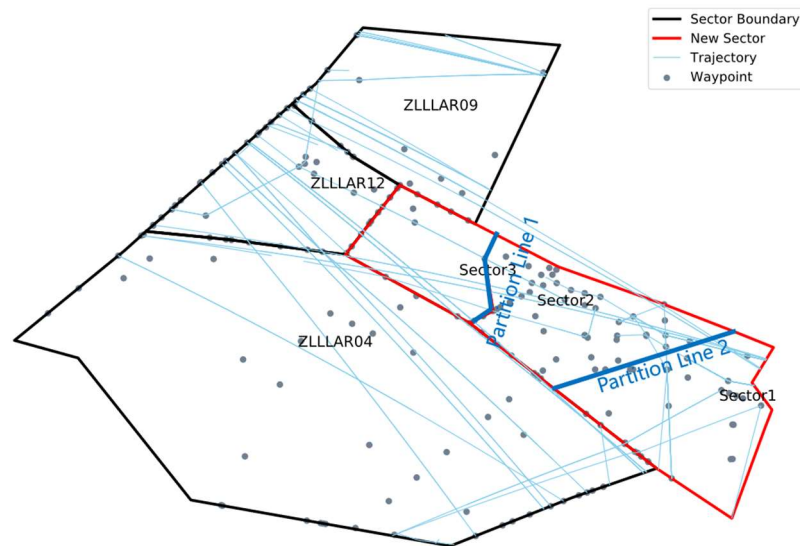


Figure 4.20(b) 10:00–11:59 After two-stage.

Table 4.10 10:00–11:59 Workload values for each sector before and after optimization.

	<b>Before</b>			<b>After One-Stage</b>		<b>After Two-Stage</b>	
	10:00–10:59	11:00–11:59		10:00–10:59	11:00–11:59	10:00–10:59	11:00–11:59
<b>ZLLAR06</b>	23.5529	23.8674	<b>Sector1</b>	68.8843	60.4926	68.8843	60.4926
<b>ZLLAR07</b>	11.5431	21.3622	<b>Sector2</b>	65.5155	58.6889	65.5155	58.6889
<b>ZLLAR08</b>	77.3584	69.3848	<b>Sector3</b>	14.9662	12.2904	14.9662	12.2904

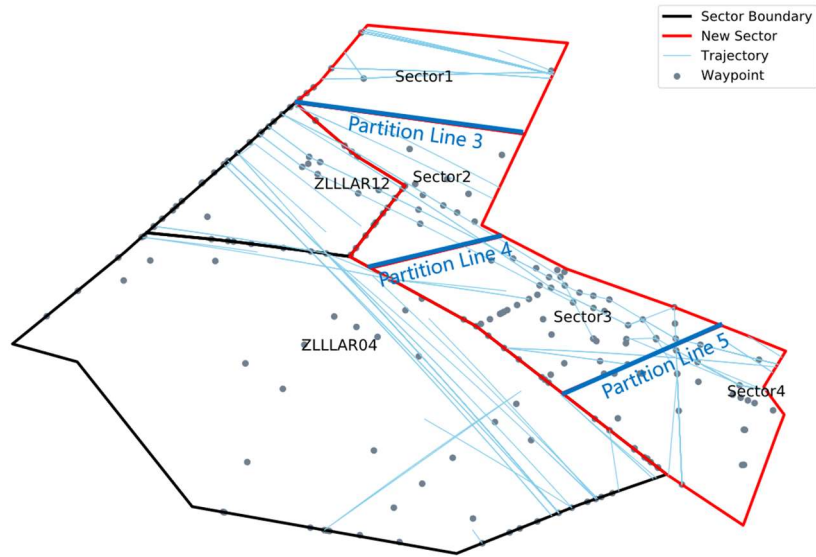


Figure 4.21(a). 12:00–13:59 After one-stage.

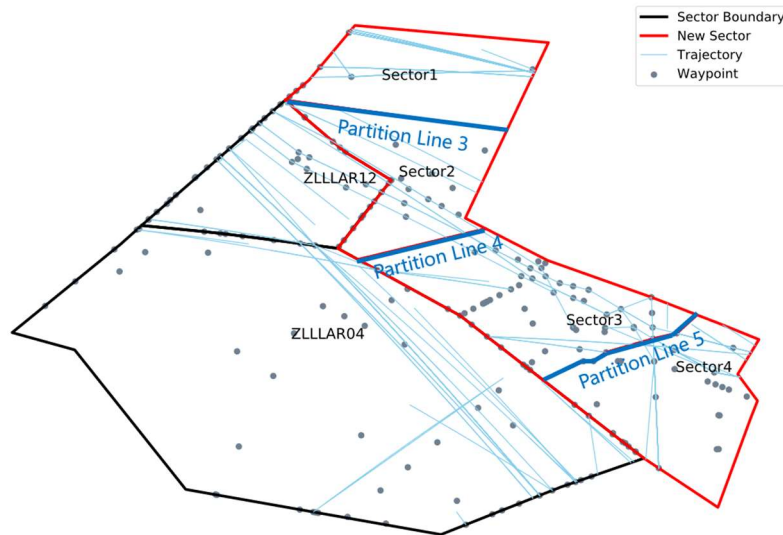


Figure 4.21(b). 12:00–13:59 After two-stage.

Table 4.11 12:00–13:59 Workload values for each sector before and after optimization.

	Before			After One-Stage		After Two-Stage	
	12:00–12:59	13:00–13:59		12:00–12:59	13:00–13:59	12:00–12:59	13:00–13:59
<b>ZLLAR06</b>	62.0566	26.6573	<b>Sector1</b>	23.8674	65.2802	23.8674	65.2802
<b>ZLLAR07</b>	16.336	16.336	<b>Sector2</b>	63.8403	57.8604	63.8403	57.8604
<b>ZLLAR08</b>	73.7572	71.565	<b>Sector3</b>	69.565	51.9123	68.7609	51.9123
<b>ZLLAR09</b>	75.7915	63.5467	<b>Sector4</b>	68.5118	59.1439	68.5118	59.9098

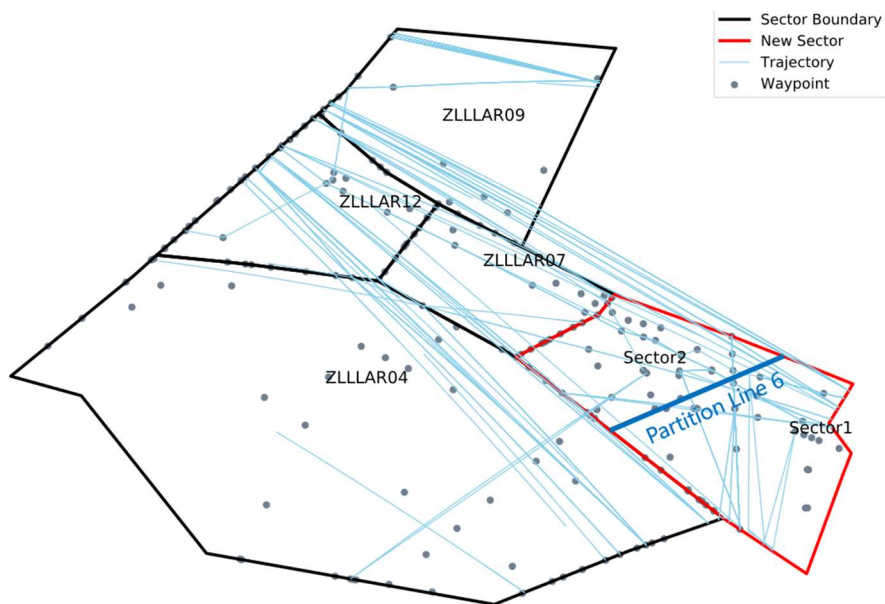


Figure 4.22(a) 14:00–15:59 After one-stage.

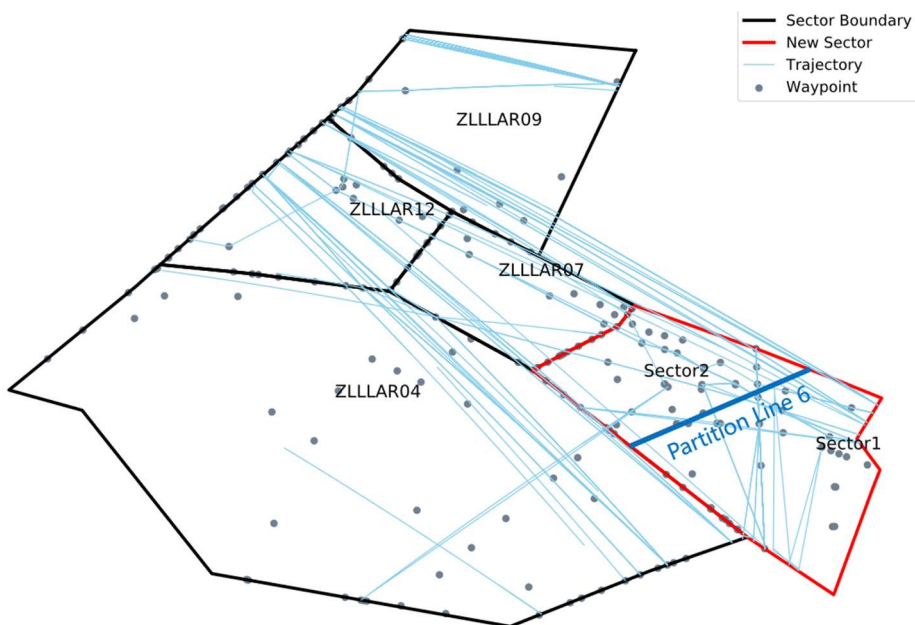


Figure 4.22(b) 14:00–15:59 After two-stage.

Table 4.12 14:00–15:59 Workload values for each sector before and after optimization.

	<b>Before</b>			<b>After One-Stage</b>		<b>After Two-Stage</b>	
	14: 00– 14:59	15:00– 15:59		14: 00– 14:59	15:00– 15:59	14: 00– 14:59	15:00– 15:59
<b>ZLLAR06</b>	22.5844	21.813	<b>Sector1</b>	69.142	37.879	69.142	37.879
<b>ZLLAR08</b>	70.7609	21.813	<b>Sector2</b>	23.8674	21.813	23.8674	21.813

## 5.3. OPERATION PROCEDURES FOR FERA MANAGEMENT

In dynamic airspace management, all available airspace should be managed flexibly. The dynamic airspace management process should include dynamic flight routes and provide optimal operational solutions. When segregation is required, the size, shape and time zone of the airspace should be determined based on the different types of operational modes to minimize the impact on operations. At the same time, the use of the airspace should be coordinated and monitored to meet the conflict requirements of all users and to minimize any restrictions on operations. Airspace reservations should be planned in advance and dynamically changed where possible. The system shall also accommodate the unplanned requirements for short notice. Noted that the operational complexity may limit the effectiveness of flexibility in airspace management.

### 5.3.1. THE OPERATION MODE OF FERA-WOC

Based on China's national and air conditions, the FERA-WoC operation mode is designed by combining FUA and FRA concepts. FERA-WoC can dynamically adapt to airspace resource availability and flexible civil-military airspace use mechanisms, and is a modular airway airspace with on-demand combination, which aims to improve spatial freedom and support semi-free-airway four-dimensional trajectory operation in Flexible Airway Airspace. The FERA-WoC flexibility component is shown in Figure 4.23, and the basic concepts and features are as follows.

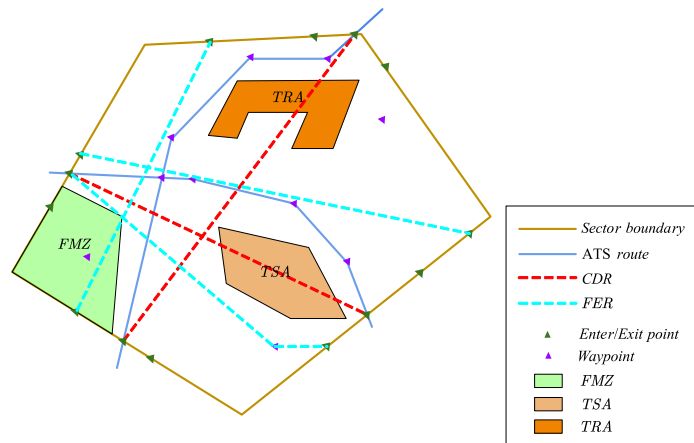


Figure 4.23 The basic operation mode of FERA-WoC

Feature 1: Retain or adjust the original ATS routes and establish the Free Maneuvering Zone (FMZ) as a supplement to the ATS routes, allowing air traffic controllers to manage tactical trajectories and spacing through intermediate waypoints or within the FMZ.

Feature 2: Temporary Segregated Area (TSA) and Temporary Reserved Area (TRA) are established to supplement, replace or modify the existing special airspace structure. Establish Conditional Route (CDR) associated with TSA and TRA.

ATS routes that are only available for use and flight planning under specified conditions. A Conditional Route may have more than one category, and those categories may change at specified times:

CDR1 routes are available for flight planning during times published in the relevant National Aeronautical Information Publication (AIP).

CDR2 routes may be available for flight planning. Flights may only be planned on a CDR2 by the daily published conditions.

CDR3 routes are not available for flight planning at all. Flights must not be planned on these routes but ATC Units may issue tactical clearances on such route segments.

TSA is a defined volume of airspace normally under the jurisdiction of one aviation authority and temporarily segregated, by common agreement, for the exclusive use of another aviation authority and through which other traffic will not be allowed to transit.

Feature 3: Configure sector entry and exit points and intermediate waypoints. The sector entry and exit points can be published as significant points or defined as any latitude and longitude coordinates with unique names, while the intermediate waypoints can only be defined by the navigation equipment. Each kind of point is introduced in Figure 4.24. The airspace users are free to plan routes between a pair of entry/exit points and intermediate waypoints based on published route availability (domestic or international route categories) without referring to the ATS route network.

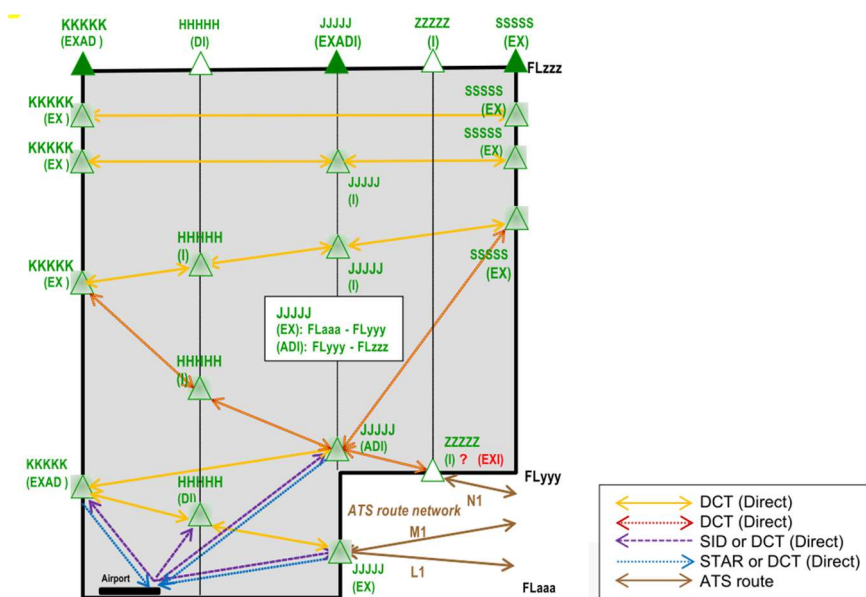




Figure 4.24 The significant definitions of FERA-WoC

### 5.3.2. THE WORKFLOW OF DYNAMIC AIRSPACE MANAGEMENT

In the process of dynamic airspace management, each airspace user should make collaborative decisions and share information to complete the dynamic management of airspace. Therefore, the workflow of dynamic airspace management is shown in Figure 4.25.

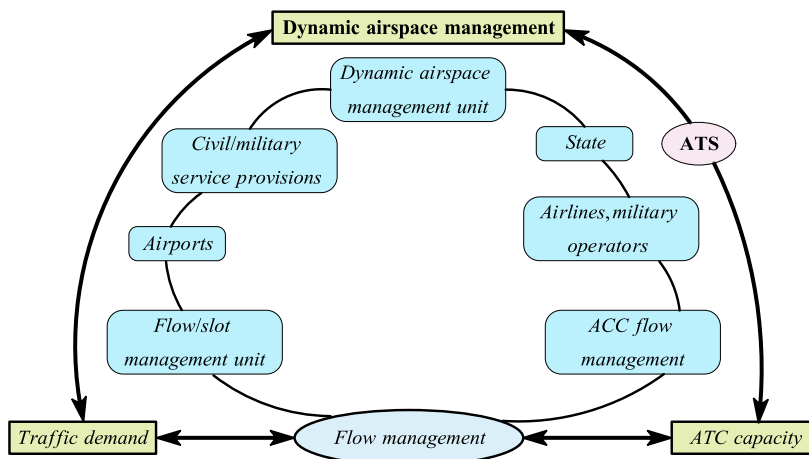


Figure 4.25 The workflow of dynamic airspace management

#### 5.3.2.1 STRATEGIC DYNAMIC AIRSPACE MANAGEMENT

The dynamic airspace management workflow in the strategic phase is shown in Figure 4.26, which is described in detail in each section below.

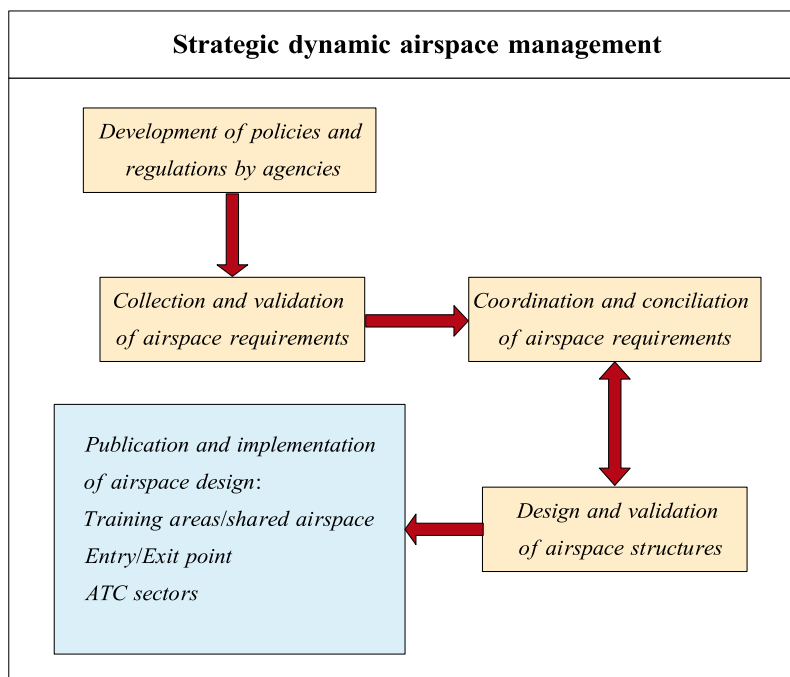


Figure 4.26 The dynamic airspace management workflow in the strategic phase

### 5.3.2.1.1 DEVELOPMENT OF POLICIES AND REGULATIONS BY AGENCIES

The National Air Traffic Control Commission (NATCC) of China shall ensure the effective sharing of airspace and efficient use of airspace by civil and military users through joint civil/military strategic planning and pre-tactical airspace allocation to enhance the safety and efficiency of FERA operations. The written agreements or arrangements shall be put in place between the competent civil and military units, based on timely data processing for airspace assessment and resource allocation, to enable them to take into account the activation and deactivation of temporary structures (i.e., manage the availability of the flexible routes). And the efficient operations at ASM Level 3 are put in place including the establishment of coordination procedures between civil and military ATS Units, and between them and military controlling units to support a process exploiting the airspace capacity dynamically.

Where appropriate, the FERA-WoC shall conclude agreements with neighboring fixed route airspace to enable cross-boundary operations. The FERA-WoC shall authorize their competent agencies to negotiate and conclude necessary written agreements that could contain specific operational and technical aspects related to pre-tactical and tactical airspace management, and arrangements for the Air Traffic Services provision, if and where applicable, and such agreements shall include all relevant legal, operational and technical issues for cooperation and interaction covering all relevant civil and military issues (e.g. defense, operations, environment and search and rescue), and the following:

- a) Determination of the responsibility for the provision of Air Traffic Services;
- b) Designation of competent civil and military authorities involved in ASM activities;
- c) Air Defence coordination and notification procedures;
- d) Priority allocation rules, time-based parameters, and booking assurance processes;
- e) Coordination procedures and interaction rules concerning the activation and release of the cross boundary airspace reservation;
- f) Services in the area(s) concerned following the principle of delegation of responsibility, where applicable;
- g) Contingency procedures;
- h) Other operational issues pertinent to cross boundary operations as appropriate;
- i) Compatibility of communication and flight data exchange systems between civil and military parties, including usage of technical enablers (eg. ASM/ATFM tool).

The NATCC shall ensure the shared use of airspace in respect of all users and the establishment of a joint civil and military process for the effective application of the flexible use of airspace concept at a strategic, pre-tactical, and tactical level, and shall conduct regular assessments of the airspace network to monitor the FERA-WoC operations. It shall also establish policies, and define mechanisms and processes to assess and approve activities that require airspace reservations or restrictions.

The NATCC shall establish a consultation mechanisms with all relevant partners and organizations, and:

- a) Shall ensure that consultations with airspace users, ATM Bureau, and other relevant bodies are conducted to obtain consensus, wherever possible, before making changes in the planning or design of airspace arrangements.
- b) Shall ensure that the functional responsibilities of the persons/authorities are defined.

#### 5.3.2.1.2 COLLECTION AND VALIDATION OF AIRSPACE REQUIREMENT

Air traffic services units and users shall make the best use of the available airspace. Thus, the airspace requirements of all airspace users should be collected. The airspace users are included as follows: a) military aviation; b) other military users; c) civil air transport; d) general, sporting, and aerial work users; e) business aviation; f) air test-civil and military; g) any other airspace users; h) national and international organizations representing groups of users. The NATCC should ensure the integration of ASM and ATFM functions at the national level, and publish processes and mechanisms to review and update user requirements. And it shall define mechanisms and establish processes to regularly review civil and military airspace requirements, to reconcile their operational needs. It shall also ensure the consistency between mechanisms and establish processes to regularly review civil and military airspace requirements.

#### 5.3.2.1.3 COORDINATION AND CONCILIATION OF AIRSPACE REQUIREMENTS

NATCC shall ensure that additional procedures for the delineation and allocation of airspace and associated dissemination of information to respond to specific short-notice airspace requirements and/or flexible route optimization are created. It shall also ensure that processes for periodic assessment and analysis of FREA network structures and operations based on a non-discrimination principle considering both civil and military requirements are in place intending to continuously optimize the flexible airspace structures and operational procedures. The assessment policy is subject to ongoing (at least yearly) review.

The assessment processes include:

- a) Identification of demand;
- b) Review airspace resource and capacity;
- c) Analysis of the potential impact;
- d) Decision to proceed, e.g., the FREA boundary/entry-exit points/SUA/CDR adjustment, operational rules optimization, etc.;
- d) Consultation;
- e) Approval;
- f) Publication.

NATCC shall define the circumstances when an air traffic services unit or controlling military unit is responsible for the separation between civil and military flights, eg. in the case of the shared portion of airspace, the tactical crossing of ATS/flexible routes, and tactical crossing of temporary reserved/restricted areas, and:

- a) Determine the conditions under which the responsibility for separation between civil and military flights may rest on the air traffic services units or controlling military units.
- b) Define the criteria for determining the responsibility for providing separation between civil and military flights.
- c) Ensure that the conditions and criteria for the responsibility for separation between civil and military flights are contained in written agreements or other appropriate arrangements.

#### 5.3.2.1.4 DESIGN AND VALIDATION OF AIRSPACE STRUCTURES

NATCC shall ensure that airspace structures for temporary use by users in response to their specific needs including the possibility of subdividing these airspace structures are defined and established, and ensure that consultations with airspace users, service providers, and other relevant bodies are conducted to obtain consensus, wherever possible, before making changes in the planning or design of airspace arrangements.

- a) Shall establish and publish procedures for airspace allocation and use for activities that require airspace reservation or restriction;
- b) Shall ensure these procedures provide for multiple choice of airspace reservations and related flexible route segments taking into account the National ATM network effect;
- c) Shall ensure that procedures are in place to promulgate airspace reservations;

d) Shall make provisions for dynamic airspace management processes, at national ASM Level 2 and 3;

e) Shall establish procedures for airspace allocation and use for activities that require a mobile airspace reservation or restriction, where appropriate.

NATCC shall ensure that the principles for adjusting lateral and vertical limits of FERA airspace structures including the subdividing of airspace reservations into elementary modules on ASM Levels 2 & 3 are defined.

a) Shall define criteria for designing FERA to enable adjustable lateral and vertical limits of airspace structures, including the subdividing of airspace reservations into elementary modules.

b) Shall define criteria and procedures for adjusting the lateral and vertical dimensions of FERA sector structures based on subdivided airspace reservations into elementary modules on ASM Levels 2 & 3.

After determining the dynamic airspace structure, the route planning is completed based on the airspace user requirements to configure the entry and exit points and intermediate points. With the goal of green, safe and efficient air traffic operation, the optimal airspace structure is obtained by refined and adaptive algorithms. The flow chart of airspace structure design is shown in the Figure 4.27.

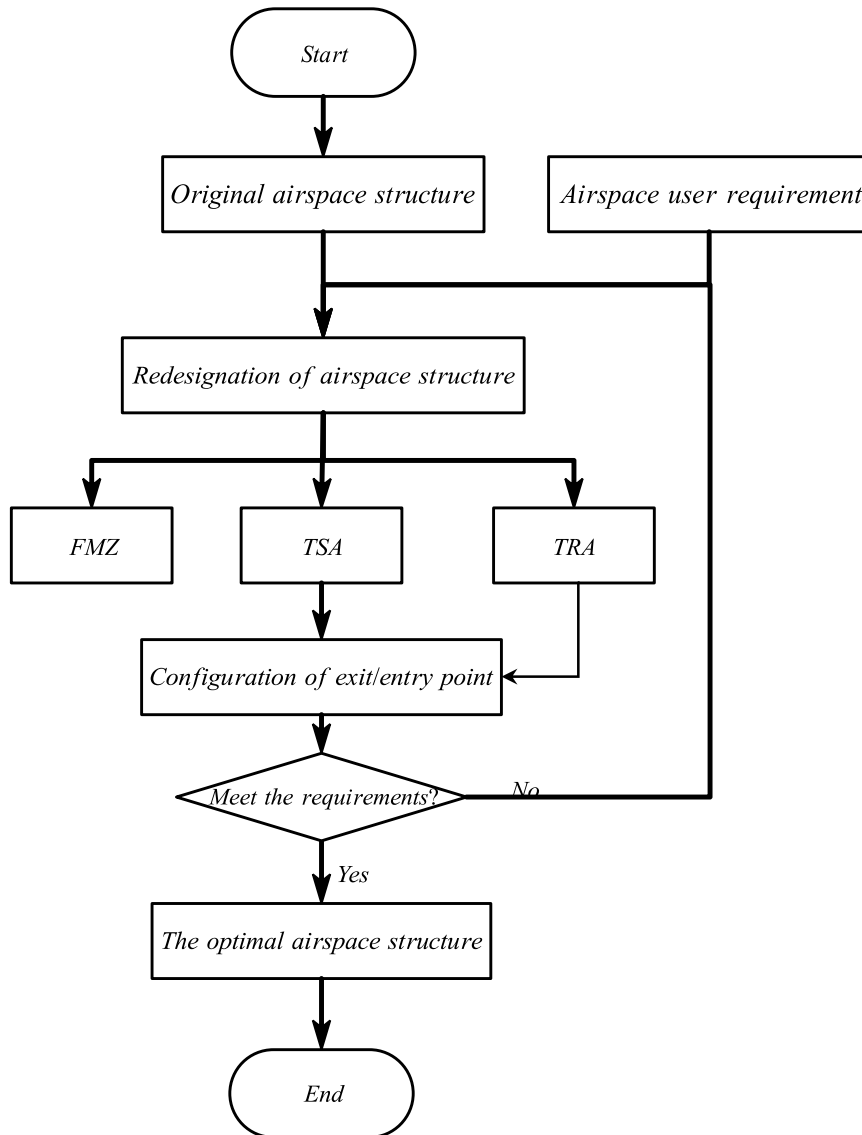


Figure 4.27 The flow chart of airspace structure design

### 5.3.2.1.5 PUBLICATION AND IMPLEMENTATION OF AIRSPACE STRUCTURE

After the FERA design is completed, it should be fed back to various departments and airspace users. The relevant military control units and air traffic services units exchange any modification of the planned activation of airspace in a timely and effective manner and notify to all affected users the current status of the airspace.

### 5.3.2.2 PRE-TACTICAL AIRSPACE MANAGEMENT

A dynamic airspace management cell is established to allocate airspace by the conditions and procedures. Both civil and military authorities are responsible for or involved in airspace management in a joint civil-military operation manner.

In the pre-tactical phase, the NATCC shall:

- a) Appoint a focal point, or establish and authorize hierarchical (e.g., national level, ACC level, TMA level) airspace management cells, or joint civil and military airspace management cells.
- b) Authorise the cells to conduct airspace allocation and management in a decisive, timely, and efficient manner and resolve conflicting airspace requirements.
- c) Ensure that staff is adequately trained in the knowledge and operation of the airspace allocation process and use of supporting systems.
- d) Ensure that the cells collaboratively collect and analyze all airspace requests and decide the daily airspace allocation taking into account the user requirements, available capacity, and the effect on the network.
- e) Ensure that the cells are responsible for the conduct of day-to-day Level 2 airspace allocation and management.

In particular, the dynamic airspace management cells:

- a) Shall collect and analyze all Airspace Requests which may require temporary airspace segregation, including airspace allocation decisions taken at ASM Level 1 in respect of major military exercises, air shows, etc.;
- b) Shall monitor and forecast the airspace situation and dynamic capacity;
- c) Shall analyze the CDR availability requests together with the traffic demand, anticipated ATC capacity problems, and expected delay information;
- d) Shall resolve conflicting requests for TSA/TRA and FMZs/CDRs utilizing all relevant information;
- e) Shall resolve conflicts between incompatible or conflicting airspace requests by the application of approved priorities, re-negotiation, rescheduling, or segregation;
- f) Shall coordinate with adjacent cells the harmonized availability of "cross-boundary" CDRs;
- g) Shall respond to any additional request for assistance by Air Traffic Flow Management, the ACCs, and other Approved Agencies or matters arising from major flexible or ATS routes inconsistencies or unexpected events;
- h) Shall activate CDR2 following established procedures and for a minimum time of two hours (2H), but with no limit when it is the extension of the availability of the same route with CDR 1 status;
- i) Shall decide following criteria established at Level 1 on the provisional closure of CDRs 1 to be handled in real-time at ASM Level 3 in conjunction with the notification of activity in associated TSA(s)/TRA(s) and/or AMC-Manageable D and R area(s);
- j) Shall promulgate the airspace allocation by transmitting the Airspace Use Plan to adjacent cells and ACCs, and to the Air Traffic Flow Management Unit.

- k) Shall provide dynamic sector configuration plans (e.g., open/closure, boundary adjustment, etc.) to relevant air traffic control units.
- l) Shall participate in a post-analysis of airspace allocation;
- m) Shall conduct, where authorized, some Level 3 coordination tasks.

### 5.3.2.3 TACTICAL REAL-TIME OPERATIONS

Establish civil/military coordination procedures and communication facilities between appropriate air traffic service units and controlling military units permitting the mutual provision of airspace data to allow the real-time activation, deactivation, or reallocation of the airspace allocated at tactical level. The relevant controlling military units and air traffic services units exchange any modification of the planned activation of airspace in a timely and effective manner and notify to all affected users the current status of the airspace.

In the tactical phase, the NATCC shall:

- a) Ensure the definition, agreement, and enforcement of co-ordination procedures between civil and military ATS units and between them and controlling military units, vested with agreements, to facilitate real-time activation, de-activation, re-allocation or modification of the airspace allocated at pre-tactical level.
- b) Ensure that the determination of these coordination procedures and communication facilities takes into account the national ATM network effect.

The NATCC shall ensure that coordination procedures between civil and military ATS/controlling military units are defined and agreed and operated to ensure safety when managing interactions between civil and military flights. That the procedures between civil and military ATS units and between them and controlling military units and the facilities are designed to minimise the negative impact on all airspace users. Where appropriate, a civil or military presence in respective control facility, where not already co-located.

### 5.3.3. EMERGING SITUATION

#### 5.3.3.1 COMMUNICATION FAILURE

This procedure is suitable for the en route control unit in FERA to deal with the loss of communication of aircraft in the control area. Any event that the on-site controller judges that the aircraft lost communication has occurred or may occur may refer to this procedure.

When the radar shows that the transponder code of the aircraft is A7600, the on-site controller should immediately call the aircraft to determine whether the aircraft has lost communication. Open the relevant navigation equipment, and use surveillance equipment to grasp the aircraft position. Regardless of whether the



aircraft has a transponder code A7600 or not, when calling an aircraft for many times without answering, it should use various methods such as transponder identification, instruct the aircraft to change the transponder code, and instruct it to change the course to determine whether the aircraft is capable of receiving, and then take measure. If it is confirmed that the aircraft can receive the ground call through the above method, it is judged as "the communication equipment on the aircraft can receive normally but the transmission failure", otherwise it is judged as "the communication equipment on the aircraft has a failure to receive".

#### 5.3.3.1.1 AIRCRAFT ON-BOARD COMMUNICATION EQUIPMENT CAN RECEIVE NORMALLY BUT TRANSMISSION FAILURE

- a. Continue to issue instructions to the aircraft, and use various methods, such as transponder identification, to determine whether the aircraft has received control instructions, requiring each control instruction to be repeated twice and confirming that the aircraft has received relevant instructions through transponder identification;
- b. When the standby frequency is turned on, direct the aircraft to contact the standby frequency;
- c. Report the situation to the relevant aircraft and instruct the relevant aircraft to avoid;
- d. Vector the aircraft to the ATS route and assign the flight level in accordance with regulations.
- e. When the aircraft is heading to the alternate airport, provide the flight information required to reroute to the alternate airport.
- d. Provide all necessary informations to adjacent control units.
- e. Assess the impact and issue air traffic flow restriction if necessary.

#### 5.3.3.1.2 THE AIRCRAFT'S ON-BOARD COMMUNICATION RECEPTION AND TRANSMISSION ARE BOTH FAULTY

- a. Maintain a vertical separation of not less than 600 meters or a horizontal separation in compliance with the regulations between aircraft with communication failure and other aircraft;
- b. Considering that an aircraft that has lost communication may descend autonomously when approaching the destination airport, when the aircraft is approaching its expected descent point, other aircraft located below the aircraft's expected flight path should be directed to avoid and maintain sufficient horizontal

separation between the expected trajectory based on the airspace and flexible route availability in the FERA.

- c. Uninterruptedly call the communication-failed aircraft within the frequency, try to establish a communication link with the communication-failed aircraft by means of airborne aircraft transfer calls, and continuously blindly send air traffic information and meteorological information to the communication-failed aircraft;
- d. Closely monitor the flight operations of aircraft with communication failure;
- e. Turn on the emergency frequency and all other possible frequencies on the intercom panel to call the aircraft with communication failure.
- f. Notify the adjacent control units that may be affected.
- g. Request the relevant control unit to assist in calling the communication disabled aircraft within its frequency.
- h. Notify the military aviation control department.
- i. Assess the impact and issue air traffic flow restriction if necessary.

### 5.3.3.2 LOSS OF CABIN PRESSURISATION

When an aircraft reports cabin depressurization and immediate descent is required:

- a. Command the aircraft below the malfunctioning aircraft to avoid emergency and maintain the safe horizontal separation.
- b. Vector the malfunctioning aircraft to the ATS route and allow the aircraft to descend to an altitude below 4,000 meters, above the safe altitude.
- c. After the malfunctioning aircraft is in stable flight, learn about the reasons for the loss of pressure in the cockpit of the aircraft, the endurance time, the intention of the captain, the casualties of the people on board, and the working conditions of the equipment.
- d. Provide the flight information of the destination or alternate airport according to the captain's request, and provide the shortest flight route in the flexible en route airspace network if necessary.
- e. Coordinate the downstream sectors or control units to evade the aircraft in an emergency.
- f. Special coordination and handover with relevant control units.
- g. Provide the necessary information of the malfunctioning aircraft to the relevant control unit.
- h. Apply for the flexible rerouting with the military aviation control department if the rerouting path pass SUAs.

### 5.3.3.3 ENGINE FAILURE

This procedure is suitable for the en route control unit to deal with engine failure events in the control area. Where the on-site controller judges that an engine failure event has occurred or may occur, it can be implemented with reference to following procedure.

- a. Considering the maneuverability of the aircraft with engine failure and the ability to maintain altitude, vector the aircraft with engine failure to the nearest ATS route and allow the aircraft to descend to a flight level above the minimum safe altitude.
- b. Quickly command other neighboring aircraft to avoid the malfunctioning aircraft.
- c. Understand the failure conditions, endurance time and captain's intentions, and provide information on nearby airports and flight information.
- d. Provide aircraft with all possible convenience and priority permission.
- e. Coordinate with the control unit or sector into which the aircraft will enter to inform them of the aircraft's intentions.
- f. According to the decision of the captain, notify the relevant control unit to tell the aircraft to prepare for the rescue at the airport where the aircraft is going to land.
- g. Notify the military aviation control department to apply for the airspace of the aircraft's maneuvering activities.
- h. Assess the impact and issue air traffic flow restriction if necessary.

### 5.3.3.4 SPATIAL DISORIENTATION

This procedure is suitable for the en route control unit to deal with spatial disorientation incidents in this control area. Where the on-site controller judges that a spatial disorientation incident has occurred or may occur, it can be implemented with reference to the following procedure.

- a. Use radar equipment to locate the disorientation aircraft and guide the aircraft to the ATS route until it resumes autonomous navigation.
- b. Notify the relevant control unit.
- c. Apply for the reroute airspace with to the military aviation control department.

### 5.3.3.5 RADIO COMPASS FAILURE

This procedure is applicable to the en route control unit to deal with radio compass failures in the control area. Where the on-site controller judges that the failure of the radio compass has occurred or may occur, it can be implemented with reference to this procedure.

- a. Ask about the information and cause of radio compass failure, and the crew's intentions.
- b. Use radar to monitor and vector the aircraft to ATS route.
- c. According to the decision of the crew, assist the aircraft to continue the flight or land at the nearest airport.
- d. Provide the crew with the weather and navigation facilities of the nearest airport and alternate airport.
- e. Immediately notify the relevant control unit of the failure of the aircraft's radio compass and the assistance needed, and make a special handover to the adjacent control unit.
- f. Notify the military aviation control department to apply for the airspace where the aircraft may maneuver.

## 6. REFERENCES

- [1] Air Traffic Management Bureau of civil Aviation Administration of China. 2019 Civil Aviation Airspace Development Report[R]. Beijing: Air Traffic Management Bureau of civil Aviation Administration of China, 2019.
- [2] Dai Dezhong. A Preliminary Study on the Use and Management of temporary routes[J]. Air Transport & Business, 2012, 000(011):4-8.
- [3] Yang Xincheng, Wang Jiakuan, Wan Chunlian. Study and analysis of evaluation index of temporary route[C]. Proceedings of "Decision-making Forum Symposium on Management Science and Business" (part 2). 2016.
- [4] Civil Aviation Administration of China. Management measures for the allocation and use of international navigation rights resources [Z]. 2018-10-01.
- [5] Li Limin. Application of flight information processing system in flexible route replacement mechanism [J]. Electronic technology and software engineering, 2020(07): 170-171.
- [6] Banavar S ,Shon G ,Kapil S ,Karl D B . Initial Study of Tube Networks for Flexible Airspace Utilization[C]. AIAA Guidance, Navigation, & Control Conference, 2006.
- [7] Zhang Huili. Research on generating System of Airspace Flexible Use Strategy [D]. Nanjing University of Aeronautics and Astronautics, 2009.
- [8] Air Traffic Management Bureau of civil Aviation Administration of China. Airspace management Manual applying the concept of airspace flexible use [Z], 1996.
- [9] Mitchell J S B. On maximum flows in polyhedral domains[J]. Journal of Computer and System sciences, 1990, 40:88-123.
- [10] Xie Zheng, Wang Jianping. Network algorithm and complexity theory[M]. Beijing: National Defense University of science and Technology Press, 1995:113-132.
- [11] Strang G. Maximal flow through a domain[J]. Mathematical Programming, 1983,26(2): 123-143.
- [12] Iri M. Survey of mathematical programming[J]. North-Holland, Amsterdam, Netherlands, 1979.
- [13] Mitchell J S B. On maximum flows in polyhedral domains[J]. Journal of Computer and System Sciences, 1990, 40(1): 88-123.
- [14] Ji Yabao. Research and Applications for the Problem of Maximum Flow Minimum Cut Algorithms[D]. Nanjing University of Posts and Telecommunications, 2017.

- [15] Krozel J. Maximum Flow Rates for Capacity Estimation in Level Flight with Convective Weather Constraints[J]. *Air Traffic Control Quarterly*, 2007, 15(3).
- [16] Li Huan. Research on Sector Planning and Optimization Technology Based on Complexity[D]. Civil Aviation University of China, 2019.
- [17] Comendador G, A Valdés, Vidosavljevic, et al. Impact of trajectories' uncertainty in existing ATC complexity methodologies and metrics for DAC and FCA SESAR concepts[J]. *Energies*, 2019, 12(8): 59-84.
- [18] Comendador V, RMA Valdés, MV Díaz, et al. Bayesian Network Modelling of ATC Complexity Metrics for Future SESAR Demand and Capacity Balance Solutions[J]. *Entropy*, 2019, 21(4):379-396.
- [19] Cong Wei, Hu Minghua, Xie Hua, et al. An Evaluation Method of Sector Complexity Based on Metrics System[J]. *Journal of Transportation Systems Engineering and Information Technology*, 2015, 15(5): 136-141.
- [20] Jelena D, Bernd L, Hartmut F. Air traffic control complexity as workload driver[J]. *Transportation Research Part C*, 2010, 18: 930-936.
- [21] Zhao Yuandi, Wang Chao, Li shanmei, Zhang Zhaoyue. Dependable clustering method of flight trajectory in terminal area based on resampling[J]. *Journal of Southwest Jiaotong University*, 2017, 52(04): 817-825.
- [22] Du Shi, Che Yutong, Wang Lihang, Ren Jingrui. K-means track clustering based on dynamic time warping metric[J]. *China Sciencepaper*, 2019, 14(06): 664-669.
- [23] Wang Bo, Wang Jianhui, Su Gang, et al. Integrated Evaluation for Operation Performance of Controlled Airspace Based on AIRTOP Simulation[J]. *Aeronautical Computing Technique*, 2020, 50(7): 61-65.
- [24] Deng Siyuan, Zhou Lanting, WANG Fei, et al. XGBoost-LSTM Variable Weight Combination Prediction Model for Dam Deformation and Its Application[J]. *Journal of Yangtze River Scientific Research Institute*, 2021, 37(10):1-9.
- [25] Sun Zhaoyun, Lv Hongyun, Yang Rongxin, et al. Traffic volume prediction for highway service areas based on XGBoost model with improved particle swarm optimization[J]. *Journal of Beijing Jiaotong University*, 45(5):74-83.
- [26] Zhao Zheng, Feng Shicheng, Song Meiwen, et al. Prediction Method of Dynamic Taxi Time Based on XGBoost[J]. *Advances in Aeronautical Science and Engineering*.
- [27] Zhang Kaiqing, Zhou Yongwu. Application of parallel nested genetic algorithm in centralized inventory routing problem[J]. *Journal of Hefei University of Technology*, 2009, 32(7): 1020-1024.
- [28] Sun Junyan, Chen Zhirui, Zhu Yaru, et al. Joint Optimization of Picking Operation based on Nested Genetic algorithm[J]. *Journal of Computer Applications*, 2020, 40(12): 3687-3694.

## ANNEX 1: ABBREVIATION

2D	Two-dimensional
ANSP	Air Traffic Service Providers
ARTCC	En-Route Control Centers
ASBU	Aviation system block upgrade
ASM	Airspace Management
ATC	Air Traffic Control
ATM	Air Traffic Management
ATS	Air Traffic Services
CAAC	Civil Aviation Administration of China
CAAMS	Civil Aviation Modern Air Traffic Management System
CR	Conditional Routes
CTA	Controlled Time of Arrival
DCB	Demand and Capacity Balancing
DSS	Decision Support System
DST	Dongshan VOR
EASA	European Union Aviation Safety Agency
FABCE	Central Europe FAB
FABEC	European Center FAB
FABs	Functional Airspace Blocks
FERA	Flexible En Route Airspace
FERA-WoC	Flexible En Route Airspace in West of China
FIR	Flight Information Region
FL	Flight Level
FRA	Free Route Airspace
FRTO	Free-route Operations
FSRA	Flow-based Sector Resource Availability
FUA	Flexible Use of Airspace
HERAM	Heterogeneous En Route Airspace Management
HFE	Hefei VOR

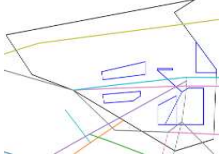
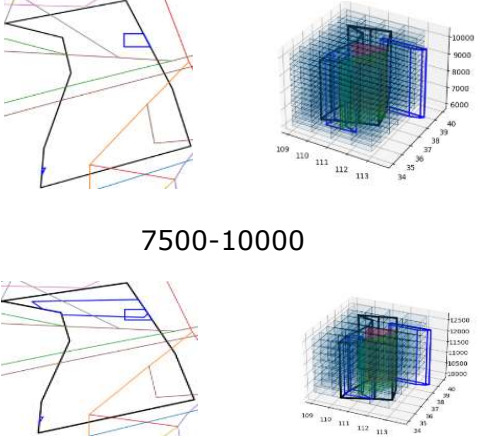
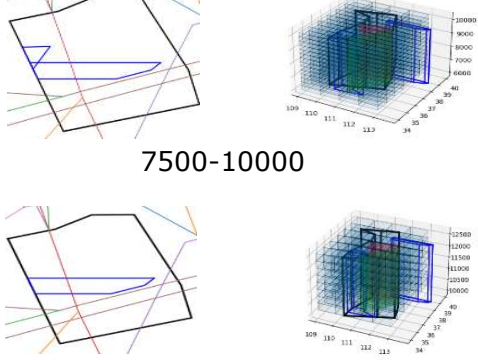
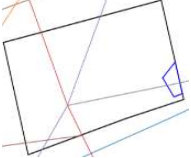
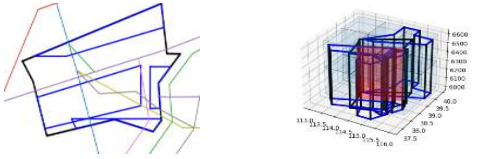
ICAO	International Civil Aviation Organization
LKO	Longkou VOR
MC	Minimum Cut
NAS	National Airspace System
NEFAB	Nordic FAB
NOTAMs	NOtice To AirMen
PRDs	Prohibited, Restricted and Dangerous Areas
RA	Resource Availability
RAM	Resource Availability Map
RCA	Reduced Coordinated Airspace
SESAR	Single European Sky Air Traffic Management Research
TOL	Tonglu VOR
TS	Temporary Route
TSV	Total Sector Volume
UAS	Unmanned Aircraft Systems
WXI	Weixian VOR

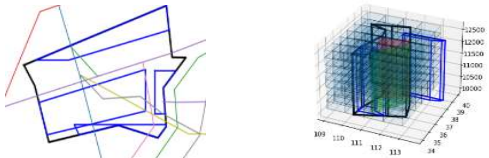
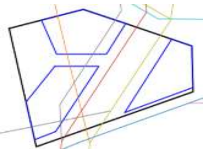
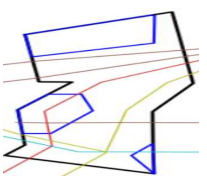
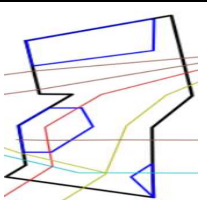
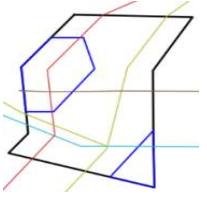
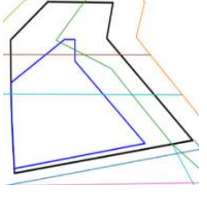


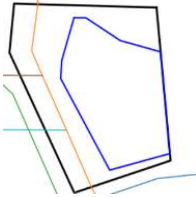
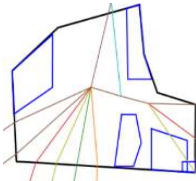
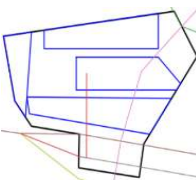
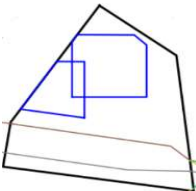
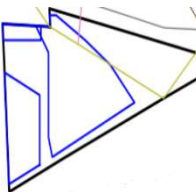

# ANNEX 2: RESOURCE AVAILABILITY OF EN-ROUTE SECTORS IN CHINA

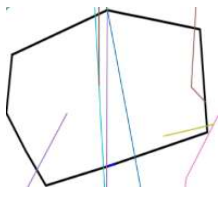
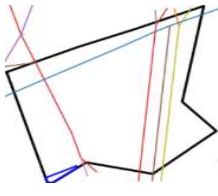
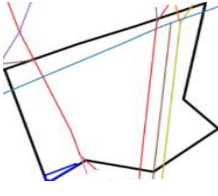
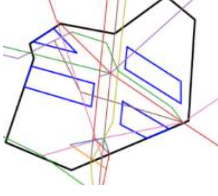
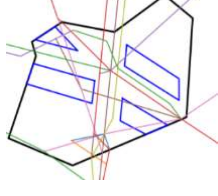
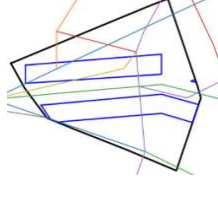
Sector	<b>2D/3D View(Altitude range(m) )</b> (Black: sector boundary,Blue: PRDs boundary Other Color lines: air routes)	Resource Availability
ZBAAAR01	<p style="text-align: center;">7800-8900</p>	0.8204
	<p style="text-align: center;">8900-12500</p>	
ZBAAAR02	<p style="text-align: center;">6000-8000</p>	0.0979
	<p style="text-align: center;">8000-9000</p>	
	<p style="text-align: center;">9000-12500</p>	
ZBAAAR03		0.3320

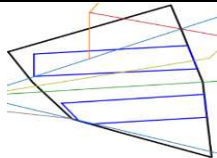
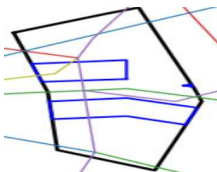
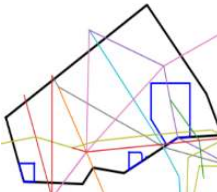
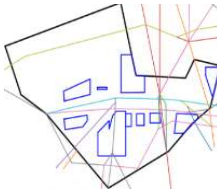
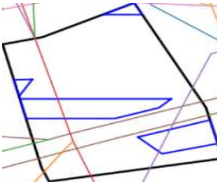
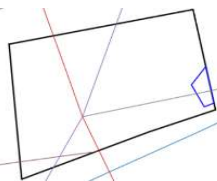
	<p>6000-8000</p> <p>8000-12500</p>	
ZBAAAR04	<p>6000-8000</p> <p>8000-12500</p>	1.0000
ZBAAAR05	<p>6000-6600</p> <p>6600-12500</p>	0.5964
ZBAAAR06	<p>6000-12500</p>	1.0000
ZBAAAR07	<p>7800-12500</p>	1.0000

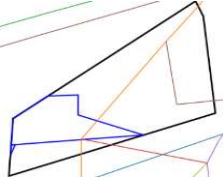
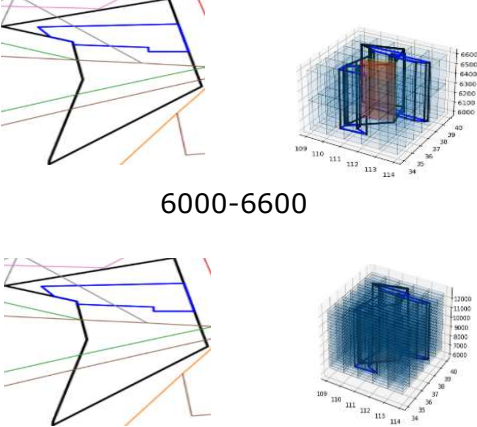
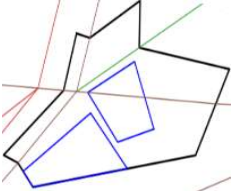
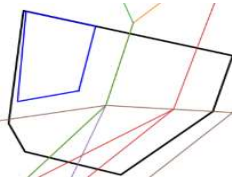
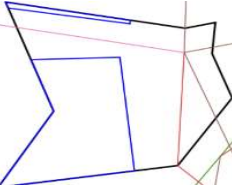
<p>ZBAAAR08</p>	 <p>7800-12500</p>	<p>0.7044</p>
<p>ZBAAAR09</p>	 <p>7500-10000</p> <p>10000-12500</p>	<p>0.9314</p>
<p>ZBAAAR10</p>	 <p>7500-10000</p> <p>10000-12500</p>	<p>1.0000</p>
<p>ZBAAAR11</p>	 <p>7800-12500</p>	<p>1.0000</p>
<p>ZBAAAR12</p>	 <p>6000-6600</p>	<p>0.6484</p>

	 <p>6600-12500</p>	
ZBAAAR13	 <p>6000-8400</p>	0.6882
ZBAAAR14	 <p>8400-12500</p>	0.5215
ZBAAAR15	 <p>6000-8400</p>	0.5215
ZBAAAR16	 <p>8400-12500</p>	0.5177
ZBAAAR17	 <p>6000-12500</p>	1.0000

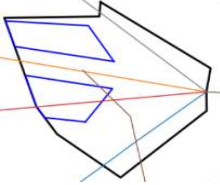
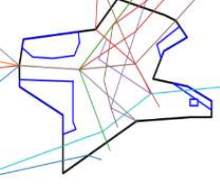
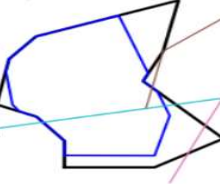

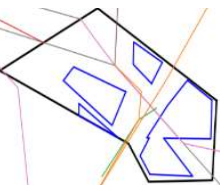
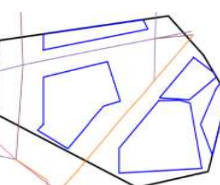
ZBAAAR18	 <p>6000-12500</p>	0.4209
ZBAAAR19	 <p>6000-12500</p>	0.5916
ZBAAAR20	 <p>6000-12500</p>	0.6031
ZBAAAR21	 <p>6000-12500</p>	1.0000
ZBAAAR22	 <p>6000-12500</p>	1.0000
ZBAAAR23	 <p>7800-12500</p>	1.0000

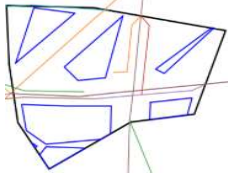
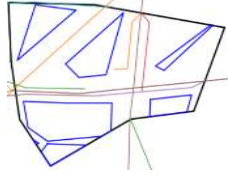
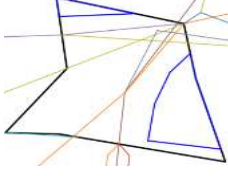
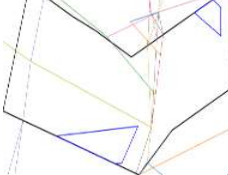

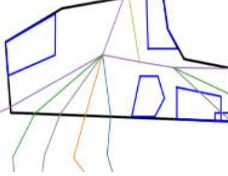
ZBAAAR24	 <p>7800-12500</p>	0.9934
ZBAAAR25	 <p>9800-12500</p>	0.8131
ZBAAAR26	 <p>7800-9800</p>	0.8131
ZBAAAR27	 <p>9800-12500</p>	0.6788
ZBAAAR28	 <p>7800-9800</p>	0.6788
ZBAAAR29	 <p>9800-12500</p>	1.0000

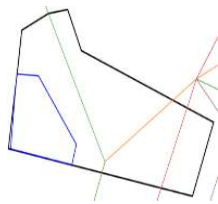
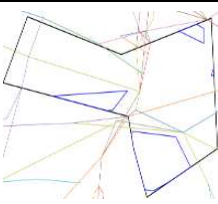
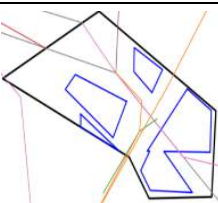
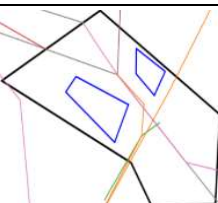
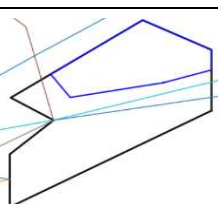
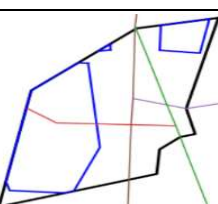
ZBAAAR30	 7800-9800	0.2893
ZBAAAR31	 7800-9800	0.7340
ZBHAR01	 6000-7800	0.7882
ZBHAR02	 6000-7800	0.7709
ZBYNAR01	 6000-7800	0.5937
ZBYNAR02	 6000-7800	1.0000

<p>ZBYNAR03</p>	 <p>6000-7800</p>	<p>1.0000</p>
<p>ZBYNAR04</p>	 <p>6000-6600</p> <p>6600-7800</p>	<p>1.0000</p>
<p>ZGGGAR01</p>	 <p>6000-12500</p>	<p>0.3390</p>
<p>ZGGGAR02</p>	 <p>6000-8400</p>	<p>1.0000</p>
<p>ZGGGAR03</p>	 <p>6000-12500</p>	<p>0.5248</p>

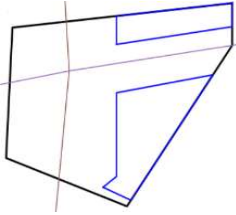
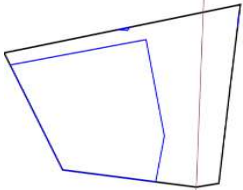
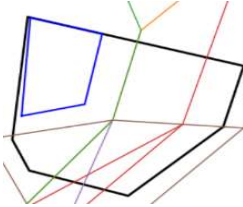
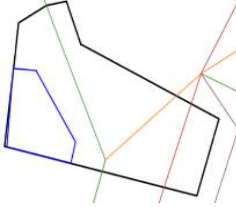
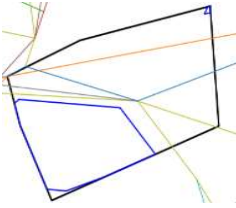
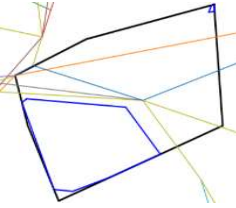


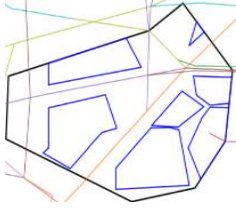
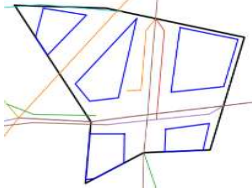
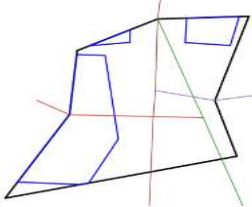
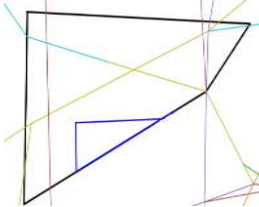
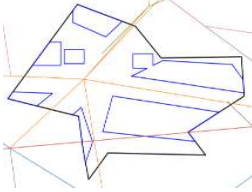
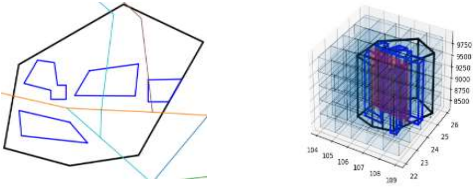
<p>ZGGGAR04</p>	 <p>6000-8400</p>	<p>1.0000</p>
<p>ZGGGAR05</p>	 <p>6000-9800</p>	<p>0.7285</p>
<p>ZGGGAR06</p>	 <p>6000-12500</p>	<p>0.7742</p>
<p>ZGGGAR08</p>	 <p>6000-12500</p>	<p>0.9125</p>
<p>ZGGGAR11</p>	 <p>9200-12500</p>	<p>0.4149</p>
<p>ZGGGAR12</p>	 <p>8400-12500</p>	<p>0.6275</p>

<p>ZGGGAR13</p>	 <p>8400-9800</p>	<p>0.4605</p>
<p>ZGGGAR14</p>	 <p>9800-12500</p>	<p>0.4605</p>
<p>ZGGGAR15</p>	 <p>7800-9800</p>	<p>0.6192</p>
<p>ZGGGAR16</p>	 <p>7800-9800</p>	<p>0.4985</p>
<p>ZGGGAR17</p>	 <p>7800-12500</p>	<p>1.0000</p>
<p>ZGGGAR19</p>	 <p>7800-9200</p>	<p>0.5378</p>

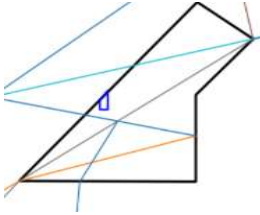
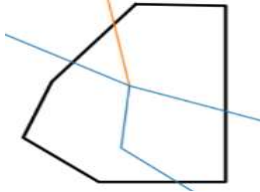
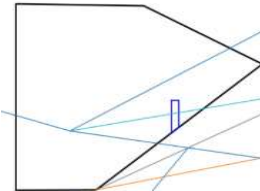
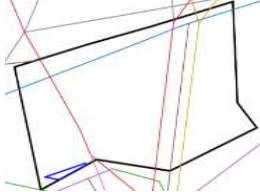
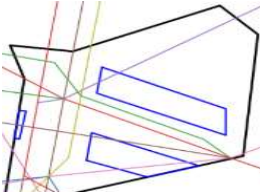
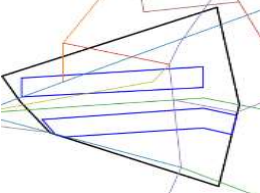
ZGGGAR20	 6000-9800	0.7566
ZGGGAR21	 9800-12500	0.5242
ZGGGAR22	 7800-9200	0.4156
ZGGGAR23	 6000-12500	0.4553
ZGGGAR24	 6000-12500	0.8750
ZGGGAR25	 7800-9800	0.6974

ZGGGAR26	<p>8400-9200</p>	1.0000
ZGGGAR27	<p>9800-12500</p>	0.4744
ZGGGAR28	<p>6000-12500</p>	1.0000
ZGGGAR29	<p>9800-12500</p>	0.7284
ZGGGAR30	<p>8400-12500</p>	0.7868
ZGGGAR31	<p>7800-9800</p>	0.7460

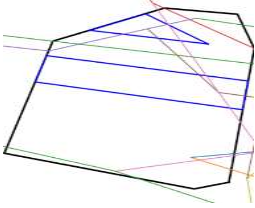
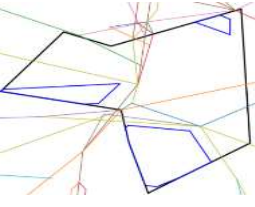
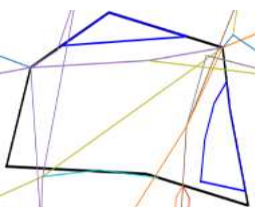
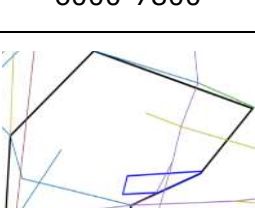
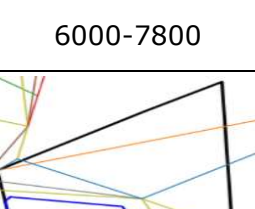
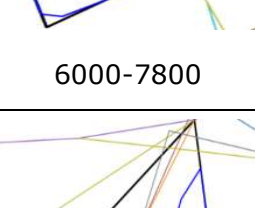
<p>ZGGGAR32</p>	 <p>7800-12500</p>	<p>0.5808</p>
<p>ZGGGAR33</p>	 <p>6000-12500</p>	<p>0.3041</p>
<p>ZGGGAR34</p>	 <p>8400-12500</p>	<p>1.0000</p>
<p>ZGGGAR35</p>	 <p>9800-12500</p>	<p>0.7566</p>
<p>ZGGGAR36</p>	 <p>7800-9800</p>	<p>0.6530</p>
<p>ZGGGAR37</p>	 <p>7800-9800</p>	<p>0.6530</p>

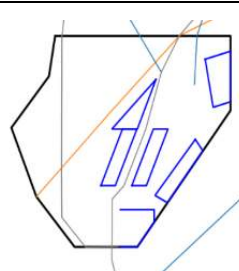
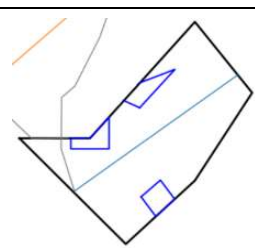
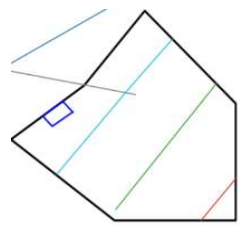
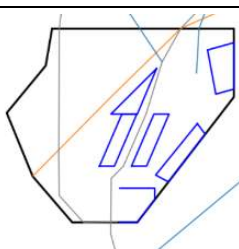
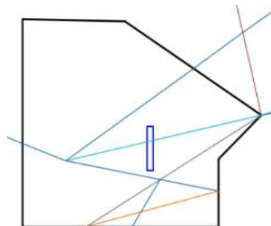
<p>ZGHAAR01</p>	 <p>6000-7800</p>	<p>0.4755</p>
<p>ZGHAAR02</p>	 <p>6000-7800</p>	<p>0.3513</p>
<p>ZGHAAR03</p>	 <p>6000-7800</p>	<p>0.4042</p>
<p>ZGHAAR04</p>	 <p>6000-7800</p>	<p>0.5972</p>
<p>ZGNNAR01</p>	 <p>6000-9800</p>	<p>0.3950</p>
<p>ZGNNAR02</p>	 <p>8500-9800</p>	<p>0.4531</p>

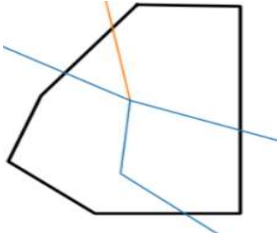

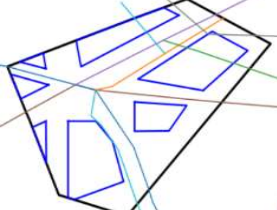
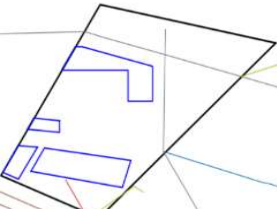
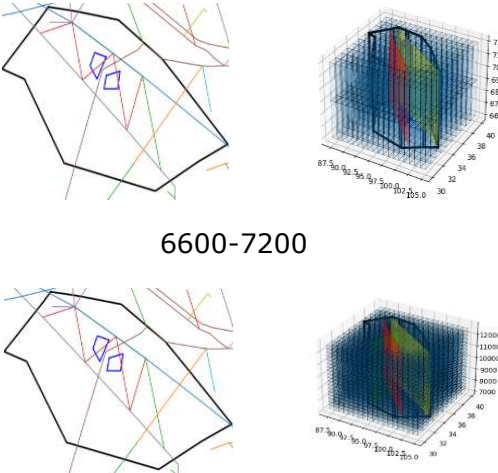
	<p>6000-8500</p>	
ZGNNAR03	<p>8500-9800</p> <p>6000-8500</p>	0.5051
ZGNNAR04	<p>9800-12500</p>	0.3950
ZGNNAR05	<p>9800-12500</p>	0.4684
ZGNNAR06	<p>9800-12500</p>	0.5168

<p>ZGZJAR01</p>	 <p>6000-7800</p>	<p>1.0000</p>
<p>ZGZJAR02</p>	 <p>6000-8900</p>	<p>1.0000</p>
<p>ZGZJAR03</p>	 <p>6000-7800</p>	<p>0.8236</p>
<p>ZHCCAR01</p>	 <p>6000-7800</p>	<p>1.0000</p>
<p>ZHCCAR02</p>	 <p>6000-7800</p>	<p>0.6331</p>
<p>ZHCCAR03</p>	 <p>6000-7800</p>	<p>0.6214</p>

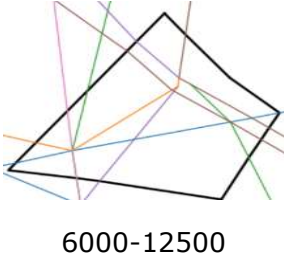
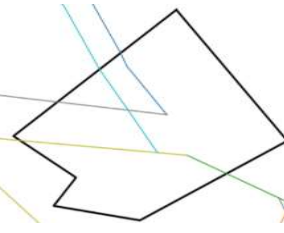


<p>ZHCCAR04</p>	 <p>6000-7800</p>	<p>0.8035</p>
<p>ZHHHAR01</p>	 <p>6000-7800</p>	<p>0.4796</p>
<p>ZHHHAR02</p>	 <p>6000-7800</p>	<p>0.4943</p>
<p>ZHHHAR03</p>	 <p>6000-7800</p>	<p>1.0000</p>
<p>ZHHHAR04</p>	 <p>6000-7800</p>	<p>0.7368</p>
<p>ZHHHAR05</p>		<p>0.5849</p>

	6000-7800	
ZJSYAR01		0.7297
	9200-12500	
ZJSYAR02		1.0000
	6000-12500	
ZJSYAR03		1.0000
	6000-12500	
ZJSYAR04		0.7297
	6000-9200	
ZJSYAR11		1.0000
	7800-12500	

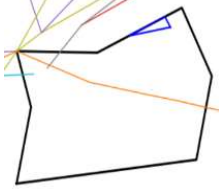
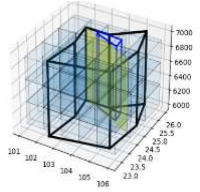
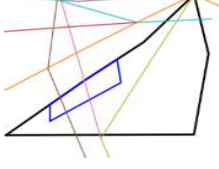
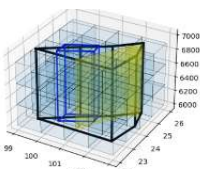
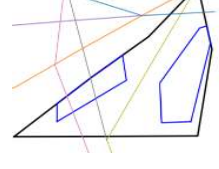
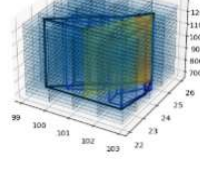

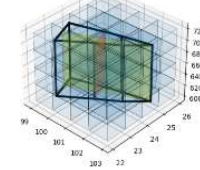
<p>ZJSYAR12</p>	 <p>8900-12500</p>	<p>1.0000</p>
<p>ZLLAR01</p>	 <p>6000-7800</p>	<p>1.0000</p>
<p>ZLLAR02</p>	 <p>6000-8900</p>	<p>0.4053</p>
<p>ZLLAR03</p>	 <p>6000-12500</p>	<p>0.4822</p>
<p>ZLLAR04</p>	 <p>6600-7200</p>	<p>1.0000</p>

	<p>7200-12500</p> <p>6000-6600</p>	
ZLLAR06	<p>7800-8900</p>	0.8301
ZLLAR07	<p>6000-12500</p>	1.0000
ZLLAR08	<p>7800-8900</p>	1.0000
ZLLAR09	<p>6000-12500</p>	1.0000

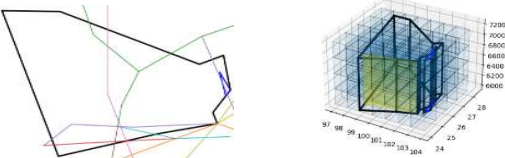
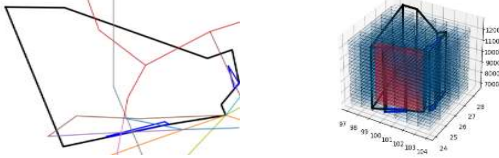
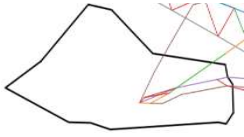
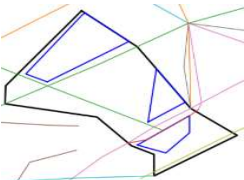
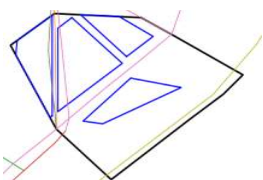
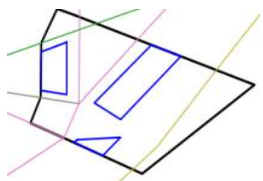
<p>ZLLAR11</p>	 <p>6000-8900</p>	<p>0.5721</p>
<p>ZLLAR12</p>	 <p>6000-12500</p>	<p>1.0000</p>
<p>ZLXYAR01</p>	 <p>6000-8900</p>	<p>0.7997</p>
<p>ZLXYAR02</p>	 <p>6000-8900</p>	<p>0.7930</p>
<p>ZLXYAR03</p>	 <p>6000-8900</p>	<p>0.8560</p>
<p>ZLXYAR04</p>		<p>0.7148</p>

	6000-8900	
ZLXYAR05	 8900-12500	0.8560
ZLXYAR06	 8900-12500	0.7997
ZLXYAR07	 8900-12500	0.7930
ZLXYAR08	 8900-12500	0.7148
ZLXYAR09	 8900-12500	1.0000
ZLXYAR10	 11000-12500	0.7096

	<p>8900-11000</p>	
ZLXYAR11	<p>8900-12500</p>	0.7498
ZLXYAR12	<p>6000-8900</p>	0.5317
ZLXYAR13	<p>8900-12500</p>	0.5317
ZPPPAR01	<p>6000-12500</p>	0.8972
ZPPPAR02	<p>6000-12500</p>	0.3852

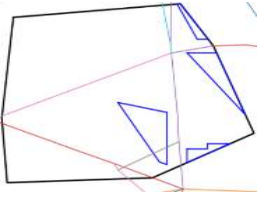
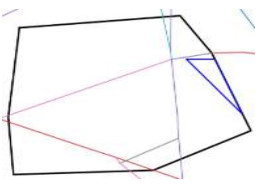
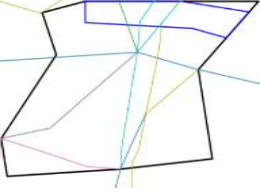
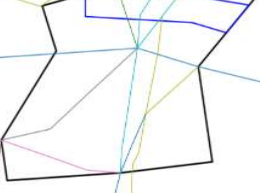
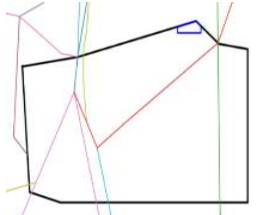
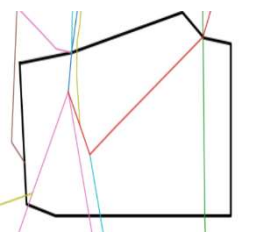
	6000-12500	
ZPPPAR03	 	0.5784
	6000-7000	
= ZPPPAR04	7000-12500	0.6812
	 	
ZPPPAR05	6000-7000	0.8754
	 	
ZPPPAR06	7000-12500	0.9437
	 	

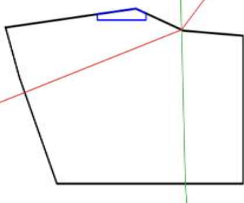
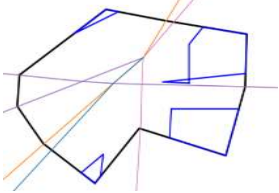
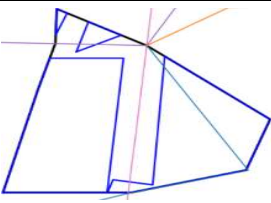
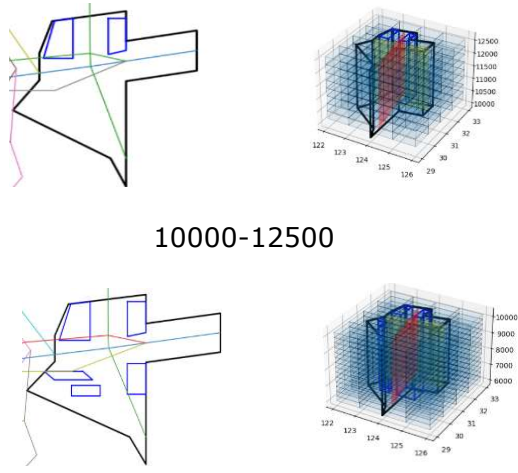
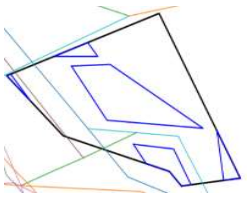


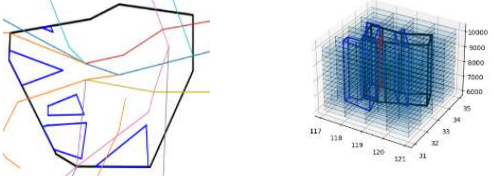
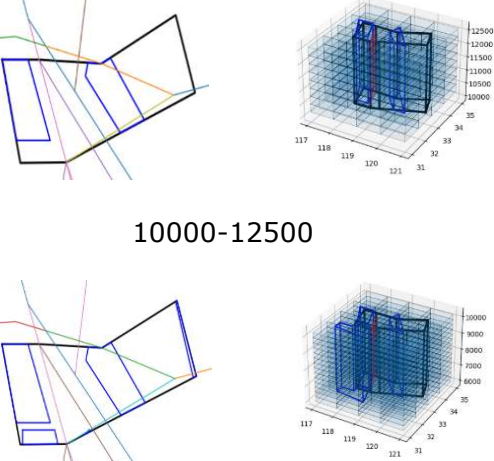
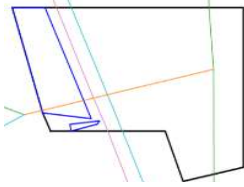
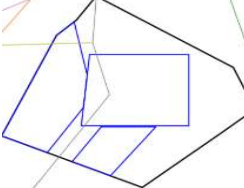
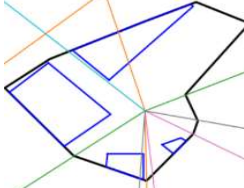
	 <p>6000-7000</p>  <p>7000-12500</p>	
ZPXX01	 <p>6000-12500</p>	1.0000
ZSAMAR01	 <p>6000-7800</p>	0.7529
ZSAMAR02	 <p>6000-7800</p>	0.1729
ZSAMAR03	 <p>6000-7800</p>	0.7043

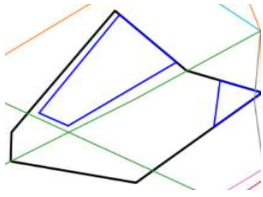
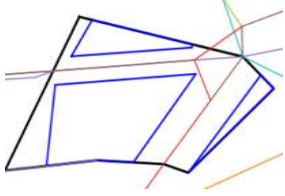
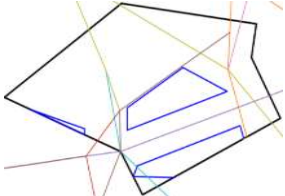
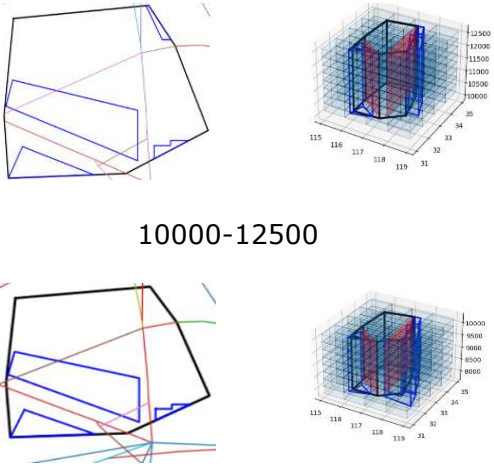
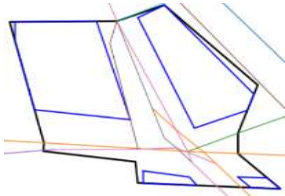
ZSAMAR04	<p>6000-7800</p>	0.6797
ZSCNAR01	<p>6000-7800</p>	0.7965
ZSCNAR02	<p>6000-7800</p>	0.5007
ZSCNAR03	<p>6000-7800</p>	0.3807
ZSCNAR04	<p>6000-7800</p>	0.5443
ZSJNAR01	<p>6000-7800</p>	1.0000

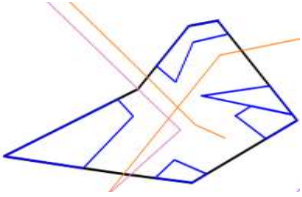
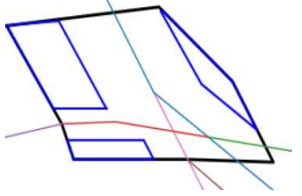
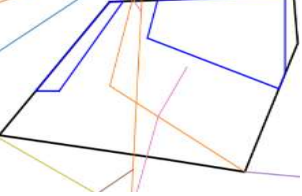
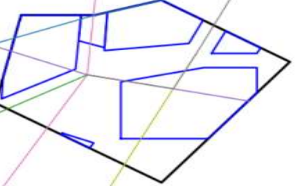
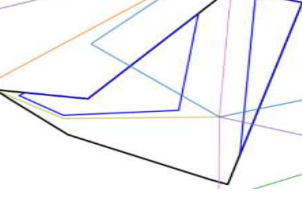
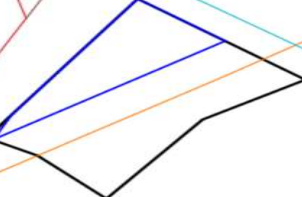
ZSJNAR02	<p>6000-7800</p>	1.0000
ZSJNAR03	<p>6000-7800</p>	1.0000
ZSOFAR01	<p>6000-7800</p>	1.0000
ZSOFAR02	<p>6000-7800</p>	0.2992
ZSOFAR03	<p>6000-7800</p>	1.0000
ZSOFAR04	<p>6000-7800</p>	0.7763

<p>ZSOFAR05</p>	 <p>6000-7800</p>	<p>0.4946</p>
<p>ZSQDAR01</p>	 <p>6000-12500</p>	<p>1.0000</p>
<p>ZSQDAR02</p>	 <p>9800-12500</p>	<p>0.5375</p>
<p>ZSQDAR03</p>	 <p>6000-8900</p>	<p>0.5375</p>
<p>ZSQDAR06</p>	 <p>6000-12500</p>	<p>0.7341</p>
<p>ZSQDAR07</p>	 <p>8400-12500</p>	<p>1.0000</p>

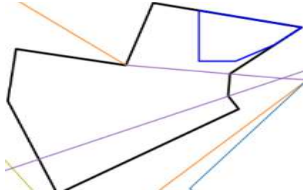
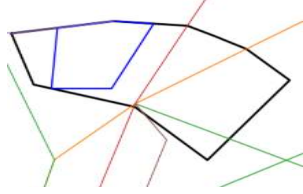
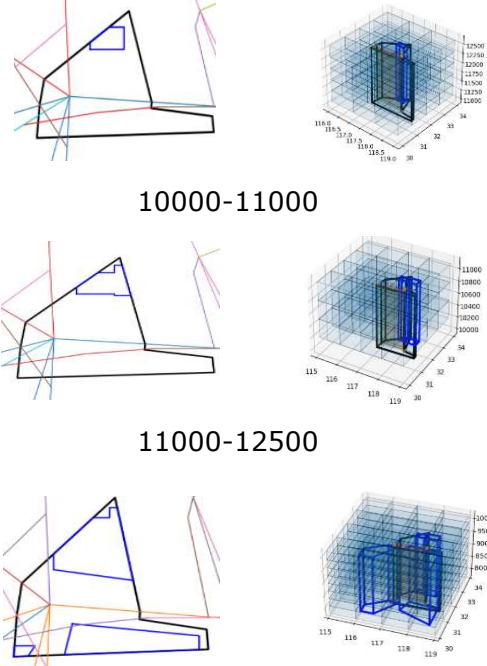
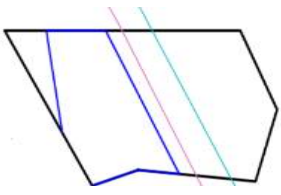
<p>ZSQDAR08</p>	 <p>6000-12500</p>	<p>0.7341</p>
<p>ZSSAR01</p>	 <p>6000-12500</p>	<p>0.5616</p>
<p>ZSSAR02</p>	 <p>6000-12500</p>	<p>1.0000</p>
<p>ZSSAR03</p>	 <p>10000-12500</p> <p>6000-10000</p>	<p>0.8199</p>
<p>ZSSAR04</p>	 <p>6000-12500</p>	<p>0.5159</p>

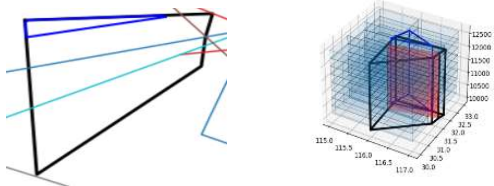
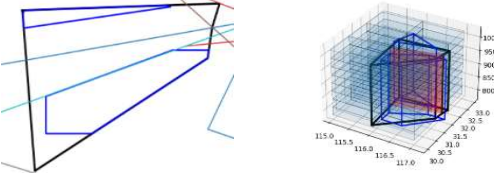
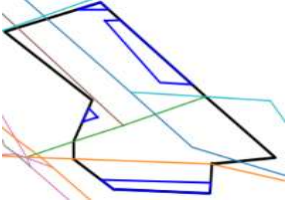
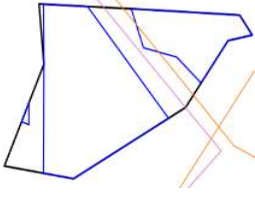
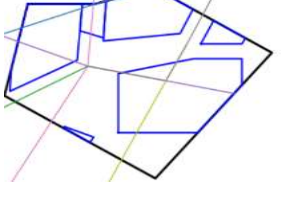
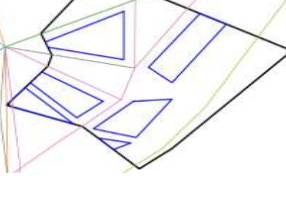
<p>ZSSSAR05</p>	 <p>6000-12500</p>	<p>0.7445</p>
<p>ZSSSAR06</p>	 <p>10000-12500</p> <p>6000-10000</p>	<p>0.5541</p>
<p>ZSSSAR07</p>	 <p>6000-12500</p>	<p>0.8035</p>
<p>ZSSSAR08</p>	 <p>6000-12500</p>	<p>0.9749</p>
<p>ZSSSAR09</p>	 <p>7800-12500</p>	<p>1.0000</p>

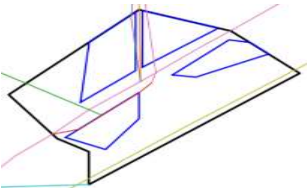
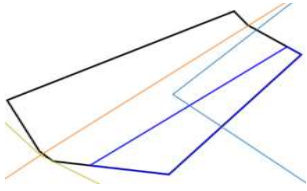
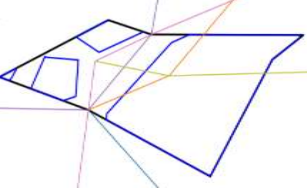

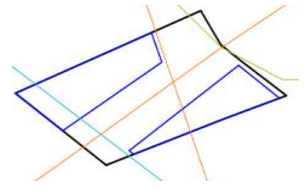
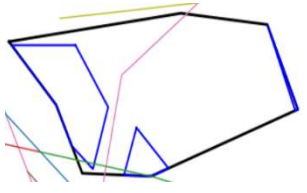
<p>ZSSSAR10</p>	 <p>7800-12500</p>	<p>0.5250</p>
<p>ZSSSAR11</p>	 <p>7800-12500</p>	<p>0.5183</p>
<p>ZSSSAR12</p>	 <p>7800-12500</p>	<p>0.6083</p>
<p>ZSSSAR13</p>	 <p>10000-12500</p> <p>7800-10000</p>	<p>0.2424</p>
<p>ZSSSAR14</p>	 <p>6000-7800</p>	<p>0.7069</p>

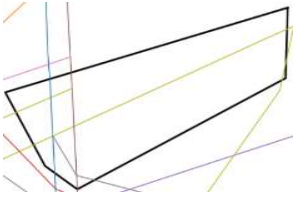
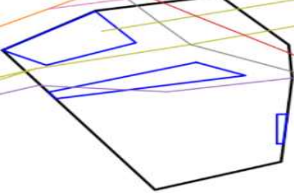
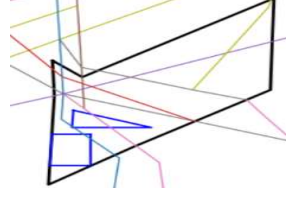
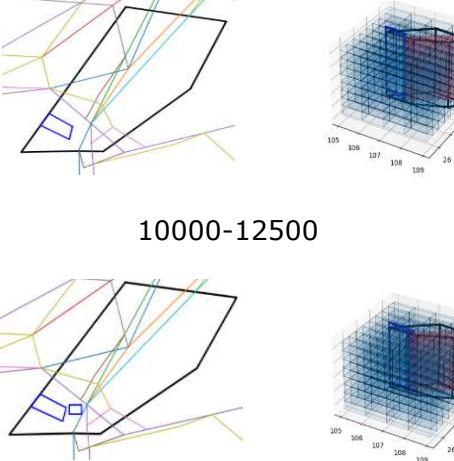
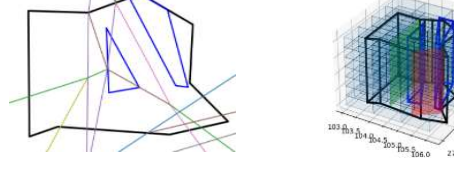
<p>ZSSSAR15</p>	 <p>6000-12500</p>	<p>0.4603</p>
<p>ZSSSAR16</p>	 <p>6000-12500</p>	<p>1.0000</p>
<p>ZSSSAR17</p>	 <p>7800-12500</p>	<p>0.3918</p>
<p>ZSSSAR18</p>	 <p>6000-9800</p>	<p>1.0000</p>
<p>ZSSSAR19</p>	 <p>6000-12500</p>	<p>1.0000</p>
<p>ZSSSAR20</p>	 <p>7800-12500</p>	<p>1.0000</p>

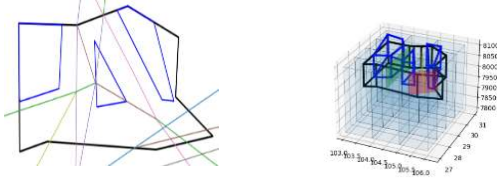
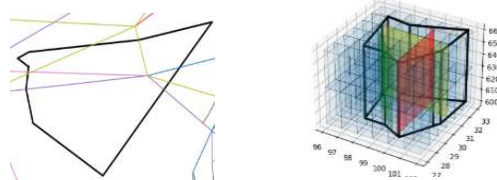
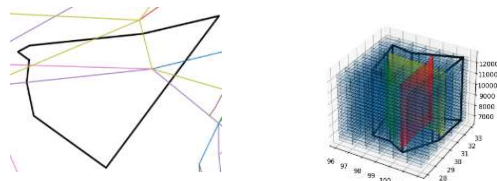
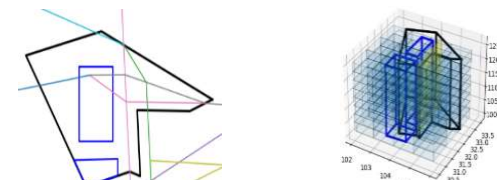
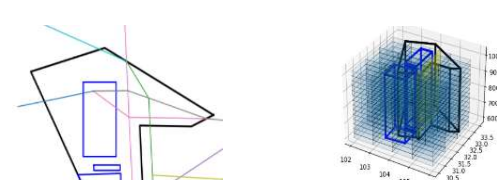
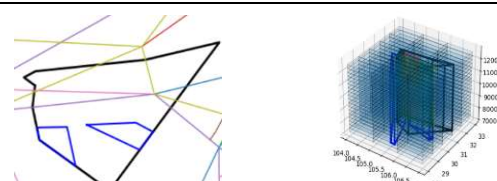


<p>ZSSSAR21</p>	 <p>6000-12500</p>	<p>1.0000</p>
<p>ZSSSAR22</p>	 <p>7800-12500</p>	<p>1.0000</p>
<p>ZSSSAR23</p>	 <p>10000-11000</p> <p>11000-12500</p> <p>7800-10000</p>	<p>0.8778</p>
<p>ZSSSAR24</p>	 <p>6000-12500</p>	<p>0.6495</p>
<p>ZSSSAR25</p>		<p>0.9076</p>

	 <p>10000-12500</p>  <p>7800-10000</p>	
ZSSSAR26	 <p>6000-12500</p>	0.8678
ZSSSAR27	 <p>6000-12500</p>	0.1783
ZSSSAR28	 <p>9800-12500</p>	1.0000
ZSSSAR29	 <p>7800-12500</p>	0.6420

<p>ZSSAR30</p>	 <p>7800-12500</p>	<p>0.6882</p>
<p>ZSSAR31</p>	 <p>6000-12500</p>	<p>1.0000</p>
<p>ZSSAR32</p>	 <p>6000-12500</p>	<p>0.2498</p>
<p>ZSSAR34</p>	 <p>7800-12500</p>	<p>0.7069</p>
<p>ZSSAR35</p>	 <p>7800-12500</p>	<p>0.6797</p>
<p>ZSSAR36</p>	 <p>6000-12500</p>	<p>0.4642</p>

<p>ZUGYAR01</p>	 <p>6000-7800</p>	<p>1.0000</p>
<p>ZUGYAR02</p>	 <p>6000-7800</p>	<p>0.8622</p>
<p>ZUGYAR03</p>	 <p>6000-7800</p>	<p>0.9604</p>
<p>ZUUUAR01</p>	 <p>10000-12500</p> <p>7800-10000</p>	<p>1.0000</p>
<p>ZUUUAR02</p>	 <p>6000-8000</p>	<p>0.8216</p>

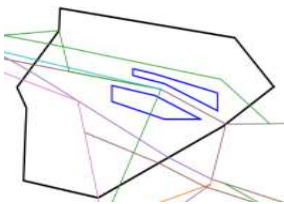
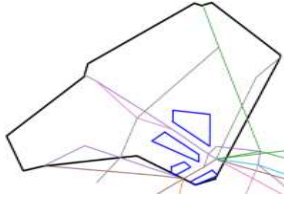
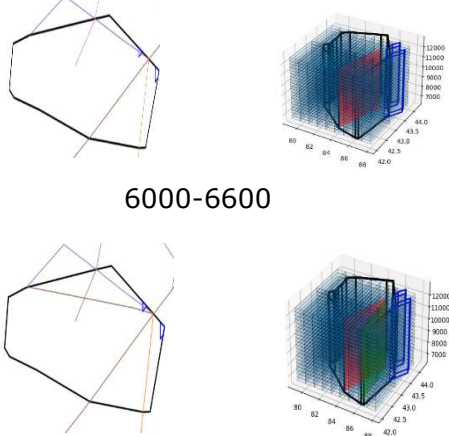
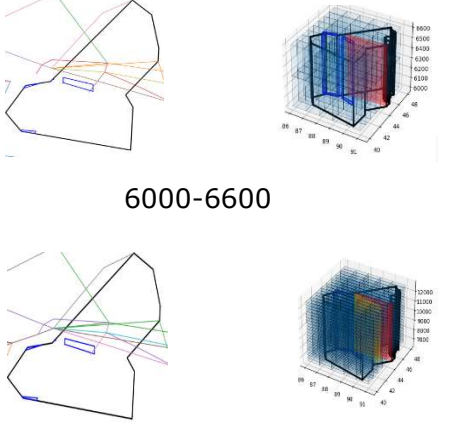
	 <p>8000-8100</p>	
ZUUJAR03	 <p>6000-6600</p>  <p>6600-12500</p>	1.0000
ZUUJAR04	 <p>10000-12500</p>  <p>6000-10000</p>	0.2601
ZUUJAR05	 <p>7200-12500</p>	1.0000

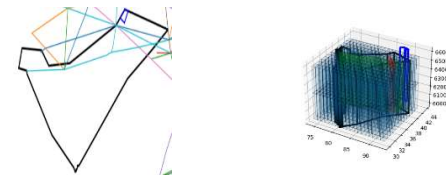

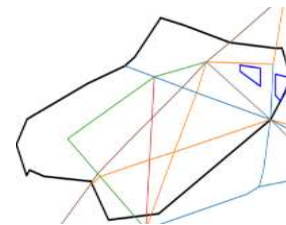
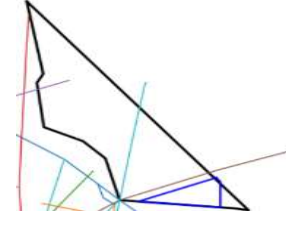
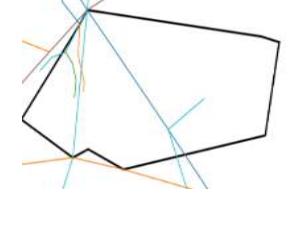

	<p>6000-7200</p>	
ZUUUAR06	<p>6000-7800</p>	1.0000
ZUUUAR07	<p>6000-7800</p>	1.0000
ZUUUAR08	<p>8100-12500</p>	1.0000
ZUUUAR09	<p>6000-12500</p>	1.0000
ZUUUAR11(1)	<p>8000-12500</p>	0.7761
ZUUUAR11		

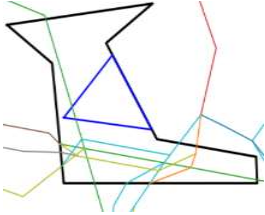
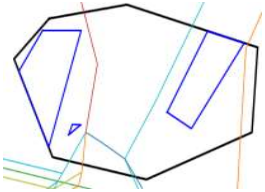
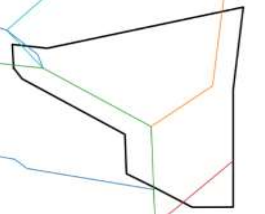
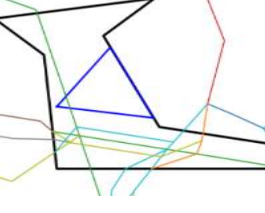
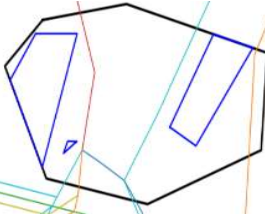
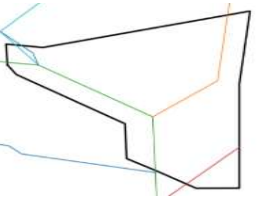
	<p>6000-8000</p>	
ZUUUAR12	<p>6000-12500</p>	1.0000
ZUUUAR13	<p>7800-12500</p>	1.0000
ZUUUAR15	<p>6000-12500</p>	1.0000
ZUUUAR16	<p>6000-12500</p>	1.0000
ZUUUAR17	<p>8000-12500</p>	0.9271

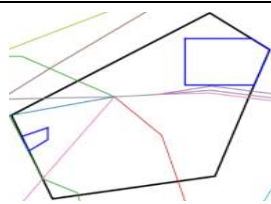
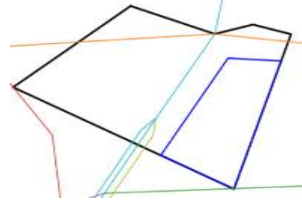
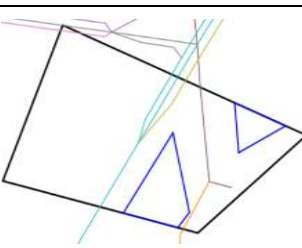
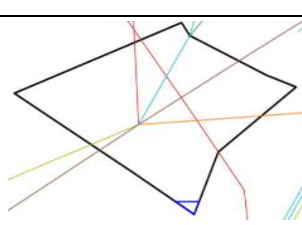
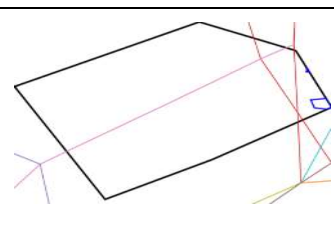
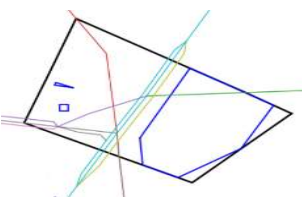
	<p>6000-8000</p>	
ZUUUAR18	<p>8100-12500</p>	0.6944
ZUUUAR19	<p>6000-7800</p>	0.9615
ZUUUAR21	<p>7800-12500</p>	1.0000
ZUUUAR22	<p>7800-12500</p>	0.7105
ZUUUAR23	<p>7800-12500</p>	1.0000

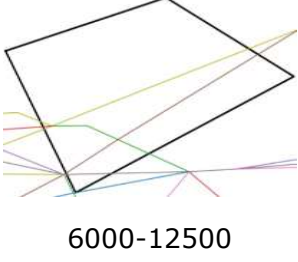
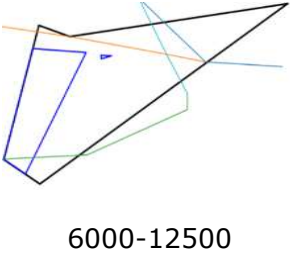
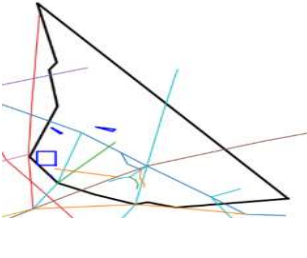


<p>ZWWWAR01</p>	 <p>6000-12500</p>	<p>0.9973</p>
<p>ZWWWAR02</p>	 <p>6000-12500</p>	<p>1.0000</p>
<p>ZWWWAR03</p>	 <p>6000-6600</p> <p>6600-12500</p>	<p>0.8282</p>
<p>ZWWWAR04</p>	 <p>6000-6600</p> <p>6600-12500</p>	<p>1.0000</p>
<p>ZWWWAR05</p>		<p>0.7257</p>

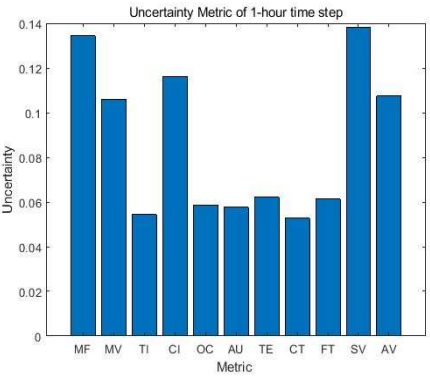
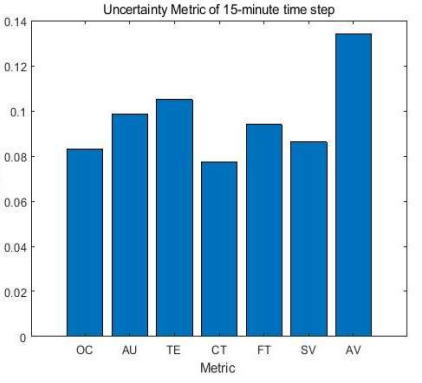
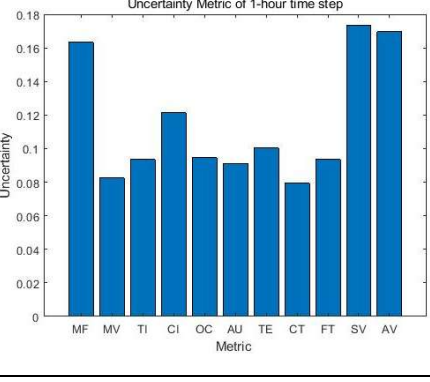
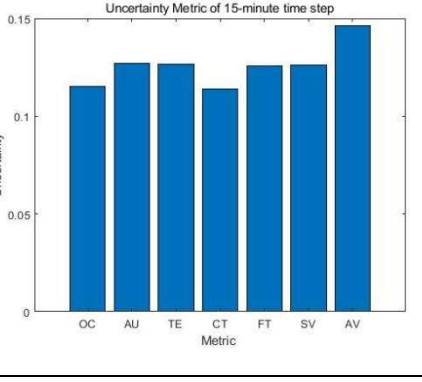
	 <p>6000-6600</p>  <p>6600-12500</p>	
ZWWWAR06	 <p>6000-12500</p>	0.9736
ZYHBAR01	 <p>6000-9800</p>	1.0000
ZYHBAR02	 <p>6000-9800</p>	1.0000
ZYHBAR03	 <p>6000-9800</p>	1.0000

<p>ZYTLAR01</p>	 <p>8900-12500</p>	<p>0.7023</p>
<p>ZYTLAR02</p>	 <p>8900-12500</p>	<p>1.0000</p>
<p>ZYTLAR03</p>	 <p>8900-12500</p>	<p>1.0000</p>
<p>ZYTLAR04</p>	 <p>6000-8900</p>	<p>0.7023</p>
<p>ZYTLAR05</p>	 <p>6000-8900</p>	<p>1.0000</p>
<p>ZYTLAR06</p>		<p>1.0000</p>

	6000-8900	
ZYTXAR01	 <p>6000-12500</p>	0.7827
ZYTXAR02	 <p>6000-12500</p>	0.5560
ZYTXAR03	 <p>6000-12500</p>	0.8052
ZYTXAR04	 <p>6000-12500</p>	1.0000
ZYTXAR05	 <p>6000-12500</p>	1.0000
ZYTXAR06	 <p>6000-12500</p>	0.4587

<p>ZYTXAR07</p>	 <p>6000-12500</p>	<p>1.0000</p>
<p>ZYTXAR08</p>	 <p>6000-12500</p>	<p>0.8332</p>
<p>ZYTXAR09</p>	 <p>9800-12500</p>	<p>1.0000</p>

# ANNEX 3: THE UNCERTAINTY OF COMPLEXITY INDICATORS IN REPRESENTATIVE SECTORS IN CHINA

	Complexity indicator uncertainty (1 hour)	Complexity indicator uncertainty (15 minutes)
ZBAAAR03		
ZBAAAR22		
ZBAAAR25	